THE
PHYSICAL REVIEW

A journal of experimental and theoretical physics established by E. L. Nichols in 1893

SECOND SERIES, VOL. 73, NO. 2 JANUARY 15, 1948

Calculation of Nuclear Quadrupole Effects in Molecules

J. BARDEEN AND C. H. TOWNES
Bell Telephone Laboratories, Murray Hill, New Jersey
(Received October 9, 1947)

Methods are given for the computation of nuclear quadrupole interactions in molecules. They apply primarily to the interpretation of microwave spectra of linear and symmetric top molecules in which either one or two nuclei on the molecular axis show quadrupole coupling to the molecular field. Tables are given of the energy values, based on Casimir's formula, for the quadrupole coupling of a single nucleus, and also of transformation coefficients for application to the case of intermediate coupling when two nuclei are involved. Spectral intensities are discussed briefly. Examples are given to illustrate various aspects of the theory. The molecules BrCN and ClCN show quadrupole effects resulting from the nitrogen nucleus as well as to the halogen. In the latter case, the intermediate coupling theory is required for a complete explanation of the observed microwave-absorption lines, as there are significant deviations from the first-order linear approximation.

NUCLEAR quadrupole effects in molecules were first discovered by Rabi[1] and his associates by the use of molecular beam spectroscopy. Recently the resolution afforded by microwave spectroscopy has made possible detection and measurement of these effects in microwave-absorption spectra of gases. It appears that nuclear quadrupole effects will be found in many spectra in the microwave region and will yield considerable nuclear and molecular information. Casimir's formula[2] for nuclear quadrupole-coupling energies in an isolated atom has previously been extended[1–5] to cases where a single atom shows quadrupole coupling in a linear or symmetric top molecule. There are also a number of interesting molecules containing two atoms with measurable quadrupole coupling; a comparison between experimental and theoretically expected spectra of some of these has already been published.[6] The theory applicable to these molecules, as well as to similar cases involving other types of coupling, is developed here. This theory, plus tables which are included, allow a fairly convenient method for interpreting quadrupole effects caused by either one or two nuclei on the axis of a linear or symmetric top molecule. Since experimental measurements of quadrupole effects in molecules and their theoretical explanation have developed together, a number of cases which test theoretical expectations are available, and these are briefly discussed.

The Hamiltonian for interaction between a nuclear quadrupole moment and molecular elec-

[1] J. M. B. Kellogg, I. I. Rabi, N. F. Ramsey, and J. R. Zacharias, Phys. Rev. **57**, 677 (1940).
[2] H. B. G. Casimir, *On the Interaction between Atomic Nuclei and Electrons* (Teyler's Tweede Genootschap, E. F. Bohn, Haarlem, 1936).
[3] A. Nordsieck, Phys. Rev. **58**, 310 (1940).
[4] D. K. Coles and W. E. Good, Phys. Rev. **70**, 979 (1946).
[5] J. H. Van Vleck, Phys. Rev. **71**, 468 (1947).
[6] C. H. Townes, A. N. Holden, J. Bardeen, and F. R. Merritt, Phys. Rev. **71**, 644 (1947); C. H. Townes, A. N. Holden, and F. R. Merritt, Phys. Rev. **72**, 513 (1947).

TABLE I. Values of $[\frac{3}{4}C(C+1)-I(I+1)J(J+1)]/2I(2I-1)(2J-1)(2J+3)$, where $C=F(F+1)-I(I+1)-J(J+1)$.

	I	1	3/2	2	5/2	3	7/2	4	9/2
J	F								
	11/2								0.05000
	5							0.05000	
	9/2						0.05000		−0.13333
	4					0.05000		−0.13750	
1	7/2				0.05000		−0.14286		0.09167
	3			0.05000		−0.15000		0.09821	
	5/2		0.05000		−0.16000		0.10714		
	2	0.05000		−0.17500		0.12000			
	3/2		−0.20000		0.14000				
	1	−0.25000		0.17500					
	1/2		0.25000						
	0	0.50000							
	13/2								0.07143
	6							0.07143	
	11/2						0.07143		−0.08333
	5					0.07143		−0.08929	
2	9/2				0.07143		−0.09694		−0.08333
	4			0.07143		−0.10714		−0.08291	
	7/2		0.07143		−0.12143		−0.08163		0.00595
	3	0.07143		−0.14286		−0.07857		0.01403	
	5/2		−0.17857		−0.07143		0.02551		0.13095
	2	−0.25000		−0.05357		0.04286		0.14031	
	3/2		0		0.07143		0.15306		
	1	0.25000		0.12500		0.17143			
	1/2		0.25000		0.20000				
	0			0.25000					
	15/2								0.08333
	7							0.08333	
	13/2						0.08333		−0.05556
	6					0.08333		−0.06250	
	11/2				0.08333		−0.07143		−0.09167
3	5			0.08333		−0.08333		−0.09464	
	9/2		0.08333		−0.10000		−0.09762		−0.06111
	4	0.08333		−0.12500		−0.10000		−0.05595	
	7/2		−0.16667		−0.10000		−0.04762		0.00556
	3	−0.25000		−0.09167		−0.03333		0.01786	
	5/2		−0.05000		−0.00667		0.03571		0.08333
	2	0.20000		0.05000		0.06333		0.09821	
	3/2		0.20000		0.11000		0.11905		0.15278
	1			0.20000		0.15000		0.16369	
	1/2				0.20000		0.17857		
	0					0.20000			

tric fields is given by Casimir's expression[2]

$$H(\mathbf{I},\mathbf{J})=2eQ\{\sum_k e_k(3\cos^2\theta_k-1)/R_k^3\}_{Av}F(\mathbf{I},\mathbf{J}), \quad (1)$$

where

$$F(\mathbf{I},\mathbf{J})=\frac{3(\mathbf{I}\cdot\mathbf{J})^2+\frac{3}{2}(\mathbf{I}\cdot\mathbf{J})-I(I+1)J(J+1)}{2J(2J-1)2I(2I-1)},$$

e = electronic charge,

Q = quadrupole moment of nucleus (defined below),

$\mathbf{R}_k$ = radius vector from nucleus to individual charge e_k in molecule,

θ_k = angle between $\mathbf{R}_k$ and an axis fixed in space,

$\mathbf{I}$ = nuclear spin in units of $h/2\pi$,

$\mathbf{J}$ = angular momentum caused by molecular rotation in units of $h/2\pi$.

The average is taken over the normal electronic state, the appropriate vibrational state, and the rotational state with $m_J=J$, that is, the one for which the projection of $\mathbf{J}$ along the fixed axis is a maximum.

When applied to a linear molecule, or to a symmetric top molecule with the nucleus on the axis of symmetry, Casimir's expression reduces to[3]

$$H(\mathbf{I},\mathbf{J})=eQq(3\cos^2\theta-1)_{Av}F(\mathbf{I},\mathbf{J}), \quad (2)$$

where θ is now the angle between the molecular axis and the axis fixed in space, and the average is over the rotational wave function with $m_J=J$.

TABLE I.—*Continued.*

	I	1	3/2	2	5/2	3	7/2	4	9/2
J	*F*								
	17/2								0.09091
	8							0.09091	
	15/2						0.09091		−0.03788
	7					0.09091		−0.04546	
	13/2				0.09091		−0.05520		−0.08658
	6			0.09091		−0.06818		−0.09172	
	11/2		0.09091		−0.08636		−0.09740		−0.07955
	5	0.09091		−0.11364		−0.10325		−0.07711	
	9/2		−0.15909		−0.10779		−0.07189		−0.03788
4	4	−0.25000		−0.10552		−0.06104		−0.02667	
	7/2		−0.07143		−0.03766		−0.00928		0.02056
	3	0.17857		0.01786		0.01948		0.03873	
	5/2		0.17857		0.07143		0.06540		0.08117
	2			0.17857		0.10714		0.10239	
	3/2				0.17857		0.13265		0.13258
	1					0.17857		0.15179	
	1/2						0.17857		0.16667
	0							0.17857	
	19/2								0.09615
	9							0.09615	
	17/2						0.09615		−0.02564
	8					0.09615		−0.03365	
	15/2				0.09615		−0.04396		−0.08013
	7			0.09615		−0.05769		−0.08677	
	13/2		0.09615		−0.07692		−0.09432		−0.08547
5	6	0.09615		−0.10577		−0.10256		−0.08517	
	11/2		−0.15385		−0.11026		−0.08242		−0.05769
	5	−0.25000		−0.11218		−0.07457		−0.04808	
	9/2		−0.08333		−0.05385		−0.03205		−0.01068
	4	0.16667		0		−0.00385		0.00801	
	7/2		0.16667		0.05000		0.03663		0.04380
	3			0.16667		0.08333		0.06937	
	5/2				0.16667		0.10714		0.09615
	2					0.16667		0.12500	
	3/2						0.16667		0.13889
	1							0.16667	
	1/2								0.16667

Our definition of q differs from previous usage, as will be discussed below. If we define

V = electrostatic potential produced by all charges except those inside a small sphere surrounding the nucleus,

z = coordinate along the molecular axis,

then our q is defined as

$$q \equiv \partial^2 V/\partial z^2.$$

Notation for the expression $eQ(\partial^2 V/\partial z^2)$ is in a rather confused state, a number of different forms having appeared in the literature. Kellogg *et al.*[1] and Nordsieck[3] define and use quantities q and q', where

$$q' = (1/2e)(\partial^2 V/\partial z^2) \quad \text{and} \quad q = (-2J/(2J+3))q'.$$

In addition, they use a quantity written as $\partial^2 V/\partial z^2$, which is our $\partial^2 V/\partial z^2$ divided by e. Coles and Good,[4] in an expression which will be discussed later, use Q for the quadrupole moment, which is our Q multiplied by $-(2I+3)/2I$. They also use a symbol q which is twice Kellogg and Nordsieck's q'. Van Vleck[7] has given an expression with a symbol Q differing from the usual Q by a factor of 4. The Q defined here appears to be that most widely used, and is

$$\frac{1}{e}\left[\rho r^2(3\cos^2\theta - 1)\right]_{Av},$$

where the average is over the nuclear charge density ρ and θ is the angle between the spin vector and the radius r to the element of charge. Since there is already so much notational confusion, and notation used in the past does not

[7] B. P. Dailey, R. L. Kyhl, M. W. P. Strandberg, J. H. Van Vleck, and E. B. Wilson, Jr., Phys. Rev. **70**, 984 (1946).

seem to us particularly suited to our discussion, we have taken the liberty of redefining the symbol q as the fundamental molecular quantity $\partial^2 V/\partial z^2$.

QUADRUPOLE COUPLING FOR A SINGLE NUCLEUS

If only one nucleus of a linear molecule shows appreciable coupling, and if no vibrational bending modes are excited, the energy caused by nuclear quadrupole effects may be expressed in terms of the quantum number F for the total angular momentum, $\mathbf{F}=\mathbf{I}+\mathbf{J}$. The energy is[1-3]

$$E=-eQq\frac{\frac{3}{4}C(C+1)-I(I+1)J(J+1)}{2I(2I-1)(2J-1)(2J+3)}, \quad (3)$$

where

$$C=F(F+1)-I(I+1)-J(J+1).$$

Table I gives the values of the factor multiplying $-eQq$ in Eq. (3) for all possible values of F, for $0<J\leq 5$, and for $1\leq I\leq 9/2$. If $J=0$ or $I<1$, the quadrupole-coupling energy is identically zero. This table for energy levels plus published tables for relative intensities of different transitions[8] allows a rapid calculation of the quadrupole splitting of molecular rotational lines involving low values of J. It may be noted from the table that when $F=J+I$ or $F=J-I$, the interaction energy is independent of I. The tabulated function becomes, indeed, $J/4(2J+3)$ when $F=J+I$ and $(J+1)/4(2J-1)$ when $F=J-I$. If $I=1$ and $F=J$, it becomes -0.25. The table also shows that for any I and J, positive quantities are obtained for extreme values of F, and negative quantities for intermediate F's. This is because the interaction varies approximately as the square of the cosine between $\mathbf{I}$ and $\mathbf{J}$.

Van Vleck[5] and Coles and Good[4] showed that for a single nucleus in a symmetric top molecule, expression (3) should be multiplied by $(1-3K^2/J(J+1))$, where K is the quantum number for angular momentum about the symmetry axis. Their result follows from the fact that $(3\cos^2\theta-1)$ averaged over the symmetric top wave function, with the magnetic quantum number m_J equal to the total angular momentum J, is $(-2J/(2J+3))(1-3K^2/J(J+1))$. The linear molecule is a special case of the symmetric top in which $K=0$, and in this case $(3\cos^2\theta-1)_{Av}$ is $-2J/(2J+3)$. Good examples of quadrupole effects in a symmetric top molecule are afforded by the now famous ammonia inversion spectrum,[4,7] and by the rotational spectra of CH_3I, CH_3Br, and CH_3Cl.[9] Table I may be used for energy levels of symmetric top molecules if the correction factor $(1-3K^2/J(J+1))$ is applied.

The expression for quadrupole energy levels in a symmetric top molecule also applies to linear molecules excited to bending vibrational states. Because of the degeneracy of the bending modes of a linear molecule, excitation of one of these modes produces an angular momentum around the molecular axis. Under this condition the molecule is almost a symmetric top, its two larger moments of inertia generally differing by about one part in a thousand. It should, therefore, be expected that the symmetric top formula for quadrupole splitting holds to a high degree of accuracy if K is replaced by l, the quantum number for angular momentum produced by this type of vibration. The result may be more rigorously demonstrated by calculating $(3\cos^2\theta-1)_{Av}$. The wave functions for each of the two states of a molecule undergoing a bending vibration involve a combination of symmetric top functions with l positive and l negative.[10] The quantity $(3\cos^2\theta-1)_{Av}$ is, however, independent of the sign of l and becomes

$$\frac{-2J}{2J+3}\left(1-\frac{3l^2}{J(J+1)}\right).$$

Examples of quadrupole splitting in linear molecules with excited bending modes are afforded by BrCN and ClCN. Spectra of their excited molecules agree well with the above theory.[6]

QUADRUPOLE COUPLING FOR TWO NUCLEI

In case there are two nuclei with angular momenta I_1 and I_2 contributing to the interaction, the Hamiltonian is a combination of functions such as expression (2):

$$H=H_1(\mathbf{I}_1, \mathbf{J})+H_2(\mathbf{I}_2, \mathbf{J}). \quad (4)$$

[8] E. U. Condon and G. H. Shortley, *The Theory of Atomic Spectra* (Cambridge University Press, New York 1935).

[9] W. Gordy, A. G. Smith, and J. W. Simmons, Phys. Rev. **71**, 917 (1947); **72**, 249 (1947); **72**, 344 (1947).

[10] See, for example, G. Herzberg, *Infrared and Raman Spectra of Polyatomic Molecules* (D. Van Nostrand Company, Inc., New York, 1945), p. 377.

TABLE II. Transformation coefficients $c(F_1, F_2)$ for $I_1=I_1$, $I_2=1$.
$\Sigma=I+J+F+1$

F_2 \ F_1	$F-1$	F	$F+1$
$J-1$	$\left(\frac{(\Sigma-2F-1)(\Sigma-2F)(\Sigma-2J-1)(\Sigma-2J)}{2J(2J+1)2F(2F+1)}\right)^{\frac{1}{2}}$	$\left(\frac{2(\Sigma-2F-1)(\Sigma-2I-1)\Sigma(\Sigma-2J)}{2J(2J+1)2F(2F+2)}\right)^{\frac{1}{2}}$	$\left(\frac{(\Sigma-2I-1)(\Sigma-2I)\Sigma(\Sigma+1)}{2J(2J+1)(2F+1)(2F+2)}\right)^{\frac{1}{2}}$
J	$\left(\frac{2(\Sigma-2F)(\Sigma-2I-1)\Sigma(\Sigma-2J-1)}{2J(2J+2)2F(2F+1)}\right)^{\frac{1}{2}}$	$\frac{2(F-I)(2F+2)+2(\Sigma-2F-1)(\Sigma-2I)}{(2J(2J+2)2F(2F+2))^{\frac{1}{2}}}$	$-\left(\frac{2(\Sigma-2F-1)(\Sigma-2I)(\Sigma-2J)(\Sigma+1)}{2J(2J+2)(2F+1)(2F+2)}\right)^{\frac{1}{2}}$
$J+1$	$\left(\frac{(\Sigma-2I-1)(\Sigma-2I)\Sigma(\Sigma+1)}{(2J+1)(2J+2)2F(2F+1)}\right)^{\frac{1}{2}}$	$-\left(\frac{2(\Sigma-2J-1)(\Sigma-2F)(\Sigma-2I)(\Sigma+1)}{(2J+1)(2J+2)2F(2F+2)}\right)^{\frac{1}{2}}$	$\left(\frac{(\Sigma-2J-1)(\Sigma-2J)(\Sigma-2F-1)(\Sigma-2F)}{(2J+1)(2J+2)(2F+1)(2F+2)}\right)^{\frac{1}{2}}$

We shall continue to represent the total angular momentum of the molecule by **F**, and introduce, in addition, the quantity $\mathbf{F}_1$, which is the vector sum of **J** and the spin $\mathbf{I}_1$ of the first nucleus, and the quantity $\mathbf{F}_2$, which is the vector sum of **J** and the spin $\mathbf{I}_2$ of the second nucleus. Wave functions for the combined system may be obtained by first obtaining functions with F_1 fixed:

$$\mathbf{F}_1=\mathbf{J}+\mathbf{I}_1, \quad F_1=|I_1+J|, \quad \cdots, \quad |I_1-J|,$$

and then combining $\mathbf{I}_2$ with $\mathbf{F}_1$ to obtain the total angular momentum **F**:

$$\mathbf{F}=\mathbf{F}_1+\mathbf{I}_2, \quad F=|F_1+I_2|, \quad \cdots, \quad |F_1-I_2|.$$

Let $\Psi_1(F, F_1)$ be the wave functions for states specified by the quantum numbers F and F_1. Different values of F_1, when combined with I_2, may lead to the same value of F. Thus there may be a number of wave functions, specified by different F_1, which all have the same total angular momentum, F. If the interaction H_2 is negligible, the states specified by different F, but with the same value of F_1, will all have the same energy. This degeneracy is removed if H_2 is appreciable.

Alternatively, it would be possible to first combine $\mathbf{I}_2$ with **J** to get states for fixed F_2, and then combine $\mathbf{F}_2$ with $\mathbf{I}_1$ to get states for fixed F. The number of different states with given F is just the same as before, and the two sets of wave functions are linearly related. Thus we may write

$$\Psi_1(F, F_1)=\sum_{F_2} c(F_1, F_2)\Psi_2(F, F_2). \qquad (5)$$

The matrix $c(F_1, F_2)$ is unitary, and the phases may be chosen so that the coefficients are real. The reverse transformation is then

$$\Psi_2(F, F_2)=\sum_{F_1} c(F_1, F_2)\Psi_1(F, F_1). \qquad (6)$$

As will be shown below, the secular determinant for the energy levels can be set up from the transformation matrix and the energy values for the individual interactions.

An expression for the matrix coefficients may be found by expanding both $\Psi_1(F, F_1)$ and $\Psi_2(F, F_2)$ in terms of a fundamental set of wave functions characterized by the quantum numbers (m_1, m_2, m_J) representing the components of I_1, I_2, and J. If these expansions are substituted into Eq. (5), and the coefficients of the wave functions of the fundamental set on the two sides are equated, a set of linear equations is obtained for $c(F_1, F_2)$. These may be solved simply in a formal way, but the resulting series expression is difficult to use for numerical calculations. Dr. G. H. Shortley has pointed out to us that Racah[11] recently obtained a closed formula for the coefficients, which, although still rather involved, is simpler to use than one which we had developed independently and used in our calculations. We shall accordingly refer to Racah's paper for the formula and its derivation. We will not reproduce it here because of its length. Our coefficient becomes in Racah's notation:

$$c(F_1, F_2)=(JI_1(F_1)I_2F|\,JI_2(F_2)I_1F). \qquad (7)$$

The closed formula of Racah[11] is his Eq. (5) of III, which refers back to his Eq. (36′) of II.

Since the general expression is complicated, we have computed expressions for the coeffi-

[11] G. Racah, I Phys. Rev. **61**, 186 (1942); II **62**, 438 (1942); **63**, III 367 (1943).

TABLE III. Transformation coefficients $c(F_1, F_2)$ for $I_1=I$, $I_2=\frac{3}{2}$.
$\Sigma=I+J+F+\frac{3}{2}$

F_2	$F_1=F-\frac{3}{2}$	$F_1=F-\frac{1}{2}$
$J-\frac{3}{2}$	$\left(\frac{(\Sigma-2F-2)(\Sigma-2F-1)(\Sigma-2F)(\Sigma-2J-2)(\Sigma-2J-1)(\Sigma-2J)}{(2F-1)2F(2F+1)(2J-1)2J(2J+1)}\right)^{\frac{1}{2}}$	$\left(\frac{3(\Sigma-1)(\Sigma-2F-2)(\Sigma-2F-1)(\Sigma-2J-1)(\Sigma-2J)(\Sigma-2I-2)}{(2F-1)(2F+1)(2F+2)(2J-1)2J(2J+1)}\right)^{\frac{1}{2}}$
$J-\frac{1}{2}$	$\left(\frac{3(\Sigma-1)(\Sigma-2F-1)(\Sigma-2F)(\Sigma-2J-2)(\Sigma-2J-1)(\Sigma-2I-2)}{(2F-1)2F(2F+1)(2J-1)(2J+1)(2J+2)}\right)^{\frac{1}{2}}$	$\frac{[2(2F-1)(\Sigma-2I-1)+(\Sigma-2F)(-3I+3J+F-\frac{1}{2})]((\Sigma-2F-1)(\Sigma-2J-1))^{\frac{1}{2}}}{((2F-1)(2F+1)(2F+2)(2J-1)(2J+1)(2J+2))^{\frac{1}{2}}}$
$J+\frac{1}{2}$	$\left(\frac{3(\Sigma-1)\Sigma(\Sigma-2F)(\Sigma-2J-2)(\Sigma-2I-2)(\Sigma-2I-1)}{(2F-1)2F(2F+1)2J(2J+1)(2J+3)}\right)^{\frac{1}{2}}$	$\frac{[(2F-1)(\Sigma-2I)+(\Sigma-2F)(-3I+3J-F+\frac{1}{2})]((\Sigma)(\Sigma-2I-1))^{\frac{1}{2}}}{((2F-1)(2F+1)(2F+2)2J(2J+1)(2J+3))^{\frac{1}{2}}}$
$J+\frac{3}{2}$	$\left(\frac{(\Sigma-1)\Sigma(\Sigma+1)(\Sigma-2I-2)(\Sigma-2I-1)(\Sigma-2I)}{(2F-1)2F(2F+1)(2J+1)(2J+2)(2J+3)}\right)^{\frac{1}{2}}$	$-\left(\frac{3\Sigma(\Sigma+1)(\Sigma-2F)(\Sigma-2J-2)(\Sigma-2I-1)(\Sigma-2I)}{(2F-1)(2F+1)(2F+2)(2J+1)(2J+2)(2J+3)}\right)^{\frac{1}{2}}$
	$F_1=F+\frac{1}{2}$	$F_1=F+\frac{3}{2}$
$J-\frac{3}{2}$	$\left(\frac{3(\Sigma-1)\Sigma(\Sigma-2F-2)(\Sigma-2J)(\Sigma-2I-2)(\Sigma-2I-1)}{2F(2F+1)(2F+3)(2J-1)2J(2J+1)}\right)^{\frac{1}{2}}$	$\left(\frac{(\Sigma-1)\Sigma(\Sigma+1)(\Sigma-2I-2)(\Sigma-2I-1)(\Sigma-2I)}{(2F+1)(2F+2)(2F+3)(2J-1)2J(2J+1)}\right)^{\frac{1}{2}}$
$J-\frac{1}{2}$	$\frac{[2F(-3I-J+3F+\frac{1}{2})+3(\Sigma-2F-1)(\Sigma-2I-2)](\Sigma(\Sigma-2I-1))^{\frac{1}{2}}}{(2F(2F+1)(2F+3)(2J-1)(2J+1)(2J+2))^{\frac{1}{2}}}$	$-\left(\frac{3\Sigma(\Sigma+1)(\Sigma-2F-2)(\Sigma-2J)(\Sigma-2I-1)(\Sigma-2I)}{(2F+1)(2F+2)(2F+3)(2J-1)(2J+1)(2J+2)}\right)^{\frac{1}{2}}$
$J+\frac{1}{2}$	$\frac{-[2F(-3I+J+3F+\frac{1}{2})+3(\Sigma-2F)(\Sigma-2I-1)]((\Sigma-2F-1)(\Sigma-2J-1))^{\frac{1}{2}}}{(2F(2F+1)(2F+3)2J(2J+1)(2J+3))^{\frac{1}{2}}}$	$\left(\frac{3(\Sigma+1)(\Sigma-2F-2)(\Sigma-2F-1)(\Sigma-2J-1)(\Sigma-2J)(\Sigma-2I)}{(2F+1)(2F+2)(2F+3)2J(2J+1)(2J+3)}\right)^{\frac{1}{2}}$
$J+\frac{3}{2}$	$\left(\frac{3(\Sigma+1)(\Sigma-2F-1)(\Sigma-2F)(\Sigma-2J-2)(\Sigma-2J-1)(\Sigma-2I)}{2F(2F+1)(2F+3)(2J+1)(2J+2)(2J+3)}\right)^{\frac{1}{2}}$	$-\left(\frac{(\Sigma-2F-2)(\Sigma-2F-1)(\Sigma-2F)(\Sigma-2J-2)(\Sigma-2J-1)(\Sigma-2J)}{(2F+1)(2F+2)(2F+3)(2J+1)(2J+2)(2J+3)}\right)^{\frac{1}{2}}$

cients $c(F_1, F_2)$for two cases

(1) $I_1=1$; I_2, J arbitrary;
(2) $I_1=\frac{3}{2}$; I_2, J arbitrary.

The values are listed in Tables II and III. These should be sufficient for a large fraction of the molecules of practical interest.

We turn now to the calculation of the energy levels. In case both interactions, H_1 and H_2, are appreciable, the eigenfunctions are not given by either $\Psi_1(F, F_1)$ or $\Psi_2(F, F_2)$, but by an appropriate linear combination of either set. Let the correct wave function be given by the expansion

$$\Psi(F)=\sum_{F_1} a(F_1)\Psi_1(F, F_1). \quad (8)$$

The Hamiltonian equation $H\Psi=E\Psi$ becomes

$$\sum_{F_1} H_1(\mathbf{I}_1, \mathbf{J})a(F_1)\Psi_1(F, F_1) + \sum_{F_1} H_2(\mathbf{I}_2, \mathbf{J})a(F_1)\sum_{F_2} c(F_1, F_2)\Psi_2(F, F_2) = E\sum_{F_1} a(F_1)\Psi_1(F, F_1), \quad (9)$$

in which use has been made of (5). By use of the relations

$$H_1(\mathbf{I}_1, \mathbf{J})\Psi_1(F, F_1)=E_1(F_1)\Psi_1(F, F_1), \quad (10)$$
$$H_2(\mathbf{I}_2, \mathbf{J})\Psi_2(F, F_2)=E_2(F_2)\Psi_2(F, F_2), \quad (11)$$

followed by replacement of Ψ_2 by (6), Eq. (9) reduces to

$$(A(F_1, F_1)+E(F_1)-E)a(F_1) + \sum_{F_1'\neq F_1} A(F_1, F_1')a(F_1')=0, \quad (12)$$

where

$$A(F_1, F_1')=\sum_{F_2} c(F_1, F_2)c(F_1', F_2)E_2(F_2). \quad (13)$$

The energies are determined by setting the determinant of the coefficients of the $a(F_1)$ equal to zero. If the interaction H_2 may be treated as a small perturbation and there is no degeneracy, energy values to the first order are

$$E=E(F_1)+A(F_1, F_1). \quad (14)$$

In general, the complete secular determinant must be solved.

It will be noted that this method for setting up the secular determinant makes no use of the specific form of the operator for the quadrupole interaction. The method can be used for any Hamiltonian of the general form of Eq. (4).

Another method for setting up the secular determinant is to calculate the elements of the

determinant directly,

$$A(F_1, F_1') = \int \Psi_1(F, F_1') H_2(I_2, J) \Psi_1(F, F_1) d\tau,$$

making use of the form of $H_2(I_2, J)$. This method has recently been applied by Foley[12] to the case of a homonuclear diatomic molecule. It may be easier to use in some cases than the method described above, particularly if only first-order effects are desired. It is perhaps also the easiest method to use if more than two nuclei are involved in quadrupole interactions.

Because of the form of the interaction operator (Eq. (1)), the matrix elements of $(\mathbf{I}_2 \cdot \mathbf{J})$ and of $(\mathbf{I}_2 \cdot \mathbf{J})^2$ are required. Condon and Shortley (p. 71) give a general expression for the matrix elements of the scalar product of any two vectors **P** and **Q**. Use may be made of their results if we make the correlation

$$\begin{aligned} j_1 &= F_1, \quad j_2 = I_2, \\ J &= F, \\ P &= I_2, \quad Q = J. \end{aligned}$$

The non-vanishing matrix elements of $\mathbf{I}_2 \cdot \mathbf{J}$, as obtained from the expressions of Condon and Shortley, are

$$(F_1, I_2, F|\mathbf{I}_2 \cdot \mathbf{J}|F_1, I_2, F) = \tfrac{1}{2}(F_1|J|F_1)(F(F+1) - F_1(F_1+1) - I_2(I_2+1)),$$

$$(F_1, I_2, F|\mathbf{I}_2 \cdot \mathbf{J}|F_1-1, I_2, F) = -\tfrac{1}{2}(F_1|J|F_1-1)\{(F+F_1-I_2)(F+I_2-F_1+1)(F+F_1+I_2+1)(F_1+I_2-F)\}^{\frac{1}{2}}, \quad (16)$$

$$(F_1, I_2, F|\mathbf{I}_2 \cdot \mathbf{J}|F_1+1, I_2, F) = -\tfrac{1}{2}(F_1|J|F_1+1)\{(F+F_1-I_2+1)(F+I_2-F_1)(F+F_1+I_2+2)(F_1+I_2-F+1)\}^{\frac{1}{2}},$$

in which

$$(F_1|J|F_1) = \frac{J(J+1) - I_1(I_1+1) + F_1(F_1+1)}{2F_1(F_1+1)},$$

$$(F_1|J|F_1-1) = \left\{\frac{(F_1-J+I_1)(F_1+J-I_1)(F_1+J+I_1+1)(J+I_1-F_1+1)}{4F_1^2(2F_1-1)(2F_1+1)}\right\}^{\frac{1}{2}}, \quad (17)$$

$$(F_1|J|F_1+1) = \left\{\frac{(F_1-J+I_1+1)(F_1+J-I_1+1)(F_1+J+I_1+2)(J+I_1-F_1)}{4(F_1+1)^2(2F_1+1)(2F_1+3)}\right\}^{\frac{1}{2}}.$$

The matrix for $(\mathbf{I}_2 \cdot \mathbf{J})^2$ can be obtained by squaring that for $\mathbf{I}_2 \cdot \mathbf{J}$. The general expressions are rather complicated, but it might not be too difficult to carry out the numerical calculations for a particular case.

The methods described above, together with the tables, allow a fairly convenient determination of energy levels, although in some cases considerable computation is still required.

INTENSITIES

In addition to energy levels, intensities are generally required. Let us assume that the intensity of a molecular line can be calculated if no quadrupole effects are present, and call its intensity A. If the quadrupole interaction of one nucleus splits this line, relative intensities of each of the hyperfine components may be found from tables in Condon and Shortley,[8] as pointed out above. The intensity of each component is then

$$\frac{AS(I_1J|F_1|I_1J'F_1')}{\sum_{F_1}\sum_{F_1'} S(I_1JF_1|I_1J'F_1')}, \quad (33)$$

where $S(I_1JF_1|I_1J'F_1')$ can be obtained from the tables. If a second nucleus produces a quadrupole interaction, but its coupling is small compared with the coupling of the first nucleus, the tables may be again applied to find intensities of all components of the still more finely split hyperfine structure. They are proportional to

[12] H. M. Foley, Phys. Rev. **71**, 751 (1947).

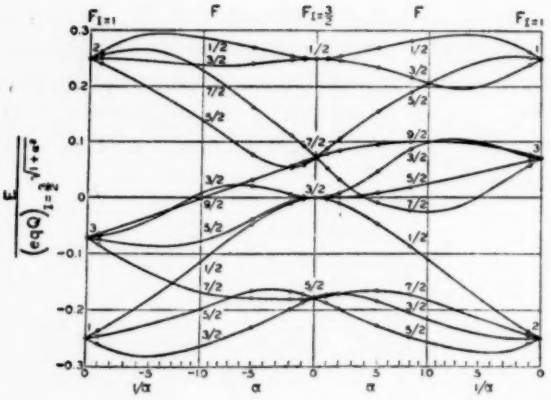

FIG. 1. Energies E resulting from quadrupole coupling of two nuclei of spin 1 and $\frac{3}{2}$, when $J=2$. Parameter $\alpha=(eqQ)_{I=1}/(eqQ)_{I=3/2}$. Minus sign should be placed in front of eqQ.

$S(I_1JF_1|I_1J'F_1')S(I_2F_1F|I_2F_1'F')$. If coupling of the two nuclei is not widely different, then true intensities cannot be found so directly, but a fair approximation to the intensities may be obtained by interpolating between the two extreme cases when coupling of the first nucleus is large compared to coupling of the second nucleus, and when it is small. Intensities for these extreme cases are thus proportional to

$$S(I_1JF_1|I_1J'F_1')S(I_2F_1F|I_2F_1'F')$$

and

$$S(I_2JF_2|I_2J'F_2')S(I_1F_2F|I_1F_2'F'),$$

respectively.

Exact intensities may, of course, be obtained in cases of intermediate coupling by making use of the energy values obtained by the method described above and solving equations of the type (12) for the $a(F_1)$. Relative intensity for a transition from state i to state j may then be written as

$$|\sum_{F_1'}\sum_{F_1} a_i(F_1)a_j(F_1')\times S^{\frac{1}{2}}(I_1JF_1|I_1J'F_1')S^{\frac{1}{2}}(I_2F_1F|I_2F_1'F')|^2.$$

Careful attention must be paid to the phases (see Condon and Shortley,[8] p. 277). This procedure would, however, be tedious and could in most cases be replaced by the more rapid method of the preceding paragraph.

EXAMPLES

As an illustration of the above theory for quadrupole coupling of two nuclei, the energy levels for the case $J=2$, $I_1=\frac{3}{2}$, $I_2=1$ are plotted in Fig. 1 as a function of the ratio of the quadrupole couplings of the two nuclei. This ratio,

$$\alpha=\left\{eQ\frac{\partial^2V}{\partial z^2}\right\}_{I=1}\Big/\left\{eQ\frac{\partial^2V}{\partial z^2}\right\}_{I=3/2}=(eqQ)_{I=1}/(eqQ)_{I=3/2},$$

is plotted along the axis of abscissae, the function $(1+\alpha)/(1+\alpha^2)^{\frac{1}{2}}$ being plotted linearly for positive α and $(1-\alpha)/(1+\alpha^2)^{\frac{1}{2}}$ linearly for negative α. Energy is plotted along the ordinate axis, $E/[(-eqQ)_{I=3/2}(1+\alpha^2)^{\frac{1}{2}}]$ being plotted linearly. Such a plot produces smooth curves and allows α a range from $-\infty$ to $+\infty$. Values for $1/\alpha$ rather than α are marked off in the region where $|\alpha|>1$. The curves are very similar to those for electronic energy levels showing coupling type ranging from pure LS to pure JJ. Points at which energy values were computed are shown by small circles; the solid curves were drawn to pass smoothly through all computed points. In the center of the figure the energy levels converge to those that would be obtained for the coupling of a single nucleus of spin $\frac{3}{2}$ to a rotational momentum 2, giving the various values of the sum of these two indicated by $F_{I=3/2}$. On the two edges, the levels converge to the proper values for positive and negative coupling of the nucleus of spin 1 with the rotational momentum

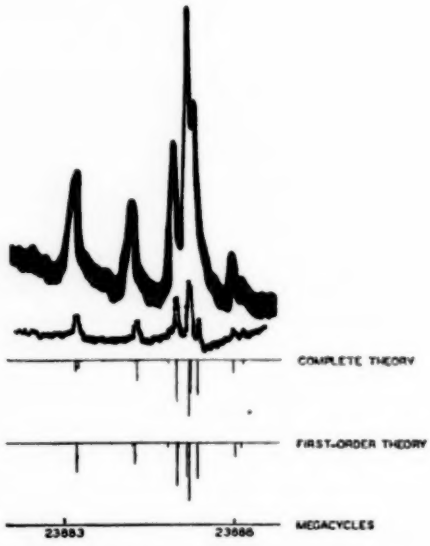

FIG. 2. Comparison of portion of observed spectrum of $Cl^{35}CN$ with first-order and complete theories.

2 to give a sum F_{I-1}. Between these three points, the levels split and are designated by the total angular-momentum quantum number F resulting from the sum of J and the spins of both nuclei. It may be seen that the first-order approximation to the complete theory, giving the initial slope of each energy level, is fairly accurate for $|\alpha|<0.1$ or $|1/\alpha|<0.1$, but that in intermediate ranges the first-order approximation gives little indication of the behavior of the energy levels.

Rotational transitions for BrCN ($J=2\rightarrow3$) and ClCN ($J=1\rightarrow2$) have been observed in the microwave region[6] and show in each case quadrupole effects resulting from two nuclei, N^{14} and the halogen. The above theory is found to fit the observed spectra well, with a value for $\alpha=(eqQ)_{N^{14}}/(eqQ)_{\text{Halogen}}$ about equal to 0.005 for BrCN and 0.05 for ClCN. In these cases the first-order approximation to the theory is rather good, although in the case of ClCN a deviation from the first-order theory can be seen which is explained by the complete theory. The rotational line $J=1\rightarrow2$ for ClCN lies at about 23,885 megacycles, and the line is split by the Cl quadrupole into a number of components with separations between 2 and 30 megacycles. Each of these lines is further split into several components separated by one megacycle or less because of the N^{14} quadrupole. Figure 2 shows the comparison between theoretically expected splitting and plots of a portion of the $Cl^{35}CN$ spectrum as produced on the oscilloscope of the detecting apparatus. The upper experimental spectrum is at a pressure of about 10^{-3} mm Hg, while the lower one is at a somewhat lower pressure. In the latter case this produced narrower lines, but with considerably reduced intensity because of saturation effects.[13] As may be seen, the first-order effects account for the main features of the spectrum, but deviations of about 50 kilocycles from the first-order theory can be observed which are explained by the complete theory. These deviations are best seen in the separations of the three strong lines in the center of the spectrum, and in the distance between the two weak lines at the high frequency end of the spectrum.

Experimental details and further experimental results will be presented in a later paper.

[13] C. H. Townes, Phys. Rev. **70**, 665 (1946).

A Determination of the $S^{32}(n,p)P^{32}$ Cross Section for Neutrons Having Energies of 1.6 to 5.8 Mev*

E. D. KLEMA** AND A. O. HANSON**
University of California, Los Alamos Scientific Laboratory, Santa Fe, New Mexico

(Received October 6, 1947)

Sulfur was irradiated with known fluxes of monoenergetic neutrons having energies of 1.6 to 5.8 Mev. The formation of P^{32} by the $S^{32}(n,p)P^{32}$ reaction was detected by means of the P^{32} beta-activity. The cross section for the reaction at the lower neutron energies has the same form as the penetrability of the protons from the reaction through the Coulomb barrier. At the higher energies the cross section for the reaction reaches an approximately constant value of 0.3×10^{-24} cm².

1. INTRODUCTION

THE production of radioactive phosphorus by the bombardment of fast neutrons on sulfur was reported by Fermi and his collaborators in 1934.[1] They reported a moderately strong activity having a half-life of about 13 days which was produced by neutrons from a radon-beryllium source.

Since that time a number of other workers have studied the production of P^{32} by other means[2] and also have measured the half-life and beta-spectrum with considerable accuracy. These studies indicate that the half-life is 14.295 days,[3] that the beta-spectrum has an upper limit of about 1.72 Mev,[4] and that there is no appreciable number of γ-rays accompanying the beta-decay.[5]

It should be pointed out that there are at least two reactions which occur on bombardment by neutrons of energies considered here. These are

$$(1)\qquad {}_{16}S^{32}+{}_0n^1\rightarrow{}_{15}P^{32}+{}_1H^1+Q_1;$$
$${}_{15}P^{32}\rightarrow{}_{16}S^{32}+\beta^-+1.72\text{ Mev}$$
$$(2)\qquad {}_{16}S^{32}+{}_0n^1\rightarrow{}_{14}Si^{29}+{}_2He^4+Q_2.$$

These reactions were studied by Huber,[6] using 2.76-Mev neutrons incident upon an ionization chamber filled with SO_2. From the heights of the pulses in the chamber he deduced values of $Q_1=-0.93\pm0.1$ Mev and $Q_2=1.2\pm0.1$ Mev.

The end-point energy of the β-spectrum (1.72 Mev) leads to a value of $Q_1=-0.97$ Mev or a threshold energy for the neutrons of 1.00 Mev.

The present work is concerned with the determination of the yield of reaction (1) when sulfur is bombarded by known fluxes of monoenergetic neutrons having energies of 1.6 to 5.8 Mev.

2. EXPERIMENTAL METHOD

A. General Arrangement

Although different sources of neutrons were used in the present work, the arrangement of the sulfur samples and neutron monitor with respect to the sources remained about the same and is shown in Fig. 1.

The sublimed elemental sulfur was melted and cast into disks 2-in. in diameter and $\frac{1}{4}$-in. thick. Two such disks (S), enclosed in spun cadmium covers, were placed on the two electrodes of an ionization chamber, as shown in the figure. A metal foil containing a thin deposit of uranium, also 2 in. in diameter, was placed inside the ionization chamber on the high voltage electrode.

* This document is based on work performed at Los Alamos Scientific Laboratory of the University of California under Government Contract No. W-7405-eng-36, and the information contained therein will appear in Division V of the National Nuclear Energy Series (Manhattan Project Technical Section) as part of the contribution of the Los Alamos Laboratory.

** Now at the University of Illinois.

[1] E. Fermi, E. Amaldi, O. D'Agostino, F. Rasetti, and E. Segrè, Proc. Roy. Soc. **A146**, 483 (1934); E. Amaldi, O. D'Agostino, E. Fermi, B. Pontecorvo, F. Rasetti, and E. Segrè, Proc. Roy. Soc. **A149**, 522 (1935).

[2] H. W. Newson, Phys. Rev. **51**, 624 (1937); H. Fahlenbrach, Zeits. f. Physik **96**, 503 (1935).

[3] N. B. Cacciapuoti, Nuovo Cimento **15**, 213 (1938).

[4] E. M. Lyman, Phys. Rev. **51**, 1 (1937); J. L. Lawson, Phys. Rev. **56**, 131 (1939); C. M. Witcher, Phys. Rev. **60**, 32 (1941); Kai Siegbahn, Phys. Rev. **70**, 127 (1946).

[5] F. N. D. Kurie, J. R. Richardson, and H. C. Paxton, Phys. Rev. **49**, 368 (1936); H. W. Newson, see reference 2.

[6] P. Huber, Helv. Phys. Acta **14**, 163 (1941).

The ionization chamber was connected to an amplifier and recorder system which served to measure the total number of fissions which occurred in the uranium foil during a given irradiation period. This number of fissions occurring in the uranium foil of known mass was then used to determine the flux of neutrons which passed through the ionization chamber.

B. Neutron Sources

Neutrons of 1.63- and 1.83-Mev energy were obtained from the $Li^7(p,n)Be^7$ reaction using protons accelerated by the Wisconsin electrostatic generator.[7] The protons were incident upon a thin film of lithium metal evaporated on a tantalum backing plate. The spread in energy of the neutrons was due primarily to the thickness of the lithium target, which was sufficient to reduce the energy of the protons by about 0.100 Mev. The uncertainty in the neutron energy was therefore estimated as ± 0.050 Mev.

The points at 2.5 and 2.9 Mev were obtained with neutrons from the $d-d$ reaction, using deuterons accelerated by the Illinois Cockcroft-Walton set.[8] The deuterons were incident upon a thick heavy-ice target with an energy of 200 kev. The point at 2.5 Mev was obtained with the samples at right angles to the direction of the deuteron beam, while the point at 2.9 Mev was obtained in the forward direction. The effective spread in energy for these points was estimated to be approximately ± 0.3 Mev.

The neutrons of 3.4, 4.3, 4.6, and 5.8 Mev energy were obtained from the $d-d$ reaction using the Wisconsin machine for accelerating the deuterons. The deuterons in this case were made to pass through a thin nickel foil into a gas cell containing deuterium. The spread in energy caused by target thickness and other causes was estimated to be approximately ± 0.15 Mev.

C. Relative Cross Sections

After irradiation, the sulfur was remelted and cast into cylinders 4.5 in. long with a wall thickness of 2.5 mm and an inner diameter of $\frac{7}{8}$ in. These cylinders, protected by being cast inside of brass sleeves, fitted snugly around a thin-walled aluminum Geiger counter which had a length of 7 in. and a uniform wall thickness of 0.007 in. The counting rate caused by a small beta-active sample moved along the length of the counter was independent of the position of the sample for the 4.5-in. length covered by the sulfur cylinders.

The irradiated sulfur samples were counted in this geometry, and the initial activity of the sulfur in counts/min./g was determined from the observed counting rates and the known time after the neutron irradiation. These initial activities, divided by the known flux of neutrons through the various samples, are proportional to the cross section of the $S^{32}(n,p)P^{32}$ reaction. The initial activities, after subtraction of natural background counts, are listed in Table I.

Since the measurements extended over a period of several months, the sensitivity of the Geiger counter was checked frequently by means of a short cylinder of uranium glass which fitted snugly over the counter in a standard position. The counting rate attributable to the uranium glass was found to remain constant to within 1 percent during these measurements, although the threshold voltage rose slightly and the length of the plateau decreased as the counter aged.

The initial activity of the sample irradiated with 4.3-Mev neutrons was quite high, and it was followed for about 30 days. The activity was found to decay with a half-life of 14.35 ± 0.05 days, which is to be compared with the value of 14.295 days obtained by Cacciapuoti.[9]

D. Efficiency of Counting

In order to obtain an absolute value for the magnitude of the $S^{32}(n,p)P^{32}$ cross section, it is

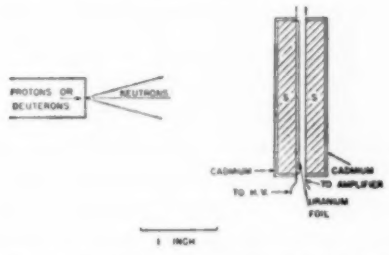

FIG. 1. Experimental arrangement. The sulfur disks, S, were covered with 30-mil cadmium.

[7] R. G. Herb, C. M. Turner, C. M. Hudson, and R. E. Warren, Phys. Rev. **58**, 579 (1940).

[8] L. J. Haworth, J. H. Manley, and E. A. Luebke, Rev. Sci. Inst. **12**, 591 (1941).

[9] N. B. Cacciapuoti, see reference 3.

TABLE I. Summary of results of measurement.

Source	Bombarding energy in Mev	E_n average neutron energy in Mev	ΔE_n in Mev	Approx. time of bombardment in hours	ϕ neutrons/ $cm^2 \times 10^8$	C counts/* minute/ gram of sulfur	$\sigma_{n,p}$ $\times 10^{-25}$ cm^2
Li(p,n)	3.36	1.63	±0.05	9	32.2	1.56	0.0131
	3.56 (0°)	1.83	±0.05	7	8.48	1.61	0.0509
$d-d$	0.2	2.5	±0.3	8	4.42	12.9	0.784
	0.2 (90°)						
	0.2 (0°)	2.9	±0.3	8	9.42	54.4	1.55
$d-d$	1.24	3.4	±0.07	2	0.732	5.56	2.04
	1.86	4.3	±0.11	8.1	9.66	125.0	3.49
	2.13	4.6	±0.15	2	2.16	23.1	2.88
	3.09 (0°)	5.8	±0.17	2	2.42	27.0	3.00

* Average thick sample contained 44±2 grams of sulfur. Average background count on counter about 65 counts/minute.

necessary to know the efficiency of counting the beta-rays from the P^{32} in the counting geometry used. This counting efficiency was determined in the following way. A small cylindrical sample of finely powdered sulfur was given an intense neutron irradiation by placing it in the center of the small reactor (waterboiler) at Los Alamos for a fraction of a minute. The sample was then thoroughly mixed and part of it was weighed accurately and mixed with a known amount of unirradiated sulfur. This mixture was then melted and cast into a cylindrical sample of the same dimensions as those used in the previous work.

Another part of the sulfur irradiated in the small reactor was made up into a thin sample by dusting a small amount of the powder on a cylinder made of a single layer of Scotch Tape with its sticky side out. Another layer of Scotch Tape was put over the cylinder and served to protect the sulfur. The sample was about 2 in. long, and it fitted snugly around the counter tube. The Scotch Tape used had a mass of about 9 mg/cm². The weight of sulfur in the sample was obtained by weighing the cylinder of Scotch Tape before and after the sulfur had been deposited. Blank checks with similar Scotch Tape cylinders showed that the Scotch Tape lost a small amount of weight because of drying, but this effect amounted to only 1 percent of the weight of the sulfur and was easily taken into account.

The ratio of the counting rates/g of activated sulfur was determined for a number of sets of thin and thick diluted samples. The average of these results gave a value of 0.214±0.03 for the ratio of the counting rate/g of a thick sample to that of a thin one. To make certain that the activity induced in the sulfur by the fission neutrons from the small reactor was the same as that produced by the other neutron sources, the activity of one of the samples was followed for a period of two weeks and was found to have the correct half-life.

In order to obtain the efficiency for counting the thin irradiated sulfur samples in the geometry used, an attempt was made to estimate the total number of beta-particles emitted by a very active thin sample of P^{32}. This sample was deposited on a 1-mil aluminum foil in an area about 2 mm in diameter. It was then counted by placing it at a distance of 2 cm from a circular aperture 1 cm in diameter in a 0.16-cm lead sheet, obtaining the counting rate in a cylindrical Geiger counter with aluminum walls having a thickness of 4.5 mil (31 mg/cm²).

This counting rate, after subtracting the appropriate background and correcting for the absorption in the counter wall (20 percent), was used as the total number of beta-particles emitted in the solid angle defined by the lead aperture. The same sample was then counted through the same amount of absorber and in the same geometry used for the thin irradiated

sulfur samples. The net counting rate in this case, divided by the total number of beta-particles emitted by the sample as determined by the previous experiment, gave a value of 0.29 for the efficiency of counting the thin irradiated sulfur sample through 57 mg/cm² of absorber. This value for the efficiency is about 15 percent lower than that obtained simply by correcting for the exponential absorption obtained through various thicknesses of absorber in the same geometry and assuming that the counting rate extrapolated to zero absorber thickness corresponds to ½ of all the beta-particles emitted.

By the use of the value of 0.29 for the efficiency of counting the thin sulfur samples, the efficiency of counting the thick samples is 0.214×0.29 or 0.062 count/disintegration. The uncertainty in this efficiency is difficult to estimate, but it may be of the order of 15 percent and is therefore the largest source of error in the determination of the absolute values obtained for the cross section of the (n,p) reaction in sulfur.

RESULTS

The data previously discussed are shown in Table I. The cross section for the reaction can be expressed by the following relation:

$$\sigma(n,p)=C/EN_s\lambda\phi=2.69\times10^{-17}\ C/\phi,$$

where C is the initial counting rate of the thick sample in counts/min./g; ϕ is the number of neutrons/cm² which passed through the sulfur during the irradiation period; E is the efficiency of counting (0.062); N_s is the number of S^{32} atoms/g of sulfur (1.79×10^{22}); λ is the fraction of the P^{32} atoms decaying/min. (3.35×10^{-5}).

The values of the cross section are shown in Fig. 2. Although these values do not lie nicely on a smooth curve, it appears that the cross section at the higher energies remains at a fairly constant value of 0.3×10^{-24} cm².

3. DISCUSSION

It might be expected that the (n,p) cross section for S^{32} would show resonance effects as a function of neutron energy. Such resonances have been observed in the capture of fast neutrons by N^{14}.[10] However, an examination of the excitation function (Fig. 2) indicates that the curve is smooth within the limits of resolution obtained in this experiment; and it would appear that the penetration of the Coulomb barrier by the emitted proton is the predominant factor determining the cross section.

In order to obtain an estimate of the cross section expected for the reaction, it might be assumed that the cross section for the formation of the intermediate S^{33} nucleus can be represented by

$$\sigma_n{}^I=S\pi\lambda^2\xi,$$

where S is a statistical factor of the order of $2l_n+1$, l_n being the effective angular momenta of the incoming neutrons giving rise to the intermediate nucleus; λ is the wave-length of the neutron divided by 2π; ξ is the sticking probability, which in this case includes the penetrability (P_n) of the incoming neutrons, and which will be considered to be constant.

If the intermediate nucleus can disintegrate either by proton or neutron emission, the fraction of the intermediate nuclei which disintegrate by proton emission is given by P_p/P_n+P_p, where P_p is the penetrability of the Coulomb barrier for

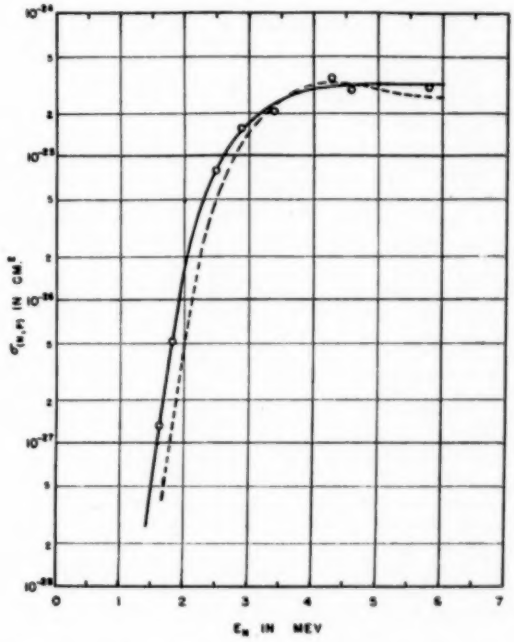

FIG. 2. Solid curve: observed cross section for the $S^{32}(n,p)P^{32}$ reaction as a function of the energy of the incident neutrons. Broken curve: cross section for the $S^{32}(n,p)P^{32}$ reaction calculated from Eq. (1).

[10] H. H. Barschall and M. E. Battat, Phys. Rev. **70**, 245 (1946).

the emitted protons.[11] P_n is the effective penetrability of the angular-momentum barrier for the emitted neutrons.

In the present discussion it is assumed that there is no distinction between the emission of a neutron or a proton except for the influence of the Coulomb barrier. P_n will be taken as unity, since it is not known which of the various angular momenta may contribute to the reaction. This approximation has very little effect on the shape of the cross-section curve, since P_n for $l_n \leq 2$ varies only slightly as compared to P_p in the energy range considered here. The expression for the (n,p) cross section then becomes

$$\sigma(n,p) = S\pi\lambda^2\xi \cdot \frac{P_p}{1+P_p}. \quad (1)$$

The curve calculated on this basis is shown as the broken line of Fig. 2. It can be seen that the calculated curve represents the observed data quite well except for a shift of the curve toward higher energy by about 0.2 Mev. One could obtain better agreement between the observed and calculated curves by using a larger value for the nuclear radius or by increasing the energy available to the emitted proton by about 0.2 Mev, since both of these quantities enter directly into the calculation of P_p. It is difficult to explain so large a shift at the lower energies by the uncertainty in the nuclear radius, since a 10 percent change in the radius corresponds to a shift of only 0.05 Mev at these lower energies (i.e., $E_n \sim 1.5$ Mev, $E_p \sim 0.5$ Mev). It is just possible, however, that a shift of 0.2 Mev might be accounted for by errors in the absolute values of the proton accelerator voltage,[12] the effective target thickness, and the value of Q_1.

It might be of interest to examine the value of $S\xi$ needed to obtain numerical agreement with the cross section found experimentally. If we use the observed value of 0.3×10^{-24} cm^2 at 5 Mev, we find that $S\xi$ must be assigned a value of 4.6 which might seem to indicate that $S \geq 5$. On the simplified assumption that $S = 2l_n + 1$, this value would indicate that neutrons of angular momentum $l_n = 2$ would be necessary to explain this large cross section.

Although the above description gives a fairly good agreement with the data, it is not the only possible interpretation. Since the shape of the curve is primarily determined by the proton penetration factor, any other description giving the correct magnitude of the cross section at the high energy points would be equally permissible. Another simple method of getting a cross section of 0.3×10^{-24} cm^2 at the high energy points is to assume that the cross section for the formation of the compound S^{33} nucleus is just the geometrical cross section (πR^2) of the sulfur nucleus, which may be taken as 10^{-24} cm^2, and to assume that this intermediate nucleus may disintegrate by the emission of a neutron, a proton, or an alpha-particle with equal probability, since each of these particles has a penetrability close to unity at the higher energies. Previous measurements of the effective cross section for the (n,α) reaction seem to indicate a very high cross section for this process (0.065×10^{-24} cm^2 for 2.76-Mev neutrons).[13]

An unambiguous interpretation of these reactions must, therefore, await further studies giving more information about the relative yields and possibly the angular distributions of the particles emitted.

We wish to express our appreciation to Professors E. J. Konopinski and S. M. Dancoff for valuable discussions on the interpretation of these results.

The neutron irradiations and the preliminary determination of the cross section were made at Los Alamos. The work on the redetermination of the efficiency of counting the thin P^{32} samples, using the method described above, was done at the University of Illinois.

[11] The proton penetrabilities were calculated by means of Eq. (600) of H. A. Bethe, Rev. Mod. Phys. 9, 166 (1937) for protons having zero angular momentum. A nuclear radius of 5.6×10^{-13} cm was used, in accordance with the experiments of Sherr (R. Sherr, Phys. Rev. 68, 240 (1945)).

[12] E_n from the Li(p,n) reaction was calculated on the basis that the threshold of the reaction is at 1.86 Mev (A. O. Hanson and D. L. Benedict, Phys. Rev. 65, 33 (1944)).

[13] P. Huber, see reference 6.

Delayed Neutrons from Fission of U^{235} *

D. J. HUGHES, J. DABBS, A. CAHN, AND D. HALL**
Argonne National Laboratory, Chicago, Illinois

(Received October 3, 1947)

The periods, yields and energies of the delayed neutrons from fission of U^{235} have been measured with a pneumatic transfer apparatus ("rabbit") at the heavy water pile of the Argonne Laboratory. The following periods account for the saturated decay curve of delayed neutrons for times longer than 0.02 sec. after irradiation ceases:

Half-life	Energy	Yield (relative to total neutron emission)
55.6 sec.	250 kv	0.025%
22.0	560	0.166
4.51	430	0.213
1.52	620	0.241
0.43	420	0.085
0.05		0.025
		Total yield 0.755%

The application of the delayed neutron data to the constants of pile kinetics is discussed and the value of the inhour (the pile reactivity unit) is calculated.

I. INTRODUCTION

ABOUT one percent of the neutrons produced by the fission of uranium are not emitted instantaneously but are "delayed" several seconds on the average. Before the beginning of the Manhattan Project, a small amount of information had already been published on the subject of these delayed neutrons. Roberts, Meyer and Wang[1] had observed the emission of neutrons from uranium after fission in the uranium had ceased. Later Meyer and Wang[2] showed that these "delayed" neutrons were not simply the result of $(\gamma-n)$ reactions of γ's from the fission products but probably came directly from the fission products in some way. The delayed neutrons were observed to decay with a period of about 12 sec. Booth, Dunning and Slack[3] found two periods for the delayed neutrons of half-life 45 and 10–15 sec., and an initial intensity of roughly one delayed neutron per 60 fissions. The delayed neutrons have been studied intensively on the Manhattan Project because of their very important function in aiding pile stability. In fact, even with reactivities of several hundred "inhours" (see Section III G), a pile is above critical because of the contribution of delayed neutrons, and its period is of the order of seconds rather than tenths of a second as it would be if all the neutrons were emitted instantaneously.

Early studies both with the pile and cyclotron showed that the delayed neutrons were not emitted according to a single radioactive period but according to several periods ranging up to about one minute. The most accurate work in identifying the periods at the time the present experiments were begun was that of Snell, Nedzel and Ibser[4] using the cyclotron and of Redman and Saxon,[5] using the graphite Argonne pile. The results of the two groups of experiments agreed rather well in demonstrating the existence of delayed neutrons of half life about 55, 23 and 4.5 sec, but showed some disagreement on several shorter periods. Fermi[6] had estimated the

* This document is based on work performed under Contract No. W-7401-eng-37 for the Atomic Energy Project, and the information contained therein will appear in Division IV of the *National Nuclear Energy Series* (Manhattan Project Technical Section) as part of the contribution of the Argonne National Laboratory. It was submitted for declassification on April 25, 1947.

** J. Dabbs, Clinton Laboratories; A. Cahn, Bureau of Standards, Washington, D. C.; D. Hall, Los Alamos Laboratory.

[1] R. B. Roberts, R. C. Meyer, and P. Wang, Phys. Rev. **55**, 510 (1939).

[2] R. B. Roberts, L. R. Hafstad, R. C. Meyer, and P. Wang, Phys. Rev. **55**, 664 (1939).

[3] E. T. Booth, J. R. Dunning, and F. G. Slack, Phys. Rev. **55**, 876 (1939).

[4] Smyth Report, Rev. Mod. Phys. **17**, 459 (1945).

[5] Unpublished Manhattan Project Work (1943).

[6] Unpublished Manhattan Project Work (1943).

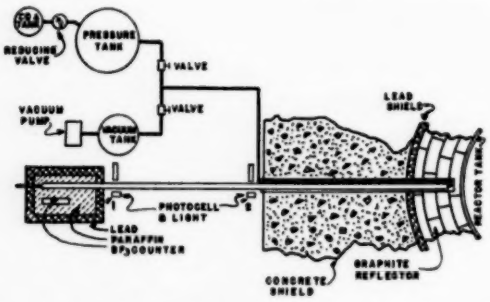

FIG. 1. The rapid transfer tube ("rabbit") and associated apparatus.

energy of the delayed neutrons by measuring their range in the graphite standard pile, and obtained 640 kv as an "average" energy which emphasized greatly the 23 sec. period.

Even though the knowledge of the delayed neutrons from U^{235} was thus in a rather satisfactory state, it was decided to extend the measurements, utilizing the Argonne heavy water pile. The decision was made on the following basis: (1) The available flux was higher than had been used in the previous work; (2) The recently constructed rapid transfer apparatus at the pile would simplify investigation of the region of short periods where most doubt existed; (3) A careful analysis of the periods and yields of U^{235} would serve as a standard of comparison for future work planned on the other fissionable isotopes.

II. APPARATUS

In order to analyze the delayed neutron periods, it is necessary to transfer a uranium sample from a region of high flux to a standard position near a well-shielded neutron counter in a fraction of a second, then to record the rapidly changing counting rate as a function of time in as detailed a manner as possible. The "rabbit" and associated apparatus fulfills these conditions in quite a satisfactory manner.

The rabbit is an electronically controlled pneumatic transfer device. It moves a sample which is to be irradiated to a position near the reactor tank of the pile and out again to a counter as rapidly as is practicable, using CO_2 as an operating medium. The device (Fig. 1) consists of the following pieces of equipment: CO_2 tank with reducing valve; pressure reservoir; two soloneoid-operated valves; vacuum reservoir; vacuum pump; a relay circuit to open and close the valves; two photo-cell units with appropriate circuits; BF_3 counter and circuits; electrocardiograph for recording counting rates, and the necessary piping including a properly shielded transfer tube.

The transfer tube is of aluminum, 3.5 cm inside diameter and 7 meters long, about half the length being enclosed in an 8 in. square plug which fits into the concrete shield of the pile. The plug is of paraffin and lead shot, and the transfer tube is bent from one corner of the plug to the diagonally opposite corner to prevent radiation leakage. The pressure tank is of about 150 liter capacity, while the vacuum tank is about 25 liters and is evacuated by a Megavac pump. All piping losses have been reduced as far is practicable in order to speed gas flow. The valves are pilot piston operated; i.e., the pressure differential does the actual opening and closing. The relay control circuit is designed in such a way that the valves may be opened at the touch of a button and close automatically at a time variable up to about one second later.

The cartridges containing the uranium samples (several grams of enriched oxide) are of lusteroid and fit very loosely in the transfer tube. Friction losses are small as are pressure losses past the cartridge. The cartridges are relatively light, of the order of 20 gm when full. The photo-cell units which are used to time the irradiation operate on the dark pulse caused when a light beam is interrupted by the passage of the sample. Holes cut in the pipe and covered with sheet plastic are used for the light beam. The sample, after irradiation, is blown out of the pile and comes to rest at the end of the tube where it is held in a fixed position by a catch. The end of the tube is buried in a paraffin block and a BF_3 counter is located in the paraffin at a variable distance from the sample. The delayed neutrons emitted by the sample are slowed in the paraffin and detected by the counter. The shielding of the pile itself and that around the paraffin geometry keeps the background down to about 12 counts per minute. The BF_3 counter is connected to a preamplifier located in the paraffin block, then to a fast amplifier and a scaler (scale of 512). The counter is operated at a voltage several hundred volts less than the usual operating potential (about 1600 v instead of 1850 v). It was found

during this work that at the usual voltage the counter would respond to γ-rays, when suddenly subjected to them, for a period of some seconds after which it would cease to count the γ's. Such an effect would interfere seriously with recording the delayed neutrons, of course, but fortunately disappeared at the lower voltage.

The scaler pulses are recorded on an electrocardiograph tape. The electrocardiograph is a standard portable model, consisting of a light source, an Eindhoven string galvanometer (current sensitive), an optical system and a slit camera. Light passes through the galvanometer, and an image of the string (a gold plated quartz fiber), magnified 500×, is focused on the slit, past which the sensitized paper travels at a constant rate of 2.5 cm/sec. The paper comes in rolls of 50-ft. length, 25 ft. of which are usually used in making a run (about $44\frac{1}{4}$ minutes running time). The paper has crosswise lines put on by a rotating marker every 25th of a second, and from these markings it is possible to interpolate to about 0.004 sec. in time. The following marks are applied to the paper: pulses when opening and closing the valves, when the cartridge passes each photo-cell, and the scaler kicks. The scaler pulse is a square wave form which is produced by the recorder driver tube output, properly attenuated. The galvanometer sensitivity is about 0.3μ amp. per cm (after magnification) and its period is 0.0015 sec. It can handle counting rates up to 2.5×10^6 cts/min. (40,000 c.p.s.) with a scale of 512. Figure 2 shows the initial portion of a typical tape containing the timing marks mentioned above.

It is desirable to use very high counting rates in order to get statistical accuracy for the short periods. The limitation, of course, lies in the "dead time" of the apparatus associated with the BF_3 counter, the counter itself having a negligible dead time. The dead time of the apparatus was made as low as possible by using a fast scaler and amplifier and mounting a preamplifier with the counter in the paraffin block. The dead time was measured by recording the gross decay curve of the delayed neutrons on a tape at a pile power such that the dead time correction would be small, then again at a power about ten times as great. The ratio of the observed counting rates for the two runs was plotted as a function of time. The ratio, which would, of course, be a constant (10) if there were no dead time correction, was less than 10 at the initial part of the curve and increased to 10 when the rates became low. The ratio actually showed a linear decrease with counting rate (Fig. 3), as is to be expected, and the rate of decrease (slope

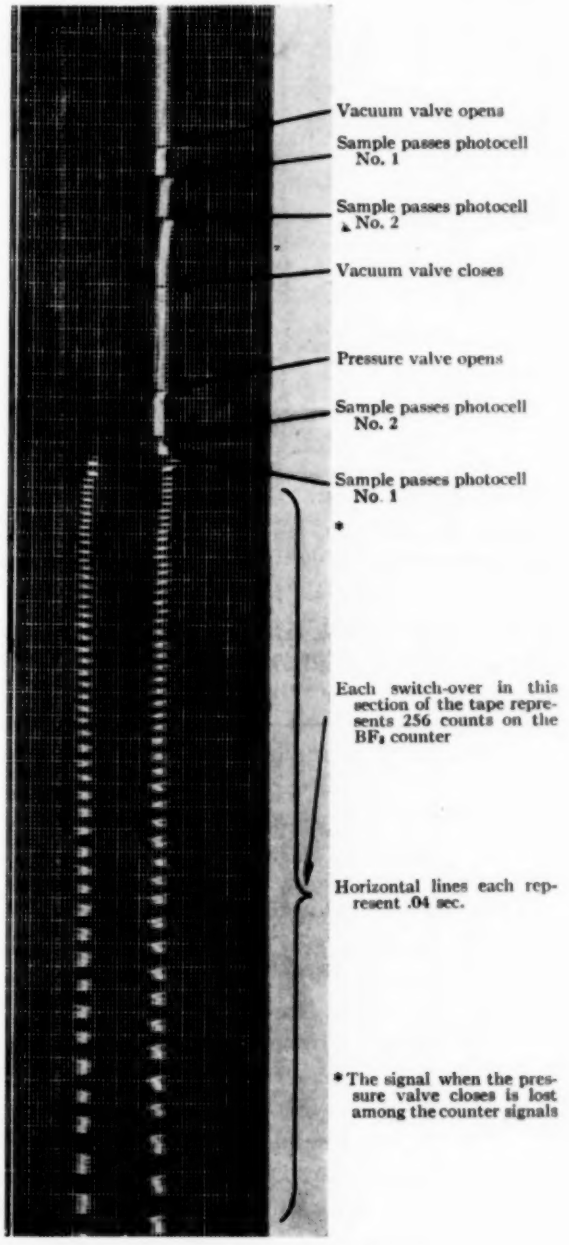
Vacuum valve opens
Sample passes photocell No. 1
Sample passes photocell No. 2
Vacuum valve closes
Pressure valve opens
Sample passes photocell No. 2
Sample passes photocell No. 1
*
Each switch-over in this section of the tape represents 256 counts on the BF_3 counter
Horizontal lines each represent .04 sec.
* The signal when the pressure valve closes is lost among the counter signals

FIG. 2. Initial portion of a typical electrocardiograph tape showing timing marks and the beginning of the delayed neutron decay curve.

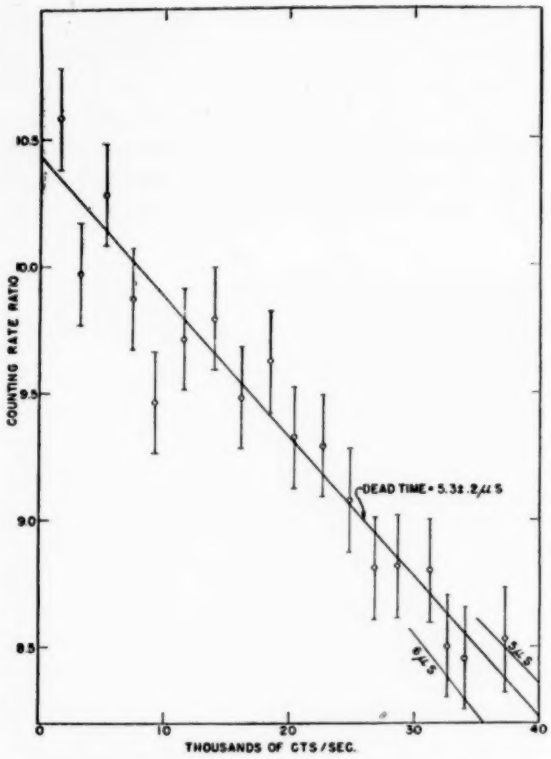

FIG. 3. Counting rate ratio for a high and low power run as a function of counting rate from which the dead time of the counting circuits is determined.

of the curve in Fig. 3) gives the dead time as 5.3 ± 0.2 microseconds. This value of the dead time means that the correction will become 10 percent at a rate of 19,000 c.p.s.

By assuming constant accelerations and using the length of time between photo-cell pulses, together with the known distances involved, it is possible to calculate the time that the cartridge arrived at, and left, the inner end of the transfer tube to an accuracy of about 0.02 or 0.03 sec. The transfer times which have been generally used are of the order of 0.6 sec. on the "in" transfer and 0.4 sec on the "out" transfer. This latter figure has been reduced on occasion to about 0.25 sec. by the use of higher pressure in the pressure reservoir.

III. MEASUREMENTS AND ANALYSIS

The various periods were studied by the usual method of determining the longest period first, then treating it as known in getting the next longest, etc., adjusting the time and intensity of irradiation to emphasize the desired period as much as possible. The discussion of the results will follow the same order.

A. The 55-Second Period

Here the method is simply to use full intensity, irradiate about 5 minutes then start counting only after the shorter lives have died out (about 5 minutes). A tape from such a run will then

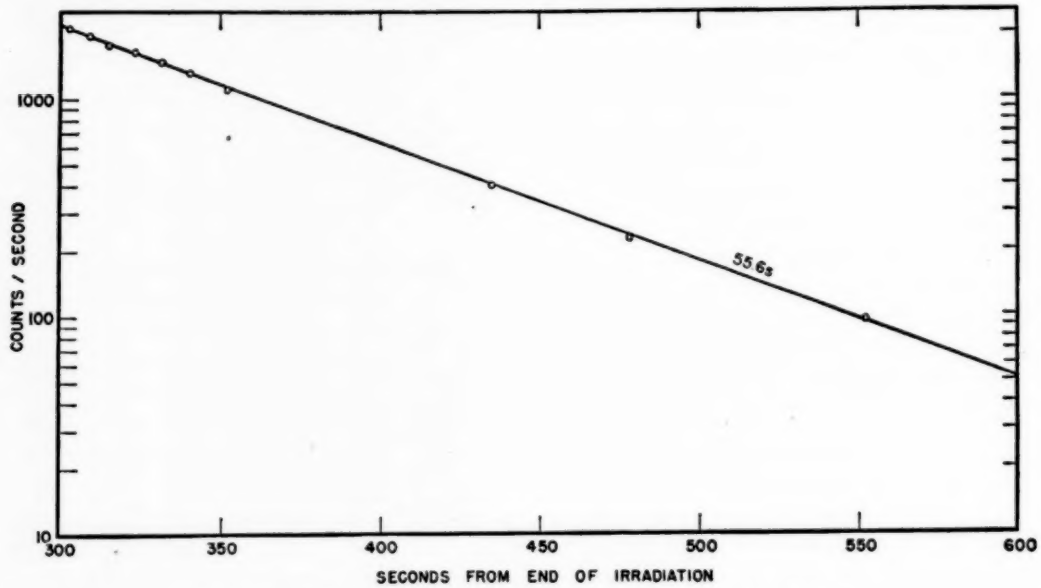

FIG. 4. Delayed neutron decay curve following a 5-min. irradiation.

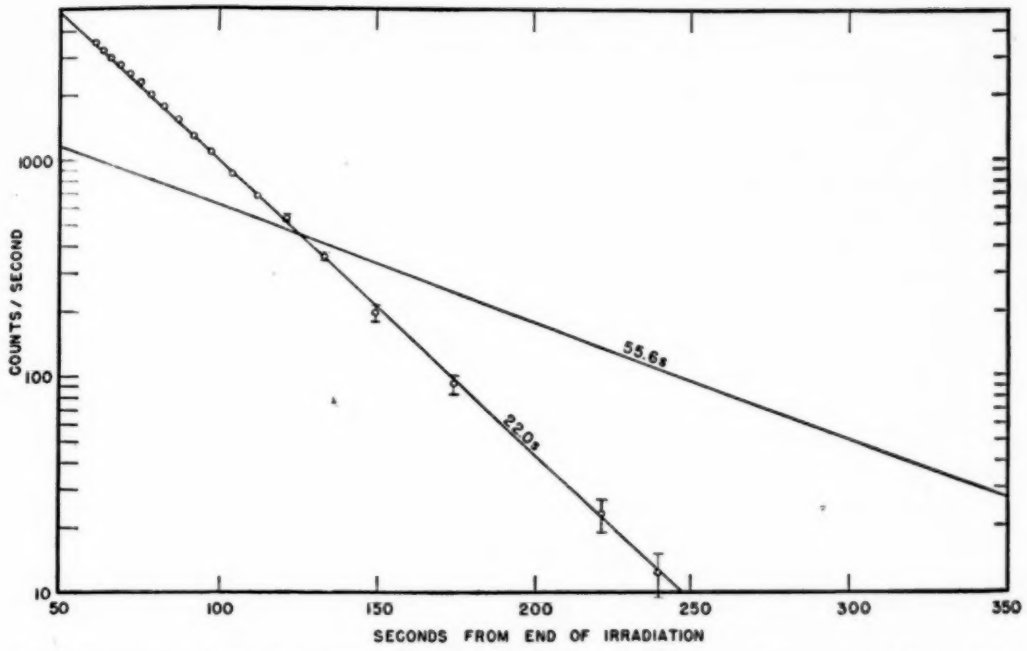

FIG. 5. Decay curve following a 30-sec. irradiation. The 55.6-sec. line shows the amount of that activity which has been subtracted.

cover the time from, say, 300 to 600 seconds after the end of the irradiation and contain a total of several hundred thousand counts. The tape is "scaled" by determining the *times* on the tape corresponding to the completion of a given number of counts, 10,240 in the present case (20 marks on tape). The number of counts divided by the time interval is then listed as the raw counting rate for the midpoint of the particular time interval. Each point has the same percent statistical error in spite of the decreasing counting rate.

Corrections to the raw counting rate are then applied in the following order, (1) for dead time as discussed under II, (2) for background, determined close to the time of irradiation because of changes caused by pile conditions, (3) for placement, because only for a time interval very short compared to the mean life would it be correct to plot the above *rate* at the center of the interval. The quantity actually measured is the number of counts divided by the time, $\Delta c/\Delta t$, whereas the correct rate at the midpoint would be

$$\frac{\Delta c e^{-\Delta t/2\tau}}{\tau(1-e^{-\Delta t/\tau})}$$

which is smaller than $\Delta c/\Delta t$. Hence, the measured rate is decreased by the difference between the above quantities. This correction, of course, assumes a knowledge of the period, τ, which is being investigated, but it is always known accurately enough for the purpose. The runs were made and scaled in such a way that all the above corrections were kept below a few percent.

Figure 4 shows the corrected data for a "55-second" run (5-min. irradiation). The period can be determined simply by drawing a straight line through the points and measuring its slope. However, it is difficult to determine what probable error to assign the result in such a case and difficult to prevent subjective errors in the process. For this reason and because errors in the long period would carry over into the work on the shorter periods, it was decided to determine the long period in a more quantitative manner, the graph showing quite convincingly that only one period is present after five minutes.

Theoretically, if only one period is present, one can determine the period most accurately from a given total number of counts by taking the ratio of the counts from t to infinity, to the total number of counts, where t is such that the ratio will be about $\frac{1}{3}$. This method was approximated by measuring the integral number of counts with

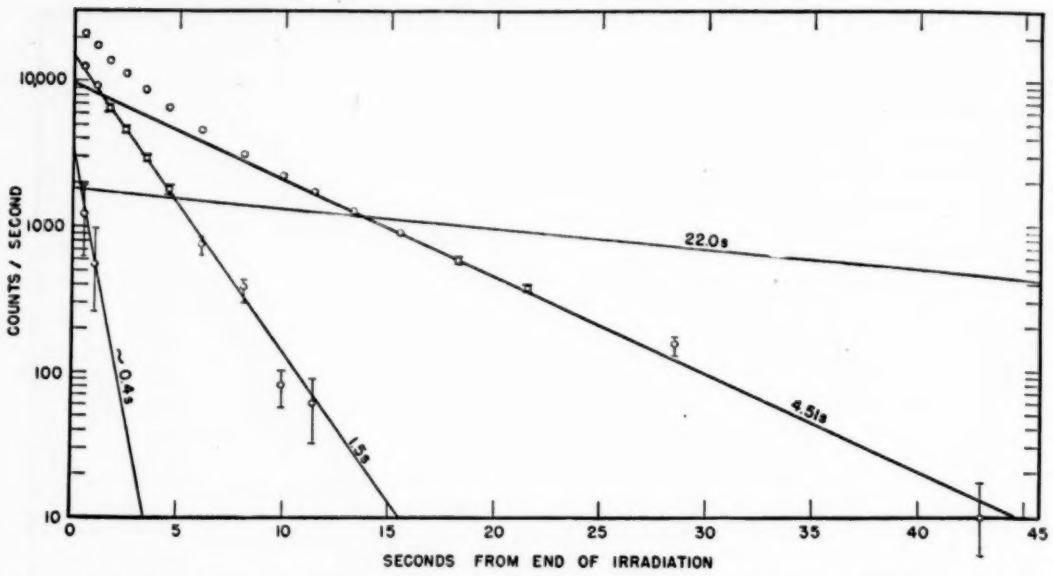

FIG. 6. A 6-sec. irradiation for the determination of the short periods with the 55.6- and 22.0-sec. periods subtracted.

a mechanical recorder (no tape being used) for two intervals, say 5–7 and 8–13 minutes, from the ratio of which the period can quickly be determined. The result of 19 such mechanical recorder runs gave 55.6±0.2 sec. for the half-life. The line shown in Fig. 1 is the one calculated from the above integral method, both for slope and magnitude, *for that particular run*. The correspondence between the line and the points scaled from the tape illustrates the agreement between the integral method and simple curve-fitting.

B. The 22-Second Period

An irradiation time of about 30 sec. at an intensity such that the counting rate is the maximum usable (about 15,000 c.p.s.) 50 sec. after irradiation (when the shorter periods have died out) gives the best conditions for determining the 22-sec. period. The longer period, taken as 55.6 sec., must be subtracted from the raw data as an additional correction in this case. However, there are not sufficient counts remaining after 300 sec. to give a 55 sec. curve with an accuracy sufficient for such correction. The amount of 55-sec. correction was actually determined by recording the *integral* number of counts occurring after 300 sec. with the mechanical counter—this number and an assumed period of 55.6 sec. gives the amount of 55.6 sec. activity to be subtracted from the earlier points. It was felt that this method was less subjective than subtraction of an amount of 55.6 activity adjusted to make the remainder lie on a straight line.

Figure 5 is a run analyzed in the above manner. The line labeled 55.6 shows the amount of this activity (as determined from the mechanical recorder count after 300 sec.) subtracted from the data to give the experimental points shown. Unlike Fig. 4, the experimental error now increases with time because although all original points have the same error, those at later times have a larger amount of 55.6 activity subtracted, leaving a larger relative error. The period shown by the 22.0 line in Fig. 2 was determined by a least-squares fit of the experimental points. This method was considered to be of somewhat better value than a graphical fit, the method used for the 55.6 period being inapplicable because the activity could not be followed over a sufficiently large number of half-lives. A series of five tapes, made under the same conditions as those of Fig. 2, was analyzed and the half-life determined by the least-squares fit for each run. The average of the results for the half-life is 22.0±0.2 sec.

The ratio of the saturated initial activity of

the 55.6 sec. to the 22.0 sec. activity ("relative yield" of the former) can be obtained of course from the initial values of each activity given from curves as in Fig. 2. However, it is more accurate to determine the yield, after the 22.0 sec. half-life is known accurately, by measuring the integral number of counts (after a run of a special length) for two time intervals chosen such that the 22.0 sec. activity predominates during the first and the 55.6 sec. during the second interval. The relative yield is then a simple function of the ratio of the two integral counts (corrected of course for dead time and background). The mean result of six such mechanical recorder runs is

$$Y(55)=0.172\pm0.003.$$

C. The Short Periods

Irradiations of several seconds duration were made at low enough intensities so that the initial counting rate would be about the maximum usable value. The intensity was read from the tape and the 22.0 and 55.6 sec. activities subtracted, using the integral number of counts obtained for the time after the short periods had disappeared, together with the measured 55.6/22.0 yield to calculate the amounts to be subtracted. The method is the same as described in B except that the contributions of two periods were being treated here.

The intensity remaining after subtraction of the long periods was then simply plotted on log paper and analyzed into separate activities by graphical methods. The use of integral counts on the mechanical recorder to get yields was used only for one period (4.5/22.0 yield) as the times which would be involved for the shorter periods would be too short to handle. Five separate runs with different irradiation times were analyzed this way, giving essentially the same periods each time, so it was felt that the graphical method was satisfactory for these short periods. Figures 6 and 7 of about 6- and 1-sec. irradiation time, respectively, show the analysis of two of these runs. The latter run was designed to accentuate the shortest periods and does show quite clearly the presence of two periods shorter than the 4.5-sec. period, of 1.5- and 0.43-sec. half-life. The two short periods agree with the findings of Snell and indicate that the 1.1-sec. activity found by

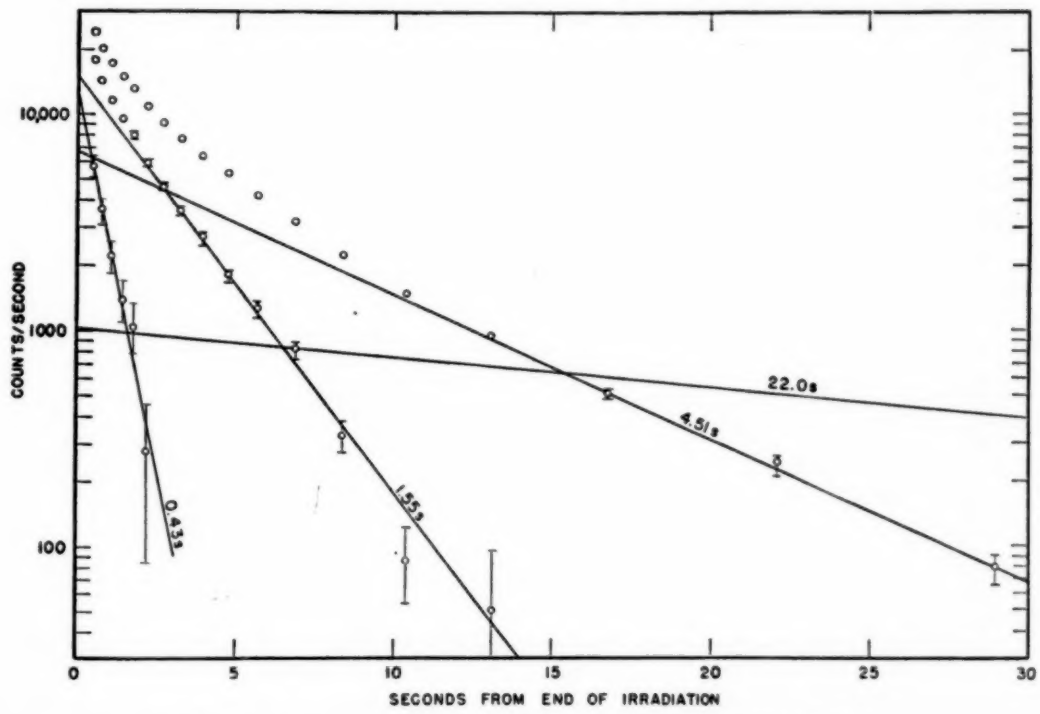

FIG. 7. A one-sec. irradiation for the determination of the shortest periods.

Redman and Saxon was really a combination of the above two activities.

The average of the five runs give the following values of the half-lives and relative yields for the short periods (again taking 22.0 sec. as the standard).

$T\frac{1}{2}$	Yield
4.51±0.1 sec.	1.42±0.06
1.52±0.05	1.35±0.06
0.43±0.05	0.57±0.04

The periods were determined simply from the graphical analysis, and the yields from the extrapolation of the periods back to zero time. In addition, values for the yield of the 4.5 sec. activity obtained from mechanical counter integral values (as mentioned in the paragraph above) were used in obtaining the average value for the 4.5 sec. yield. The probable error given is only a reasonable estimate because of the subjective nature of the graphical analysis.

An over-all check of the period and yield values was made by calculating the total decay curve of all the delayed neutrons, after a saturated run, from the measured period and yield values. A saturated run was then made and the total decay curve plotted. The calculated curve and the experimental points (equated at $t=0$) are compared in Fig. 8, and it is seen that the five periods and yields represent the total curve quite well. Some runs were also made with extremely short irradiation times (about 0.1 sec.), and compared with curves calculated from the above periods, to investigate possible shorter periods. The results showed that for times greater than 0.25 sec. after the end of a saturated irradiation the periods and yields above completely accounted for the decay curve. This means that if any shorter periods are present, they die out within 0.25 sec. after irradiation. The detection of an extremely short period was carried out later by a different method which will be described in Section III G.

D. Energy of the Delayed Neutrons

It is possible that the yields measured above do not give the true relative numbers of the neutrons of the different periods. The detecting apparatus used probably has an efficiency that varies with neutron energy; hence, it would not

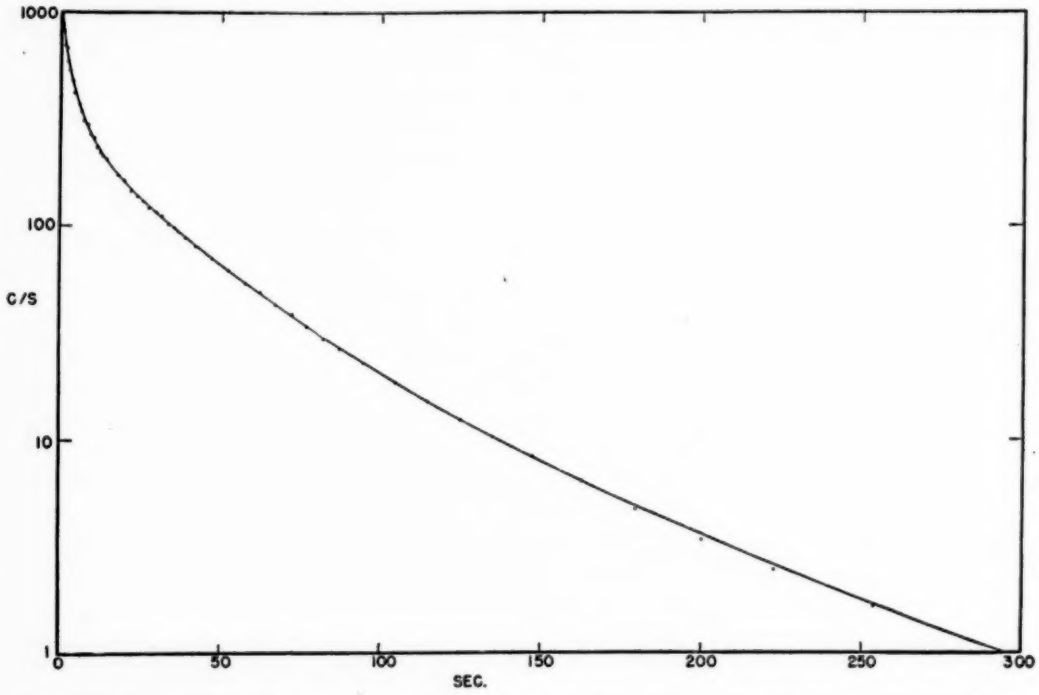

FIG. 8. The decay curve following a saturated irradiation (points) compared to the curve calculated from the periods and yields of Table I.

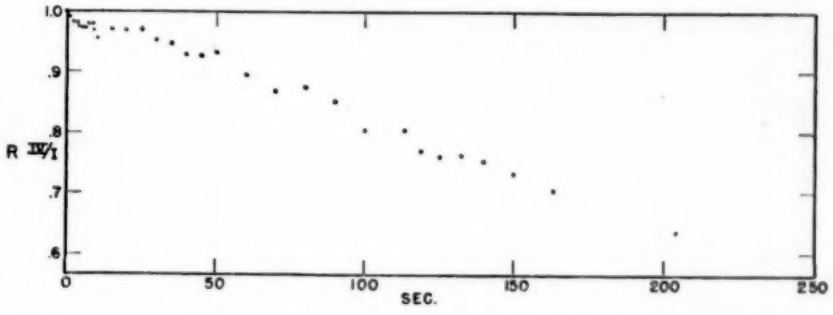

FIG. 9. Ratio of delayed neutron intensity at two different positions in the paraffin block as a function of time after saturated irradiation. The decrease in the ratio means a decrease in the average energy of the delayed neutrons as a function of time.

give true yields for periods made up of neutrons of different energies.

To investigate the possible difference in energy of the neutron periods, a saturated decay curve was obtained with the counter 20 cm from the sample in the paraffin block ("position IV") and compared with a similar curve obtained in the position 8 cm from the sample ("position I") which had been used for all the period and yield work. The two saturated curves, both set equal to unity at $t=0$ (actually the intensity was ~ 30 times greater in position I) were compared and the ratio IV/I is shown in Fig. 9. The ratio of the two curves is not constant but decreases with time showing that the energies of the different periods are not the same and, as the longer periods become more predominant, the decrease of intensity in going from I to IV becomes greater, i.e., the average energy becomes less.

The actual shape of the slowing down curve in the paraffin was obtained for the 55.6- and the 22.0-sec. periods by analyzing the decay curve into its components at four different positions in the paraffin. Figure 10 gives the results where I is the intensity of the period and r the distance from source to counter. The curves obtained with two photo-neutron sources (Na-Be, 920 kv and Na-D_2O, 280 kv) are also shown. The curves show that the 55.6 period is much less energetic than the 22.0 period and the photo-neutron sources allow an energy calibration of the curves, putting the former period at 250 kv and the latter at 560 kv.

One might expect from the curve of Fig. 9 (which showed that the *average* energy keeps dropping after $t=0$) that, for the shorter periods also, the energy would increase as the period decreases. The energy of the individual shorter periods was measured by analyzing runs made in position IV and obtaining the relative (taking 22.0 as 1.00 again) yields of the short periods in this position much as had been done in position I. It will then be true that a relative yield in IV *greater* than that in I means that the particular period has an energy *higher* than the 22-sec. energy. The ratio of the yields in IV to those in I are shown in Fig. 11 for all the periods. The observed ratios do not indicate any monotonic change of energy with half-life but merely a trend toward higher energy with shorter half-life. An energy scale based on the photo-neutron source measurements is shown in Fig. 9 also. Thus, the approximate energy values may be estimated as 430, 620 and 420 kev. for the 4.51, 1.52 and 0.43 periods, respectively, each with an error of about 60 kev.

The actual variation of energy values of the individual periods seems so great that it is sur-

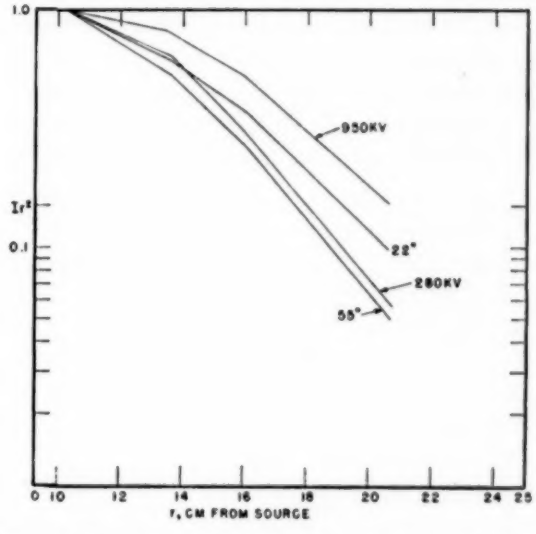

FIG. 10. Intensity of two delayed neutron periods and of two standard photo-neutron sources as a function of position in the paraffin block.

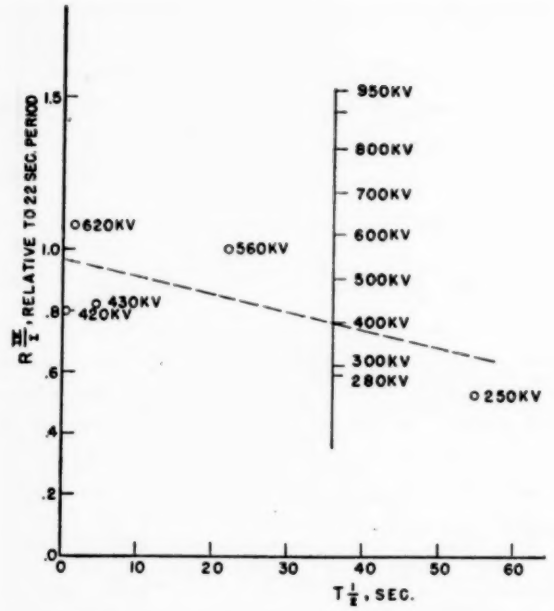

FIG. 11. Values of the intensity ratio at two positions in the paraffin block for the individual periods. The energy scale is based on the standard photo-neutron sources and gives the delayed neutron energy values shown.

prising that Fig. 9 shows such a continuous decrease in energy with time (i.e., decrease in ratio IV/I). To investigate any possible discrepancy, the value of R, the ratio IV/I, to be expected as a function of time after a saturated run, was calculated from the R's for each period given in Fig. 11. This was done by weighting the R for each period according to the amount of that period present at a given time after irradiation. The resulting ratio drops almost continuously from a value of 0.92 (at $t=0$) to 0.52 (when only the 55.6-sec. period is left) showing that the *average* energy at $t=0$ is slightly less than the 22-sec. period, say 510 kv, and drops (almost) continuously to a steady value of 250 kv. The calculated average ratio IV/I, set equal to unity at $t=0$, is shown in Fig. 12 compared with the experimental points of Fig. 9. The agreement between the calculated and experimental ratio shows that there is no discrepancy between the average energy and the individual period values. The approximate energy scale included in Fig. 12 gives the average energy of the delayed neutrons as a function of time after a saturated run.

E. Correction of the Measured Yields for Energy

It is certain that, because of the difference in energy of the periods, the yields measured in position I should be corrected for energy dependence. However, the magnitude of the correction, or even its sign, is difficult to calcuate. If a thermal detector is very close to a fast neutron source, it will favor the low energies, while if it is far from the source, it will favor the high energies. Because of the finite size of the paraffin block and the various gaps in it (the rabbit pipe, BF_3 counter, pre-amplifier, etc.), the actual distribution curve of thermal neutrons in the paraffin is impractical to calculate. What is needed, of course, for the true yield is the value of Ir^2 integrated from zero to infinity, whereas only the intensity at a fixed r was actually measured.

The correction was made experimentally by measuring the value of two of the relative yields with the "long counter" [7] which is very nearly energy-independent. For the long counter measurements, the sample was shot clear through the usual geometry out to a position (in the center

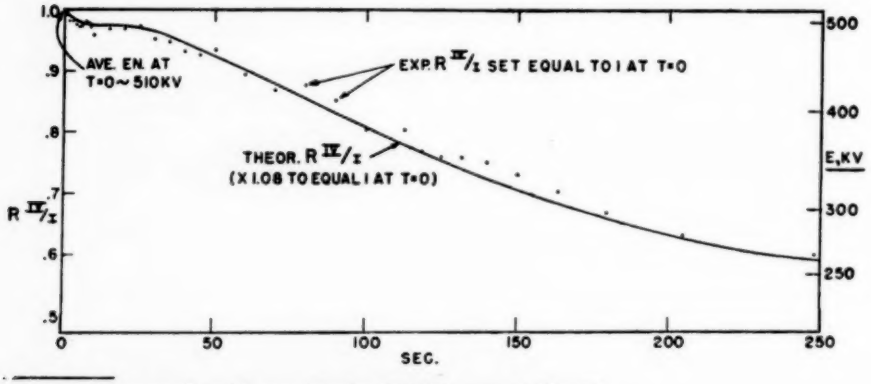

FIG. 12. Average value of delayed neutron energy after a saturated irradiation (right-hand scale) and the observed *vs.* calculated intensity ratio (left-hand scale).

[7] A. O. Hanson, Los Alamos Declassified Document No. 59.

TABLE I. Properties of delayed neutron periods.

Half-life	Energy	Relative yield, position I	Yield, corrected for energy
55.6 ±0.2 sec.	250±60 kv	0.172±0.003	0.153±0.004
22.0 ±0.2	560±60	1.000	1.000
4.51±0.1	430±60	1.42 ±0.06	1.28 ±0.08
1.52±0.05	620±60	1.35 ±0.06	1.45 ±0.08
0.43±0.05	420±60	0.57 ±0.04	0.51 ±0.05

TABLE II. Absolute yields of delayed neutron periods.

Half-life	Absolute yield
55.6 sec.	2.5×10^{-4}
22.0	16.6
4.51	21.3
1.52	24.1
0.43	8.5
	73.0×10^{-4}

of the room adjoining the pile) in front of the long counter. The yields of the 55.6- and the 4.5-sec. periods (relative to the 22.0) were determined by taking integral counts over appropriate time intervals in the same manner as these yields were measured in position I. In each measurement the back-scattering correction was made by use of a paraffin cone in front of the long counter; its amount was about 20 percent so the back-scattering in the room was not excessive.

The long counter relative yields for the 55.6- and the 4.5-sec. periods are both lower than the values measured in position I, which shows that, for position I, the low energies are emphasized (because the energy of the 22-sec. period is higher than that of the other two). It was not possible to measure the yields of the short periods with the long counter because of insufficient intensity, so the true relative yields for the short periods were obtained by comparison with the corrections for the 4.5- and 55.6-sec. corrections. The largest correction (for the 55.6 sec.) was only 12 percent, so the error in estimating the correction for the short periods by interpolation is probably not serious. The final values for the corrected yields, together with the other petinent data, are listed together in Table I for convenience. The estimated errors are based partly on statistical error and partly on variation in results of successive runs.

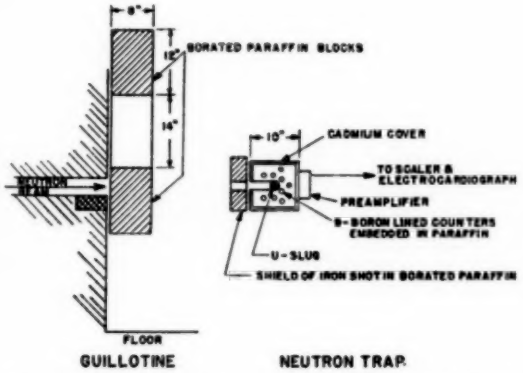

FIG. 13. Apparatus for the determination of absolute yield of delayed neutrons and of short period delayed neutrons.

The results given here cannot be compared very easily with those already published, for the energy dependence of the apparatus actually used for other measurements would have to be considered. However, in general, the yield values of Redman and Saxon agree quite well with the yields found here for the long periods (they did not resolve the two shortest periods). The half-life values agree reasonably well with Snell's and especially well for the short lives where, however, he obtained no yield values. Burgy *et al.*[8] have recently published energy values for the delayed neutrons, based on measurement of proton recoils in a cloud chamber, which correspond very well with those of Table I.

F. Absolute Yield of Delayed Neutrons and Applications to Pile Behavior

Nagle, Redman and Saxon[9] determined the absolute yield (the fraction of the total neutrons emitted which are delayed) by comparing the activation of indium foils in a graphite block by delayed neutrons with the activation by instantaneous neutrons. In making the comparison it was necessary to extrapolate back over a period of about 15 seconds, using the known periods, to obtain the initial intensity of the delayed neutrons. Use of their experimental data but the present periods and yields, corrected for energy (i.e., five periods instead of their four), raises the absolute yield from their calculated value of 0.0078 to 0.0081. The latter value, of course, refers only to those delayed neutron periods of

[8] M. Burgy, L. A. Pardue, H. B. Willard, and E. O. Wollan, Phys. Rev. **70**, 104A (1946).
[9] Unpublished Manhattan Project Work (1943).

0.43 sec. or longer—the presence of shorter periods would mean a larger absolute yield. Because the absolute yield value of 0.0081 seemed high compared to the yield obtained from actual pile behavior, the absolute yield was re-measured by an independent method.

The apparatus is shown diagrammatically in Fig. 13. When the "guillotine" is dropped from the position shown, it allows a 0.19 sec. irradiation of the uranium slug as the opening passes the beam of thermal neutrons. For the yield work, however, the guillotine was held in the open position to measure the total neutron omission from the metal slug and then dropped to give the delayed neutron decay curve. The decay curve was recorded on an electrocardiograph tape in the same manner as was used for the work at the rabbit. The initial intensity of the decay curve (which was 100 times background) compared to the intensity with the beam open then gives the absolute yield directly. Actually the open beam intensity was measured at a low pile power and converted to high power by means of a fission chamber monitor located inside the pile shield. The initial intensity of the decay curve was obtained by extrapolating the experimental points back from $t=1$ sec. to $t=0$ according to the five periods of Table I. This was done because of the presence of a hitherto unknown short period present at shorter times (see Section G).

The "neutron trap," designed primarily for high efficiency (about 1 percent), was intended to be somewhat independent of energy (through placement of counters) but, unfortunately, has a rather large energy dependence. Therefore, it is necessary to correct the observed yield for the difference in energy of fission neutrons and delayed neutrons (which have an average energy of about 500 kv at $t=0$). The energy sensitivity of the trap was measured, by comparison with the long counter, for several different neutron energies; for Ra-Be, Na-Be, 22-sec. delayed neutron period, 55-sec. period, and Na-D_2O neutrons. It was found from these standards that the sensitivity decreases smoothly with increasing energy and that the conversion factor between fission neutrons and 500 kv neutrons is 1.36 ± 0.06. The observed yield was (0.99 ±0.04 percent) which then becomes (0.73+0.05 percent), when corrected for energy sensitivity. This yield, of course, does not include periods shorter than the five of Table I. The absolute

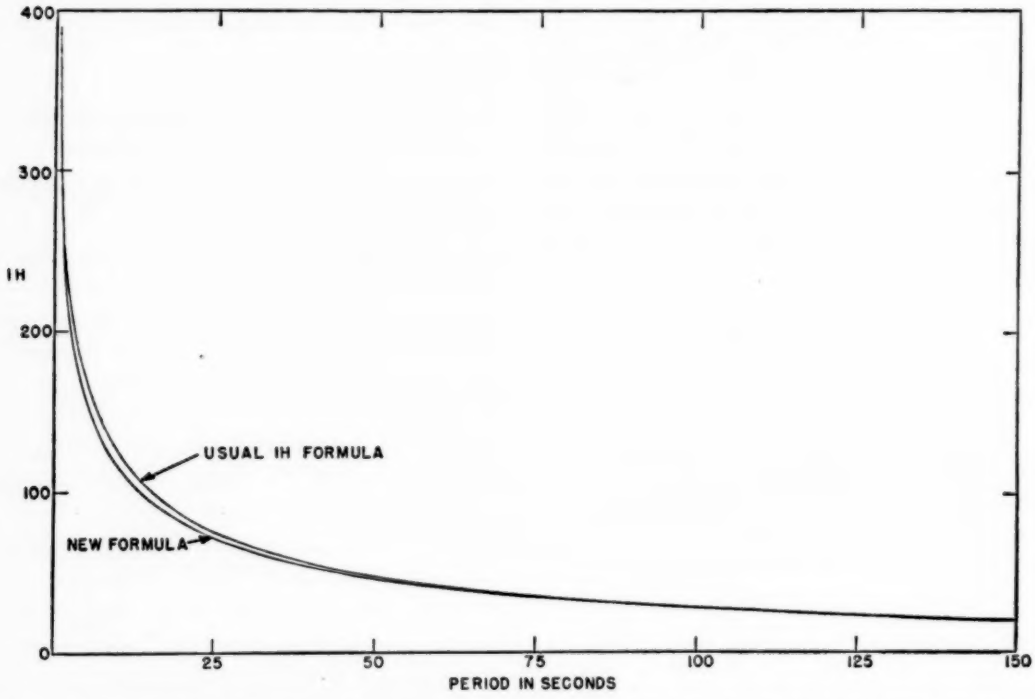

FIG. 14. The relationship between the excess reactivity of a pile and its period (the "inhour formula").

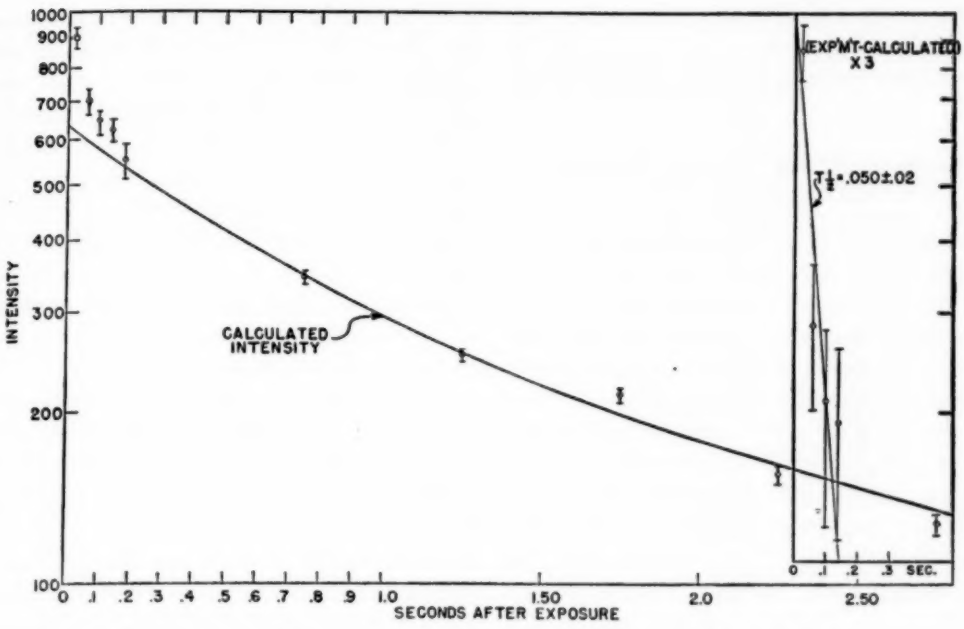

FIG. 15. Delayed neutron decay curve after a 0.19-sec. irradiation obtained with the apparatus of Fig. 13. The initial part of the curve (shown on larger scale also in right hand box) is evidence for an activity of 0.05-sec. half-life.

yield of 0.0073 can be combined with the relative yields of Table I to obtain the absolute yield values of the individual periods which are listed in Table II.

It is a simple matter to ascertain whether the absolute yields are consistent with observed pile behavior. Observations[10] with graphite-uranium piles have shown that the amount of reactivity ("excess k") which will give a pile period of one hour is $2.5\pm0.5\times10^{-5}$. This amount of reactivity is by definition one "inhour." The excess k corresponding to one inhour also follows directly[11] from the absolute yields:

$$(k-1)_{1\ ih}=\frac{l_0}{3600}+\sum_i\frac{y_i\tau_i}{3600+\tau_i},$$

where l_0 is the average lifetime of the neutrons in the pile and y_i is the absolute yield of the ith delayed neutron group of period τ_i (in seconds). The value of l_0 is about 1.5×10^{-3} sec.[12]; its exact value is unimportant. Substitution of numerical values gives

$$(k-1)_{1\ ih}=(2.6\pm0.2)\times10^{-5},$$

which is in good agreement with, and more accurate than, the value obtained directly from pile behavior.

The periods and yields reported here also make it possible to give a more accurate formulation of the relationship between the reactivity in inhours and the pile period (the "inhour formula") than that given in reference 10. Substitution of the new values into the formula given as Eq. 3 of reference 11 gives the following relationship:

$$ih \text{ of reactivity}=\frac{54}{T}+\frac{20.3}{T+0.62}+\frac{204}{T+2.19}+\frac{535}{T+6.5}+\frac{2036}{T+31.7}+\frac{787}{T+80.3}$$

and the two formulas (old and new) are compared in Fig. 14. It is to be noted that the present formula is adjusted to equal unity for $T=3600$ in accordance with the definition of the inhour, while the formula of reference 10 (aside from the older yield and period values) differ

[10] Anderson, Fermi, Wattenberg, Weil and Zinn, Phys. Rev. **72**, 16 (1947).
[11] L. W. Nordheim, Manhattan District Declassified Document No. 35, Eq. 3, June 14, 1946.
[12] E. Fermi, MDDC No. 74, June 18, 1946.

slightly in that the sum of the numerators is set equal to 3600 and, hence, the reactivity is slightly less than one inhour for a period of one hour.

G. New Short Period Delayed Neutron Activity

The guillotine of Fig. 13 was also used to investigate a possible short-period, delayed neutron activity whose existence seemed likely from some measurements made during the absolute yield work. A 0.19 sec. irradiation was obtained by dropping the guillotine past the beam and the resulting decay curve, recorded on the electrocardiograph tape, was compared with a theoretical curve made up of the five known periods (in amounts corrected for relative saturation and energy sensitivity of the neutron trap). The results are shown in Fig. 15 where the theoretical curve is equated to the experimental in the region 0.5–2.5 sec., the experimental points being the sum of the counts obtained on a number of runs. The presence of a short period is evident, and it turns out to have a half-life of 0.05 ± 0.02 sec. and a relative intensity (22 sec. period = 1.00) of approximately 0.15, which is about the same yield as the 55 sec. period. The reality of the period was checked by removing the uranium slug and cutting a hole in the Cd cover of the trap to obtain a high counting rate from the thermal neutrons when the beam was open. The experiment was repeated under these conditions and the rate dropped to background instantly when the beam was cut off, thus eliminating any spurious source of the short-lived activity (such as mechanical shock, bouncing, etc.). The guillotine actually shuts off the beam in about 1 millisecond and the decay curve can be measured immediately, limited only by the speed of the recording circuit and the available counting rate.

The absolute total yield value of 0.73 percent, which was described in Section F, does not include the 0.05 sec. period, of course. Inclusion of this period raises the yield to 0.755 percent, a change which is uncertain by a negligible amount because of the unknown energy of the 0.05 sec. period. The short period has very little effect in a saturated run, being only about 4 percent of the total initially and dropping to less than 1 percent within 0.2 sec. Because this period is much shorter than the usual pile periods, it also has no effect on the considerations of Section F concerning the value of the inhour or the inhour formula.

A separate experiment was performed in an attempt to determine if any periods shorter than 0.05 sec. exist. The set-up was the same as Fig. 13 with the addition of a rotating shutter in the beam before the uranium slug and a timing device, so that only those counts in a certain time interval after each burst of neutrons would be detected. The apparatus was actually the "chopper" velocity selector[13] used to detect short periods rather then neutron times-of-flight. The lower limit to the lifetimes which could be detected by this method was about one millisecond and was set by the time of flight of the neutrons plus the lifetime of the neutrons in the neutron trap.

Because of the high background inherent in such an adaptation of the chopper, the experimental uncertainty turned out to be quite high. However, the absolute yield obtained (by comparing the "instantaneous" neutrons with those delayed) for all periods greater than one millisecond is 0.0084 ± 0.0012 which agrees, within experimental error, with the value of 0.00755 for the six periods already discussed. Thus, no periods between one and 50 milliseconds were found, and any such periods, if present, must constitute only a small part of the total delayed neutron emission.

[13] T. Brill and H. Lichtenberger, to be published.

The Polarizability of the Neutron in an Electrostatic Field*

KENNETH M. WATSON
Department of Physics, University of Iowa, Iowa City, Iowa
(Received October 1, 1947)

In an applied electrostatic field the meson-charge cloud about a neutron should become polarized. The dipole moment for a neutron in an electrostatic field $\mathbf{E}$ is $(\epsilon^2 g^2/\mu^3)\mathbf{E}$. This should give rise to an attractive force between a neutron and a charged particle.

THE direct experimental detection of the effects of the finite extension of the meson-charge cloud about a neutron or proton would be of considerable interest. An attempt along this line to account for the discrepancy in the fine structure of the hydrogen atom energy levels as resulting from the breakdown of the Coulomb potential for a point charge was made by Frohlich, Heitler, and Kahn.[1] They ascribed the breakdown of the $1/r$ potential to the "smearing out" of the charge of the proton by the meson field. Subsequent investigation[2] indicated that the effect was much too small to account for the observed discrepancy in the levels.

The polarization of the meson-charge cloud in an external electrostatic field presents another possibility of accounting for the fine-structure splitting. The polarization of the meson field about a neutron might also be measured directly. Again the effect is too small to account for the fine-structure splitting (and of the wrong sign[3]) and too small to be directly measured. However, as the possibility of polarizing the neutron is of some interest in itself and as improved experimental techniques may make the effect detectable, it was thought worth while to record the results of the present calculations.

The calculations were made for scalar, pseudoscalar, and vector meson fields. In all three cases the results were the same except for slight differences in the numerical coefficients.

One begins with the Schroedinger equation

$$(H_\mu+H_1+H_2)\Omega=i\frac{d\Omega}{dt} \tag{1}$$

(we use as units $\hbar$, c, and cm), where H_μ is the free meson-field Hamiltonian, H_1 represents the interaction of the meson field with the applied electrostatic field, and H_2 represents the interaction of the meson field with the neutron (see, for instance, Kemmer[4]). It was necessary to solve Eq. (1) by the usual perturbation methods to the third order. We neglect the recoil of the neutron, which gives a relative error of the order μ/M (μ is the meson rest mass, M is the neutron mass).

Having determined Ω from Eq. (1), the "expectation value" of the charge density is given by

$$\bar{\rho}=\Omega^*\rho\Omega, \tag{2}$$

where ρ is the charge density operator of the meson field. If the neutron is taken at the origin of the coordinate system, the neutron dipole moment will be given by

$$\alpha=\int \mathbf{Z}\bar{\rho}d^3Z, \tag{3}$$

where Z is the coordinate vector measured from the position of the neutron.

The work was carried out rigorously in the scalar theory, but in the pseudoscalar and vector theories only the dominant terms in $\bar{\rho}$ were kept (with third-order accuracy in Ω, in the vector theory there were 64 non-vanishing terms to evaluate in Eq. (2)). Thus for the latter two meson fields the estimated accuracy was within 40 percent. Certain of the terms in the vector theory diverged, but could be made convergent with the lambda limiting process.

From Eq. (3) the dipole moment of a neutron (or proton) plus meson field turned out to be

$$\alpha\cong 0.1\frac{\epsilon^2 g^2}{\mu^3}\mathbf{E}. \tag{5}$$

* This paper contains the results of a thesis submitted in partial fulfillment of the requirements for the degree of Doctor of Philosophy at the University of Iowa.

[1] Frohlich, Heitler, and Kahn, Proc. Roy. Soc. **A177**, 269 (1939).

[2] J. M. Blatt, Phys. Rev. **67**, 205 (1945).

[3] Unpublished calculations of Professor J. M. Jauch.

[4] N. Kemmer, Proc. Roy. Soc. **A166**, 501 (1938).

Here ϵ is the electronic charge, μ is the meson rest mass, g is the dimensionless coupling constant of the meson field with the heavy particle field ($\cong 0.2$), and $\mathbf{E}$ is the strength of the applied electrostatic field at the position of the neutron.

If the applied electrostatic field is not constant in the vicinity of the neutron, its potential ϕ can be expanded in a power series in the coordinate $\mathbf{Z}$:

$$\phi = \phi_0 - \mathbf{E}\cdot\mathbf{Z} + \sum_{i,j=1}^{3} \phi_{ij} Z_i Z_j + \cdots. \tag{6}$$

The electrostatic potential ϕ causes a decrease in energy of the meson field. This decrease in energy can be represented by a series of terms corresponding uniquely to the terms of Eq. (6). The constant term in Eq. (6) gives no effect, but the succeeding two terms give, respectively, the dipole and quadrupole energies of the polarized meson field, which are

$$V_d \cong -0.1 \frac{\epsilon^2 g^2}{\mu^3} \mathbf{E}\cdot\mathbf{E}, \tag{7}$$

$$V_Q \cong -0.03 \frac{\epsilon^2 g^2}{\mu^5} \sum_{i,j=1}^{3} \phi_{ij}\phi_{ij}. \tag{8}$$

For a point charge ϵ at a distance r from the neutron (or proton) Eqs. (7) and (8) become

$$V_d = -0.1\mu \frac{\epsilon^4 g^2}{(\mu r)^4}, \tag{7'}$$

$$V_Q = -0.04\mu \frac{\epsilon^4 g^2}{(\mu r)^6}. \tag{8'}$$

These expressions are valid for $\mu r > 1$. As a rule, only Eq. (7') need be considered. This represents an attractive electrostatic force between either a proton or an electron and a neutron, or an additional force to be added to the potential of a proton and an electron.

In any case, the interaction given by Eq. (7') is too small to be of importance in shifting the energy levels of the hydrogen atom. It is also doubtful whether it could be detected by the scattering of charged particles by neutrons.

A process similar to the polarizability of the meson field would be its "vibrations" in an external electromagnetic field. This would cause γ-rays incident on a neutron to be scattered elastically. Calculations show that the cross section is again very small. For low energy γ-rays it is of the order of 10^{-32} cm^2, rising to about 10^{-30} cm^2 for γ-rays of energy equal to the meson rest mass.

The author would like to express his appreciation to Dr. J. M. Jauch for suggesting the problem and for his helpful comments concerning its solution.

The Multiple Production of Mesons

H. W. LEWIS, J. R. OPPENHEIMER, AND S. A. WOUTHUYSEN
*Department of Physics, University of California, Berkeley, California**

(Received October 2, 1947)

In this paper an attempt is made to treat the impacts of nucleons of very high energy ($\gg Mc^2$). These impacts lead to meson emission, despite the relatively small momentum transfers to be expected, because changes of nuclear charge and spin require a readjustment of the nuclear meson fields. Where the fields are strong (as e.g., in the pseudoscalar case), meson emission is multiple, and the multiplicity increases with energy. For weaker coupling (e.g., scalar fields) this is not true.

Two closely related methods are developed for a more quantitative description of these collisions. These methods may be expected to give valid results when the collision time is short compared to the periods of the emitted mesons, and when the emission of mesons into the various modes can be treated as statistically independent. Under these conditions the total cross section may be expected to be about 10^{-26} cm^2, and the multiplicity to approach for high energies $2g^{\frac{1}{2}}(ME_0/2\pi\mu^2c^2)^{\frac{1}{4}}$, with E_0 the primary energy and g the dimensionless coupling constant.

Some applications to the calculation of positive excess, primary spectrum, angular distribution, and the theory of auger showers, are discussed briefly in the final section.

I. QUALITATIVE CONSIDERATIONS

YUKAWA'S original argument, which anticipated the existence of mesons, was based on the role which they would play in accounting for nuclear stability and the forces between nucleons. On the one hand, very extensive theoretical study has failed to devise a theory which accounts at all reasonably for the quantitative aspects of nuclear forces; on the other hand, decisive experience with cosmic-ray mesons, both with the absorption and scattering of the penetrating component, and with the capture of mesons brought to rest in matter, fails to reveal the evidences of any strong interaction. Only one phenomenon shows, if not yet conclusively, that there is a strong interaction between mesons and nuclear matter. This is the phenomenon of the production of mesons, which takes place with very high probability, and with characteristic and high multiplicity when the primary cosmic rays traverse the matter of the earth's atmosphere.[1] These present notes give some considerations about the theoretical treatment of these collisions.

Quite apart from the inadequacy of current theoretical methods and concepts, to which we will have to return over and over again in the discussion of this problem, it appears that a somewhat more complex model may have to be invoked to reconcile the strong interactions manifested in meson creation with the absence of subsequent interactions between cosmic-ray mesons and nuclear matter. Especially if one compares the processes of production with the processes of meson absorption, let us say, in the domain of ten billion volts, one is led to an apparent lack of correspondence between elementary processes and their approximate inverses quite at variance with preceding experience. In the discussions of this problem, which has definitely not been resolved by such theoretical development as the "strong coupling" theory, it was recognized at the Shelter Island Conference[2] that the most natural interpretation lay in the existence of "structure," either for the nucleons or the mesons, or both. Thus Weisskopf suggested the existence of long-lived metastable states for the nucleons formed during the primary collision and subsequently decaying with a long lifetime to yield the mesons; whereas Marshak proposed the equally satisfactory view that the mesons originally created were metastable with regard to disintegration into those actually observed, as might, for instance, be the case if they had a higher mass.

In making this study, we shall, of course, not

* Now at the Institute for Advanced Study, Princeton, New Jersey.

[1] M. Schein, W. P. Jesse, and E. O. Wollan, Phys. Rev. 59, 615 (1941); M. Schein, M. Iona, and J. Tabin, Phys. Rev. 64, 253 (1943).

[2] June 1947, sponsored by the National Academy of Sciences.

be able to account for copious meson production without assuming a strong coupling between mesons and nucleons; but it is to be understood that much of the argument does not depend on a direct identification of the mesons with those observed in cosmic rays, nor on the exclusion of metastable states for nuclear matter. In fact, the arguments which originally led Yukawa to the view that charged quanta must exist have in no way been weakened by recent experience in the domain of nuclear physics: the scattering, by neutrons and protons, of neutrons of high energy reveals the important part played by charge exchange in these phenomena; and the measurement of the magnetic moment of the triton strongly suggests, if it does not prove, the existence of electromagnetic currents associated with nuclear attractions.[3]

Even under the assumption of strong coupling, such as, for instance, characterized the symmetric pseudoscalar or "mixed" theories, or the pair theories, of nuclear forces, an understanding of the phenomena of meson production is by no means trivial. There seem to be two characteristics of these collisions which are well established: The first is that they correspond to a cross section very close to the size of the nucleus; the second is that the typical act is a multiple one in which a considerable number of mesons, perhaps 5 or so, for typical cosmic-ray energies, are created.[4] When one remembers that these collisions occur at distances of encounter for which nuclear forces as normally experienced are extremely weak, one must ask two questions: Why do these encounters lead to such strong emission, and why is this emission characteristically multiple?

To these two questions one would like to give simple qualitative answers. To the first: although relatively remote collisions are not accompanied by large momentum transfers between nucleons, they probably are accompanied by changes of spin and isotopic spin. Thus, the collision produces a discrepancy between the meson fields which are actually present about the nucleon, and those which are appropriate to its new state. Insofar as it is possible to idealize the collision processes as rapid, compared to the time of emission of mesons, this would lead us to expect a very probable emission. As to the second question,[5] and guided by similar qualitative arguments, we may suppose that if the fields of nucleons are indeed very intense, so that large numbers of mesons are present in these fields, then the effect of a sudden change of spin or isotopic spin will be to release considerable numbers of mesons, as is observed. Whether and how this number will depend on the energy of the collision must, as the future analysis will show, depend importantly on detailed characteristics of the field. But even at this stage we may say that if the collisions between nucleons involved no change other than a small transfer of momentum, the large radiation cross sections would not be intelligible, and that if the fields surrounding the nucleons were in fact as weak and as weakly dependent on position as the Coulomb field, this radiation process would not be highly multiple.

It should be observed that in these discussions we have assumed that the primary cosmic ray is itself a nucleon, an assumption which is now current. Some support for the view that meson production is in fact the result of the collision of nucleons comes from the study of so-called penetrating showers throughout the atmosphere, and at sea level.[6] In fact, the characteristics and number of such showers at sea level, and the equal distribution between charged and neutral initiators, suggests quite strongly that these phenomena are what is left of the primary collisions in the upper atmosphere, after the absorption of the primaries and of their secondary protons and neutrons. At least this assumption that protons initiate these collisions in the upper atmosphere underlies the work of this paper.

Most of the evidence of multiple production and of collision cross section comes from the typical cosmic ray, of energy say ten billion volts. It is possible so to interpret the very large air showers as to obtain evidence bearing on much higher energies. It seems to be true that these showers have their origin quite near the top of

[3] Felix Villars, Phys. Rev. **72**, 256 (1947).
[4] Cf. reference 1.
[5] J. R. Oppenheimer and J. Schwinger, Phys. Rev. **60**, 150 (1941); H. A. Bethe, Phys. Rev. **70**, 787 (1946).
[6] L. Jaǹossy, Proc. Roy. Soc. **A179**, 361 (1942); L. Jaǹossy and G. D. Rochester, Proc. Roy. Soc. **A181**, 399 (1943); W. B. Fretter, Bull. Am. Phys. Soc. Stanford meeting, July 1947.

the atmosphere, and that they involve an intimate mixture of meson and soft radiation. A natural, but by no means unique, interpretation of this is that the soft radiation arises primarily from the decay of neutral mesons, though little in our arguments would be altered were the decay process to involve transitions from heavier to lighter particles, provided the time of such decay were short enough to satisfy the Mills-Christy condition,[7] and long compared to all collision times. If these suggestions prove to be correct, they will bring with them the consequence that, even for energies in the range of the 10^{14} volts, and perhaps higher, collision cross sections must be of the order of nuclear areas, and must lead to the conversion of a large part of the primary energy into mesons and their decay products. As we shall see, the interpretation of such collisions on the basis of meson-field theories gives us information about field strengths of very great magnitude, such as might obtain in the immediate neighborhood of the nucleon.

It is, of course, not possible, even adopting one of the more or less standard forms of meson theory, to compute what will happen in a collision between two nucleons of high energy, because of this clearly depends on a reliable theory of the reaction of meson radiation on the collision process. Even in the simple case of the electromagnetic radiation of a slow electron deflected by a scatterer no such theory exists; nor do even the most radical attempts at altering electrodynamics give an answer which is finite and acceptable.[8] But precisely for this reason, attempts at treating meson radiation may not be entirely devoid of methodological interest, since effects of radiation reaction, which in electrodynamics may be small and only barely susceptible to observation, are here of decisive importance.

For analogy, we may be guided by the problem of electromagnetic radiation. Here, as Bloch and Nordsieck first showed, the problem can be very simply treated insofar as one may make three assumptions: (1) the collision time is short compared to the periods of the emitted radiation; (2) the effect of the emitted radiation, in particular its recoil, on the source may be neglected; (3) only those components of the radiation field will be considered for which these conditions are satisfied. The difficulties, of course, arise from the fact that in any radiation problem, the "virtual" effects of components for which conditions 1 and 2 are not satisfied cannot legitimately be ignored. When these three conditions are fulfilled, one has two simple results: The radiated spectrum can be obtained as the difference between the quasi-static fields of the radiator as it is and as it should be after the scattering process, and (2) the total probability of collision is not altered, though collisions are now accompanied by the emission of radiation, which would have been regarded as elastic had not the coupling with the radiation field been considered.

In the following we shall attempt to develop methods based on the three assumptions above, and appropriate to meson-producing collisions. To this end, we shall first modify the Bloch-Nordsieck method of canonical transformation to make it apply to characteristic meson fields. As is well known, this means physically regarding the nucleon, plus its quasi-static field, as the elementary ingredient of the collision rather than the bare nucleon itself. Although it is easy to carry through these calculations, they may nevertheless leave something to be desired, and that for the following reason: in nuclear impacts and for the emission of mesons, the spin and isotopic spin of the nucleons change. On the one hand, these changes cannot be consistently taken into account by a theory which neglects the effects of radiation on the source. On the other hand, just these changes in spin would appear to be decisive for the course of the collision. For this reason we have supplemented the Bloch-Nordsieck treatment by a species of perturbation theory, which in the electromagnetic case would itself be its equivalent, and which again exploits, but to a more limited extent, the statistical independence of the emission process. In this treatment we considered the process of emitting a fixed number of mesons, and calculated its

[7] M. M. Mills and R. F. Christy, Phys. Rev. **71**, 275 (1947).

[8] W. Pauli, Helv. Phys. Acta **19**, 234 (1946); H. A. Bethe and J. R. Oppenheimer, Phys. Rev. **70**, 451 (1946). *Note added in proof:* Recently, in connection with the work of Lamb, Schwinger, Bethe and Weisskopf on the term shifts of hydrogen, one of us (H. W. L.) has solved this problem (Physical Review; to be published). The extension of this work to meson problems clearly deserves intensive study. It is to be hoped that it makes many of the assumptions of this paper unnecessary.

cross section to the lowest order in all coupling constants in which it appears in the formal treatment. We then compare the cross sections for various numbers of mesons emitted, always working in their lowest order. We *assume* that although these absolute cross sections are manifestly meaningless, their ratios are correctly given by this means of calculation. In fact, this assumption means that all calculated cross sections will be reduced by the effects of radiation damping, so that, as in the electromagnetic case, the sum of all cross sections is the same as we would obtain for the elastic cross section with the neglect of radiation processes and, further, that the factor by which the calculated cross section must be reduced varies not at all, or only slowly, with the number of mesons emitted. It is clear that quite apart from deeper questions, some consideration needs to be given to the momentum relations in these collisions, since collisions involving large transfers of momentum from one nucleon to another can take place only for correspondingly small impact parameters. Some comments on this point will be found in the course of the actual calculations.

Thus the calculations which follow make no pretense to an estimate of total cross sections, but take these over from the estimate of the probability of the corresponding elastic collisions. It may be agreed that on the basis of what is known about nuclear forces and of the measurement on the collisions of 100-million volt neutrons with protons and neutrons,[9] the cross section observed for the cosmic-ray processes would seem to be a reasonable extrapolation. In fact, if one assumes that there are no serious singularities in the potentials between neutrons and protons, and adjusts their range and strength to agree with nuclear experience, one obtains elastic cross sections in the relativistic domain which are constant, and have the value of about 10^{-26} cm^2 per nucleon. This is in reasonable enough accord with cosmic-ray experience.

One final comment may perhaps be appropriate. These calculations have been carried out in the relativistic domain, that is, where the primary energies are large compared to a billion volts; this has been done in part in an attempt to make the results applicable to the great auger showers, and this in turn in part because this application of theory extends to the most intense fields and the smallest distances. Since it will be clear from the following calculations that in theories like the scalar theory, where these fields are only moderate, one does not obtain a high and increasing multiplicity of meson production, the question arises as to what meaning to ascribe to the enormously greater field strengths characteristic, e.g., of the pseudoscalar, or pair, theories. For certainly we know one thing: the nucleon response to these fields gives no direct evidence of their existence; the nucleons act as though the forces between them were free of important singularities, not only in the normal phenomena of nuclear physics, but even by the collisions of 100-million volt nucleons, where quite small momentum exchanges are the rule. Nevertheless, the possibility should not be overlooked that these strong fields may have meaning, in the sense that they can be radiated under suitable circumstances, and yet not be susceptible of familiar interpretation in terms of the behavior of the nucleons which are subject to them. Much will have to be learned before even the partial validity of this notion can be regarded as established.

In summary of the results of the calculations which have just briefly been described, it may be said that a scalar theory gives an energy independent, and, in general, a small multiplicity of production; that a theory which involves no internal change in the nucleons when they scatter each other, such as charge or spin exchange, will give a very small probability of radiation; that the symmetrical pseudoscalar theory, and a similar formulation of pair theory, do in fact give large probabilities and large multiplicity of meson production; and that in the forms here considered, and at extremely high energies, the multiplicity rises with the cube root of the primary energy. Some physical applications of these results are discussed in a quite tentative way in Section IV of the paper.

II. BLOCH-NORDSIECK METHOD

A. Symmetrical Scalar Theory

We will now treat the collision of two nucleons in the symmetrical scalar theory by a method

[9] We are indebted to Dr. E. MacMillan for information on n–p and n–n *total* cross sections at about 90 Mev.

similar to that of Bloch and Nordsieck. The meson field will be considered to interact with the nucleon through the latter's isotopic spin, which will be treated classically. A canonical transformation will be performed to find the quasi-static meson field associated with the nucleon for a definite orientation of its isotopic spin (definite charge state). We will describe charge exchange in the collision by introducing a potential, V, which can change the isotopic spin of the nucleons in the collision. The corresponding change in the quasi-static field appropriate to the isotopic spin orientation will give us the radiation in the collision. Thus the primary interaction between nucleons could, for instance, be of the form $(\tau_1\cdot\tau_2)V(r)$; of V we shall assume that its Fourier transform tends to zero for momenta $\gg\mu c$. As will be obvious, we should obtain no radiation (in the approximation here considered) were we to omit the charge exchange $(\tau_1\cdot\tau_2)$ from the interaction. It should further be observed that here we neither assume nor deny that the interaction can be derived from the meson interactions themselves. Following Bloch and Nordsieck,[10] we use the Dirac equation for the heavy particle coupled to the meson field, and neglect recoils. The Hamiltonian is then,*

$$H=\boldsymbol{\alpha}\cdot\mathbf{P}+\beta M+\sum_{\alpha k}\frac{k_0}{2}(Q_{k\alpha}^2+P_{k\alpha}^2)$$
$$+\beta g(4\pi)^{\frac{1}{2}}\sum_{\alpha k}\frac{\tau_\alpha}{k_0^{\frac{1}{2}}}(Q_{k\alpha}\sin\mathbf{k}\cdot\mathbf{r}+P_{k\alpha}\cos\mathbf{k}\cdot\mathbf{r}) \quad (1)$$

which, by the Bloch-Nordsieck argument,** can be replaced by its positive energy part,

$$H=\mathbf{v}\cdot\mathbf{P}+\frac{M}{\gamma}+\sum_{\alpha k}\frac{k_0}{2}(Q_{k\alpha}^2+P_{n\alpha}^2)$$
$$+\frac{g}{\gamma}(4\pi)^{\frac{1}{2}}\sum_{\alpha k}\frac{\tau_\alpha}{k_0^{\frac{1}{2}}}(Q_{k\alpha}\sin\mathbf{k}\cdot\mathbf{r}+P_{k\alpha}\cos\mathbf{k}\cdot\mathbf{r}), \quad (2)$$

where the isotopic spin vector τ is treated as a classical unit vector. M is the mass of the heavy particle, and the meson field is represented by

$$\varphi_\alpha=\sum_k k_0^{-\frac{1}{2}}(Q_{k\alpha}\sin\mathbf{k}\cdot\mathbf{r}+P_{k\alpha}\cos\mathbf{k}\cdot\mathbf{r}), \quad (3)$$

where the $Q_{k\alpha}$ and $P_{k\alpha}$ are canonically conjugate.

We make the canonical transformation

$$\begin{aligned}&P_{k\alpha}=P_{k\alpha}'-a_{k\alpha}\cos\mathbf{k}\cdot\mathbf{r}',\\&Q_{k\alpha}=Q_{k\alpha}'-a_{k\alpha}\sin\mathbf{k}\cdot\mathbf{r}',\\&\mathbf{r}=\mathbf{r}',\\&\mathbf{P}=\mathbf{P}'+\sum_{\alpha k}\mathbf{k}a_{k\alpha}(Q_{k\alpha}'\sin\mathbf{k}\cdot\mathbf{r}'\\&\qquad+P_{k\alpha}'\cos\mathbf{k}\cdot\mathbf{r}'-\tfrac{1}{2}a_{k\alpha}),\end{aligned} \quad (4)$$

with

$$a_{k\alpha}=\frac{g\tau_\alpha(4\pi/k_0)^{\frac{1}{2}}}{\gamma(k_0-\mathbf{v}\cdot\mathbf{k})},$$

obtaining finally, for the transformed wave equation,

$$\left\{\mathbf{v}\cdot\mathbf{P}'+\frac{M}{\gamma}+\sum_{\alpha k}\frac{k_0}{2}(Q_{k\alpha}^2+P_{k\alpha}^2)\right.$$
$$\left.-\sum_k\frac{2\pi g^2}{\gamma^2(k_0-\mathbf{v}\cdot\mathbf{k})}-E\right\}u'(\mathbf{r}',Q_{k\alpha}')=0, \quad (5)$$

whose solution is

$$u'=\chi\exp[iM\gamma\mathbf{v}\cdot\mathbf{r}']\prod_{\alpha k}h_{m\alpha k}(Q_{k\alpha}'), \quad (6)$$

where χ is a normalized spinor, and the $h_{m\alpha k}$ are normalized Hermite polynomials.

Now, transforming back to the old coordinates, we have

$$u(\mathbf{r},Q_{k\alpha})=\chi\exp[iM\gamma\mathbf{v}\cdot\mathbf{r}]$$
$$\prod_{\alpha k}\exp[-ia_{k\alpha}\cos\mathbf{k}\cdot\mathbf{r}(Q_{k\alpha}+\tfrac{1}{2}a_{k\alpha}\sin\mathbf{k}\cdot\mathbf{r})$$
$$\times h_{m\alpha k}(Q_{k\alpha}+a_{k\alpha}\sin\mathbf{k}\cdot\mathbf{r}). \quad (7)$$

The cross section for scattering by a potential V, with emission of $n_{\alpha k}$ mesons in each mode $\alpha\mathbf{k}$, is

$$d\sigma=\frac{P_0Q_0Q}{P}\frac{d\Omega}{4\pi^2}|V_{PQ}|^2\prod_{\alpha k}\frac{w_{\alpha k}{}^{n_{\alpha k}}}{n_{\alpha k}!}e^{-w_{\alpha k}}, \quad (8)$$

where $(\mathbf{P},P_0)$ and $(\mathbf{Q},Q_0)$ are the initial and final momentum and energy of the nucleon, and

$$w_{\alpha k}=\frac{2\pi g^2(\Delta\tau_\alpha)^2}{\gamma^2k_0(k_0-\mathbf{v}\cdot\mathbf{k})^2}, \quad (9)$$

where $\Delta\tau_\alpha$ is the change in τ_α during the scattering process.

It should be observed that the term $e^{-w_{\alpha k}}$ above is independent of the $n_{\alpha k}$ and should be summed over all the modes available. This would

[10] F. Bloch and A. Nordsieck, Phys. Rev. **52**, 54 (1937).

* $c=\hbar=\mu=$ mass of the meson $=1$.

** It will be seen in Section III that virtual pair production does not play an important part in these processes. In (1), α and β are the usual Dirac matrices, $Q_{k\alpha}$ is the amplitude of the mode of the meson field with wave number $\mathbf{k}$ and charge coordinate α, $P_{k\alpha}$ is the momentum conjugate to $Q_{k\alpha}$, k_0 is $[1+k^2]^{\frac{1}{2}}$, and g^2 is the dimensionless coupling constant, γM is the energy of the nucleon.

make the total cross section zero, corresponding to the fact that the virtual emissions are not restricted by the energy conservation conditions. A similar result was found by Pauli and Fierz[11] for the electromagnetic case. However, the fact that this factor is independent of the n_{ak} means that its effect is to cut down the total cross section, but it does not affect the *ratio* of the probabilities of emitting N and $N+1$ mesons. We will *assume* that the inadequacy of the assumptions inherent in this method, as discussed in Section I, does not destroy this characteristic of the damping. In this way we can give sense to the calculation, since we will calculate only the most probable number of mesons emitted, and will attach no significance to the total cross section. Therefore we omit these terms, and all others that do not depend upon the number of emitted mesons. We also replace $n_{ak}!$ by 1, since the finite rest mass makes it unlikely that more than one meson will be emitted into any particular mode. We have, then,

$$\sigma \sim |V_{PQ}|^2 \prod_{ak} w_{ak}, \tag{10}$$

where the product is carried out over all the modes into which a meson is emitted.

Now to obtain the total cross section for the emission of N mesons, with total energy loss ϵ, this has to be summed over all the modes satisfying the energy loss condition. Thus

$$\sigma(N,\epsilon)d\epsilon \sim |V_{PQ}|^2 \left(\frac{g^2}{4\pi^2\gamma^2}\right)^N \sum \int \cdots \times \int \prod_n \frac{d\mathbf{k}_n}{k_{0n}(k_{0n}-\mathbf{v}\cdot\mathbf{k}_n)^2} \prod_\alpha \frac{(\Delta\tau_\alpha^2)^{N_\alpha}}{N_\alpha!}, \tag{11}$$

where the sum is taken over all N_α such that $\sum N_\alpha = N$, and the integral over the volume in momentum space corresponding to an energy loss between ϵ and $\epsilon+d\epsilon$.*** The $N_\alpha!$ arise from the indistinguishability of mesons of each type. We have, then,

$$\sigma(N,\epsilon)d\epsilon \sim |V_{PQ}|^2 \left(\frac{g^2}{2\pi\gamma^2}\right)^N \frac{(\Delta\tau^2)^N}{N!} \times \int \cdots \int \prod_n \frac{k_n dk_{0n} d\mu_n}{(k_{0n}-v\mu_n k_n)^2}, \tag{12}$$

where μ_n is the cosine of the angle the nth meson makes with the direction of motion of the nucleon. Now, in order to find the limits of integration, it is necessary to take into account the longitudinal momentum transfer from the other nucleon (for which exactly these same considerations hold, provided we are in a coordinate system in which each nucleon is near the speed of light).

If the momentum transfer between the nucleons is $\mathbf{K}$, then the equations of conservation of energy and momentum are

$$\begin{aligned} \Delta P_{1z} &= -\sum^{N_1} k_z - K_z, \\ \Delta P_{2z} &= -\sum^{N_2} k_z + K_z, \\ \Delta E_1 &= -\epsilon_1 = \mathbf{v}_1 \cdot \Delta \mathbf{P}_1 = -v_1 \sum^{N_1} k_z - v_1 K_z, \\ \Delta E_2 &= -\epsilon_2 = \mathbf{v}_2 \cdot \Delta \mathbf{P}_2 = v_2 \sum^{N_2} k_z - v_2 K_z, \end{aligned} \tag{13}$$

where the z axis is taken along the direction of motion of the first nucleon. Thus, since

$$\begin{aligned} \sum^N k_{0n} &= \epsilon_1 + \epsilon_2, \\ \epsilon_1 &= \frac{v_1}{v_1+v_2} \sum^N (k_{0n} + v_2 k_{zn}) = \sum^N \alpha_n, \\ \epsilon_2 &= \frac{v_2}{v_1+v_2} \sum^N (k_{0n} - v_1 k_{zn}) = \sum^N \beta_n. \end{aligned} \tag{14}$$

Now making the transformation from μ_n, k_{0n} to α_n, β_n we have, since

$$k dk_0 d\mu = \frac{v_1+v_2}{v_1 v_2} d\alpha d\beta \sim 2 d\alpha d\beta,$$

$$\sigma(N_1 N_2 \epsilon_1 \epsilon_2) d\epsilon_1 d\epsilon_2 \sim |V(K_z)|^2 \left(\frac{g^2}{4\pi}\right)^{N_1+N_2} \times \frac{(\Delta\tau_1^2)^{N_1}(\Delta\tau_2^2)^{N_2}}{\gamma_1^{2N_1}\gamma_2^{2N_2} N_1! N_2!} \int \cdots \int \prod_n \frac{d\alpha_n d\beta_n}{(\alpha_n^2)^{N_2}(\beta_n^2)^{N_1}}, \tag{15}$$

where in the denominator α^2 appears for each meson emitted by the second nucleon, and β^2 for each emitted by the first. The integration is over the sheet

$$\epsilon_1 \leqslant \sum^N \alpha_n \leqslant \epsilon_1 + d\epsilon_1, \quad \epsilon_2 \leqslant \sum^N \beta_n \leqslant \epsilon_2 + d\epsilon_2. \tag{16}$$

For ϵ_1 and ϵ_2 large compared to μc^2, the integral

[11] W. Pauli and M. Fierz, Nuovo Cimento **15**, 167 (1938).

*** It should be noted that the continuous decrease in γ affects only the absolute magnitude of the cross section, so that the initial value may be used here.

in (15) becomes

$$\int\cdots\int\prod^{N_1}\left(\frac{4\gamma_1^2\alpha_n d\alpha_n}{\alpha_n^2+\gamma_1^2}\right)\cdot\prod^{N_2}\left(\frac{4\gamma_2^2\beta_n d\beta_n}{\beta_n^2+\gamma_2^2}\right),$$

since for a given α the lower limit of β is $(\alpha^2+\gamma_1^2)/4\alpha\gamma_1^2$, and inversely. This can be approximately evaluated when $\epsilon_1/N_1\gamma_1$ and $\epsilon_2/N_2\gamma_2$ are either much less than or much greater than one. We shall see that the most probable multiplicity and energy losses occur in the latter region, so we will evaluate the integral in that case. The major contributions will then come from $\alpha_n\sim\epsilon_1/N_1$, $\beta_n\sim\epsilon_2/N_2$, and the integral becomes, in this limit,

$$4^N\gamma_1^{2N_1}\gamma_2^{2N_2}\left(\ln\frac{\epsilon_1}{\gamma_1}\right)^{N_1-1}\left(\ln\frac{\epsilon_2}{\gamma_2}\right)^{N_2-1}\frac{N_1N_2}{\epsilon_1\epsilon_2}d\epsilon_1 d\epsilon_2.$$

Thus

$$\sigma(N_1N_2\epsilon_1\epsilon_2)d\epsilon_1 d\epsilon_2\sim|V(K_z)|^2\times\left(\frac{g^2}{\pi}\right)^N\frac{N_1N_2}{\epsilon_1\epsilon_2}(\Delta\tau_1^2)^{N_1}(\Delta\tau_2^2)^{N_2}\times\frac{(\ln\epsilon_1/\gamma_1)^{N_1-1}}{N_1!}\frac{(\ln\epsilon_2/\gamma_2)^{N_2-1}}{N_2!}d\epsilon_1 d\epsilon_2. \quad (17)$$

Now to account for the different distributions of the mesons among the nucleons, this has to be multiplied by the binomial coefficient $C_{N_1}{}^N$, and summed over N_1 to obtain the cross section for the emission of N mesons, with energy losses ϵ_1 and ϵ_2.

$$\sigma(N\epsilon_1\epsilon_2)d\epsilon_1 d\epsilon_2\sim\left(\frac{g^2}{\pi}\right)^N N!\sum_{N_1=0}^{N}|V(K_z)|^2\times\frac{N_1N_2}{\epsilon_1\epsilon_2}(\Delta\tau_1^2)^{N_1}(\Delta\tau_2^2)^{N_2}\times\frac{(\ln\epsilon_1/\gamma_1)^{N_1-1}}{N_1!^2}\frac{(\ln\epsilon_2/\gamma_2)^{N_2-1}}{N_2!^2}d\epsilon_1 d\epsilon_2. \quad (18)$$

The $|V|^2$ is placed inside the sum, since, from (13), setting $v_1\sim v_2\sim c$,

$$2K_z=\epsilon_1+\epsilon_2+\sum^{N_2}k_z-\sum^{N_1}k_z=\epsilon_1+\epsilon_2-\sum^{N}k_{\|n}, \quad (19)$$

so that the longitudinal momentum transfer required depends upon the distribution of the mesons between the nucleons. We can obtain an idea of what is required by using the average values of the k_{zn} as given by the distribution (11).

Here the resonance denominators force the emissions to be forward for the most part, and K_z is of the order $N\mu c$. Now our assumption that both nucleons are moving near the speed of light requires us, for large energy losses, to work in a coordinate system in which neither nucleon reverses its direction of motion. For large equal energy losses this is the center of mass system. We therefore† go into the center of mass system, setting $\gamma_1=\gamma_2=\gamma$, and suppose that $N\ll\gamma$. This corresponds to the condition that the mesons emitted have energies greater than Mc^2. The Fourier analysis of the scattering potential should be flat up to momentum transfers of order $\gamma\mu c$, so that the $|V|^2$ can now be taken out of the sum.

Integrating over-all energy losses, we obtain

$$\sigma(N)\sim\left(\frac{g^2}{\pi}\right)^N N!\left(\ln\frac{\epsilon_{\max}}{\gamma}\right)^N\sum_{N_1=0}^{N}\frac{(\Delta\tau_1^2)^{N_1}(\Delta\tau_2^2)^{N_2}}{N_1!N_2!}, \quad (20)$$

where $\epsilon_{\max}$ is the maximum energy a nucleon can lose in the center of mass system. This probably is somewhere between $(\gamma-1)M$ and $(\gamma-2)M$, since the nucleon does not convert its rest energy into mesons, and probably stops appreciable emissions when its velocity becomes sensibly less than that of light. Thus this factor becomes $\ln M/\mu$ for high energies, greater than around 10^{11} volts.

Now for a symmetrical potential of the form $(\tau_1\cdot\tau_2)V(r)$ as is given by the symmetrical meson theories, $\tau_1+\tau_2$ is a constant of the motion in a scattering process, so $\Delta\tau_1=-\Delta\tau_2=\Delta\tau$, and, since the sum in (20) may be replaced to sufficient accuracy by its largest term, we have,

$$\sigma(N)\sim\left(\frac{4g^2\Delta\tau^2}{\pi}\right)^N\frac{1}{N!}\left(\ln\frac{\epsilon_{\max}}{\gamma}\right)^N, \quad (21)$$

since $(\frac{1}{2}N)!\sim 2^{-N/2}(N!)^{\frac{1}{2}}$. This is valid for $N<\epsilon_{\max}/\gamma$. The cross section has a maximum at

$$\bar{N}=\frac{4g^2\Delta\tau^2}{\pi}\ln\frac{\epsilon_{\max}}{\gamma}, \quad (22)$$

which is small for most reasonable values of g^2, and gives a most probable multiplicity which

† Thus, if E_0 is the primary energy,

$$\gamma M=[\tfrac{1}{2}M(E^0+M)]^{\frac{1}{2}}.$$

does not increase with energy.†† This corresponds to the fact that the scalar meson field has only a r^{-1} singularity near the source, and contains only a logarithmically infinite number of mesons.

B. Symmetrical Pseudoscalar Theory

We will now use essentially the same method to treat the case of a symmetrical pseudoscalar field, which is different from the scalar theory in two respects. First, we will use a coupling in which both the isotopic and ordinary spins appear, so that changes in either one can cause meson emission. Second, we will use a gradient coupling so that the quasi-static field has a worse singularity near the source than was the case for the scalar field ($1/r^2$ instead of $1/r$). As we will see, this latter leads to a more copious meson emission, corresponding to the much stronger meson-field strengths in the vicinity of the source. We will suppose that the internucleonic potential can effect either ordinary or isotopic spin changes, but that it is free of singularities—and its Fourier transform small for $k \gg \mu c$—as would not be the case were the interaction to be derived directly from the meson fields; such singular interaction can clearly not be treated as small. The procedure is then exactly analogous to that for the scalar field, with the Namiltonian

$$H=\boldsymbol{\alpha}\cdot\mathbf{P}+\beta M+\sum_{\alpha k}\frac{k_0}{2}(Q_{k\alpha}^2+P_{k\alpha}^2)+g(4\pi)^{\frac{1}{2}}\sum_{\alpha k}\frac{\tau_\alpha}{k_0^{\frac{1}{2}}}(\boldsymbol{\sigma}\cdot\mathbf{k}-\gamma_5 k_0)\times(Q_{k\alpha}\cos\mathbf{k}\cdot\mathbf{r}-P_{k\alpha}\sin\mathbf{k}\cdot\mathbf{r}), \quad (23)$$

which can be replaced by

$$H=\mathbf{v}\cdot\mathbf{P}+\frac{M}{\gamma}+\sum_{\alpha k}\frac{k_0}{2}(Q_{k\alpha}^2+P_{k\alpha}^2)-g(4\pi)^{\frac{1}{2}}\sum_{\alpha k}\frac{\tau_\alpha\sigma_{||}}{k_0^{\frac{1}{2}}}(k_0-k_{||})\times(Q_{k\alpha}\cos\mathbf{k}\cdot\mathbf{r}-P_{k\alpha}\sin\mathbf{k}\cdot\mathbf{r}) \quad (24)$$

for $v\sim c$. The canonical transformation is similar to the scalar one, and we obtain again

$$\sigma\sim|V_{PQ}|^2\prod v_{\alpha k}, \quad (25)$$

where now

$$v_{\alpha k}=(2\pi g^2/k_0)[\Delta(\tau_\alpha\sigma_{||})]^2, \quad (26)$$

so that

$$\sigma(N_1N_2\epsilon_1\epsilon_2)d\epsilon_1d\epsilon_2\sim|V(K_s)|^2\left(\frac{g^2}{\pi}\right)^N\frac{q_1^{N_1}q_2^{N_2}}{N_1!N_2!}\times\int\cdots\int\prod^N d\alpha_n d\beta_n, \quad (27)$$

where

$$q=\sum_\alpha[\Delta(\tau_\alpha\sigma_{||})]^2.$$

The integration yields,

$$\sigma(N_1N_2\epsilon_1\epsilon_2)d\epsilon_1d\epsilon_2\sim|V(K_s)|^2\left(\frac{g^2}{\pi}\right)^N\frac{q_1^{N_1}q_2^{N_2}}{N_1!N_2!}\times N^2\frac{(\epsilon_1\epsilon_2)^{N-1}}{N!^2}d\epsilon_1d\epsilon_2. \quad (28)$$

Again multiplying by CN_1^N and summing, we have

$$\sigma(N\epsilon_1\epsilon_2)d\epsilon_1d\epsilon_2\sim\left(\frac{g^2}{\pi}\right)^N\frac{N^2(\epsilon_1\epsilon_2)^{N-1}}{N!}d\epsilon_1d\epsilon_2\sum_{N_1=0}^{N}|V(K_s)|^2\frac{q_1^{N_1}q_2^{N_2}}{(N_1!N_2!)^2}. \quad (29)$$

Now, however, for large energy losses in the center of mass system the spherical symmetry gives

$$K_s\sim\tfrac{1}{2}(\epsilon_1+\epsilon_2),$$

which can be as large as $\epsilon_{\max}$, which is larger than $\gamma\mu c$ for incident proton energies greater than about 5×10^{10} ev. However, the spherical symmetry also makes the momentum transfer independent of the distribution of the mesons between the two nucleons, so that the matrix element can be taken out of the summation, and we will return to the question of the large momentum transfers below.

Replacing the sum, as before, by its largest term, which occurs at $N_1=f_1N$ and $N_2=f_2N$, where $f_1=q_1/(q_1+q_2)$ and $f_2=q_2/(q_1+q_2)$, we have

$$\sigma(N\epsilon_1\epsilon_2)d\epsilon_1d\epsilon_2\sim\left(\frac{g^2}{\pi}\right)^N\frac{N^2(\epsilon_1\epsilon_2)^{N-1}}{N!^3}\left(\frac{q_1+q_2}{f_1^{f_1}f_2^{f_2}}\right)^N d\epsilon_1d\epsilon_2, \quad (30)$$

†† Were we to assume very large values of g^2, we should have the other limiting case $N\gg\epsilon_{\max}/\gamma$; here (21) would be replaced by

$$\sigma(N)\sim\left(\frac{4g^2M^2\Delta\tau^2}{\pi}\right)^N\left(\frac{\epsilon_{\max}}{\gamma M}\right)^{2N}\frac{1}{N!^3}, \quad (21a)$$

which yields

$$\bar{N}\sim(4g^2\Delta\tau^2\epsilon_{\max}^2/\pi\gamma^2)^{\frac{1}{2}},$$

which, though large for large enough g^2, still does not increase with increasing energy.

and, integrating over-all energy losses in the center of mass system,

$$\sigma(N)\sim\left(\frac{g^2}{\pi}\right)^N\frac{\epsilon_{\max}{}^{2N}}{N!^3}\left(\frac{q_1+q_2}{f_1{}^{f_1}f_2{}^{f_2}}\right)^N, \quad (31)$$

(31) has a maximum at

$$\bar{N}=\left(\frac{g^2\gamma^2M^2}{\pi}\right)^{\frac{1}{4}}\left(\frac{q_1+q_2}{f_1{}^{f_1}f_2{}^{f_2}}\right)^{\frac{1}{4}}\left(\frac{\epsilon_{\max}}{\gamma M}\right)^{\frac{1}{4}} \quad (32)$$

which increases as $\gamma^{\frac{1}{4}}$ or as the cube root of the primary energy. This corresponds to the inverse square singularity of the pseudoscalar meson field, which gives an unlimited supply of mesons. We have assumed that the $|V(K_s)|^2$ varies more slowly with N than the other factors, even in the region of large momentum transfers.

We note, for future reference, that the case of a neutral pseudoscalar field is obtained by setting $f_1=f_2=\frac{1}{2}$, and $q_1=q_2=[\Delta(\tau_s\sigma_{||})]^2$, for the case of a symmetrical interaction between the nucleons. Thus, the cross section becomes,

$$\sigma(N)=\left(\frac{4g^2}{\pi}\right)^N\frac{\epsilon_{\max}{}^{2N}}{(N!)^3}[\Delta(\tau_s\sigma_{||})]^{2N}$$

and gives

$$\bar{N}=\left(\frac{4g^2\gamma^2M^2}{\pi}\right)^{\frac{1}{4}}[\Delta(\tau_z\sigma_{||})]^{\frac{1}{4}}\left(\frac{\epsilon_{\max}}{\gamma M}\right)^{\frac{1}{4}}. \quad (32a)$$

We note also that the number of mesons of each charge type depends upon the change in $\tau_\alpha\sigma_{||}$ so that with a potential that doesn't discriminate among the different τ_α we should expect that an average of one-third of the mesons would be neutral, and two-thirds charged.

C. Comparison and Total Cross Section

The preceding considerations have illustrated a number of general features of the radiation process. First, it is clear from the method, as well as from the examples, that the radiation occurs through a change in the source—in particular, a change in some feature of the source to which the meson field is coupled. Thus the scalar field can be radiated by a change in the isotopic spin of the source, and the pseudoscalar by a change in either the ordinary or isotopic spin.

Secondly, the number of mesons emitted is largely determined by the number previously existing in the virtual field. Therefore, in order to obtain an appreciably energy-dependent multiplicity of production, we must have a badly singular meson field (worse than $1/r$), and cannot cut off the singularity except at very short distances. This makes the self-energy and nuclear forces difficulties acute, and a quantitative discussion of the cut-off question will be deferred to Section IV.

Another difference between the scalar and pseudoscalar theories is in the angular distribution of the emitted mesons. For the scalar case the average perpendicular momentum of an emitted meson is of order μc, whereas for the pseudoscalar mesons the distribution is spherically symmetric in the center of mass system. This has the consequence that the emission of scalar mesons requires only a small momentum exchange between the nucleons, and the absolute cross section is not limited by this. Thus we might suppose that the total cross section for inelastic scattering is of the same order as that for elastic scattering, around $(\hbar/\mu c)^2$, which is in rough accord with the data on the absorption of primaries at the top of the atmosphere.

On the other hand, the pseudosclar mesons require a momentum exchange between the nucleons of the order γMc in the center of mass system, and, if the potential between them is similar to a Lorentz-contracted Yukawa well, this means an impact parameter $\hbar/Mc$. However, this extreme situation obtains only for energies greater than around 10-in. volts. For lower energies the factor $\epsilon_{\max}/\gamma M$ becomes important, and the important impact parameters become of order $\hbar c\gamma/\epsilon_{\max}$ which increases the cross section somewhat. Thus, at 10^{10} volts primary energy, $\epsilon_{\max}$ is perhaps 3 to $5\mu c^2$ and $\hbar c\gamma/\epsilon_{\max}\sim\frac{1}{2}\hbar/\mu c$, which is not too small.

The evaluation of the physical consequences of these considerations is not unambiguous. For they show that only for close impact ($<\hbar/Mc$ for extremely high energies) can probabilities of meson emission be regarded as statistically independent; and only to this case are the methods of this paper applicable. For the more distant collisions, in which large momentum

transfers are not readily available, there are two possibilities: either the statistical independence upon which the methods of this paper are based will be maintained, in which case such distant collisions will not, in general, be accompanied by radiation. Or the requirement of small momentum transfers may force correlations among the successive emissions, in which case the methods here used are no longer applicable. However, one might schematize the correlations by supposing, for example, that the volume in momentum space available to the mesons is decreased by the momentum transfer requirement. In order, for instance, to cut down the momentum transfer from γMc to $\gamma\mu c$, a factor of roughly ten, the emissions might be concentrated forward, into about one-fifth of the previously available momentum space per meson. Thus a factor of $1/5^N$ might be introduced into Eq. (31), and 5^{-1} or 0.6 into Eq. (32).

Although present theoretical methods do not settle which alternative will be realized, the experimental evidence for auger showers shows that even at these energies the cross sections for converting primary into cascade radiation are still of the order of 1/100 barn per nucleon.

We also note that 'cut-off' procedures in the meson fields would tend to concentrate the emissions forward, level off the multiplicity as a function of energy, and decrease the required momentum transfer between the nucleons.

We may also note some more general features of the multiplicity laws. The fact that the differential cross section must be a relativistic invariant, for all numbers of mesons emitted, means, in the case of statistical independence of the successive emissions, that that part of the cross section which involves the meson emission must be a product of invariant factors. Thus, in the scalar case we have

$$\Pi \frac{d\mathbf{k}_n}{k_{0n}\gamma^2(k_{0n}-\mathbf{v}\cdot\mathbf{k}_n)^2},$$

and in the pseudoscalar $\prod d\mathbf{k}_n/k_{0n}$. In the case where the emissions are statistically independent, (and only in this case) the cross section will break up into a product. Since only the two four-vectors $(\mathbf{k}, k_0)$ and $(\mathbf{P}, E)$ can appear, the cross section must then have the form

$$\Pi \frac{d\mathbf{k}_n}{k_{0n}} f[\gamma(k_{0n}-\mathbf{v}\cdot\mathbf{k}_n)].$$

The two cases studies so far correspond to $f(x)$ a simple power, $f(x)=1/x^2$ for the scalar theory, and $f(x)=1$ for the pseudoscalar, For a general case $f(x)=x^\nu$, some of the properties of the solution are immediately clear. First, for ν negative the emissions are concentrated in a forward direction, increasingly so as ν becomes more negative. For $\nu=0$, we have spherically symmetric emissions in the center of mass system, and for $\nu>0$ the mesons tend to be concentrated backward somewhat. One can do the integrations over the momentum space roughly, and finds that, for $\nu \geqslant 0$, $\sigma(N)\sim\gamma^{(2\nu+2)N}/N!^{3+\nu}$, apart from numerical factors. The case of the pseudoscalar field corresponds to $\nu=0$.

If ν is less than zero, the cross section behaves as const./$N!^{3+\nu}$ for $N\ll M/\mu$, and const./$N!^{1-\nu}$ for $N\gg M/\mu$, so that no negative values of ν give a multiplicity which varies appreciably with energy. The scalar field corresponds to $\nu=-2$. As ν increases, the multiplicity will also tend to increase more rapidly with energy.

III. PERTURBATION METHOD

A. Neutral Pseudoscalar

Now, in order to take into account the quantum properties of the ordinary and isotopic spin in a more consistent manner, we will treat the case of a neutral pseudoscalar field by a sort of perturbation theory,[12] giving an explicit form to the spin and isotopic spin dependence of the potential function. In the electromagnetic case this would be the formal equivalent of the Bloch-Nordsieck method. We will use the Born approximation, in the sense that each process will be considered only in the first order in which it occurs, and we will use a potential function proportional to $(\boldsymbol{\tau}\cdot\mathbf{T})(\boldsymbol{\sigma}\cdot\boldsymbol{\Sigma}-\gamma_5\Gamma_5)$, which has the property of flipping either the spin or isotopic spin of the nucleons. Here, as later, the small Greek letters refer to the first nucleon, and the large ones to the second. The matrix elements for the emission of a meson by the first or second

[12] We are indebted to Dr. H. A. Bethe for helpful methodological discussions during the early part of this work.

nucleon, respectively, are

$$g\left(\frac{2\pi}{k_0}\right)^{\frac{1}{2}}\tau_z\sigma_{||}(k_0-k_z),$$
$$g\left(\frac{2\pi}{k_0}\right)^{\frac{1}{2}}T_z\Sigma_{||}(k_0+k_z), \tag{33}$$

where, as before, the pair-producing parts have been omitted, and the nucleons have been supposed near the speed of light. We take only the even parts since the large energy denominators associated with pair production will cut down the contribution of the odd parts as $1/\gamma$ so that one can neglect them.

The matrix element for the emission of N_1 and N_2 mesons by the first and second nucleon, respectively, is

$$H=\frac{(2\pi g^2)^{N/2}\prod_n b_n}{\prod_n k_{0n}^{\frac{1}{2}}}\times\sum\frac{\chi_f^*\Lambda_f\sigma_{||}\tau_z\Sigma_{||}T_z\cdots V_{\text{scatt}}\sigma_{||}\tau_z\cdots\Lambda_i\chi_i}{\text{energy denominators}}, \tag{34}$$

where χ_i and χ_f are the initial and final state spinors (each for two nucleons), Λ_i and Λ_f are the corresponding projection operators, and b_n is $k_{0n}-k_{zn}$ for a meson emitted by the first nucleon, and $k_{0n}+k_{zn}$ for one emitted by the second nucleon. The energy denominators are of the form

$$b_1(b_1+b_2)\cdots(-b_{N-1}-b_N)(-b_N),$$

where the break occurs at the scattering act. If there are n_1 emissions by the first nucleon before the scattering, and n_2 by the second, then the sum is over n_1, n_2, the combinations of n_1 and n_2 mesons, and all the permutations of the emissions before and after the scattering. Since the $\sigma_{||}$, $\Sigma_{||}$, τ_z, and T_z all commute, the sum over permutations is done directly, and with

$$\sum_{\text{Perm}}\frac{1}{b_1(b_1+b_2)(b_1+b_2+b_3)\cdots}=\frac{1}{\prod_n b_n}$$

yields

$$H=\frac{(2\pi g^2)^{N/2}}{\prod_n k_{0n}^{\frac{1}{2}}}\sum[(-)^{n_1+n_2}\chi_f^*\Lambda_f(\sigma_{||}\tau_z)^{N_1-n_1}\times(\Sigma_{||}T_z)^{N_2-n_2}V_{\text{scatt}}(\sigma_{||}\tau_z)^{n_1}(\Sigma_{||}T_z)^{n_2}\Lambda_i\chi_i]. \tag{35}$$

Now the operator part of V_{scatt} can be broken up into a part that commutes with the $\sigma_{||}\tau_z$ and a part that anticommutes. Thus

$$(\boldsymbol{\tau}\cdot\mathbf{T})(\boldsymbol{\sigma}\cdot\boldsymbol{\Sigma}-\gamma_5\Gamma_5)=[\tau_zT_z(\sigma_z\Sigma_z-\gamma_5\Gamma_5)+(\boldsymbol{\tau}_\perp\cdot\mathbf{T}_\perp)(\boldsymbol{\sigma}_\perp\cdot\boldsymbol{\Sigma}_\perp)]+[\tau_zT_z(\boldsymbol{\sigma}_\perp\cdot\boldsymbol{\Sigma}_\perp)+(\boldsymbol{\tau}_\perp\cdot\mathbf{T}_\perp)\sigma_z\Sigma_z] \tag{36}$$

and, calling the former of these A^+ and the latter A^-, we have

$$H=V(K_z)\frac{(2\pi g^2)^{N/2}}{\prod_n k_{0n}^{\frac{1}{2}}}\{\chi_f^*\Lambda_f(\sigma_{||}\tau_z)^{N_1}(\Sigma_{||}T_z)^{N_2}\times\sum[(-)^{n_1+n_2}A^++A^-]\Lambda_i\chi_i\}, \tag{37}$$

where

$$\Sigma[(-)^{n_1+n_2}A^++A^-]=\sum_{n_1n_2}C_{n_1}^{N_1}C_{n_2}^{N_2}[(-)^{n_1+n_2}A^++A^-]=2^NA^-.$$

The loss of the A^+ means that only that part of the potential that can flip either the spin or isotopic spin of the nucleons is effective in causing radiation. We have then,

$$H=V(K_z)\frac{(8\pi g^2)^{N/2}}{\prod_n k_{0n}^{\frac{1}{2}}}[\chi_f^*\Lambda_f(\sigma_{||}\tau_z)^{N_1}\times(\Sigma_{||}T_z)^{N_2}A^-\Lambda_i\chi_i]. \tag{38}$$

Squaring, then averaging over the initial and summing over the final spins (ordinary and isotopic), we have

$$|H|^2=\tfrac{1}{16}|V(K_z)|^2\frac{(8\pi g^2)^N}{\prod_n k_{0n}}Sp[\Lambda_fA^-\Lambda_iA^-]. \tag{39}$$

The spur is non-vanishing, and independent of the N, so

$$|H|^2\sim|V(K_z)|^2\frac{(8\pi g^2)^N}{\prod_n k_{0n}}, \tag{40}$$

and

$$d\sigma\sim|V(K_z)|^2\left(\frac{g^2}{\pi^2}\right)^N\prod^N\frac{d\mathbf{k}_n}{k_{0n}}. \tag{41}$$

Now the integration over the momentum space of the mesons, and summation over N_1, can be carried out as in Section II, yielding

$$d\sigma\sim|V(K_z)|^2\left(\frac{8g^2}{\pi}\right)^N\frac{N^2(\epsilon_1\epsilon_2)^{N-1}}{N!^3}d\epsilon_1d\epsilon_2, \tag{42}$$

which, as before, favors large energy losses, and

$$\sigma(N)\sim\left(\frac{8g^2}{\pi}\right)^N\frac{\epsilon_{\max}{}^{2N}}{N!^3} \tag{43}$$

for the integrated cross section in the center of mass system, which has a maximum at

$$\bar{N}=\left(\frac{8g^2\gamma^2M^2}{\pi}\right)^{\frac{1}{4}}\left(\frac{\epsilon_{\max}}{\gamma M}\right)^{\frac{1}{2}}. \tag{44}$$

Comparing (43) with the result for the neutral pseudoscalar field obtained by the Bloch-Nordsieck method in Section II, we see that the only difference is the replacement of $(\Delta\tau_z\sigma_{||})^2$ by 2, indicating that an exchange potential is in fact equivalent to a large spin change in the Bloch-Nordsieck method.

We could, of course, treat a neutral scalar field by exactly this same method, with similar results.

The extension of the above to the case of the symmetrical theory is not trivial, since the feature that made the combinatorics simple, namely, the commutativity of the τ_z, is not present when charged mesons appear. Thus the successive emissions are not independent, and the simplicity is lost. In this particular case the non-commutativity of the successive emissions is related to the conservation of charge. In our treatment by the Bloch-Nordsieck method we neglected this difficulty by treating the isotopic spin vector classically. Such classical treatment would correspond to an extreme form of the so-called strong coupling theories, implying in particular the existence of charge isobars of the nucleons. Thus the charge asymmetry of the emitted mesons is compensated for by the fact that the heavy particles emerge from the collision in isobar states, in such a way as to effect the over-all conservation of charge. This problem does not exist in a neutral theory.

B. A Pair Theory

We wish now, in view of the fact that the emission of single mesons may be almost forbidden, to consider a typical spinor-pair theory. We use an interaction that is sensitive to spin changes of the nucleons,

$$H_{\text{int}}=g\Psi^*\psi^*(\sigma\cdot\Sigma-\gamma_5\Gamma_5)\psi\Psi, \tag{45}$$

where the capital letters refer to the heavy particle, and the small ones to the mesons. Taking the even part for the heavy particle, we can replace this by

$$H_{\text{int}}=g\Psi^*\Sigma_{||}\Psi\psi^*(\sigma_{||}-\gamma_5)\psi, \tag{46}$$

where we will later take the odd part of the light particle operators.

Writing down the matrix element for the emission of N *pairs* in an exactly analogous manner to that used in the preceding section, and with the same potential between the nucleons, we obtain

$$H=V(K_z)\frac{(2g)^N}{\prod_n b_n}[\chi_f{}^*\Lambda_f\Sigma_{1||}{}^{N_1}\Sigma_{2||}{}^{N_2}(\Sigma_{1\perp}\cdot\Sigma_{2\perp})\Lambda_i\chi_i]\cdot\prod_n\psi_n{}^*\lambda_n{}^+(\sigma_{||}-\gamma_5)\lambda_n{}^-\psi_n, \tag{47}$$

where, as before, the Λ and λ are the projection operators for the heavy and light particles, respectively, and

$$b_n=\epsilon_n{}^++\epsilon_n{}^--p_{n||}{}^+-p_{n||}{}^-.$$

Squaring, then summing over final and averaging over initial spins, we have

$$|H|^2=\frac{1}{4}|V(K_z)|^2\frac{(4g^2)^N}{\prod_n b_n{}^2}\cdot Sp[\Lambda_f(\Sigma_{1\perp}\cdot\Sigma_{2\perp})\Lambda_i(\Sigma_{1\perp}\cdot\Sigma_{2\perp})]\cdot\prod_n Sp[\lambda_n{}^+(\sigma_{||}-\gamma_5)\lambda_n{}^-(\sigma_{||}-\gamma_5)]. \tag{48}$$

The former spur is non-vanishing, and independent of N, and the latter, since the momentum of the "positron" is the negative momentum of the negative energy state, is

$$(2/\epsilon_n{}^+\epsilon_n{}^-)(\epsilon_n{}^+-p_{n||}{}^+)(\epsilon_n{}^--p_{n||}{}^-).$$

Therefore,

$$d\sigma\sim(8g^2)^N\prod_n\frac{d\mathbf{p}_n{}^+d\mathbf{p}_n{}^-}{\epsilon_n{}^+\epsilon_n{}^-}\times\frac{(\epsilon_n{}^+-p_{n||}{}^+)(\epsilon_n{}^--p_{n||}{}^-)}{(\epsilon_n{}^++\epsilon_n{}^--p_{n||}{}^+-p_{n||}{}^-)^2}, \tag{49}$$

which has an invariant form of the sort discussed in Section II. Integration of this expression over the momentum space available, followed by summation over N_1, would give the total cross

section for the emission of N pairs, but, unfortunately, the integration is not as simple as in the previous cases. However, to obtain an estimate of energy dependence, we may set the final factor in (49) equal to unity, and have

$$\sigma(N)\sim\epsilon_{\max}{}^{4N}/N!^2(2N)!^2,$$

which has a maximum for

$$\bar{N}\sim\epsilon_{\max}{}^{\frac{1}{2}}$$

which, by coincidence, is the same result as was found for the single pseudoscalar theory.

IV. SOME APPLICATIONS

A. Angular Distribution

We wish now to apply the foregoing results to the auger showers, and to the primary production of mesons. For this purpose we will use the results of the symmetrical pseudoscalar theory, as obtained in Section II. We found there that the weighting in momentum space was proportional to

$$\prod_n \frac{d\mathbf{k}_n}{k0_n}\propto\prod_n d\alpha_n d\beta_n,$$

with the α_n and β_n defined by (14). Averaging over all the mesons except one, we have for the average value of any function of α and β

$$\langle f(\alpha,\beta)\rangle_{Av}=\frac{(N-1)^2}{(\epsilon_1\epsilon_2)^{N-1}}\int_0^{\epsilon_2}\int_0^{\epsilon_1} f(\alpha,\beta)\times(\epsilon_1-\alpha)^{N-2}(\epsilon_2-\beta)^{N-2}d\alpha d\beta. \quad (50)$$

Thus the average energy of the emitted mesons is obtained by setting $f(\alpha,\beta)=\alpha+\beta$, and gives

$$\langle k_0\rangle_{Av}=(\epsilon_1+\epsilon_2)/N,$$

as it must.

Now approximating the distribution function for high energies, and transforming it to the laboratory system, we have a convenient form for applications,

$$P(\mathbf{k})d\mathbf{k}\cong\frac{N^2}{2\pi ME_0}\exp\left[-N\left(\frac{k_0}{E_0}+\frac{1}{2Mk_0}\right)\right]\times\exp[-Nk_0\vartheta^2/2M]\frac{d\mathbf{k}}{k_0}, \quad (51)$$

where, as before, energies are measured in units of μc^2 and masses in units of the meson mass.

In order to obtain the angular distribution alone, we have to integrate this over k_0, and obtain approximately, for small ϑ,

$$P(\vartheta)d\Omega\cong\frac{2M}{\pi E_0}\exp\left[-\frac{N^2}{4M^2}\left(\vartheta^2+\frac{2M}{E_0}\right)\right]\times\frac{d\Omega}{(\vartheta^2+2M/E_0)^2}. \quad (52)$$

This involves, however, an integration over meson momenta as low as $N/2M$, many of which will not reach sea level, and, in order to find the sea level angular distribution, we should only go down to energies of the order of 2×10^9 ev, which is the energy required to come through the atmosphere. With the lower limit $\eta=2\times10^9$ ev we find

$$P'(\vartheta)d\Omega\cong\frac{2M}{\pi E_0}\exp\left[-\frac{N\eta}{2M}\left(\vartheta^2+\frac{2M}{E_0}\right)\right]\times\frac{d\Omega}{(\vartheta^2+2M/E_0)^2}, \quad (53)$$

which has two characteristic widths

$$\vartheta_1\sim(2M/E_0)^{\frac{1}{2}},\quad \vartheta_2\sim(2M/N\eta)^{\frac{1}{2}}, \quad (54)$$

and we must choose whichever is smaller. Estimating the coefficients in (32), we find $\bar{N}\sim2E_0{}^{\frac{1}{4}}$ so that for the most probable multiplicity,

$$\vartheta_1\sim4E_0{}^{-\frac{1}{4}},\quad \vartheta_2\sim E_0{}^{-1/6}, \quad (55)$$

and for $E_0>5\times10^{10}$ ev, ϑ_1 is smaller, and we have roughly

$$P''(\vartheta)d\Omega\sim\frac{2M}{\pi E_0}\frac{d\Omega}{(\vartheta^2+2M/E_0)^2} \quad (56)$$

for angles less than ϑ_2.

This corresponds to spherically symmetric emissions in the center of mass system, and corresponds to an extremely wide distribution for the most highly populated primary energies. In the region of the auger showers, where $E_0\sim10^{14}$ or 10^{15} ev, the half-width is around 4×10^{-3} radian. This is, of course, the spread of the hard core of the showers, and the initial spread of the neutral mesons that form the soft part. The latter

is later considerably spread by multiple scattering.

If the showers are created at altitudes of (say) 20 km, this angle corresponds to a diameter of approximately 80 meters at sea level.

B. Primary Spectrum

The fact that the average multiplicity of production increases with the energy of the primary proton causes the energy spectrum of the mesons to be different from that for the primary protons. In particular, if the primary spectrum is proportional to $E_0^{-\lambda}dE_0$ and the average multiplicity is proportional to E_0^r, then the average energy ϵ of an emitted meson is E_0^{1-r} and the meson spectrum at the place of production is proportional to

$$\epsilon^{-\lambda/(1-r)}\cdot\epsilon^{1/(1-r)-1}d\epsilon\cdot\epsilon^{r/(1-r)} \quad \text{or} \quad \epsilon^{-(\lambda-2r)/(1-r)}d\epsilon.$$

Thus, if we take the meson spectrum as $\epsilon^{-2.8}d\epsilon$ and take $r=\frac{1}{3}$, the primary spectrum implied is $E_0^{-2.5}dE_0$ in the relatively high energy region for which these considerations are valid, E_0 greater than around 10-in. ev. For lower energies the multiplicity changes more rapidly, and if the primary spectrum predicted above persists below 10^{11} volts, we should expect the high altitude meson spectrum to deviate from an $\epsilon^{-2.8}$ law, the deviation being toward increased numbers of slow mesons. Of course the decay of the slower mesons and the magnetic effects on the primaries will influence these results.

C. Positive Excess

If we suppose that all final charge states of the nucleons are equally probable, then the fact that the primaries are positively charged causes an excess of positive mesons to be produced. If the number of charged mesons is N_c, then the average number of positive mesons will be $\frac{1}{4}(2N_c+1)$ and of negative $\frac{1}{4}(2N_c-1)$ so that the positive excess is $2/(2N_c-1)\sim 1/N_c$. This is both energy dependent and depends upon the absolute number of mesons produced. Taking, as above, $\overline{N}\sim 2E_0^{\frac{1}{4}}$ and $N_c\sim\frac{2}{3}\overline{N}\sim 1.3E_0^{\frac{1}{4}}$, we have

$$\text{Pos. excess}\sim 0.8E_0^{-\frac{1}{4}}\sim\epsilon^{-\frac{1}{4}}, \tag{57}$$

since $\epsilon_N=E_0/N\cong\frac{1}{2}E_0^{\frac{3}{4}}$. This gives the positive excess as a function of meson energy at the point of production, and around 2×10^9 ev must be added to energies at sea level to extrapolate back to the top of the atmosphere. For energies of a few Bev at sea level, this corresponds to an excess of between 15 and 20 percent, which is in accord with the experiments. No data are yet available on the variation of the excess with meson energy.

D. Range of Fields and Distances Involved

Integrating the distribution (51) over angles, we obtain for the energy distribution in the laboratory system, which is the initial rest system for the air nucleon,

$$P(k_0)dk_0\cong\frac{N}{E_0}\exp\left[-N\left(\frac{k_0}{E_0}+\frac{1}{2Mk_0}\right)\right]dk_0. \tag{58}$$

Thus the energy distribution is uniform from around $k_0\sim N/2M$ to $k_0\sim E_0/N$, and the average energy is indeed E_0/N. Thus we are exploring the meson field to distances of order N/E_0 which, for $N=\overline{N}\sim 2E_0^{\frac{1}{4}}$ is $2E_0^{-\frac{1}{4}}$. Thus a cut-off at a few times the proton Compton wave-length, as is suggested by magnetic moment, nuclear force, and self-energy consideration, would modify our results in the entire cosmic-ray range. The proton Compton wave-length itself becomes important at around 10^{10} ev, and at 10^{15} volt we are exploring the meson field to distances of about 1/1000 of $\hbar/Mc$.

Radiations from Scandium[46] and Titanium[51] *

C. E. MANDEVILLE AND MORRIS V. SCHERB
Bartol Research Foundation of the Franklin Institute, Swarthmore, Pennsylvania

(Received September 22, 1947)

Sc^{46} and Ti^{51} have been prepared in the Clinton pile. The characteristic radiations of these isotopes have been investigated by absorption and coincidence methods.

Sc^{46} was found to emit beta-rays having a range of 0.076 gram/cm² in aluminum and gamma-rays having a maximum energy of 1.0 Mev as determined by coincidence absorption. No hard beta-rays having an end point in the vicinity of 1.5 Mev were observed to be emitted by Sc^{46}. The beta-gamma-coincidence rate was found to be 1.4×10^{-3} coincidence per beta-particle and independent of the beta-ray energy, while the gamma-gamma-coincidence rate was $(0.62\pm0.06)\times10^{-3}$ coincidence per gamma-ray. These coincidence rates suggest that each beta-ray is followed by two gamma-rays.

The 72-day isomer of Ti^{51} emitted beta-rays having a range of 0.09 gram/cm² in aluminum and gamma-rays having a maximum energy of 1.0 Mev by coincidence absorption. The beta-gamma-coincidence rate was 0.9×10^{-3} coincidence per beta-ray and was independent of the beta-ray energy. The gamma-gamma-coincidence rate was $(0.35\pm0.03)\times10^{-3}$ coincidence per gamma-ray. These coincidence rates indicate that the beta-transition leads to an excited state of the V^{51} residual nucleus and that some or all of the residual nuclei de-excite with the emission of two or more gamma-rays in cascade.

1. INTRODUCTION

THE isotopes of scandium and titanium of long half-period have been the subject of several investigations.[1–6] The half-periods of scandium[46] and titanium[51] have been established as 85 ± 1 days and 72 ± 2 days, respectively.[1,2] The radioactive materials with which the experiments of this paper were carried out were prepared at the Clinton pile. The energies of the beta-rays and gamma-rays were measured by absorption in aluminum, and coincidence rates were observed in order to obtain some information as to the disintegration schemes.

2. APPARATUS

Thin-walled Geiger counters of two types were used. For measuring the energy of beta-rays, aluminum foils were placed between the radioactive source and a glass bubble counter having a window thickness of 0.0013 cm. For coincidence absorption measurements wherein the gamma-ray energies were determined, two Geiger counters in coincidence, each having a wall thickness of 0.013 cm, were used. The cathodes of the two counters were of Aquadag, the thickness of the Aquadag layer being 0.0006 cm.

Two identical Aquadag counters were placed with axes parallel, as in Fig. 1, when gamma-gamma-coincidences were to be observed. Aluminum blocks were placed between the counters and the source so that no primary beta-rays would be recorded. The block before C_2 was then removed, and the beta-gamma-coincidence rate was observed. The wires of the counters were attached to the input grids of a conventional coincidence circuit of the Rossi type. The output

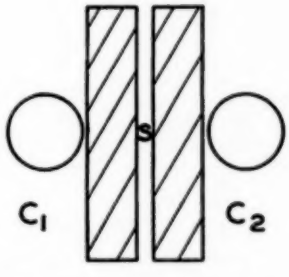

FIG. 1. Counter arrangement for gamma-gamma-coincidences. The counters are denoted by C_1 and C_2, and the radioactive source is placed at S.

* Supported by the Office of Naval Research.

[1] H. Walke, E. J. Williams, and G. R. Evans, Proc. Roy. Soc. **171A**, 360 (1939).
[2] H. Walke, Phys. Rev. **57**, 163 (1940).
[3] H. Walke, communication to G. T. Seaborg, Rev. Mod. Phys. **16**, 1 (1944).
[4] Lise Meitner, Arkiv. f. Mat. Astron. och Fysik, **28B**, No. 14 (1942); *ibid.*, **32A**, No. 6 (1945).
[5] I. Feister and L. F. Curtiss, J. Research Nat. Bur. Stand. **38**, 411 (1947).
[6] A. E. Miller and M. Deutsch, Bul. Am. Phys. Soc. **22**, 7 (1947).

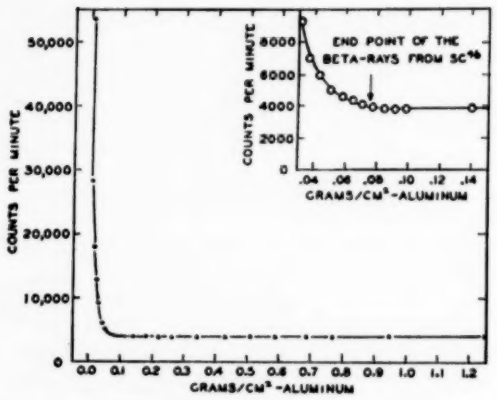

FIG. 2. Absorption of the beta-rays from Sc^{46}. The constant counting rate beyond the beta-ray group arises from the gamma-ray background.

tube of this circuit fed a scale of sixty-four and mechanical recorder.

When the beta-gamma-coincidence rate was computed, corrections were made for gamma-gamma-coincidences, accidentals, and gamma-ray counts in the beta-ray counter. The accidental correction was calculated from the usual equation

$$A = N_1 N_2 (K\tau),$$

where N_1 and N_2 were the single counting rates in either counter, and $K\tau$ was 2.5 microseconds. The coincidence rates of the two identical counters of Fig. 1 were used to form an estimate of the number of gamma-rays following each beta-particle. For obtaining beta-gamma-coincidences as a function of the beta-ray energy, C_2 was replaced by a thin bubble counter.

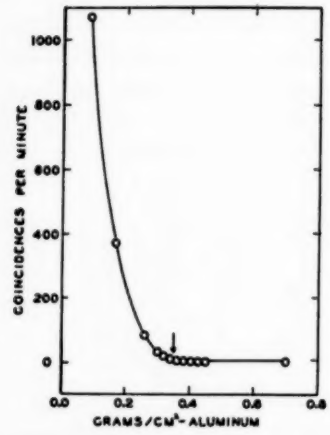

FIG. 3. Coincidence absorption of the Compton secondaries of the gamma-rays from Sc^{46}.

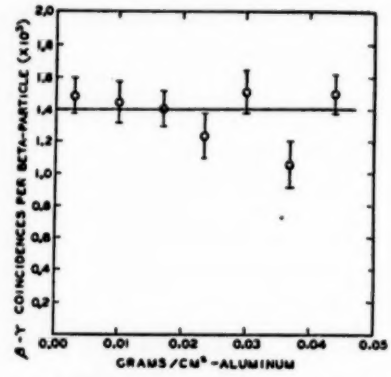

FIG. 4. Genuine beta-gamma-coincidences in the disintegration of Sc^{46}.

3. SCANDIUM[46]

The beta-rays from Sc^{46} have been measured with conflicting results. Walke[2] has reported two groups of beta-rays having energies of 0.26 Mev and 1.5 Mev. Meitner[4] found the group of low energy but attributed Walke's group of hard beta-rays to secondary effects. More recently, Feister and Curtiss[5] have verified that only the low energy group is present, whereas Peacock and Wilkinson[7] have reported the presence of a beta-ray group having an end point at 1.49 Mev and of about the same intensity relative to the main group as that of Walke's initial report.

The absorption curve for the beta-rays from Sc^{46} is given in Fig. 2. The end point occurs at 0.076 gram/cm² in aluminum. According to these measurements, only one group of beta-rays is present. The counting rate is seen to be constant over the entire region where contributions from the 1.5 Mev group might be found. Every effort was made to eliminate scattering and secondary effects as described by Deutsch[8] and Meitner.[9] This absorption curve certainly does not resemble that given by Walke on the interval beyond the main group of low energy beta-rays. The end point of Fig. 2 corresponds to a beta-ray energy of about 0.29 Mev.[10]

[7] Charles Peacock and R. G. Wilkinson, Phys. Rev. **72**, 251 (1947).

[8] M. Deutsch, Phys. Rev. **61**, 672 (1941).

[9] Lise Meitner, Phys. Rev. **63**, 73 (1943).

[10] Following Walke's convention, this energy has been estimated from the range-energy relation for homogeneous beta-rays, since the equations of Feather and Sargent do not apply for beta-ray energies below 0.7 Mev. The value 0.36 Mev obtained by Feister and Curtiss, Miller and Deutsch, and Peacock and Wilkinson, using spectrometer techniques, is naturally more desirable than that computed from the absorption limit.

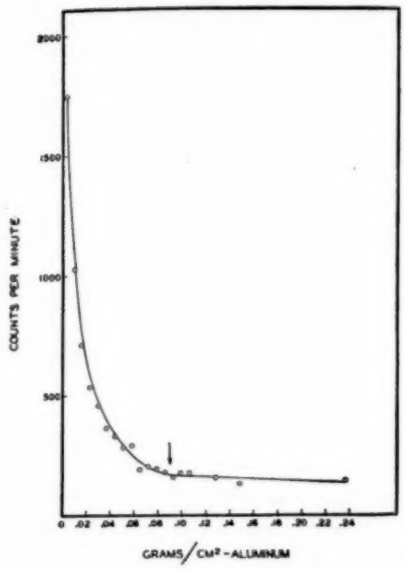

FIG. 5. Absorption of the beta-rays from Ti^{51}.

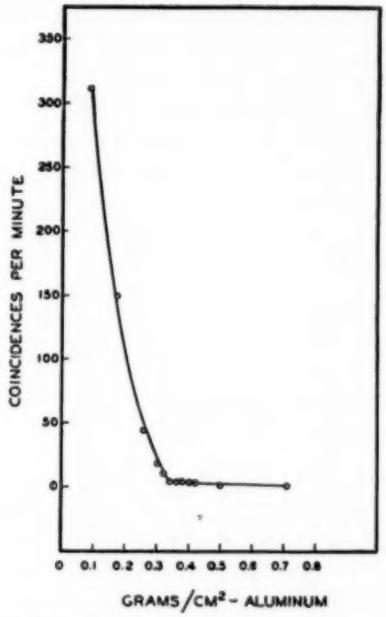

FIG. 6. Coincidence absorption of the Compton secondaries of the gamma-rays from Ti^{51}.

The maximum energy of the gamma-rays emitted by Sc^{46} was measured by coincidence absorption. The curve for these data is given in Fig. 3, where the end point occurs at 0.345 gram/cm². This corresponds to a quantum energy of 1.0 Mev.[11]

Using a thin bubble counter on the "beta-ray side," beta-gamma-coincidences were investigated. These data are given in Fig. 4. The genuine beta-gamma-coincidence rate was found to be 1.4×10^{-3} coincidence per beta-ray recorded in the beta-ray counter, and from the curve it is seen that the coincidence rate is independent of the beta-ray energy, suggesting that only one beta-ray spectrum is present. Corrections were made for gamma-gamma-coincidences in the beta-gamma-counting arrangement.

The two identical Aquadag counters of Fig. 1 gave coincidence rates of $(1.40\pm0.05)\times10^{-3}$ beta-gamma-coincidence per beta-ray and $(0.62\pm0.06)\times10^{-3}$ gamma-gamma-coincidence per gamma-ray. According to these coincidence rates, each beta-ray is followed by two gamma-rays.[12]

4. TITANIUM[51]

The absorption curve for the beta-rays from Ti^{51} is given in Fig. 5. The end point occurs at 0.09 gram/cm² in aluminum. This corresponds to a beta-ray energy of about 0.32 Mev. The value reported by Walke *et al.*[1] was 0.36 Mev. The data for coincidence absorption of the gamma-rays from Ti^{51} are given in Fig. 6, where the end point is found to correspond to a gamma-ray energy of 1.0 Mev.[11]

Using the thin bubble counter as the beta-ray counter, a genuine beta-gamma-coincidence rate of 0.9×10^{-3} coincidence per beta-ray was observed. These data are given in Fig. 7. This coincidence rate was independent of the beta-

[11] In arriving at 1.0 Mev for the gamma-ray energy, the maximum energy of the Compton secondaries was obtained from the range-energy relation for homogeneous beta-rays, and an appropriate amount of energy was added for collisions in the forward direction. The curve of H. Maier-Leibnitz (Physik. Zeits. **43**, 333 (1942)) also gives 1.0 Mev, so that the coincidence arrangement may in a sense be regarded as calibrated.

[12] This estimate is based upon the assumption that the gamma-ray efficiency of the two identical Aquadag counters is the same for all quanta emitted in the disintegration. The general formulation of the Indiana University group has been followed (Phys. Rev. **56**, 962 (1939)); that is,

$$\frac{K}{K-1}=\frac{\alpha}{\beta},$$

where

α = beta-gamma coincidence rate = 1.4×10^{-3},
β = gamma-gamma-coincidence rate = 0.62×10^{-3},
K = number of gamma-rays per disintegration.

Then $K=1.8$ for Sc^{46}.

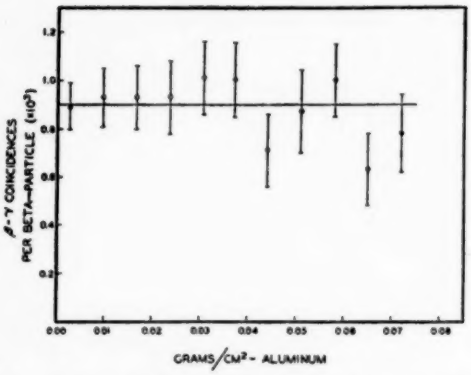

FIG. 7. Genuine beta-gamma-coincidences in the disintegration of Ti^{51}.

ray energy. The counters of Fig. 1 gave a beta-gamma-coincidence rate of $(0.90\pm0.03)\times10^{-3}$ coincidence per beta-ray and a gamma-gamma-coincidence rate of $(0.35\pm0.03)\times10^{-3}$ coincidence per gamma-ray. These coincidence rates suggest that 1.6 quanta are emitted per disintegration.[12] Ti^{51} cannot emit two gamma-rays of energy about 1.0 Mev since, for the same counters and geometry, its coincidence rates differ too greatly from that of Sc^{46}. The disintegration diagram of Fig. 8 then seems probable. About two-thirds of the disintegrations would occur by the alternate mode rather than by the emission of a single gamma-ray of energy 1.0 Mev to the ground state of V^{51}. Of course, it may be that de-excitation of the V^{51} residual nucleus occurs by only one mode with a gamma-ray of low energy in cascade with the 1.0-Mev radiation. The low detection efficiencies of the counters for the low energy quantum would then explain the coincidence rates.

5. ACKNOWLEDGMENTS

The writers are indebted to Mr. Willis E. Ramsey for many helpful discussions and to Mr. A. G. Nester who made the counters. They wish to express their particular appreciation to Professor W. B. Keighton of Swarthmore College for having carried out the chemical separations. They wish also to acknowledge the interest of Dr. W. F. G. Swann, Director of the Bartol Research Foundation.

Note added in proof: The coincidence rates of Sc^{46} have been redetermined with high statistical accuracy, and the net gamma-ray efficiency of the aquadag counters has been calculated in the usual manner.* It was assumed that Sc^{46} emits two gamma-rays in cascade of energies 0.88 and 1.12 Mev respectively. For a gamma-ray energy of 1 Mev, the net efficiency is about 0.7×10^{-3}. The coincidence rates of Ti^{51} suggest that gamma-rays having an energy of 1 Mev are in cascade with gamma radiation of low energy and having a net efficiency of about 0.2×10^{-3}. This would seem to be a more plausible disintegration scheme than that of Fig. 8.

APPENDIX I: CHEMICAL PROCEDURE FOR SCANDIUM

Two milligrams of Sc_2O_3 contained in a glass ampoule were irradiated by neutrons in the pile. The crushed ampoule was washed first with warm $6N-HNO_3$ and then with water. About fifty milligrams of aluminum were added in the form of a solution of aluminum nitrate. The solution was then diluted to ten milliliters. After the addition of 250 mg of NH_4Cl, the solution was heated to boiling, and the hydroxides of scandium and aluminum were precipitated together with ammonia. The hydroxides were washed with hot 2 percent NH_4NO_3 solution, dissolved in concentrated HCl, water was added, and the hydroxides were again precipitated.

This second hydroxide precipitate was dissolved in HCl, evaporated nearly to dryness, and dissolved in water and a few drops of HCl. To the resulting solution was added about fifty milligrams of inactive calcium as calcium nitrate solution. Calcium and scandium oxalates were precipitated together from the hot solution by adding an equal volume of saturated oxalic acid solution. After standing over night, the pre-

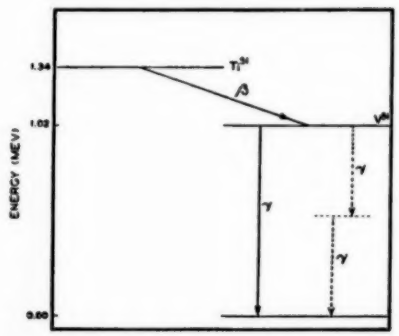

FIG. 8. Tentative disintegration scheme for Ti^{51}.

* J. V. Dunworth, Rev. Sci. Inst. 11, 167 (1940).

cipitate was washed with 1 percent oxalic acid solution, dried, and ignited at 800–1000°C. The product weighed 74 mg and consisted of CaO and practically the entire quantity (2 mg) of Sc_2O_3. The calcium was added as a carrier to assure complete recovery of the radioactive scandium.

By this procedure it was intended to obtain scandium free of radioactive phosphorus, calcium, and iron.

APPENDIX II: CHEMICAL PROCEDURE FOR TITANIUM

Chemically pure TiO_2 was irradiated by neutrons in the pile. The titanium dioxide was fused in platinum with ten times its weight of sodium carbonate. The melt was then boiled with water and filtered. The insoluble residue of titania was well washed with boiling water, and the filtrate and washings were rejected. This procedure should have removed phosphorus and part of any scandium impurity. The partly purified titania was then fused in platinum with potassium acid sulfate, and the melt was dissolved in cold $6N-H_2SO_4$. Orthotitanic acid was precipitated, at room temperature, with dilute ammonium hydroxide. The precipitate was dissolved in concentrated HCl and the solution diluted to $2N$. One volume of saturated oxalic acid solution was added to three volumes of the warm solution. After standing four hours, a trace of precipitate, which may have been calcium or scandium oxalate, was filtered out.

The filtrate was again made ammoniacal, and the orthotitanic acid precipitate was filtered out, washed, and dissolved in HCl. After dilution to $2N$, sufficient tartaric acid was added to prevent precipitation of titanium. The solution was neutralized with ammonia, made about $0.3N$ in H_2SO_4, and saturated with H_2S. Ammonia was added in decided excess, and the solution was again saturated with H_2S. The precipitate, probably iron and platinum sulfides, was filtered out. The filtrate, made strongly acid with H_2SO_4, was boiled to expel H_2S, diluted, and cooled. The titanium was precipitated with a 4 percent solution of cupferron added in excess, and the precipitate was ignited to TiO_2. The procedure outlined gave a sample of TiO_2 free of phosphorus, scandium, calcium, and iron.

PHYSICAL REVIEW VOLUME 73, NUMBER 2 JANUARY 15, 1948

The Propagation of a Pulse in the Atmosphere. Part II

C. L. PEKERIS*
The Institute for Advanced Study, Princeton, New Jersey
(Received September 5, 1947)

The previous investigation of the dispersion of long waves in the atmosphere has been extended to shorter periods of the order of one minute. Both the phase velocity and group velocity have been determined. The results are applied to the interpretation of the pressure wave produced by the Great Siberian Meteor and to the pressure oscillations recorded by microbarographs in England.

1. INTRODUCTION AND SUMMARY

FOR the purpose of interpreting the observed features of the pressure wave produced by the explosion of the Great Siberian Meteor in 1908,[1] the previous investigation by the author[2] of the dispersion of long waves in the atmosphere (Krakatoa wave, period of one hour) has been extended to shorter periods of the order of a minute. Two model atmospheres have been treated, one (*a*) having a finite height in which the temperature gradient is constant and equal to 7/11 of the adiabatic, and another (*b*) in which the same temperature gradient prevails in the troposphere, but a constant temperature is assumed above 10.3 km. The variation of phase

* This work was carried out while the writer served as consultant to project N6-ori-139, task order # 1, sponsored by the O.N.R.
[1] F. J. W. Whipple, Q. J. Roy. Meteor. Soc. **56**, 287 (1930).
[2] C. L. Pekeris, Proc. Roy. Soc. **A171**, 434 (1939); this paper will be referred to as I.

velocity with period in model a was studied by Solberg,[3] while G. I. Taylor[4] first gave the limiting value of the phase velocity at long waves for the more realistic model b. In this study both the phase velocity and group velocity have been determined. It is found (see Fig. 1) that in model a there exists, in addition to the oscillation studied by Solberg (I), a second type of oscillation (II) which is limited to periods less than the free period of the atmosphere for purely vertical oscillation (3.5 minutes). In this type II of oscillation the group velocity passes through a maximum, equal to 0.64 of the value of the sound velocity at the ground, at a period of about 2.5 minutes. No type II oscillation was found in model b. However, it turns out that in b the free oscillation of type I exists only for periods greater than 2 minutes. Shorter periods are not propagated freely without horizontal attenuation, essentially because they leak out vertically to space.

A steady-state solution is obtained for the oscillation of atmosphere b when excited by a point source situated at the ground, in which the vertical velocity w varies with time like $e^{i\omega t}$. It is found that at large distances from the source the resulting pressure oscillation at the ground has a relative maximum at a period of about 4 minutes, tending to zero both at very long periods and at the cut-off period (see curve A, Fig. 2). When this steady-state solution is used to determine the oscillation excited by an *impulsive* point source, in which the spectrum of w is uniform, the higher dispersion at the shorter periods results in an excitation which starts from zero at the cut-off period and increases in a monotone fashion towards the longer periods.

On the other hand, if the pulse is such that the *pressure variation* at the source has a uniform spectrum, the excitation is a maximum at a period equal to Brunt's period for the vertical oscillation of a particle near the ground, i.e., 9.5 minutes. These results are applied to the interpretation of the pressure wave produced by the Great Siberian Meteor and to pressure oscillations recorded by microbarographs in England.

[3] H. Solberg, Astrophys. Norvegica 2, 123 (1936).
[4] G. I. Taylor, Proc. Roy. Soc. A126, 728 (1929); H. Lamb, *Hydrodynamics* (Cambridge University Press, Teddington, England, 1932), p. 541.

2. THEORY OF ATMOSPHERIC OSCILLATIONS

The theory of atmospheric oscillations dates back to Laplace,[5] but Lamb[6] was the first to develop it without making restrictive assumptions about the physical processes involved. Since we shall be interested in periods ranging from a minute to about an hour, we may neglect the stabilizing effects arising from the earth's rotation which become significant only at periods of the order of a day.[7] We shall, therefore, confine the discussion to the oscillations of a horizontally stratified atmosphere resting on a flat ground when disturbed from static equilibrium. If the positive direction of the z axis be taken downwards, the pressure distribution in the equilibrium state is given by

$$(dp_0/dz)=g\rho_0, \quad p_0=R\rho_0 T, \tag{1}$$

$$p_0(z)=p_0(z_0)\exp\left[-(g/R)\int_z^{z_0}(dz/T)\right],$$

$$\rho_0(z)=\rho_0(z_0)(T_0/T)\exp\left[-(g/R)\int_z^{z_0}(dz/T)\right]. \tag{2}$$

Upon this equilibrium state we superimpose small oscillations which are governed by the equations of motion and continuity:

$$\rho_0\frac{\partial u}{\partial t}=-\frac{\partial p}{\partial x}, \quad \rho_0\frac{\partial v}{\partial t}=-\frac{\partial p}{\partial y}, \quad \rho_0\frac{\partial w}{\partial t}=-\frac{\partial p}{\partial z}+g\rho, \tag{3}$$

$$\frac{\partial \rho}{\partial t}+w\frac{\partial \rho_0}{\partial z}=-\rho_0\chi, \quad \chi\equiv\frac{\partial u}{\partial x}+\frac{\partial v}{\partial y}+\frac{\partial w}{\partial z}, \tag{4}$$

p and ρ denoting perturbations from equilibrium values. The adiabatic energy equation,

$$\frac{Dp}{Dt}=c^2\frac{D\rho}{Dt}, \quad c^2=\gamma p_0/\rho_0=\gamma RT_0, \tag{5}$$

yields the fifth equation for the determination of the five variables (u, v, w, p, ρ):

$$\frac{\partial p}{\partial t}+g\rho_0 w=-\gamma p_0\chi. \tag{6}$$

[5] Laplace, Mécanique Céleste, Livre 4, Chap. 5 (1845).
[6] H. Lamb, *Hydrodynamics* (Cambridge University Press, Teddington, England, 1932), p. 550; Proc. Roy. Soc. A84, 552 (1910); Proc. Lond. Math. Soc. 7, 122 (1909).
[7] In the case of long period oscillations G. I. Taylor has shown that the effect of the earth's rotation can be taken into account in the manner used in the theory of oceanic tides. Proc. Roy. Soc. A156, 378 (1936).

Eliminating p and ρ, we get

$$\frac{\partial^2 u}{\partial t^2}=\frac{\partial}{\partial x}(c^2\chi+gw), \quad \frac{\partial^2 v}{\partial t^2}=\frac{\partial}{\partial y}(c^2\chi+gw), \quad (7)$$

$$\frac{\partial^2 w}{\partial t^2}=\frac{\partial}{\partial z}(c^2\chi+gw)+\left[(\gamma-1)g-\frac{dc^2}{dz}\right]\chi. \quad (8)$$

Let the dependence on time and on $r(=(x^2+y^2)^{\frac{1}{2}})$ be given by a factor $e^{i\sigma t}J_0(kr)$, then the above equations yield

$$c^2\ddot{\chi}+(\dot{c}^2+\gamma g)\dot{\chi}+[\sigma^2-k^2(Q^2/\sigma^2)]\chi=0,$$
$$Q^2\equiv g\dot{c}^2+\sigma^2c^2-(\gamma-1)g^2, \quad (9)$$

$$\delta w=\sigma^2c^2\dot{\chi}+(g\gamma\sigma^2-gk^2c^2)\chi, \quad \delta\equiv g^2k^2-\sigma^4, \quad (10)$$

$$\delta p=i\sigma\rho_0[gc^2\dot{\chi}+(\gamma g^2-\sigma^2c^2)\chi], \text{ or}$$
$$p=(i\rho_0/\sigma)(gw+c^2\chi), \quad (11)$$

where the dots denote differentiation with respect to z.

In order to bring out the contrast with the laws of propagation of acoustic vibrations ($\sigma\to\infty$), where the motion is irrotational and is derivable from a velocity potential φ,

$$\mathbf{v}=-\nabla\varphi, \quad p=\rho_0(\partial\varphi/\partial t),$$
$$\nabla^2\varphi=(1/c^2)\partial^2\varphi/\partial t^2, \quad (12)$$

we write in (7) and (8)

$$gw+c^2\chi=-\partial^2\varphi/\partial t^2, \quad u=-\partial\varphi/\partial x,$$
$$v=-\partial\varphi/\partial y, \quad p=\rho_0\partial p/\partial t, \quad (13)$$

and find that

$$w=-(\partial\varphi/\partial z)+\Delta,$$
$$\Delta=[\dot{c}^2-(\gamma-1)g](\sigma^2\varphi+g\dot{\varphi})/Q, \quad (14)$$

$$Q^2c^2\sigma^2\ddot{\varphi}+(\gamma\sigma^2gQ^2-\sigma^2c^2\dot{Q}^2)\dot{\varphi}$$
$$+[-Q^4k^2g^2+Q^4\sigma^4+\gamma\sigma^4g^2Q^2$$
$$-\sigma^6c^2Q^2-\sigma^4c^2\dot{Q}^2g^2]\varphi/g^2=0. \quad (15)$$

The motion is now rotational, as evidenced by the Δ term in (14). This arises from the fact that, whereas when an air particle is displaced horizontally it is restrained only by elastic forces, when it is displaced vertically an additional force stemming from the vertical stable stratification comes into play. When a particle is displaced adiabatically upwards, its temperature drops in dry air at the rate of about 10° per km., the so-called dry-adiabatic lapse rate. On the other hand, the normal temperature gradient in the atmosphere is only about 0.6 of the adiabatic. Hence the particle is cooler than the surrounding air at the new elevation, and is therefore pulled down to its original position by a force which is initially proportional to the displacement. The period of free vertical oscillation of an individual air particle was shown by Brunt[8] to be determined from

$$\sigma^2c^2=(\gamma-1)g^2-g\dot{c}^2; \quad Q=0. \quad (16)$$

Only when the actual temperature gradient is equal to the adiabatic is the right-hand side of (16) equal to zero, and only then do the atmospheric oscillations become strictly isotropic. In the acoustic limit $(\partial\varphi/\partial z)\simeq(2\pi/\lambda)\varphi$, whereas

$$\Delta\simeq\varphi[(\dot{c}^2/c^2)-g(\gamma-1)/c^2]$$
$$\simeq\varphi(1/T)(dT/dz)\simeq\varphi\ 10^{-7}\ \text{cm}^{-1}.$$

Δ is then of the order of 10^{-4} smaller than $(\partial\varphi/\partial z)$. To the same degree of approximation Eqs. (9) and (15) then reduce to the acoustic wave Eq. (12). On the other hand, at periods of several minutes, in which we shall be interested in this study, the motion deviates radically from acoustic isotropy, especially near Brunt's resonant period, where Q in (9) and (15) passes through zero.

For future reference we shall point out here that Eq. (9) can be reduced by the substitution

$$u=\int_z^{z_0}\left(\frac{c_0^2}{c^2}\right)dz, \quad H_0=\frac{RT_0}{g},$$
$$q\equiv\left[\frac{c^4}{c_0^4}-\frac{1}{\gamma H_0\sigma^2}\frac{dc^2}{du}-\frac{(\gamma-1)c^2}{\gamma^2H_0^2\sigma^2}\right], \quad (17)$$

to

$$\chi=\exp(u/2H_0)\psi(u),$$
$$\frac{d^2\psi}{du^2}+\left[-\frac{1}{4H_0^2}+\frac{\sigma^2c^2}{c_0^4}-k^2q\right]=0. \quad (18)$$

3. FREE OSCILLATIONS OF AN ATMOSPHERE WITH CONSTANT TEMPERATURE

In addition to the anisotropic effects mentioned above, arising from the vertical stability, the atmosphere has free modes of oscillation that are analogous to Rayleigh waves. The nature of these can best be illustrated in the simple case of an atmosphere in which the temperature is uniform at all heights. In the case of a liquid

[8] D. Brunt, Q. J. Roy. Meteor. Soc. **53**, 30 (1927).

half-space of constant sound velocity, say an ocean of infinite depth, the field produced by a point source situated at some depth can be represented by two spherical waves emanating from the source and from its image (negative) in the surface. When the half space is rigid, Rayleigh[9] has shown that the source excites, in addition, a free surface wave whose energy decreases exponentially with depth, and which spreads out cylindrically. Two types of surface waves of this nature can be propagated in the atmosphere. These, of course, have not the same physical origin as Rayleigh's waves, since the rigidity of the air is zero.

It will be convenient in this section to take the positive z axis upwards. Equations (9) and (10) reduce in our case to

$$c^2\ddot{\chi}-\gamma g\dot{\chi}+[\sigma^2-k^2c^2+k^2(\gamma-1)g^2/\sigma^2]\chi=0, \quad (19)$$

$$(g^2k^2-\sigma^4)w=\sigma^2c^2\dot{\chi}+(gk^2c^2-g\gamma\sigma^2)\chi=0. \quad (20)$$

We also have for the distribution of normal density with height

$$\rho_0(z)=\rho_0(0)\exp(-z/H_0), \qquad H_0=(RT_0/g)=(c_0^2/\gamma g). \quad (21)$$

Assuming

$$\chi=A\cdot\exp(\lambda z+i\sigma t-ikx), \quad (22)$$

we get from (19)

$$\lambda=\frac{\gamma g}{2c^2}-\mu,$$

$$\mu=\left[\frac{\gamma^2g^2}{4c^4}-\frac{\sigma^2}{c^2}+k^2-\frac{g^2k^2(\gamma-1)}{\sigma^2c^2}\right]^{\frac{1}{2}}, \quad (23)$$

where μ is to be taken positive. The choice of the negative sign in front of μ was made in order to assure that the kinetic energy of wave motion integrated over a column of the atmosphere is finite. The kinetic energy density, which is proportional to $\rho_0(z)\chi^2$, varies then like $\exp(-2\mu z)$. In the other solution with the positive sign in front of μ, this quantity is proportional to $\exp(2\mu z)$. Now a free oscillation is possible if w vanishes at the ground, or from (20)

$$\lambda=\frac{\gamma g}{c^2}-\frac{gk^2}{\sigma^2}. \quad (24)$$

[9] Lord Rayleigh, Sci. Pap. **2**, 441 (1900); H. Lamb, Phil. Trans. Roy. Soc. **A203**, 1 (1904); C. L. Pekeris, Proc. Nat. Acad. Sci. **26**, 433 (1940).

Substituting in (23), we obtain a relation between σ and k which determines the speed of propagation $V(=\sigma/k)$ of the free waves and the group velocity $U(=d\sigma/dk)$ as functions of the frequency σ. This relation has two roots corresponding to two possible types of free oscillation:

$$\text{I.} \quad k=\sigma/c, \quad V=U=c, \quad \mu=g(2-\gamma)/2c^2, \quad \lambda=(\gamma-1)g/c^2, \quad (25)$$

$$\text{II.} \quad k=\sigma^2/g, \quad V=(g/\sigma), \quad U=\tfrac{1}{2}V, \quad \mu=\frac{\sigma^2}{g}-\frac{\gamma g}{2c^2}, \quad \lambda=\frac{\gamma g}{2c^2}-\frac{\sigma^2}{g}. \quad (26)$$

While oscillation I can exist at all frequencies, in oscillation II only frequencies above a critical value can be propagated:

$$\text{II.} \quad \sigma^2>\sigma_c^2=\gamma g^2/2c^2, \quad k>1/2H_0, \quad U<c/(2\gamma)^{\frac{1}{2}}. \quad (27)$$

When Eq. (27) is violated, no root of (23) and (24) belonging to class II exists which yields an integrable wave energy in an atmospheric column. As $\sigma\to\sigma_c$ the energy content per atmospheric column grows indefinitely, so that it becomes increasingly difficult to excite the oscillation near σ_c.

In the next section, when dealing with an atmosphere having a constant temperature in the stratosphere, we shall also find a cut-off frequency conditioned by the vanishing of μ. Then, however, frequencies less than the cut-off frequency are disallowed.

It should be noted that because the dependence on z is represented by a single exponential term, the condition of the vanishing of w at the ground makes it vanish at all heights. In an atmosphere of constant temperature the free oscillations manifest themselves only by horizontal motion u and by a pressure oscillation p,

$$u=(ikc^2/\sigma^2)\chi, \quad p=(i\rho_0c^2/\sigma^2)\chi, \quad w=0. \quad (28)$$

Had we assumed a factor

$$H_0^{(2)}(kr)\to(2/\pi kr)^{\frac{1}{2}}\exp(-ikr+i\pi/4), \quad (29)$$

instead of $\exp(-ikx)$ in (22), the displacement would have been in the r-direction, and the amplitude would have decreased like $r^{-\frac{1}{2}}$.

4. FREE OSCILLATIONS OF AN ATMOSPHERE HAVING A CONSTANT TEMPERATURE GRADIENT IN THE TROPOSPHERE AND A CONSTANT TEMPERATURE IN THE STRATOSPHERE (MODEL *b*)

With the z axis pointing downwards, let in the troposphere

$$T=\beta z,\quad m\equiv -1+(g/R\beta),\quad c^2=\gamma g z/(m+1). \tag{30}$$

Write

$$\tau=\sigma^2/gk,\quad x=2kz,$$

$$2\alpha=\left[-2-m+\frac{(m+1)\tau}{\gamma}-\frac{1}{\tau}+\frac{(\gamma-1)(m+1)}{\gamma\tau}\right], \tag{31}$$

then Eq. (9) reduces to

$$x\frac{d^2\chi}{dx^2}+(m+2)\frac{d\chi}{dx}+\left(-\frac{x}{4}+\alpha+1+\frac{m}{2}\right)\chi=0, \tag{32}$$

whose solution is

$$\chi=e^{-x/2}[AF_1(x)+Bx^{-1-m}F_2(x)],$$
$$F_1=F(-\alpha,\ m+2,\ x);$$
$$F_2=F(-\alpha-1-m,\ -m,\ x), \tag{33}$$

provided m is not an integer. The condition of the vanishing of w at the ground ($x=x_0$) yields

$$\frac{B}{A}=\frac{x_0^{1+m}[\dot F_1(x_0)-NF_1(x_0)]}{\{[N+(1+m)/x_0]F_2(x_0)-\dot F_2(x_0)\}},$$

$$N=\frac{1}{2}\left(1+\frac{1}{\tau}\right)-\frac{(m+1)}{x_0}. \tag{34}$$

In the stratosphere ($x<x_1$)

$$c^2=\gamma g x_1/2k(m+1),\quad \chi=De^{\lambda z}, \tag{35}$$

$$\frac{\lambda}{2k}=-\frac{(m+1)}{2x_1}\left\{1-\left[1+\frac{x_1^2}{(m+1)^2}-\frac{2x_1\tau}{\gamma(m+1)}-\frac{2(\gamma-1)x_1}{\gamma\tau(m+1)}\right]^{\frac{1}{2}}\right\}. \tag{36}$$

At the tropopause ($x=x_1$) we must have continuity of the perturbation pressure p and of w. From (10) and (11) it follows that both $\dot\chi$ and χ must be continuous, and therefore also $\dot\chi/\chi$. Equating $\dot\chi/\chi$ obtained from (33) and (35), we arrive at a relation which determines $\sigma(k)$:

$$g(x)=\frac{\dot F_1(x_1)+(B/A)x_1^{-1-m}[\dot F_2(x_1)-(1+m)F_2(x_1)/x_1]}{[F_1(x_1)+(B/A)x_1^{-1-m}F_2(x_1)]}-\frac{1}{2}$$
$$+\frac{(m+1)}{2x_1}\left\{1-\left[1+\frac{x_1^2}{(m+1)^2}-\frac{2x_1\tau}{\gamma(m+1)}-\frac{2(\gamma-1)x_1}{\gamma\tau(m+1)}\right]^{\frac{1}{2}}\right\}=0. \tag{37}$$

Here (B/A) is determined from (34) and

$$(x_1/x_0)=(T_s/T_0), \tag{38}$$

where T_s denotes the temperature in the stratosphere, and T_0 the temperature at the ground. For a given value of α one computes τ from (31) and then finds such a value of x_0 (and with it of x_1) that (37) is satisfied. Having obtained x_0 as a function of α, the frequency σ and associated phase velocity V and group velocity U can be determined from

$$\sigma=\left[\frac{g\tau x_0}{2H_0(m+1)}\right]^{\frac{1}{2}},\quad \frac{V}{c_0}=\left(\frac{2\tau(m+1)}{\gamma x_0}\right)^{\frac{1}{2}},$$

$$\frac{U}{c_0}=\left(\frac{2m+2}{\gamma}\right)^{\frac{1}{2}}\frac{d(\tau x_0)^{\frac{1}{2}}}{dx_0}. \tag{39}$$

It should be noted that for a given α, Eq. (31) yields two values of τ:

$$\tau_1=\frac{\gamma(2+2\alpha+m)}{2(m+1)}+\left[\frac{\gamma^2(2+2\alpha+m)^2}{4(m+1)^2}+\frac{\gamma}{(m+1)}+1-\gamma\right]^{\frac{1}{2}}, \tag{40}$$

$$\tau_2=\frac{\gamma(2+2\alpha+m)}{2(m+1)}-\left[\frac{\gamma^2(2+2\alpha+m)^2}{4(m+1)^2}+\frac{\gamma}{(m+1)}+1-\gamma\right]^{\frac{1}{2}}, \tag{41}$$

both of which are relevant to the dispersion relation. The limiting values for long wave-lengths

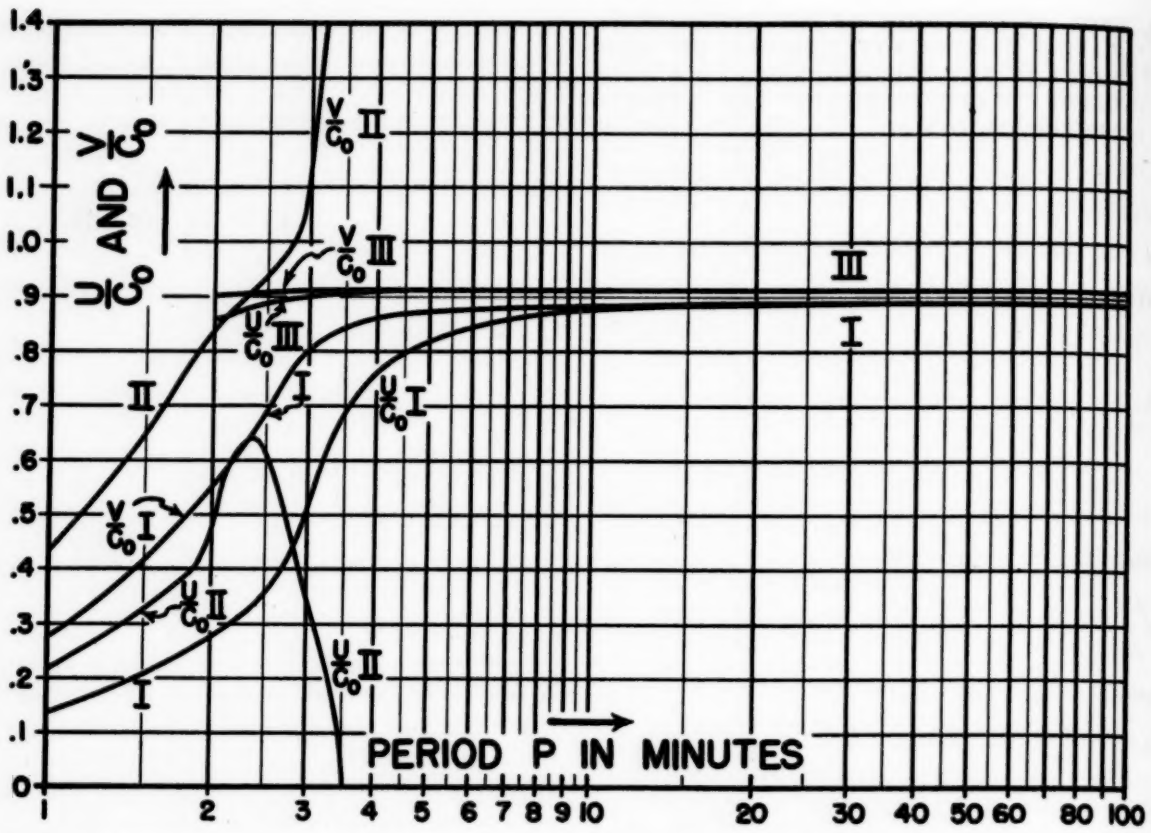

FIG. 1. Variation of phase velocity V and group velocity U in atmospheres a (I+II) and b (III). c_0=sound velocity at the ground. In model a, $\beta=(7/11)\beta_{ad}$, $m=4.5$, $T_0=288°K$, $H_0=8.43$ km. In model b, $\beta=(7/11)\beta_{ad}$ in troposphere, $T=220°K$ in stratosphere above 10.3 km.

(Lamb, Taylor, Pekeris) arise from τ_2. At moderate wave-lengths, τ_2 is replaced on this branch by τ_1 after a value of α is passed at which the radical in (41) vanishes. In model a atmosphere, however, there is, in addition, another branch of $\sigma(k)$ which arises entirely from τ_1.

In the model a atmosphere in which the tropospheric temperature gradient is assumed to extend also into the stratosphere ($x_1=0$), the solution (33) for χ cannot contain the B term. Hence it follows from (34) that the frequency relation is given by

$$F_1'(x_0)-\left[\frac{1}{2}\left(1+\frac{1}{\tau}\right)-\frac{(m+1)}{x_0}\right]F_1(x_0)=0. \quad (42)$$

One branch of the solution of (42) was studied by Solberg[3] for several integral values of m (temperature gradients). We have evaluated this branch for the case $m=4.5$, $\beta=(7/11)\beta_{ad}$, and the resulting phase velocity V and group velocity U are shown as functions of the period P by the curves I in Fig. 1. There exists another type of oscillation, labelled II in Fig. 1, which can exist only at periods less than 3.5 minutes. The latter is the free period of the atmosphere for purely vertical oscillation ($k=0$), a general formula for which was given by Lamb[6] for a model a atmosphere. In the limit of long wave-lengths ($k\to 0$), the motion in oscillation I is mainly horizontal ($w\simeq ku$), while in II the oscillation of individual particles is mainly in the vertical direction as in stellar pulsation. In the case of an atmosphere of constant temperature, discussed in the previous section, (V/c_0) and (U/c_0) of branch I are both equal to 1 for all periods, while in branch II they increase proportionately to the period from zero at $P=0$, and then terminate at the critical period.

The dispersion curves for model b, as obtained from (37), are shown by curves III in Fig. 1. These terminate at a period of two minutes. For

shorter periods the radical in (36) and (37) becomes imaginary and free waves do not exist. We note that at $P=2$, V is about 2 percent above c_1, the sound velocity in the stratosphere, while U is about 2 percent less than c_1. The limiting value of U and V for long periods is 4 percent above c_1 and 8.5 percent below c_0. It is clear that the cut-off period arises from the fact that in contrast to atmosphere a, the temperature in the stratosphere of atmosphere b is too high to allow the propagation (trapping) of slow-speed, short-period waves. It is therefore probable that other model atmospheres having a finite temperature minimum in the stratosphere would also exhibit a short period cut-off.

5. EXCITATION OF THE FREE OSCILLATION OF ATMOSPHERE b BY A POINT SOURCE SITUATED AT THE GROUND IN WHICH w HAS A UNIFORM SPECTRUM

The fact that the cut-off period of model b occurs when the radical in (37) vanishes, shows that at the cut-off the wave energy in the free oscillation per column of the atmosphere is infinite. This suggests a vanishing normalization factor, i.e., a difficulty in exciting periods near the cut-off. In order to investigate this point quantitatively, with a view of application to the pressure wave produced by the North Siberian Meteor, we shall determine first the relative amplitudes of the pressure oscillation excited by a point source situated at the ground, in which w varies with time like $e^{i\sigma t}$. Such an investigation was carried out by the writer for long periods in connection with the interpretation of the Krakatoa wave.[2] There, a w-point source suggested itself by the nature of the volcanic eruption, and the problem was to determine the relative excitation of two modes at the same frequency. In this case of the question of relative excitation of various periods in the same mode, the nature of the point source is important. One obtains a different answer if the comparison is made on the basis of a uniform spectrum of the pressure oscillation at the point source, i.e., a p-source.

Referring to Eqs. (9) and (10), we seek a solution of the form

$$\chi(z,r,t)=e^{i\sigma t}\int_0^\infty A(k,\sigma)K(z,\sigma,k)\times J_0(kr)kdk, \quad (43)$$

where, by (9),

$$c^2\ddot{K}+(\dot{c}^2+\gamma g)\dot{K}+[\sigma^2-k^2(Q/\sigma^2)]K=0. \quad (44)$$

The function $A(k,\sigma)$ has to be chosen so as to satisfy the boundary conditions at the ground and at the point source. Since the point source is at the ground, w must be zero except at the source where we shall assume it to become integrably infinite. Such a discontinuous function can be represented by the discontinuous integral

$$w(0,r,t)=e^{i\sigma t}\int_0^\infty J_0(kr)kdk. \quad (45)$$

With the aid of (10) one obtains

$$\chi(z,r,t)=e^{i\sigma t}\int_0^\infty J_0(kr)K(z,\sigma,k)kdk/W(k,\sigma), \quad (46)$$

$$W(k,\sigma)=[1/(g^2k^2-\sigma^4)]\cdot[\sigma^2c^2\dot{\chi}+(g\gamma\sigma^2-gk^2c^2)\chi]_{z=0}. \quad (47)$$

At points outside of the source, where w is zero, we get from (11)

$$p(0,r,t)=(i\rho_0c_0^2/\sigma)e^{i\sigma t}\int_0^\infty J_0(kr)\times K(0,\sigma,k)kdk/W(k,\sigma). \quad (48)$$

The integral in (48) can be evaluated by the residue method at the zeros of W, which yield the various modes of free oscillation. The contribution from the first mode can be shown to be given at large ranges r by[10]

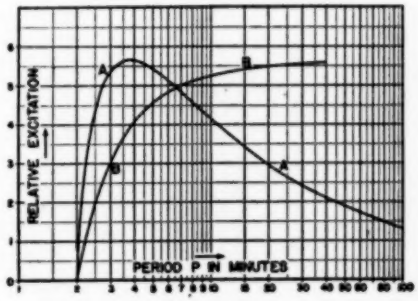

FIG. 2. Relative excitation of atmpsphere b by a w-point source situated at the ground. A = steady-state solution; B = solution for an impulsive point source (including effect of dispersion).

[10] H. Lamb, Phil. Trans. Roy. Soc. **A203**, 1 (1904); C. L. Pekeris, J. Acous. Soc. Am. **18**, 295 (1946); see also reference 2.

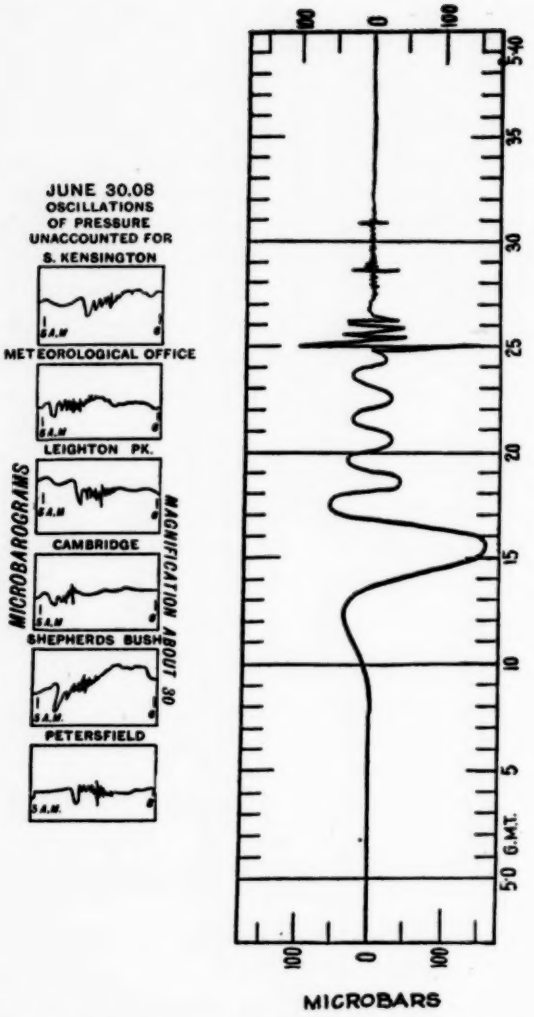

FIG. 3. Microbarograms of the pressure wave produced by the Great Siberian Meteor, recorded at English stations. On the right is a composite drawing made by F. J. W. Whipple.[1]

$$p(0, r, t) \rightarrow \frac{\rho_0 c_0^2}{2\sigma}\left(\frac{2k_1}{\pi r}\right)^{\frac{1}{2}} \exp\left(i\sigma t - ik_1 r + i\frac{3\pi}{4}\right) \times \frac{K(0, k_1, \sigma)}{(\partial W/\partial k)}. \quad (49)$$

Using the notation of (30) and (31) and putting

$$R = \frac{gW}{c_0^2 \cdot K} = \frac{2\tau}{(1-\tau^2)}\left[\frac{1}{\chi}\frac{d\chi}{dx} + \frac{(m+1)}{x_0} - \frac{1}{2\tau}\right]_{x=x_0}, \quad (50)$$

we find that

$$p(0, r, t) = Ar^{-\frac{1}{2}} \exp(i\sigma t - ik_1 r + i3\pi/4) \times [(\tau)^{\frac{1}{2}}\partial R/\partial x]^{-1}. \quad (51)$$

The quantity $[(\tau)^{\frac{1}{2}}\partial R/\partial x]^{-1}$, giving the relative excitation of the various frequencies in the pressure oscillation by a w-point source, is shown for atmosphere b by curve A of Fig. 2. As expected, it vanishes at the cut-off frequency. This curve applies only to the steady-state solution. For an impulsive excitation, such as the explosion of the Great Siberian Meteor was, one must take into account the additional weakening of the amplitude with increasing range because of the stretching of the wave by dispersion. This dispersive stretching introduces an additional factor $[r(d^2k/d\sigma^2)]^{-\frac{1}{2}}$ into (51). It arises from the evaluation of a σ-integral over (49) at the point of stationary phase of the exponential term. This factor, which is inversely proportional to the square root of the slope of the (U/c_0) curve *III* in Fig. 1, favors the short periods over the long ones. As a result, a relative excitation of atmosphere b by an impulsive w-point source, as shown by curve B in Fig. 2, is obtained. While this curve would fit the Krakatoa wave, for which the w-source is, moreover, a plausible excitation, the records of the Siberian Meteor wave shown in Fig. 3 suggest a preference for a period of from 5 to 8 minutes.

6. EXCITATION OF THE FREE OSCILLATION OF ATMOSPHERE b BY A POINT SOURCE SITUATED AT THE GROUND IN WHICH THE PRESSURE VARIATION HAS A UNIFORM SPECTRUM

In the impulsive excitation curve B of Fig. 2 the comparison was made on the basis of a uniform spectrum in w. It was, moreover, assumed that at the source the spacial distribution of w was represented by the discontinuous integral in (45). While it is of interest to analyze the field produced by a point source of well-defined characteristics, and w in (45) is a function which meets the required boundary condition at the ground, we must examine more closely the nature of the field in the immediate vicinity of a point source which radiates in a medium governed by the rather complex Eqs. (9) and (10), or (15). Because of the anisotropy resulting from the vertical stability of the atmosphere, we should not expect that the emitted wave will have even initially a spherical wave front. The deviation from initial spherical symmetry should be small at acoustic frequencies, but could become appre-

ciable near Brunt's resonant frequency. Now the integral in (45) has the following origin. In the solution of the acoustic wave equation

$$\nabla^2\varphi=(1/c^2)(\partial^2\varphi/\partial t^2), \tag{52}$$

where c^2 may be a function of z, in the form

$$\varphi(z, r, t)=e^{i\sigma t}\int_0^\infty F(z, \sigma, k)J_0(kr)dk, \tag{53}$$

$$\ddot{F}+[(\sigma^2/c^2)-k^2]F=0, \tag{54}$$

the conditions at a point source situated at $z=z_1$ are determined from the behavior of F at large wave numbers k. The asymptotic behavior of F for large k and small values of $(z-z_1)$ is $\exp[-k|z-z_1|]$, so that near the source

$$\varphi\to e^{i\sigma t}\int_0^\infty \exp[-k|z-z_1|]J_0(kr)dk = e^{i\sigma t}/[(z-z_1)^2+r^2]^{\frac{1}{2}}. \tag{55}$$

It follows from (55) that at $z=z_1$

$$\frac{\partial\varphi^-}{\partial z}-\frac{\partial\varphi^+}{\partial z}=w^+-w^-=e^{i\sigma t}\int_0^\infty J_0(kr)kdk. \tag{56}$$

where $+$ and $-$ refer to $z>z_1$ and $z<z_1$, respectively. This function is equal to the limit assumed by $2e^{i\sigma t}(z-z_1)/R$, as $z\to z_1$, namely, zero everywhere except at $r=0$, where it becomes infinite like $2e^{i\sigma t}/(z-z_1)$. The specification of a point-source solution of (52) by (56), which is attributable to Lamb,[10] gives the right result in the case of constant c and in the case of $c=az$, for which an explicit solution of the form (55) has been derived.[11]

In the free oscillations of the atmosphere, the asymptotic solution of (9), or of (15), for large k and small $(z-z_1)$ is

$$\begin{aligned} &A\exp\left[-(k/\sigma)\int_{z_1}^{z}Qdz\right], \quad z>z_1; \\ &A\exp\left[-(k/\sigma)\int_{z}^{z_1}Qdz\right], \quad z<z_1. \end{aligned} \tag{57}$$

Hence, if we are considering a point source situated at $z=z_1$ in which the *pressure p varies like* $e^{i\sigma t}$, we have for the boundary condition at the source

$$\frac{\partial p^-}{\partial z}-\frac{\partial p^+}{\partial z}=2(Q/\sigma)\int_0^\infty J_0(kr)kdk, \quad z=z_1. \tag{58}$$

We shall now obtain the complete solution for a p-point source situated at $z=z_1$, and, after allowing $z_1\to z_0$ (the ground), shall compute the relative excitation function for various periods. For the region above the source, let

$$\chi=\chi_1=CN, \quad \beta p_1=C(gc^2\dot{N}+\omega N), \quad z<z_1, \tag{59}$$

$$\beta\equiv(k^2g^2-\sigma^4)/(i\rho_0\sigma), \quad \omega\equiv(\gamma g^2-\sigma^2c^2), \tag{60}$$

where N is the solution of (9) which gives an integrable wave energy per atmospheric column. In the region between the source and the ground let

$$\begin{aligned} &\chi=\chi_2=AM+BN, \\ &\beta p_2=A(gc^2\dot{M}+\omega M)+B(gc^2\dot{N}+\omega N), \\ &\qquad\qquad z_0>z>z_1. \end{aligned} \tag{61}$$

From the boundary condition of the vanishing of w at the ground we get by (10) and (61),

$$(B/A)=-\{[\sigma^2c^2\dot{M}+g(\gamma\sigma^2-k^2c^2)M]/[\sigma^2c^2\dot{N}+g(\gamma\sigma^2-k^2c^2)N]\}_{z=z_0}. \tag{62}$$

At the source we must have continuity of p, and

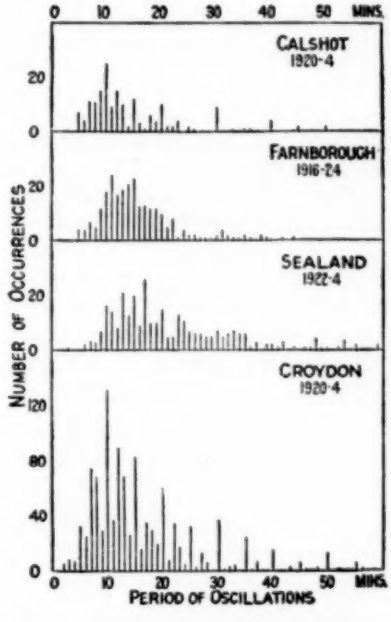

FIG. 4. Frequency of occurrence of pressure oscillations of well developed periods on microbarograms at English stations (after N. K. Johnson, reference 13).

[11] C. L. Pekeris, see reference 10.

we must satisfy (58):

$$p_1=p_2, \quad \dot{p}_1-\dot{p}_2=2(Q/\sigma)k, \tag{63}$$

which determine A, B, and C. After letting $z_1\to z_0$ in these relations, we arrive at the desired solution for a p-point source situated on the ground:

$$p(z_0, r, t)=\frac{-2\sigma c^2 e^{i\sigma t}}{Q} \times\int_0^\infty \frac{J_0(kr)kdk(gc^2\dot{N}+\omega N)}{[\sigma^2c^2\dot{N}+g(\gamma\sigma^2-k^2c^2)N]}, \tag{64}$$

where N and $\dot{N}$ are evaluated at z_0. This integral can now be evaluated in terms of normal modes by the method of residues, and the result is a steady-state excitation function of the form

$$p=Ar^{-\frac{1}{2}}\exp(i\sigma t-ik_1r+i3\pi/4) \times[(\tau)^{\frac{1}{2}}Q(\partial R/\partial x)]^{-1}, \tag{65}$$

which differs from (51) by the extra factor $(1/Q)$. The same factor attaches also to the impulsive excitation function B of Fig. 2. Since Q vanishes at Brunt's period (9.5 minutes in atmosphere b), it follows that the impulsive excitation function for a p-point source vanishes at the cut-off period of 2 m and is peaked at 9.5 m. The integral of the excitation function over a finite spectral band width, including the Brunt period, is of course finite.

7. APPLICATIONS TO THE PRESSURE WAVE PRODUCED BY THE GREAT SIBERIAN METEOR AND TO PRESSURE OSCILLATIONS RECORDED ON MICROBAROGRAPHS IN ENGLAND

Figure 3 shows some original pressure records of the Great Siberian Meteor wave of 1908 obtained on microbarographs at several stations in England, and, on the right, a composite drawing of the principal features of these records made by F. J. W. Whipple.[1] A first pressure rise, lasting about 3 minutes, is followed by a rapid drop in the next two minutes, and then by a succession of four damped oscillations of about 2 minutes' period. The ratio of the velocities of the first arrival (323 m/sec.) to that of the last of the 2-min. waves (308 m/sec.) agrees with the ratio of the corresponding group velocities in atmosphere b shown in Fig. 1. With an assumed surface temperature of 288°K, $c_0=341$ m/sec., and the group velocity at a period of 2 min. in atmosphere b is 293 m/sec. This is 5 percent less than the observed value of 308 m/sec. The difference could be due either to a lower value of the surface temperature or to an actual stratospheric temperature of about 240°K, as against the assumed value of 220°K. The fact that no periods shorter than 2 min. were recorded, suggests the cut-off period shown in Fig. 1. The shocks recorded at 5^h25^m and later are probably due to the various rays (or normal modes) which travel through the sound channel associated with a minimum sound velocity in the stratosphere, in the manner observed by Ewing and co-workers[12] in the oceanic sound channel.

Figure 4 gives an analysis made by Johnson[13] of the frequency of occurrence of oscillations of well developed periods on microbarograms at English stations. He interprets the peaks as being associated with Brunt's resonant period. This view is supported by the excitation function for a pressure point source given in (65). The lack of periods less than 2 minutes is also manifest. In this connection the following quotation from Johnson's paper is of interest:

"In the second place we may notice that oscillations with a period of two minutes (or even less) are extremely obvious and very easily detected in the records of any properly adjusted microbarograph. The small number of oscillations of short period (say less than seven minutes) shown in Fig. 1 cannot therefore be attributed to difficulty of detection."

There are a number of problems raised by this investigation to which the writer hopes to return.

[12] M. Ewing *et al.*, Bull. Geol. Soc. Am. **5**, 930 (1946); B. Gutenberg, Bull. Seis. Soc. Am. **36**, 327 (1946); J. Meteor. **3**, 27 (1946).

[13] N. K. Johnson, Q. J. Roy. Meteor. Soc. **55**, 20 (1929).

On the Theory of Ferromagnetic Resonance Absorption

CHARLES KITTEL
Bell Telephone Laboratories, Inc., Murray Hill, New Jersey
(Received October 8, 1947)

The theory of ferromagnetic resonance absorption previously developed is extended to include the effect of the shape of the specimen and, in the case of a single crystal, the effect of crystal orientation. The resonance condition may be written $\omega_0=\gamma H_{eff}$, where H_{eff} is equal to $(BH)^{\frac{1}{2}}$ for a plane surface, $H+2\pi M$ for a long circular cylinder, and H for a sphere; the latter two values apply only to the situation in which the eddy current skin depth is large in comparison with the radius of the specimen. In the case of an uniaxial crystal with the axis parallel to the static magnetic field, the value of H to be used in the resonance conditions is increased by $2K/M$, where K is the anisotropy constant. The case of a cubic crystal is also considered. A detailed discussion of macroscopic eddy current effects is given, and it is shown that the usual eddy current losses do not introduce damping terms into the expression for the permeability, when properly interpreted.

I. INTRODUCTION

FERROMAGNETIC resonance absorption is the analog of paramagnetic and nuclear resonance absorption. The ferromagnetic effect was found originally by Griffiths,[1] and further confirmation has been reported by Yager and Bozorth.[2] A theory of the resonance effect has been proposed by the present author.[3]

In a typical experimental arrangement the ferromagnetic specimen is in the form of a thin sheet or foil, which is employed as one wall of a rectangular cavity terminating a wave guide fed by a microwave generator. The ferromagnetic side of the cavity is chosen so that the magnetic vector of the microwave field is constant in direction in the plane of the wall. A static magnetic field is applied (by means of an electromagnet) also in the plane of the wall but perpendicular to the microwave magnetic field. It is found experimentally that the energy loss in the cavity goes through a maximum as the strength of the static magnetic field is increased. For example, Yager and Bozorth found a sharp resonance peak in a Supermalloy specimen for a field strength near 5000 oersted when using a frequency near 24,000 Mc/sec. The measured Q of their cavity dropped sharply from a value of several thousand on either side of resonance to a value of several hundred at resonance.

The principal result of the theory[3] is that the resonance condition for a plane surface should be given by

$$\omega_0=\gamma(BH)^{\frac{1}{2}}, \tag{1}$$

instead of the Larmor condition $\omega_0=\gamma H$; here ω_0 is the frequency at resonance; γ is the magnetomechanical ratio for an electron spin; H is the strength of the static magnetic field, and B is the magnetic induction in the specimen.

The considerations set forth below elucidate and extend certain aspects of the original theory. The discussion generally follows macroscopic and classical lines, analogous to the Bloch[4] treatment of the nuclear induction experiment. In a paper which is to appear in *The Physical Review*, Van Vleck has shown that a quantum-mechanical treatment of ferromagnetic resonance leads to the identical resonance condition as the classical theory.

II. DEPENDENCE OF RESONANCE CONDITION ON THE SHAPE OF THE SPECIMEN

The equation $\omega_0=\gamma(BH)^{\frac{1}{2}}$ was derived specifically for a plane surface. The derivation of the resonance condition is intimately related to the nature of the demagnetizing field, and it is reasonable to expect that the equation will depend on the shape of the specimen. It turns out, for example, that the resonance condition in a *small sphere* of ferromagnetic material is given by the Larmor equation $\omega_0=\gamma H_a$.

[1] J. H. E. Griffiths, Nature **158**, 670 (1946).
[2] W. A. Yager and R. M. Bozorth, Phys. Rev. **72**, 80 (1947).
[3] C. Kittel, Phys. Rev. **71**, 270 (1947).
[4] F. Bloch, Phys. Rev. **70**, 460 (1946).

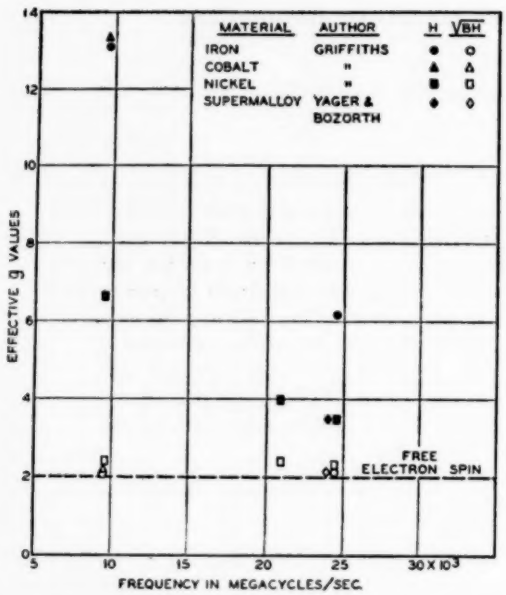

FIG. 1. Summary of data on ferromagnetic resonance in plane specimens: comparison of effective g values using both H and $(BH)^{\frac{1}{2}}$ as the effective magnetic field in the resonance condition. For an electron spin $g=2.00$.

We shall limit the discussion to shapes for which the demagnetizing factors have a rigorous meaning. We must accordingly discuss only objects which are uniformly magnetized at the frequencies under consideration. It is therefore necessary that certain dimensions of the specimens be small in comparison with the eddy current skin depth. A plane surface is in a sense an exception to this requirement.

The skin depth in the ferromagnetic metals at microwave frequencies is of the order of 10^{-5} to 10^{-4} cm, so that only very fine particles will satisfy the size requirement. However, the new ferromagnetic semi-conductor materials offer unusual possibilities for working with specimens of a convenient size. For example, Snoek[5] gives the resistivity of "Ferroxcube 4," which is a Ni-Zn ferrite, as 10^6 ohm-cm, or about 10^{11} higher than the resistivity of iron. The skin depth is ~ 3 cm at $\lambda=1$ cm and $\mu=100$. One should be able to work at microwave frequencies with a single shaped specimen of such material with dimensions of the order of 0.1 to 1 cm.

The magnetization $\mathbf{M}$ and angular momentum density $\mathbf{J}$ are related by

$$\mathbf{M}=\gamma\mathbf{J}, \tag{2}$$

where γ is the magneto-mechanical ratio and is equal to e/mc for electron spins; numerically, $\gamma/2\pi=2.80$ megacycles/oersted. The equation of motion referred to unit volume of material is

$$d\mathbf{J}/dt=\mathbf{M}\times\mathbf{H}, \tag{3}$$

since the expression on the right is the torque acting on a unit volume. This equation may be written

$$d\mathbf{M}/dt=\gamma\mathbf{M}\times\mathbf{H}. \tag{4}$$

We now consider the resonance condition for a general ellipsoid with principal axes parallel to the x, y, z axes of the coordinate system. The demagnetizing factors are N_x, N_y, N_z. The static magnetic field is H_z; the r-f field* is H_x. The effective values of the magnetic field components inside the material are:

$$H_x{}^i=H_x-N_xM_x; \tag{5a}$$

$$H_y{}^i=-N_yM_y; \tag{5b}$$

$$H_z{}^i=H_z-N_zM_z. \tag{5c}$$

The values $H_x{}^i$, $H_y{}^i$, $H_z{}^i$ should be used when substituting for H in Eq. (4). The component equations of Eq. (4) become

$$dM_x/dt=\gamma[H_z+(N_y-N_z)M_z]M_y; \tag{6a}$$

$$dM_y/dt=\gamma[M_zH_x-(N_z-N_x)M_xM_z - M_xH_z]; \tag{6b}$$

$$dM_z/dt\cong 0. \tag{6c}$$

On solving these equations with time dependence $\exp[j\omega t]$, the susceptibility $\chi_x(=M_x/H_x)$ is found to be

$$\chi_x=\frac{\chi_0}{1-(\omega/\omega_0)^2}, \tag{7}$$

[5] J. L. Snoek, *New Developments in Ferromagnetic Materials* (Elsevier, Amsterdam, 1947), p. 97; Philips Technical Review **8**, 353 (1946).

* This convention for the labeling of static and r-f fields will be followed throughout the present paper. It may be noted that the Weiss exchange field does not enter into the problem, since the exchange field is parallel to $\mathbf{M}$ and hence its vector product with $\mathbf{M}$ is identically zero. Any anisotropic term in the Lorentz local field is lumped in with the crystalline anisotropy energy, which is treated below. In the quantum-mechanical treatment the Weiss field does not enter because the operator $\Sigma\sigma_i{}^z$ commutes with the exchange interaction term in the Hamiltonian, as Van Vleck has shown.

where

$$\chi_0=\frac{M_z}{H_z+(N_z-N_z)M_z} \tag{8}$$

and the *resonance frequency* is given by

$$\omega_0=\gamma\{[H_z+(N_y-N_z)M_z] \times[H_z+(N_z-N_z)M_z]\}^{\frac{1}{2}}. \tag{9}$$

We shall consider some special cases of Eq. (9):

(a) *Plane* ($N_z=N_z=0$; $N_y=4\pi$)

$$\omega_0=\gamma(B_zH_z)^{\frac{1}{2}}. \tag{10}$$

(b) *Sphere* ($N_z=N_y=N_z=4\pi/3$)

$$\omega_0=\gamma H_z. \tag{11}$$

(c) *Infinite Circular Cylinder* ($N_z=N_y=2\pi$; $N_z=0$)

$$\omega_0=\gamma(H_z+2\pi M_z). \tag{12}$$

It is seen that, except for the special cases of a plane and a sphere, Eq. (7) predicts the *existence of a finite resonance frequency even for zero static field.* It should however be emphasized at this point that the ferromagnetic resonance effect may only be conspicuous when the entire specimen is magnetized to saturation as a *single domain;* otherwise the inhomogeneous magnetization may lead to high damping by eddy currents. It will commonly be necessary to apply at least a small static field in order to insure approximate saturation.

It is clear from the behavior in the general case just considered that the demagnetizing fields affect the resonance condition by changing the magnetic field energy associated with a given direction of the magnetization vector.

Some numerical comparisons are given below in order to show the importance of the shape effect. The material considered is iron, for which $M_z\cong1700$; for electron spins $\gamma/2\pi=2.80$ Mc/oersted.

Example A $H=1000$ oersted.
Plane: $f_0=13{,}300$ Mc/sec.
Sphere: $f_0=2{,}800$ Mc/sec.
Cylinder: $f_0=32{,}800$ Mc/sec.

Example B $H\cong0$.
Plane: $f_0=0$.
Sphere: $f_0=0$.
Cylinder: $f_0=30{,}000$ Mc/sec.

Figure 1 is based on the published data on ferromagnetic resonance in *plane* specimens. The scale of ordinates is the effective g value as calculated from the observed frequency and magnetic field at resonance. The solid points are the g-values as calculated assuming the ordinary Larmor resonance condition with H_z as the effective field. The hollow points are calculated for the same observations but using $(BH)^{\frac{1}{2}}$ as the effective field; it is seen that this assumption leads to g values very much closer to the value $g=2.00$ which obtains for an electron spin. The values remain slightly high, however; no satisfactory explanation of the residual deviation has been put forward.

Figure 2 compares the theoretical resonance conditions for a plane surface and for a small sphere. The value of the saturation magnetization is taken as for a representative ferrite.

III. EFFECT OF CRYSTALLINE ANISOTROPY ENERGY ON THE RESONANCE CONDITION

The energy of ferromagnetic crystals depends in part on the magnetization direction relative to the crystal axes; this part of the energy is called the anisotropy energy. In an uniaxial

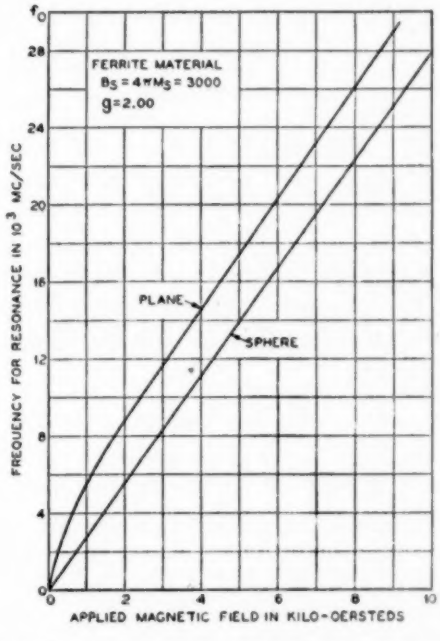

FIG. 2. Comparison of theoretical resonance conditions for a plane surface and for a small sphere (diameter small in comparison with eddy current skin depth).

crystal such as cobalt, the major term in the anisotropy energy may be written

$$f=K_1' \sin^2\theta, \tag{13}$$

where f refers to unit volume of material; θ is the angle between the magnetization and the principal axis of the crystal; K_1' is the first order anisotropy constant. Similarly in a cubic crystal

$$f=K_1(\alpha_1^2\alpha_2^2+\alpha_2^2\alpha_3^2+\alpha_1^2\alpha_3^2), \tag{14}$$

where α_1, α_2, α_3 are the direction cosines of the magnetization relative to the cube edges.

The anisotropy energy will in general effect an alteration in the resonance condition. In a single crystal one expects to find that the value of the magnetic field required for resonance at a fixed frequency will depend on the direction of the crystal axes relative to the shape axes of the specimen. In a polycrystalline specimen the resonance in general will be broader than in a single crystal of the same material, since the distribution in direction of the crystal axes causes a distribution in field strengths for resonance.

It is convenient to consider the effect of the anisotropy energy in terms of an equivalent magnetic field.[5a] The equivalent field $\mathbf{H}^e$ is defined such that the torque exerted on the specimen by such a field is equal to the torque exerted by the anisotropy energy: that is,

$$\partial f/\partial\theta=\mathbf{M}_s\times\mathbf{H}^e \tag{15}$$

where θ is a rotation about an axis parallel to the direction of $\mathbf{M}_s\times\mathbf{H}^e$. *The vector* $\mathbf{H}^e$ *is not completely determined by Eq. (15), since either the magnitude or the direction are still arbitrary.* It is often appropriate to take $\mathbf{H}^e$ parallel to the x or y axes of the specimen** and to express its magnitude in terms of an *effective demagnetizing factor* N^e defined by

$$H_x^e=-N_x^eM_x \tag{16a}$$

and

$$H_y^e=-N_y^eM_y. \tag{16b}$$

The resonance condition is then determined by adding N_x^e, N_y^e to the usual demagnetizing factors in Eq. (9), giving

$$\omega_0=\gamma\{[H_z+(N_y+N_y^e-N_z)M_z] \times[H_z+(N_x+N_x^e-N_z)M_z]\}^{\frac{1}{2}}, \tag{17}$$

as the general condition for resonance in an ellipsoidal single crystal when the static magnetic field H_z is along one of the principal axes of the ellipsoid.

It remains now to determine the values of the effective demagnetizing factors N_x^e and N_y^e for representative experimental situations.

(a) *Uniaxial crystal; H_z along axis.*

$$\partial f/\partial\theta=2K_1' \sin\theta\cos\theta=\mathbf{M}_s\times\mathbf{H}^e \cong N_x^eM_xM_x\cong N_x^eM_z^2\sin\theta, \tag{18}$$

so that, for angles near $\theta=0$,

$$N_x^e=(2K_1'/M_z^2); \tag{19a}$$

similarly,

$$N_y^e=(2K_1'/M_z^2). \tag{19b}$$

The resonance condition for a plane specimen is

$$\omega_0=\gamma\left\{\left(H_z+4\pi M_z+\frac{2K_1'}{M_z}\right)\left(H_z+\frac{2K_1'}{M_z}\right)\right\}^{\frac{1}{2}}. \tag{20}$$

This equation predicts a finite limiting frequency as $H\rightarrow 0$; in practice a small biasing field will usually be required in order to eliminate domain boundary effects. The possibility of resonance in the "anisotropy field" was first considered by Landau and Lifshitz,[6] for the special case of uniaxial crystals. Their treatment neglects the effects of demagnetizing fields and the eddy current damping associated with the movement of domain boundaries.

(b) *Cubic crystal; H_z, H_z along [100] directions.*

In a (100) plane Eq. (14) for the anisotropy energy reduces to

$$f=(K_1/4)\sin^2 2\theta, \tag{21}$$

where θ is the angle between the magnetization and a [100] axis. We have

$$\partial f/\partial\theta=K_1\sin 2\theta\cos 2\theta=N_x^eM_z^2\sin\theta; \tag{22}$$

[5a] In general the torque vector resulting from the anisotropy energy is to be treated directly as an additional torque in the equations of motion. The artifice of the effective field or effective demagnetizing factors is applicable to planes and directions of high symmetry, and is a convenience in that it often avoids solving the equations of motion over again for each situation.

** When $N_x^e=N_y^e$ it may be convenient to consider $\mathbf{H}^e$ as parallel to the z axis; see, for example, Eq. (20).

[6] L. Landau and E. Lifshitz, Physik. Zeits. Sowjetunion **8**, 153 (1935); see also J. L. Snoek, Nature **160**, 90 (1947).

so that for angles near $\theta=0$,

$$N_x^e=(2K_1/M_s^2); \tag{23a}$$

similarly,

$$N_y^e=(2K_1/M_s^2). \tag{23b}$$

The results for this orientation are similar to those worked out above for cobalt. The numerical value of the effective field in the z-direction is $2K_1/M_s\sim 7000$ oersted in Co and ~ 500 oersted in Fe, at room temperature.

(c) *Cubic crystal; H_x, H_z along [110] directions.*

Let $\epsilon=\theta-\pi/4$; then

$$\partial f/\partial\epsilon=-K_1\sin 2\epsilon\cos 2\epsilon=N_x^e M_s^2\sin\epsilon, \tag{24}$$

so that for angles near $\epsilon=0$,

$$N_x^e=-(2K_1/M_s^2); \tag{25a}$$

the negative sign should be noted. To determine N_y^e we write the anisotropy energy as

$$f=K_1(\tfrac{1}{4}\sin^2 2\theta+\alpha_3^2), \tag{26}$$

so that

$$-\partial f/\partial\theta_3=2K_1\cos\theta_3\sin\theta_3=N_y^e M_s^2\cos\theta_3, \tag{27}$$

giving, for angles near $\theta_3=\pi/2$,

$$N_y^e=(2K_1/M_s^2). \tag{25b}$$

The difference in sign between N_x^e and N_y^e may be confirmed by considering the general shape of the anisotropy energy surface. An instructive photograph of a model of the surface is given by Bitter.[7]

A comparison of cases (b) and (c) shows that the magnetic field required for resonance with a (100) crystal face is expected to be greater when H_z is in the [110] direction than when H_z is in the [100] direction. The difference ΔH_z is of the order of $4K_1/M_s$ for $H_z\ll 4\pi M_s$. The theoretical resonance conditions for [100] and [110] directions are compared in Fig. 3.

The general expression for the resonance condition in the (001) plane is given by Eq. (17) with

$$N_x^e=2K_1\cos 4\theta/M_s^2, \tag{27a}$$

$$N_y^e=(2K_1+\tfrac{1}{2}K_2\sin^2 2\theta)/M_s^2, \tag{27b}$$

where θ is the angle between the z-axis and the [100] direction; here we have taken account of the second-order term $K_2\alpha_1^2\alpha_2^2\alpha_3^2$ in the anisotropy energy.

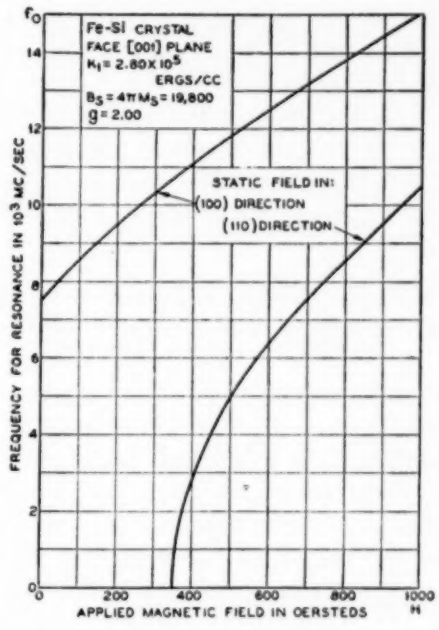

FIG. 3. Comparison of theoretical resonance condition for [100] and [110] directions in an Fe-Si single crystal with a (001) plane surface.

The discussion has supposed that the static magnetic field H_z is sufficiently large so that the static magnetization is in the direction of H_z. If this condition is not satisfied, we may under certain conditions still obtain resonance, but in the calculations it is then necessary to use as H_z the projection of the static field on the direction of the static magnetization; also, θ should be taken as the angle between the magnetization and the [100] direction.

Note added in proof: The predicted dependence of the resonance condition on angle in the (001) plane in ion has been verified approximately by Kip and Arnold (to be published) and by Yager (to be published). Kip and Arnold have also observed at 3 cm wave-length two resonance peaks for angles near [110]. Qualitatively it seems that this observation may be explained by the fact that the resonance condition may sometimes have two roots if the static field H_z is of the same order of magnitude as K_1/M_s, so that the angle between the static field and magnetization may be appreciable. The quantitative treatment of the condition for the appearance of the second peak is difficult to carry through in

[7] F. Bitter, *Introduction to Ferromagnetism* (McGraw-Hill Book Company, Inc., New York, 1937), p. 195.

detail because of uncertainty[7a] as to the actual domain structure of the crystal in the relevant range of field strength.

One may treat magnetostrictive energy due to strains on the same basis as the anisotropy energy, so that one would expect the resonance condition to depend on the state of strain of the material.

IV. FERROMAGNETIC RESONANCE IN THE PRESENCE OF MACROSCOPIC EDDY CURRENTS—PLANE SURFACE

The usual measurements and computations involved in deducing values of the effective permeability μ_R as a function of the static field H_s are listed below. In the experiments it is found that μ_R as determined in this way shows a well-defined maximum for values of H somewhere near the value predicted by Eq. (1).

(a) The cavity Q as a function of H_s is determined by means of standing wave ratio measurements[8] in a slotted section of wave guide connecting the r-f power supply to the resonant cavity.

(b) From the measured Q's and the known geometry of the cavity one can calculate[9] (at least approximately) the value of the "loss factor" $(\mu_R\rho)^{\frac{1}{2}}$ for each of the walls of the cavity separately.

(c) Taking ρ from d.c. measurements, we are able to calculate μ_R *vs.* H_s as desired.

Mention should be made of the connection between the complex permeability $\mu=\mu_1-j\mu_2$ with which the theory commonly deals and the effective permeability μ_R which emerges from the interpretation, as above, of the results of a resistive type of measurement, such as a cavity Q measurement.[10] The *resistive loss* from the skin effect is determined by the *imaginary* part of the complex wave number $k=k_1-jk_2$, which describes the spatial variation of the magnetic field within a conducting surface according to an equation of the form $H_x\sim e^{-jky}=e^{-k_2y}e^{-jk_1y}$. From the differential equation for eddy currents one finds

$$k\sim(-j\mu)^{\frac{1}{2}}=j(\mu_2+j\mu_1)^{\frac{1}{2}}=\frac{1}{\sqrt{2}}(\mu_L^{\frac{1}{2}}-j\mu_R^{\frac{1}{2}}), \quad (28)$$

where the term on the extreme right may be viewed as defining the real quantities μ_L and μ_R. This definition is consistent with the characteristic properties of μ_R and μ_L.

From Eq. (28) we find the well-known result

$$\mu_R=(\mu_1^2+\mu_2^2)^{\frac{1}{2}}+\mu_2; \quad (29a)$$

$$\mu_L=(\mu_1^2+\mu_2^2)^{\frac{1}{2}}-\mu_2. \quad (29b)$$

If μ is real, $\mu_R=\mu_L=\mu$.

By a Q measurement only μ_R is determined; μ_L is the effective permeability for an inductive measurement and may be determined from the shift in resonance frequency of the *cavity*—this is a far more difficult determination than an ordinary Q measurement.

The above discussion enables one to interpret the results of theoretical derivations for uniformly magnetized specimens—uniform with respect to both static and r-f components of magnetization—in terms of the experimental situation, which in normal ferromagnetic conductors involves the non-uniform r-f magnetization associated with eddy currents.

Because the argument may seem somewhat devious, it is intended below to treat the matter in a more direct way. In particular it will emerge clearly that, when the results of an experiment are properly interpreted, the *usual eddy current losses do not as such introduce damping terms into the expression for the permeability.*

In addition to Eq. (4) we must consider the relation between M and H given by the eddy current equation:

$$\nabla^2\mathbf{H}=(4\pi/\rho c^2)\left(\frac{d\mathbf{H}}{dt}+4\pi\frac{d\mathbf{M}}{dt}\right), \quad (30)$$

which is a consequence of Maxwell's equations for curl$\mathbf{E}$ and curl$\mathbf{H}$; here ρ is the resistivity.

[7a] A. von Engel and M. S. Wills, Proc. Roy. Soc. **A188**, 464 (1947).

[8] See, for example, J. C. Slater, Rev. Mod. Phys. **18**, 441 (1946).

[9] Actually the observed Q's do not usually agree very closely with the values calculated for cases where the permeability μ is unity and the resistivity ρ is taken from d.c. measurements. The resulting uncertainty in μ_R (in cases where this is not unity) does not affect appreciably the deduced values of the resonance frequency and the half-width of the resonance. It seems reasonable to require that μ_R approach unity as H approaches infinity, and this requirement can be invoked as a partial check on the normalization of μ_R.

[10] For a more detailed discussion of this point, see C. Kittel, Phys. Rev. **70**, 281 (1946).

For a plane surface the components of $\mathbf{H}$ are $(H_x, -4\pi M_y, H_z)$. Here H_x is the r-f field; H_z is the static field;[11] $H_y = -4\pi M_y$ as a consequence of the demagnetization factor $N_y = 4\pi$.

Neglecting products of small quantities, Eqs. (4) and (30) reduce to the following, where we have assumed solutions of the form $H_x, M_x, M_y \sim \exp[j(\omega t - ky)]$:

$$j\omega M_x - \gamma B_z M_y = 0, \tag{31a}$$

$$j\omega M_y - \gamma(M_z H_x - M_x H_z) = 0, \tag{31b}$$

$$(jp^2 + k^2)H_x + j4\pi p^2 M_x = 0. \tag{31c}$$

Here $p^2 = 4\pi\omega/\rho c^2$. The set of three homogeneous linear equations in the three unknown H_x, M_x, M_y has a non-trivial solution if the determinant

$$\begin{vmatrix} 0 & j\omega & -\gamma B_z \\ -\gamma M_z & \gamma H_z & j\omega \\ (jp^2 + k^2) & j4\pi p^2 & 0 \end{vmatrix} = 0. \tag{32}$$

The determinantal equation reduces to

$$k^2 = jp^2 \frac{\mu_0\omega_0^2 - \omega^2}{\omega^2 - \omega_0^2}, \tag{33}$$

where

$$\omega_0 = \gamma(B_z/H_z)^{\frac{1}{2}} \tag{34}$$

and

$$\mu_0 = B_z/H_z. \tag{35}$$

Now the ordinary eddy current equation for permeability μ_R leads to

$$k^2 = -j\mu_R p^2, \tag{36}$$

which is identical with Eq. (33) if we set

$$\mu = \mu_R = (\omega_0^2\mu_0 - \omega^2)/(\omega_0^2 - \omega^2). \tag{37}$$

The susceptibility χ_x is therefore

$$\chi_x = \chi_0/[1 - (\omega/\omega_0)^2], \tag{38}$$

with $\chi_0 = M_{sat}/H_z$ and $\omega_0 = \gamma(B_z H_z)^{\frac{1}{2}}$. This result is identical with that derived in the earlier paper,[3] where eddy currents were not considered explicitly; we may therefore conclude that the macroscopic eddy current losses do not enter in the expression for the susceptibility.

[11] It is assumed here that the specimen is a thin plane sheet, so that we may neglect demagnetizing corrections to the field H_z.

It is of interest to consider the form of the orbit described by the magnetization vector. Equation (31a) shows that M_x and M_y differ in phase by $\pi/2$, and $|M_x|/|M_y| = \gamma B_z/\omega$. The orbit is therefore an ellipse; at resonance the ratio of the principal axes is $(B_z/H_z)^{\frac{1}{2}}$, with the long axis parallel to the plane surface of the specimen and the short axis normal to the surface.

V. CONCLUSION

The results of this paper predict several new effects which have not as yet been reported experimentally. The resonance condition is expected to depend on the shape of the specimen, and, in the case of a single crystal, also on the orientation of the crystal. It may be possible to test the predicted shape dependence using ferromagnetic semi-conducting materials, such as the ferrites.

The considerations given here throw no light on the anomalous g value of 2.17 reported by Yager and Bozorth[2] using a Supermalloy specimen, since the anisotropy and magnetostriction of this material are very low. The quantum mechanical treatment by Van Vleck also does not account for this anomaly, since his treatment leads to the usual resonance condition.

In connection with relaxation or damping effects, it may be remarked in passing that the failure[2] of the relaxation term $-\lambda(\mathbf{M} - \chi_0\mathbf{H})$ proposed previously[3] is not particularly alarming in the absence of a detailed physical description of the relaxation process. The basis for the above term is purely formal, and the term could have been written $-\lambda'[(\mathbf{M}/\chi_0) - \mathbf{H}]$, which will fit the data of Yager and Bozorth in a satisfactory manner.

I am indebted to Professor J. H. Van Vleck for a discussion of the quantum-mechanical treatment of the problem, and to W. A. Yager for discussions of the effect of various relaxation terms. Part of the work reported here was done at the Massachusetts Institute of Technology during the tenure of a fellowship of the John Simon Guggenheim Memorial Foundation. I wish to thank Professor J. C. Slater and Professor J. A. Stratton for their hospitality, and the trustees of the Foundation for financial support.

Crystalline Stark Splitting and Microwave Resonance Absorption in Paramagnetic Salts*

C. KITTEL** AND J. M. LUTTINGER***
Research Laboratory of Electronics, Massachusetts Institute of Technology, Cambridge, Massachusetts

(Received October 6, 1947)

A theoretical discussion is given of the application of microwave-absorption measurements to the determination of energy levels in single crystals of paramagnetic salts. Selection rules are given for magnetic-dipole transitions between sublevels in the presence of crystalline electric fields of cubic, tetragonal, trigonal, and rhombic symmetry. The Zeeman effect in the presence of crystalline electric fields is discussed in some detail for three special cases: (a) $J=5/2$, cubic field; (b) $J=7/2$, cubic field; (c) $J=3/2$, trigonal field. These examples may correspond approximately to certain magnetically dilute salts containing Fe^{+++}, Gd^{+++}, and Cr^{+++} ions, respectively, provided that exchange interactions do not play an important role and that the assumed symmetries are approximately correct. Numerical values are tabulated for the relative frequencies and line strengths associated with magnetic-dipole transitions in the cases discussed. The character of the spectra may change radically between the limit where the Zeeman splitting is small in comparison with the Stark splitting, and the opposite limit where the Stark splitting may be neglected.

I. INTRODUCTION

THE present knowledge[1–4] of the quantum states of paramagnetic salts is largely derived from the interpretation of measurements of magnetic susceptibilities, specific heats, and optical-absorption spectra. The difficulties in giving a consistent account of the various phenomena have been emphasized by Van Vleck at the 1939 Strasbourg conference,[3] and by Penney and Kynch.[5]

The recent experimental discovery by Zavoisky[6] of paramagnetic resonance absorption provides a new and direct method for the investigation of closely spaced energy levels in paramagnetic materials. The method consists of observing by means of electrical measurements the quantum transitions induced by a radiofrequency or microwave electromagnetic field. The salt is placed in an r-f circuit element situated between the pole pieces of an electromagnet. As the strength of the static field is varied the power absorption in the salt is found to pass through a well defined maximum.

In the measurements reported by Zavoisky the position of the resonance satisfies closely the Larmor equation for electron spins:

$$f/H_0=\frac{e}{2\pi mc}=2.80 \text{ megacycles/oe}, \qquad (1)$$

where f=frequency, H_0=static magnetic field, e=electronic charge in e.s.u., m=electronic mass, and c=velocity of light. The applicability of Eq. (1) to electron states in solids in which the spin is free was pointed out by Frenkel.[7] Under this condition, the experiment is analogous to the nuclear magnetic resonance experiment. It may be noted that this equation also holds in the presence of strong exchange coupling between spins.

On the present picture of paramagnetic solids the energy levels of the paramagnetic ions are affected in an important way by the inhomogene-

* This work was supported in part by Joint Service Contract No. W. 36-039 sc 32037.

** Now at Bell Telephone Laboratories, Murray Hill, New Jersey.

*** Now at Eidgenössische Technische Hochschule, Zürich, Switzerland.

[1] J. H. Van Vleck, *The Theory of Electric and Magnetic Susceptibilities* (Oxford University Press, London, 1932).

[2] H. B. G. Casimir, *Magnetism and Very Low Temperatures* (Cambridge University Press, Teddington, England, 1940).

[3] Université de Strasbourg, *Le Magnétisme: Tome 3: Paramagnétisme* (Institut International de Coopération Intellectuelle, Paris, 1940).

[4] C. J. Gorter, *Paramagnetic Relaxation* (Elsevier Publishing Company, Inc., Amsterdam, 1947).

[5] W. G. Penney and G. J. Kynch, Proc. Roy. Soc. **A170**, 112 (1939); see also J. H. Van Vleck, J. Phys. Chem. **41**, 67 (1937); S. Freed, Rev. Mod. Phys. **14**, 105 (1942).

[6] E. Zavoisky, J. Phys. U.S.S.R. **9**, 211, 245, 447 (1945); **10**, 170, 197 (1946); see also R. L. Cummerow and D. Halliday, Phys. Rev. **70**, 433 (1946); R. L. Cummerow, D. Halliday, and G. E. Moore, Phys. Rev. **72**, 173 (1947).

[7] J. Frenkel, J. Phys. U.S.S.R. **9**, 299 (1945).

ous crystalline electric fields, which are caused largely by the dipole moments of the water of hydration. The crystalline Stark effect splits the degenerate energy levels of the free ions. This splitting of a single level into several components makes possible the occurrence in an r-f field of magnetic-dipole transitions between the split components, even in the absence of a static magnetic field. A second effect of the splitting is to change the character of the Zeeman effect in a static magnetic field: under certain conditions we might expect to find several lines in the absorption spectrum, in contrast to the single line found by Zavoisky.

In Section II of this paper we discuss some aspects of microwave-absorption spectra in the absence of the Zeeman effect ($H_0=0$). In Section III the combined Zeeman and crystalline Stark effects are considered for three particular situations of interest in the microwave range. All of our calculations refer to single crystals, with the static and r-f magnetic fields along crystal axes of high symmetry. The situation for powdered specimens of these salts is extremely complicated, and would probably not give as much information as the single crystals.

It is possible that in a large number of salts the effect of the Stark splitting will be erased by strong exchange coupling between ions. The prevalence of such coupling is perhaps one of the more important things which might be determined by paramagnetic resonance experiments. *The specific cases of crystalline splitting considered in this paper are presented only as illustrations of the kind of behavior to be expected in the absence of exchange interactions; our calculations are not applicable in the presence of strong exchange coupling.* Various effects of exchange coupling are considered by J. H. Van Vleck, in a paper which is to appear in *The Physical Review*. It should also be emphasized that the angular dependence of the crystalline electric fields may be more complicated than assumed here.

Note added in proof: Measurements on Chrome Ammonium Alum at microwave frequencies have been reported very recently[7a] which show clearly the expected effect of the Stark splitting.

II. MICROWAVE ABSORPTION CAUSED BY CRYSTALLINE STARK SPLITTING

The usual Stark splittings in crystals are of the order of some hundred or thousand cm^{-1}; in certain circumstances, however, the splittings are of the order of one cm^{-1}. This is the case with some of the salts studied in magnetic cooling experiments. For example, Gorter[4] gives the following over-all splittings of the ground state:

$Gd_2(SO_4)_3\cdot 8\ H_2O$	1.0 cm^{-1},
$Gd_2(C_2O_4)_3\cdot 10\ H_2O$	0.60 cm^{-1},
$KCr(SO_4)_2\cdot 12\ H_2O$	0.16 cm^{-1},
$FeNH_4(SO_4)_2\cdot 12\ H_2O$	0.13 cm^{-1}.

Splittings in the neighborhood of one cm^{-1} are in principle accessible to investigation by means of microwave methods. The selection rules, in general, permit a number of magnetic-dipole transitions. Electric dipole transitions are forbidden by the parity rule, since the parity of initial and final states are identical when these states originate from the same degenerate level of the free ion. Electric quadrupole transitions are less probable than magnetic-dipole transitions by a factor of the order of (atomic radius/wavelength)$^2\times$(Debye unit/Bohr magneton),[2] which is of the order of 10^{-12} for $\lambda=1$ cm.

Magnitude of the Effect

The magnitude and detectability of the resonance-absorption effect may be estimated by reasoning similar to that given by Torrey, Purcell, and Pound[8] for the case of nuclear resonance. We shall consider the power absorbed by a system which has two eigenstates, 1 and 2, with eigenvalues differing by the energy $\hbar\omega_0$. The transition probability between states 1 and 2 for a single system per unit time for x-polarized radiation is

$$p=(2\pi/\hbar^2)\,|\mu_{12}^x|^2 I, \qquad (2)$$

where μ_{12}^x is the matrix element of the magnetic-moment operator $\mu_x=g\mu_B J_x$ and I is the total energy in the incident radiation field per unit volume per unit frequency interval.

[7a] D. M. S. Bagguley and J. H. E. Griffiths, Nature 160, 532 (1947); P. R. Weiss, C. A. Whitmer, H. C. Torrey, and Jen-Sen Hsiang, Phys. Rev. 72, 975 (1947).

[8] H. C. Torrey, E. M. Purcell, and R. V. Pound, Phys. Rev. 69, 680 (1946).

In thermal equilibrium the number of systems in the ground state is greater than the number of systems in the excited state; the excess is

$$(N_1-N_2)=N_1(1-\exp[-\hbar\omega_0/kT])\cong\frac{N}{2}\frac{\hbar\omega_0}{kT} \quad (3)$$

for $\hbar\omega_0/kT\ll 1$; here N is the total number of systems. The power absorption is given by

$$\frac{1}{2}\frac{\hbar\omega_0}{kT}(\hbar\omega_0)Np. \quad (4)$$

Suppose that the band width of the incident electromagnetic wave is Δf and the width of the resonance line (resulting from magnetic-moment interactions) is $\Delta\omega_0(\gg\Delta f)$; then only the fraction $2\pi\Delta f/\Delta\omega_0$ of the total number of systems have their resonances within the band width of the r-f radiation field. Let $U=I\Delta f$ be the total energy density in the incident radiation field; then

$$P=\frac{2\pi^2\omega_0^2|\mu_{12}^x|^2 n}{kT\Delta\omega_0}U \quad (5)$$

is the integrated power absorption per unit volume, where n is the number of paramagnetic ions per unit volume.

Now the Q of the system is given by

$$Q^{-1}=\frac{P}{\omega_0 U}\sim\frac{\omega_0}{\Delta\omega_0}\frac{\mu^2 n}{kT}\sim\frac{\hbar\omega_0}{kT} \quad (6)$$

if the line width is considered as caused by magnetic-dipole interactions, so that $\hbar\Delta\omega_0\sim\mu^2/a^3\sim n\mu^2$.

From Eq. (6) one has, for $T=300°$K and $\lambda=1$ cm, $Q\sim 200$, which is *easily detectable* in the presence of empty cavity Q's which may be of the order of 1000 or more at this wave-length.

Selection Rules

We have pointed out that the allowed transitions are magnetic-dipole transitions. One can proceed to calculate the selection rules by group theoretical methods. The eigenfunctions corresponding to the energy levels in the crystalline electric fields transform according to the irreducible representations, Γ_i, of the symmetry group of the crystalline field. The characters of the irreducible representations are given in the papers of Bethe,[9] Tisza,[10] and Jahn.[11] The character of the magnetic-moment operator under a rotation through an angle φ is given by $\chi(\varphi)=1+2\cos\varphi$, since the magnetic-moment transforms as an axial vector.

It is a fundamental result of group theory that magnetic dipole transitions are allowed between levels m and n only if $\Gamma_m{}^*\times\Gamma_n\times\Gamma_a$ contains the identical representation Γ_1; here Γ_a is the representation of an axial vector. The allowed transitions found from the character calculations are given below; the representations are labeled according to the notation of Bethe.[9] In the cases of the one- and two-valued rhombic and trigonal groups, which were not given in detail by Bethe, the character tables are given in Appendix A.

The notation $\Gamma_{a,b}\leftrightarrow\Gamma_c$ indicates that the energy level whose eigenfunctions belong to Γ_c has allowed magnetic-dipole transitions to and from the energy levels whose eigenfunctions belong to Γ_a and Γ_b.

Cubic Group ($\Gamma_{\text{axial}}=\Gamma_4$)

$\Gamma_{1,2,4}\leftrightarrow\Gamma_4$; $\Gamma_{2,3,4,5}\leftrightarrow\Gamma_5$; $\Gamma_{6,8}\leftrightarrow\Gamma_6$; $\Gamma_{7,8}\leftrightarrow\Gamma_7$; $\Gamma_8\leftrightarrow\Gamma_8$.

Tetragonal Group ($\Gamma_{\text{axial}}=\Gamma_2+\Gamma_5=\Gamma_{(z)}+\Gamma_{(x,y)}$)

Transitions for J_z: $\Gamma_1\leftrightarrow\Gamma_2$; $\Gamma_3\leftrightarrow\Gamma_4$; $\Gamma_5\leftrightarrow\Gamma_5$; $\Gamma_6\leftrightarrow\Gamma_6$; $\Gamma_7\leftrightarrow\Gamma_7$.

Transitions for J_x, J_y: $\Gamma_{1,2,3,4}\leftrightarrow\Gamma_5$; $\Gamma_{6,7}\leftrightarrow\Gamma_6$; $\Gamma_7\leftrightarrow\Gamma_7$.

Trigonal Group ($\Gamma_{\text{axial}}=\Gamma_2+\Gamma_3=\Gamma_{(z)}+\Gamma_{(x,y)}$)

Transitions for J_z: $\Gamma_1\leftrightarrow\Gamma_2$; $\Gamma_3\leftrightarrow\Gamma_3$; $\Gamma_4\leftrightarrow\Gamma_4$; $\Gamma_5\leftrightarrow\Gamma_5$.

Transitions for J_x, J_y: $\Gamma_1\leftrightarrow\Gamma_3$; $\Gamma_2\leftrightarrow\Gamma_3$; $\Gamma_4\leftrightarrow\Gamma_5$; $\Gamma_5\leftrightarrow\Gamma_5$.

Rhombic Group ($\Gamma_{\text{axial}}=\Gamma_2+\Gamma_3+\Gamma_4=\Gamma_{(z)}+\Gamma_{(y)}+\Gamma_{(x)}$)

Transitions for Γ_2: $\Gamma_1\leftrightarrow\Gamma_2$; $\Gamma_3\leftrightarrow\Gamma_4$; $\Gamma_5\leftrightarrow\Gamma_5$.

Transitions for Γ_3: $\Gamma_1\leftrightarrow\Gamma_3$; $\Gamma_2\leftrightarrow\Gamma_4$; $\Gamma_5\leftrightarrow\Gamma_5$.

Transitions for Γ_4: $\Gamma_1\leftrightarrow\Gamma_4$; $\Gamma_2\leftrightarrow\Gamma_3$; $\Gamma_5\leftrightarrow\Gamma_5$.

The selection rules for the tetragonal case have been given previously by Bethe.[12]

The application of these selection rules may be illustrated by the case of the Gd^{+++} ion, for which $J=7/2$. According to Bethe,[9] the ground

[9] H. A. Bethe, Ann. d. Physik **3**, 133 (1929); see also E. Wigner, Göttingen Nachrichten 133 (1930).
[10] L. Tisza, Zeits. f. Physik **82**, 48 (1933).
[11] H. Jahn, Proc. Roy. Soc. **A164**, 117 (1938); see also W. Opechowski, Physica **7**, 552 (1940).
[12] H. Bethe, Zeits. f. Physik **60**, 218 (1930).

state of the ion splits in a cubic field into a twofold degenerate level belonging to Γ_6, a twofold degenerate level belonging to Γ_7, and a fourfold degenerate level belonging to Γ_8. The selection rules permit transitions between Γ_6 and Γ_8, and between Γ_7 and Γ_8, but not between Γ_6 and Γ_7.

If the over-all splitting of the ground state in $Gd_2(SO_4)_3 \cdot 8H_2O$ is 1.0 cm^{-1}, as given by Gorter,[4] the allowed transitions will correspond to wave-lengths of 1.6 cm and 2.7 cm. This follows from the fact that, if only the cubic term of the fourth degree in the crystalline potential is considered,[13] the splitting is in the ratio of 5 to 3, with the fourfold level between the two twofold levels.

Intensity Factors

Equation (5) is a quite general expression for the power absorption when the band width Δf of the incident electromagnetic wave is small in comparison with the effective band width $\Delta\omega_0$ of the resonance, and for $kT \gg h\omega_0$. In the absence of detailed knowledge regarding the dependence of $\Delta\omega_0$ on the crystalline and applied magnetic fields, we shall suppose for the sake of discussion that $\Delta\omega_0$ is a constant for any specific salt. Under this assumption the dependence of the power absorption on frequency and magnetic field intensity is determined by the factor $\omega_0^2|\mu_{12}^x|^2$ in Eq. (5).

For convenience, we prefer to discuss the dimensionless quantity

$$\Theta_{mn}^{i} = (h\omega_0/\delta)^2 |(m|J_i|n)/h|^2. \qquad (7)$$

This will be called the *intensity factor*. Here $\mathbf{J}$ is the angular-momentum operator; δ is an energy which must be defined for each specific problem—it is closely related to the purely crystalline splitting.

In general it is more convenient to work with the operators $J_+ = J_x + iJ_y$ and $J_- = J_x - iJ_y$, than with J_x or J_y separately. One has

$$J_x = \tfrac{1}{2}(J_+ + J_-); \qquad (8)$$

now from the reality of J_x and J_y,

$$(m|J_-|n)^* = (n|J_+|m), \qquad (9)$$

so that

$$(m|J_x|n) = \tfrac{1}{2}\{(m|J_+|n) + (n|J_+|m)^*\}. \qquad (10)$$

This relation is used to calculate the matrix elements of J_x from those of J_+.

Tables of numerical values of the intensity factor are given in the following sections along with the energy differences associated with the various transitions.

III. COMBINED CRYSTALLINE AND ZEEMAN SPLITTING

It is not possible to discuss in a general fashion the behavior of energy levels in the presence of combined crystalline electric fields and external static magnetic fields. Rather, it is necessary to find in detail for each individual case the solution to the quantum-mechanical perturbation problem.

Level splittings corresponding to microwave frequencies are believed to arise only in somewhat special situations, including:

(a) When the ground state of the free ion is an S state, the crystalline field causes splitting only in conjunction with spin-orbit coupling.[14] The resultant splitting is small.

(b) A small crystalline field of low symmetry may remove the degeneracy left by a larger crystalline field of higher symmetry. For example, a predominantly cubic field may have a small trigonal component which gives rise to a further splitting.

Hebb and Purcell[13] in their theoretical study of

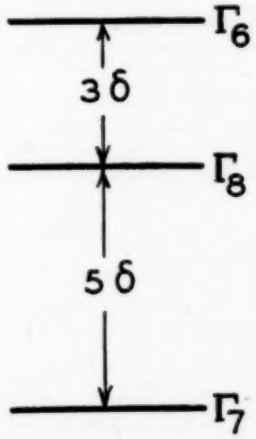

FIG. 1. Energy levels of ^8S state after splitting by cubic electrostatic potential of form $V = D(x^4+y^4+z^4)$; the over-all separation is 8δ.

[13] M. H. Hebb and E. M. Purcell, J. Chem. Phys. **5**, 338 (1937).

[14] J. H. Van Vleck and W. G. Penney, Phil. Mag. **17**, 961 (1934).

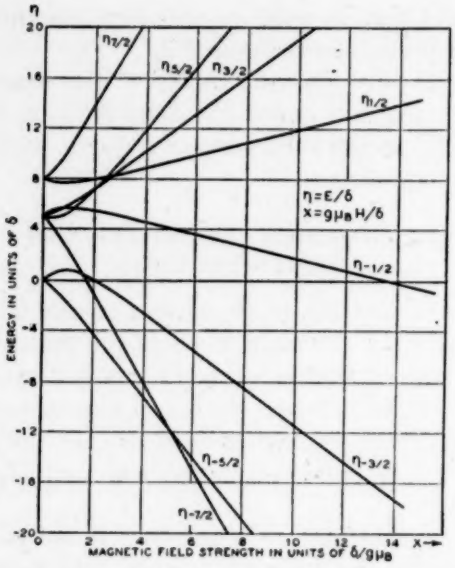

FIG. 2. Eigenvalues of ${}^8S$ state as a function of the strength of the static magnetic field in the [001] directions; a constant cubic electrostatic field is also present. The The subscripts on the η's indicate the value of the magnetic quantum number, M_J, characterizing the state for $x \gg 1$.

magnetic cooling experiments discuss examples where the splitting is of the order of magnitude of one cm^{-1}. Type (a) splitting is found, for example, in salts of trivalent gadolinium, where the ground level is ${}^8S_{7/2}$, and in Fe^{+++} and Mn^{++} (${}^6S_{5/2}$). Type (b) splitting is found, for example, in potassium chromic alum ($KCr(SO_4)_2 \cdot 12\,H_2O$), where there is thought to be a small trigonal field superposed on the predominant cubic field. The possible transitions and corresponding intensity factors for the cases just cited are discussed in detail below.

Case I. $J=7/2$ (Gd^{+++})

In the absence of external magnetic fields this state is split by a cubic electric field into two twofold levels and one fourfold level. The validity of the cubic field assumption is uncertain. According to Bethe (cf. reference 9, p. 155), the twofold levels belong to Γ_6 and Γ_7, the fourfold level to Γ_8. We assume that the splitting* takes place as in Fig. 1, which is consistent with the work of Hebb and Purcell.[13] The zero-order wave functions belonging to these representations are listed below.

$$\left.\begin{aligned}\psi_a^{(1)} &= \tfrac{1}{2}[3^{\frac{1}{2}}\Phi_{5/2}-\Phi_{-3/2}]\\ \psi_a^{(2)} &= \tfrac{1}{2}[3^{\frac{1}{2}}\Phi_{-5/2}-\Phi_{3/2}]\end{aligned}\right\}\Gamma_7,$$

$$\left.\begin{aligned}\psi_b^{(1)} &= (7/12)^{\frac{1}{2}}[\Phi_{7/2}-(5/35^{\frac{1}{2}})\Phi_{-1/2}]\\ \psi_b^{(2)} &= (7/12)^{\frac{1}{2}}[\Phi_{-7/2}-(5/35^{\frac{1}{2}})\Phi_{1/2}]\\ \psi_b^{(3)} &= \tfrac{1}{2}[\Phi_{5/2}+3^{\frac{1}{2}}\Phi_{-3/2}]\\ \psi_b^{(4)} &= \tfrac{1}{2}[\Phi_{-5/2}+3^{\frac{1}{2}}\Phi_{3/2}]\end{aligned}\right\}\Gamma_8, \quad (11)$$

$$\left.\begin{aligned}\psi_c^{(1)} &= (5/12)^{\frac{1}{2}}[\Phi_{7/2}+(7/35^{\frac{1}{2}})\Phi_{-1/2}]\\ \psi_c^{(2)} &= (5/12)^{\frac{1}{2}}[\Phi_{-7/2}+(7/35^{\frac{1}{2}})\Phi_{1/2}]\end{aligned}\right\}\Gamma_6.$$

Φ_m denotes a function with $J=7/2$, $M_J=M$. We obtain for the secular equation in the presence of an [001] directed magnetic field:

	$\psi_c^{(1)}$	$\psi_b^{(1)}$	$\psi_b^{(3)}$	$\psi_a^{(1)}$
$\psi_c^{(1)}$	$8\delta+\frac{7}{6}a-E$	$\frac{1}{3}(35)^{\frac{1}{2}}a$	0	0
$\psi_b^{(1)}$	$\frac{1}{3}(35)^{\frac{1}{2}}a$	$5\delta+\frac{11}{6}a-E$	0	0
$\psi_b^{(3)}$	0	0	$5\delta-\frac{1}{2}a-E$	$\sqrt{3}a$
$\psi_a^{(1)}$	0	0	$\sqrt{3}a$	$\frac{3}{2}a-E$

$=0.$ (12)

Here $a=g\mu_B H$ ($g=2$ since $L=0$), and there is a similar block involving $(-a)$ for (a) and the remaining functions. This result has been essentially given by Hebb and Purcell in another connection. Introducing dimensionless quantities $\eta=E/\delta$, $x=a/\delta$, one finds for the eigenvalues:

$$\left.\begin{aligned}
\eta_{\pm 7/2} &= \pm\tfrac{3}{2}x+\tfrac{13}{2}\pm\tfrac{1}{2}\left(\left(3\mp\tfrac{2}{3}x\right)^2+\tfrac{140}{9}x^2\right)^{\frac{1}{2}},\\
\eta_{\pm 5/2} &= \pm\tfrac{1}{2}x+\tfrac{5}{2}\pm\tfrac{1}{2}((5\mp 2x)^2+12x^2)^{\frac{1}{2}},\\
\eta_{\pm 3/2} &= \mp\tfrac{1}{2}x+\tfrac{5}{2}\pm\tfrac{1}{2}((5\pm 2x)^2+12x^2)^{\frac{1}{2}},\\
\eta_{\pm 1/2} &= \mp\tfrac{3}{2}x+\tfrac{13}{2}\pm\tfrac{1}{2}\left(\left(3\pm\tfrac{2}{3}x\right)^2+\tfrac{140}{9}x^2\right)^{\frac{1}{2}},
\end{aligned}\right\} \quad (13)$$

* However, the situation in the Gd^{+++} salts may not be so simple. We are indebted to Professor F. J. Belinfante for correspondence regarding a detailed treatment of the energy-level scheme in preparation by Van Dyk and himself.

TABLE I. Frequencies and intensity factors for transitions in $J=7/2$ case; cubic field. Table is labeled in terms of dimensionless quantities $\eta=E/\delta$ and $x=g\mu_B H/\delta$, where δ is as shown in Fig. 1. The intensity factor is defined by Eq. (7) and is given in this case by $\Theta_x=\frac{1}{4}|(m|J_+|n)|^2(\Delta\eta)^2$ and $\Theta_z=|(m|J_z|n)|^2(\Delta\eta)^2$. The static magnetic field is in the Z direction; this is also the [001] direction.

Transitions	Quantity	0.1	0.3	0.5	0.7	1.0	1.5	←x→ 2.0	3.0	5.0	7.5	10.0	15.0
7/2⟷ 1/2	$\Delta\eta$	0.23	0.71	1.22	1.76	2.60	4.05	5.53	8.51	14.51	22.00	29.50	44.50
	Θ_x	0.07	0.59	1.35	2.08	2.93	3.74	4.15	4.51	4.73	4.82	4.86	4.88
7/2⟷−7/2	$\Delta\eta$	3.33	4.13	5.09	6.19	7.98	11.19	14.53	21.36	35.22	52.65	70.11	105.07
	Θ_x	8.10	6.57	5.04	3.78	2.47	1.34	0.82	0.39	0.14	0.09	0.04	0.02
1/2⟷−1/2	$\Delta\eta$	2.73	2.33	2.09	1.99	1.98	2.19	2.53	3.36	5.22	7.65	10.11	15.07
	Θ_x	9.27	9.97	10.49	11.14	12.74	17.28	24.04	43.85	107.71	232.68	407.68	907.61
−1/2⟷−7/2	$\Delta\eta$	0.37	1.09	1.78	2.44	3.40	4.95	6.47	9.49	15.49	23.00	30.50	45.50
	Θ_x	0.09	0.73	1.63	2.46	3.35	4.14	4.49	4.76	4.89	4.93	4.93	4.92
7/2⟷ 5/2	$\Delta\eta$	3.17	3.56	3.98	4.40	5.00	5.84	6.53	7.72	9.85	12.40	14.93	19.96
	Θ_x	28.02	31.75	35.13	40.73	48.86	63.20	77.32	105.98	170.79	270.04	390.78	697.32
5/2⟷−1/2	$\Delta\eta$	0.21	0.52	0.66	0.66	0.42	0.41	1.53	4.16	9.88	17.24	24.68	39.62
	Θ_x	0.02	0.14	0.26	0.25	0.08	0.04	0.36	1.04	1.77	2.15	2.33	2.50
7/2⟷−3/2	$\Delta\eta$	7.99	8.08	8.34	8.74	9.58	11.41	13.53	18.16	27.88	40.24	52.68	77.62
	Θ_x	0.10	0.87	1.95	2.72	2.92	2.07	1.28	0.55	0.18	0.07	0.04	0.02
−1/2⟷−3/2	$\Delta\eta$	5.03	5.04	5.02	5.00	5.00	5.16	5.47	6.28	8.15	10.60	13.07	18.04
	Θ_x	58.41	62.23	66.32	69.50	76.14	89.59	105.55	144.42	247.28	419.62	639.47	1220.2
5/2⟷ 3/2	$\Delta\eta$	0.10	0.29	0.44	0.55	0.61	0.49	0.18	0.65	2.56	5.03	7.51	12.51
	Θ_x	0.02	0.19	0.47	0.77	2.02	0.67	0.09	1.28	19.61	75.75	169.42	469.24
3/2⟷−3/2	$\Delta\eta$	4.91	4.81	4.80	4.89	5.20	6.05	7.18	9.79	15.47	22.81	30.23	45.16
	Θ_x	17.94	15.90	13.62	11.32	8.25	4.77	2.92	1.36	0.49	0.22	0.12	0.05
5/2⟷−5/2	$\Delta\eta$	5.11	5.41	5.80	6.29	7.20	9.05	11.18	15.79	25.47	37.81	50.23	75.16
	Θ_x	19.43	20.13	19.88	18.72	15.83	10.68	7.08	3.53	1.34	0.60	0.34	0.15
−3/2⟷−5/2	$\Delta\eta$	0.30	0.89	1.44	1.95	2.61	3.49	4.18	5.35	7.44	9.97	12.49	17.49
	Θ_x	0.20	1.82	5.02	9.63	18.41	34.87	51.40	85.33	166.07	298.44	467.63	918.01
3/2⟷ 1/2	$\Delta\eta$	2.84	2.56	2.31	2.09	1.79	1.30	0.82	0.14	2.10	4.57	7.06	12.04
	Θ_x	24.52	21.19	18.08	15.21	11.36	6.15	2.47	0.08	16.46	78.19	186.47	543.19
1/2⟷−5/2	$\Delta\eta$	8.05	8.25	8.56	8.94	9.60	10.84	12.18	14.99	20.81	28.22	35.66	50.61
	Θ_x	0.09	0.68	1.44	2.10	2.80	3.35	3.55	3.62	3.43	3.29	3.18	3.07
3/2⟷−7/2	$\Delta\eta$	0.25	0.85	1.56	2.34	3.60	5.84	8.18	12.99	22.81	35.22	47.66	72.61
	Θ_x	0.02	0.12	0.23	0.31	0.35	0.32	0.27	0.17	0.08	0.04	0.02	0.01
−5/2⟷−7/2	$\Delta\eta$	4.96	4.84	4.69	4.51	4.21	3.70	3.18	2.14	0.10	2.43	4.94	9.96
	Θ_x	53.93	49.01	44.13	39.58	33.49	25.04	18.21	8.16	0.02	10.34	42.84	173.77
7/2⟷−1/2	$\Delta\eta$	2.96	3.04	3.32	3.75	4.58	6.24	8.06	11.87	19.72	29.65	39.61	59.57
	Θ_x	35.0	35.0	35.0	35.0	35.0	35.0	35.0	35.0	35.0	35.0	35.0	35.0
1/2⟷−7/2	$\Delta\eta$	3.09	3.41	3.87	4.43	5.39	7.14	9.00	12.85	20.71	30.64	40.61	60.57
	Θ_x	35.0	35.00	35.00	35.00	35.00	35.00	35.0	35.0	35.0	35.0	35.0	35.0
5/2⟷−3/2	$\Delta\eta$	4.81	4.52	4.36	4.34	4.58	5.57	7.00	10.44	18.03	27.84	37.75	57.66
	Θ_x	75.0	75.0	75.0	75.0	75.0	75.0	75.0	75.0	75.0	75.0	75.0	75.0
−5/2⟷ 3/2	$\Delta\eta$	5.21	5.70	6.24	6.84	7.81	9.54	11.36	15.13	22.91	32.79	42.72	62.65
	Θ_x	75.0	75.0	75.0	75.0	75.0	75.0	75.0	75.0	75.0	75.0	75.0	75.0

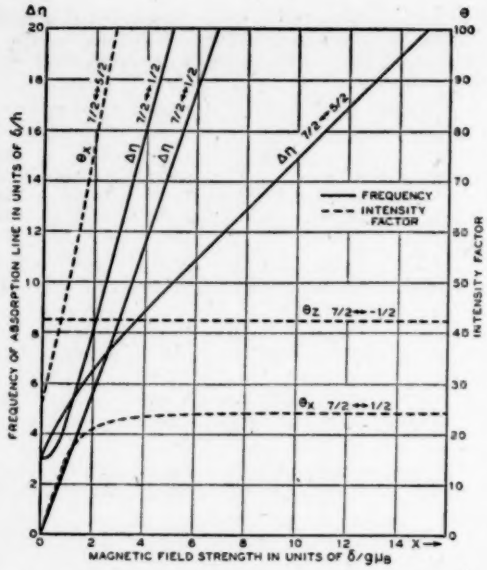

FIG. 3. Frequency and intensity factor for some typical absorption lines resulting from an ^6S state; the intensity factor is proportional to the power absorption and is defined by Eq. (7). *Note added in proof:* Two frequency curves are labeled in the figure as $7/2 \longleftrightarrow 1/2$; of these two curves the left hand one is incorrectly labeled and should read $7/2 \longleftrightarrow -1/2$.

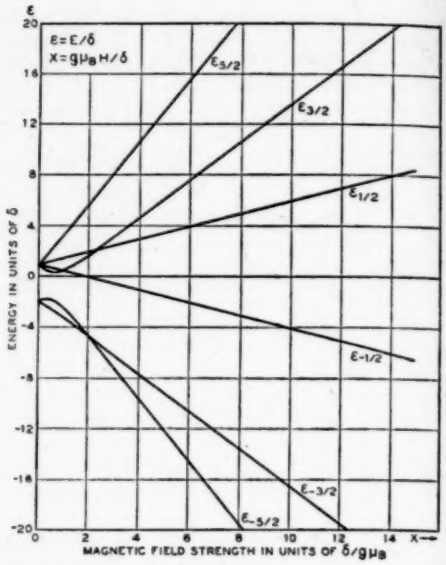

FIG. 4. Eigenvalues of ^6S state as a function of the static magnetic field in the [001] direction.

the η's being labeled according to the levels they represent in very large fields. These are plotted in Fig. 2. The numerical values of the frequencies and intensity factors corresponding to non-vanishing matrix elements are to be found** in Table I, while Fig. 3 gives plots of intensity factors and frequencies of typical lines *vs.* applied magnetic field.

The sum of the squares of all the matrix elements of J_+ is exactly 84 for $J=7/2$, independent of the value of x. This result follows from the principle of spectroscopic stability (cf. reference 1, p. 139), and provides a very useful check on the numerical calculations.

For strong magnetic fields the eigenvalues and matrix elements approach the values characteristic of free ions. From Table I we see, for example, that for large x the largest values of the intensity factors belong to those X-polarized transitions for which $\Delta M_J=\pm 1$, in agreement with the usual selection rule. An example of such a transition is $7/2 \leftrightarrow 5/2$, for which the values of the frequency and intensity factor are shown in Fig. 3. A number of lines are weak for all x: an example is $3/2 \leftrightarrow -7/2$. All of the Z-polarized lines have constant values of the intensity factor, independent of x; an example is the line $7/2 \leftrightarrow 1/2$ shown in Fig. 3. The crossing points on the eigenvalue diagram (Fig. 2) correspond to lines of zero frequency.

Case II. $J=5/2$ (Fe^{+++}, Mn^{++})

The case of $J=5/2$ is very similar to that of $J=7/2$. The roots of the secular equation for an [001] magnetic field and a cubic electric field have been given by Debye[15] and also by Kronig and Bouwkamp.[16]

We shall not discuss this state in any detail, but merely give results. The energy levels are

$$\left.\begin{aligned}
\epsilon_{\pm 1/2} &= 1 \pm \frac{1}{2}x, \\
\epsilon_{\pm 5/2} &= \pm\frac{x}{2} - \frac{1}{2} \pm 2[x^2 \pm x + (3/4)^2]^{\frac{1}{2}}, \\
\epsilon_{\pm 3/2} &= \mp\frac{x}{2} - \frac{1}{2} \pm 2[x^2 \mp x + (3/4)^2]^{\frac{1}{2}},
\end{aligned}\right\} \quad (14)$$

where, as before, $x=g\mu_B H/\delta$, $\epsilon=E/\delta$ (3δ being

** The authors have available copies of the analytical expressions for the wave functions and matrix elements as functions of x for distribution to anyone who may require them.

[15] P. Debye, Ann. d. Physik 32, 85 (1938).
[16] R. de L. Kronig and C. J. Bouwkamp, Physica 6, 290 (1939).

the over-all splitting in the crystalline electric field alone). In the case under consideration, just as in the 7/2 case, one has $L=0$ so that $g=2$. In Fig. 4 one finds these energies plotted as a function of external field. Table II gives the numerical values of the frequencies and intensity factors.

The principle of spectroscopic stability applied to the $J=5/2$ case tells us that the sum of the squares of all the matrix elements of J_+ is 35, independent of x.

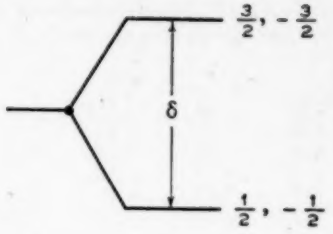

FIG. 5. Energy levels for $KCr(SO_4)_2 \cdot 12\,H_2O$ in presence of axial electrostatic field.

Case III. ($KCr(SO_4)_2 \cdot 12H_2O$)

According to Hebb and Purcell the Cr^{+++} ion in this salt is in a ${}^4FT_8$ state, which is not split by the cubic crystalline field. If one assumes that there is also present a small field of trigonal symmetry the axis of which coincides with one of the body diagonals of the cubic lattice (this is to be expected from x-ray studies of the salt), then the $J=3/2$ state does split and give rise to possibilities for microwave absorption. Now in this alum the Cr^{+++} ions lie on a face-centered cubic lattice, i.e., on interpenetrating simple cubic lattices. If one resolves the face-centered lattice into the four simple cubic lattices, then one finds that the trigonal axis of the electric field is in each case along a different body diagonal of the unit cube. We shall treat these four simple cubic system independently.***

Taking for the crystalline potential only the

TABLE II. Frequencies and intensity factors for transitions in $J=5/2$ case; cubic field. Table is labelled in terms of dimensionless quantities $\epsilon=E/\delta$ and $x=g\mu_B H/\delta$, where δ is the over-all splitting in the electric field alone. The intensity factor is defined by Eq. (7) and is given in this case by $\Theta_z=\frac{1}{2}|(m|J_+|n)|^2(\Delta\epsilon)^2$ and $\Theta_x=|(m|J_x|n)|^2(\Delta\epsilon)^2$. The static magnetic field is in the Z direction; this is also the [001] direction.

Transitions	Quantity	←x→ 0.1	0.3	0.5	0.7	1.0	1.5	2.0	3.0	5.0	7.5	10.0	15.0
3/2⟷ 1/2	$\Delta\epsilon$	0.23	0.61	0.88	1.01	1.00	0.71	0.30	0.62	2.57	5.04	7.53	12.52
	Θ_z	0.02	0.25	0.78	1.37	1.67	0.94	0.17	0.77	13.15	50.82	113.40	313.44
5/2⟷−1/2	$\Delta\epsilon$	0.24	0.75	1.29	1.85	2.70	4.15	5.62	8.59	14.56	22.04	29.53	44.52
	Θ_z	0.02	0.10	0.21	0.32	0.46	0.64	0.76	0.92	1.09	1.18	1.23	1.29
−3/2⟷−1/2	$\Delta\epsilon$	3.04	3.15	3.29	3.45	3.70	4.25	4.62	5.59	7.56	10.03	12.53	17.52
	Θ_z	16.00	18.08	20.29	22.66	26.54	35.52	42.24	62.08	113.92	201.32	313.76	613.55
−5/2⟷ 1/2	$\Delta\epsilon$	2.97	2.99	3.12	3.39	4.00	5.29	6.70	9.62	15.57	23.04	30.53	45.52
	Θ_z	14.00	11.93	9.72	7.61	5.33	3.56	2.83	2.23	1.85	1.69	1.61	1.54
5/2⟷−5/2	$\Delta\epsilon$	3.11	3.44	3.91	4.54	5.70	7.94	10.33	15.21	25.13	37.58	50.06	75.04
	Θ_z	5.28	5.45	4.89	3.82	2.34	1.10	0.62	0.27	0.10	0.04	0.02	0.01
5/2⟷ 3/2	$\Delta\epsilon$	0.37	1.06	1.67	2.16	2.70	3.36	3.92	4.97	6.99	9.49	12.00	17.00
	Θ_z	0.09	0.89	2.60	4.97	8.60	13.93	19.14	30.79	61.02	112.68	179.91	361.10
3/2⟷−3/2	$\Delta\epsilon$	2.91	2.84	2.91	3.14	3.70	4.94	6.33	9.21	15.13	22.58	30.06	45.04
	Θ_z	4.63	3.71	2.71	1.82	0.98	0.43	0.23	0.10	0.04	0.02	0.01	0.00
−5/2⟷−3/2	$\Delta\epsilon$	0.17	0.46	0.67	0.76	0.70	0.36	0.08	1.03	3.01	5.51	8.00	13.00
	Θ_z	0.02	0.17	0.42	0.62	0.58	0.16	0.01	1.34	11.34	37.89	80.07	211.38
5/2⟷−3/2	$\Delta\epsilon$	3.28	3.90	4.58	5.30	6.40	8.31	10.25	14.18	22.11	32.08	42.06	62.04
	Θ_z	20.00	20.00	20.00	20.00	20.00	20.00	20.00	20.00	20.00	20.00	20.00	20.00
−5/2⟷ 3/2	$\Delta\epsilon$	2.75	2.37	2.24	2.37	3.00	4.58	6.40	10.25	18.14	28.09	38.07	58.00
	Θ_z	20.00	20.00	20.00	20.00	20.00	20.00	20.00	20.00	20.00	20.00	20.00	20.00

*** Part of this calculation was performed previously for another purpose by L. J. F. Broer, Physica 9, 547 (1942).

TABLE III. Frequencies $\Delta\epsilon$ for transitions in case of $KCr(SO_4)_2\cdot 12H_2O$; H_z Parallel [001].*

Transition	.1	.2	.3	.4	.6	←x→ 1.0	2.0	5.0	10.0	15.0
3/2 ⟷ 1/2	.30	.57	.80	.99	1.29	1.91	3.56	8.70	17.34	25.99
3/2 ⟷ −1/2	1.03	1.13	1.31	1.56	2.17	3.52	6.95	17.33	34.65	51.96
−3/2 ⟷ 3/2	1.33	1.70	2.11	2.54	3.47	5.42	10.51	26.03	51.98	77.96
−1/2 ⟷ 1/2	.73	.55	.50	.57	.88	1.61	3.39	8.63	17.31	25.97
−3/2 ⟷ 1/2	1.03	1.13	1.31	1.56	2.17	3.52	6.95	17.33	34.65	51.96
−3/2 ⟷ −1/2	.30	.57	.80	.99	1.29	1.91	3.56	8.70	17.34	25.99

* Table is labeled in terms of dimensionless quantities $\epsilon = E/\delta$ and $x = g\mu BH/\delta\sqrt{3}$, where δ is as shown in Fig. 5.

second-order terms, we find

$$V_{\text{trig}} = D(x^2+y^2-2z^2), \tag{15}$$

where the z axis is here taken as the body diagonal. This potential has more than trigonal (i.e., it has axial) symmetry as a result of our dropping higher terms. Just because of this apparent axial symmetry, however, a magnetic field placed in the [001] crystallographic direction will look the same to each component simple cubic array. That is, the properties of the states as functions of the field should depend only on the strength of the field and the angle between the field direction and the trigonal axis. We therefore need consider only one of the component arrays, say the one with trigonal axis in the [111] direction.

We now have to solve the problem of an atom with $J=3/2$ perturbed by an interaction

$$H = V_{\text{trig}} + H_{\text{mag}} = V_{\text{trig}} + g\mu_B(\mathbf{H}\cdot\mathbf{J}). \tag{16}$$

Taking the direction of quantization to be along the [111] direction, and choosing the x and y axes such that the component of H perpendicular to the z axis lies equally between them, we have

$$\mathbf{H}\cdot\mathbf{J} = \frac{H}{\sqrt{3}}(J_x+J_y+J_z) \tag{17}$$

or

$$H_{\text{mag}} = \alpha(\tfrac{1}{2}(1-i)J_+ + \tfrac{1}{2}(1+i)J_- + J_z), \tag{18}$$

where

$$\alpha = g\mu_B H/3^{\frac{1}{2}}.$$

The level scheme in the absence of H_{mag} is as shown in Fig. 5. Here the levels are labeled by their *weak field* quantum numbers. Introducing now H_{mag}, we get as our secular equation:

$$\begin{vmatrix} \frac{3}{2} & \frac{1}{2} & -\frac{1}{2} & -\frac{3}{2} \\ \frac{3}{2} & \frac{1}{2}+\frac{3}{2}x-\epsilon & \frac{1-i}{2}3^{\frac{1}{2}}x & 0 & 0 \\ \frac{1}{2} & \frac{1+i}{2}3^{\frac{1}{2}}x & -\frac{1}{2}+\frac{1}{2}x-\epsilon & (1-i)x & 0 \\ -\frac{1}{2} & 0 & (1+i)x & -\frac{1}{2}-\frac{1}{2}x-\epsilon & \frac{1}{2}(1-i)3^{\frac{1}{2}}x \\ -\frac{3}{2} & 0 & 0 & \frac{1+i}{2}3^{\frac{1}{2}}x & \frac{1}{2}-\frac{3}{2}x-\epsilon \end{vmatrix} = 0, \tag{19}$$

where $\epsilon \equiv E/\delta$, $x \equiv \alpha/\delta$. Expanding gives

$$\epsilon^4 - \tfrac{1}{2}(1+15x^2)\epsilon^2 + \tfrac{1}{16}(1+81x^2-6x^2) = 0, \tag{20}$$

the roots of which are

$$\left.\begin{aligned} \epsilon(\tfrac{3}{2}) &= \tfrac{1}{2}(1+15x^2+6x(1+4x^2)^{\frac{1}{2}})^{\frac{1}{2}}, \\ \epsilon(\tfrac{1}{2}) &= \tfrac{1}{2}(1+15x^2-6x(1+4x^2)^{\frac{1}{2}})^{\frac{1}{2}}, \\ \epsilon(-\tfrac{1}{2}) &= -\tfrac{1}{2}(1+15x^2-6x(1+4x^2)^{\frac{1}{2}})^{\frac{1}{2}}, \\ \epsilon(-\tfrac{3}{2}) &= -\tfrac{1}{2}(1+15x^2+6x(1+4x^2)^{\frac{1}{2}})^{\frac{1}{2}}, \end{aligned}\right\} \tag{21}$$

where we have labeled the energies with their appropriate *strong field* quantum numbers. To find the selection and intensity rules it is necessary to find the wave functions $\psi(M)$ belonging to $\epsilon(M)$ and also the matrix elements of J_+, J_z. It should be remembered that these are J_z and J_+ relative to the system of quantization used in this problem. For an r-f field along the [001] axis,

for example, we will not have only J_z elements present. The wave functions and the corresponding matric elements are to be found in Appendix C.

In order to calculate the relative intensities of the different lines we must know the direction of the r-f field. If, for example, the r-f field is directed along the [001] axis, then the relative intensities are given by calculating the matrix elements of $J_x+J_y+J_z=T$. A simple calculation shows

$$\begin{aligned}|(M|T|M')|^2=&\tfrac{1}{2}|(M|J_+|M')|^2\\&+\tfrac{1}{2}|(M'|J_+|M)|^2+|(M|J_z|M')|^2\\&+Im(M|J_+|M')(M'|J_+|M)\\&+Re((M|J_+|M')(M|J_z|M')^*\\&+(M'|J_+|M)(M|J_z|M'))\\&+Im((M|J_+|M')(M|J_z|M')^*\\&\quad+(M'|J_+|M)(M|J_z|M')).\end{aligned}\tag{22}$$

All of the intensity factors for this case are very small. This is partly the consequence of taking the r-f field parallel to the static field. A plot of the eigenvalues as a function of x is given in Fig. 6; and the associated frequencies are tabulated in Table III.

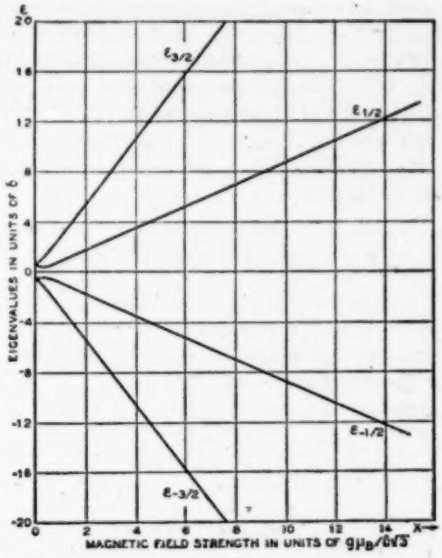

FIG. 6. Eigenvalues for $KCr(SO_4)_2\cdot 12\,H_2O$ as a function of the strength of the static magnetic field in the (001) direction.

IV. CONCLUSION

It is seen from the above treatment, which is based on the usual simplified model, that the microwave-absorption spectrum of paramagnetic crystals is expected to be a rather complicated function of the external static magnetic field. We wish to emphasize again that the influence of exchange coupling between paramagnetic ions has been entirely neglected. This coupling in many salts may submerge the effects we have considered, and may result in a simpler spectrum. Indeed, it may well be that an effect of this sort occurs in the measurements of Zavoisky and of Cummerow and Halliday, most of which were made on magnetically concentrated salts. The type of situation which we have treated is most likely to be realized in salts which are magnetically very dilute. One should also note the importance of using single crystals with the static and r-f magnetic fields along crystal axes of high symmetry.

ACKNOWLEDGMENTS

We wish to thank Professors J. H. Van Vleck, C. J. Gorter, and L. Tisza for several discussions, and Miss Ruth Krock for computational assistance. One of us (C.K.) is indebted to the John Simon Guggenheim Memorial Foundation for a Fellowship, during the tenure of which this work was carried out.

APPENDIX A

Character Table—Trigonal Double Group (after Jahn[11])

	E	R	$2C_1'$	$2C_1''$	$3C_2'$	$3C_2''$
Γ_1	1	1	1	1	1	1
Γ_2	1	1	1	1	−1	−1
Γ_3	2	2	−1	−1	0	0
Γ_4	2	−2	−2	2	0	0
Γ_5	2	−2	1	−1	0	0

Note—Γ_4 is used to denote two conjugate-complex one-dimensional representations.

Character Table—Rhombic Double Group (after Bethe[9])

	E	R	$2C_1$	$2C_2$	$2C_3$
Γ_1	1	1	1	1	1
Γ_2	1	1	−1	1	−1
Γ_3	1	1	−1	−1	1
Γ_4	1	1	1	−1	−1
Γ_5	2	−2	0	0	0

APPENDIX B

Center of Gravity Sum Rule for Crystalline Fields

Consider an unperturbed system which has a definite angular momentum J. It undergoes a perturbation re-

sulting from an external non-singular electric field satisfying Laplace's equation. We shall show that center of gravity of the $2J+1$ components of the originally degenerate energy level is not shifted to the first order, except by the amount of the Madelung potential.

Let the eigenfunctions of the perturbed system be ψ_i ($i=1; \cdots, 2J+1$). Then the center of gravity of the levels will be given by

$$\bar{W}=\frac{1}{2J+1}\sum_i \int \psi_i^* V \psi_i d\tau,$$

where V is the perturbing potential. However, this is simply the trace of V in the representation ψ_i and is invariant under choice of representation. We could, therefore, just as well use the eigenfunctions ψ_M ($M=-J, \cdots, +J$) of the unperturbed system. That is,

$$\bar{W}=\frac{1}{2J+1}\sum_M \int \psi_M^* V \psi_M d\tau$$

$$=\frac{1}{2J+1}\int d\tau V(\sum_M \psi_M^* \psi_M).$$

Now $\sum_M \psi_M^* \psi_M$ is rotationally invariant, since the ψ_M form the basis vectors of a $(2J+1)$-dimensional irreducible representation of the rotation group, and in this "representation space" the sum indicated is just a scalar product. Now by the assumption that V satisfies Laplace's equation (which is rotationally invariant), we see that V must transform as one component of some representation of the rotation group. Since the only invariant solutions of Laplace's equation are a constant (which shifts all levels equally by the Madelung potential and just amounts to a change of the energy zero point) and $1/r$ (which is singular), we can say that the representation to which V belongs does not contain the identity representation. Therefore, according to the usual group theoretical argument the integral in $\bar{W}$ vanishes, and the required result has been established. A weaker form of this theorem has been given previously by Kynch.[17]

APPENDIX C

This appendix contains the wave functions and matrix element for K Cr alum in an [001] static magnetic field. The wave functions are given by

$$\psi(M)=[\Phi_{3/2}+a_M\Phi_{1/2}+b_M\Phi_{-1/2}+c_M\Phi_{-3/2}]/[1+|a_M|^2+|b_M|^2+|c_M|^2]^{\frac{1}{2}}$$

where

$$a_M=-\frac{(\frac{1}{2}+\frac{3}{2}x-\epsilon(M))}{\sqrt{3}x}(1+i),$$

$$b_M=-i(3^{\frac{1}{2}}/2)-(1+i)\frac{(-\frac{1}{2}+\frac{1}{2}x-\epsilon(M))}{2x}a_M,$$

$$c_M=-\frac{(1+i)(3^{\frac{1}{2}}/2)xb_M}{(\frac{1}{2}-\frac{3}{2}x-\epsilon(M))}.$$

The matrix elements of J_+ and J_z are now

$$(M'|J_z|M)=\frac{\frac{3}{2}+\frac{1}{2}(a_{M'}^*a_M-b_{M'}^*b_M)-\frac{3}{2}c_{M'}^*c_M}{[(1+|a_M|^2+|b_M|^2+|c_M|^2)\times(1+|a_{M'}|^2+|b_{M'}|^2+|c_{M'}|^2)]^{\frac{1}{2}}},$$

$$(M'|J_+|M)=\frac{3^{\frac{1}{2}}a_M+2a_{M'}^*b_M+3^{\frac{1}{2}}b_{M'}^*c_M}{[(1+|a_M|^2+|b_M|^2+|c_M|^2)\times(1+|a_{M'}|^2+|b_{M'}|^2+|c_{M'}|^2)]^{\frac{1}{2}}}.$$

[17] G. J. Kynch, Trans. Faraday Soc. **33**, 1402 (1937).

On the Reactive Terms in Quantum Electrodynamics

H. W. LEWIS
Institute for Advanced Study, Princeton, New Jersey

November 24, 1947

I. INTRODUCTION

THE recent discovery by Lamp and Retherford[1] of the displacement of the $2S_{\frac{1}{2}}$ level in the hydrogen spectrum and its subsequent interpretation by Bethe[2] as a reactive* effect of radiation have suggested an investigation of the role of the inertial and reactive terms in quantum electrodynamics. Such studies have up to now been largely frustrated by the appearance of divergences, but Bethe's results in the line shift problem indicate that, at least non-relativistically, it is possible to separate the inertial and reactive effects and to identify the latter as the level shift, in good agreement with experiment. Lamb[3] has shown that this can also be done relativistically, and that all the divergent effects are indeed associated with the electromagnetic mass. The procedure that has been used is to calculate consistently the electromagnetic self-energy of the electron in the hydrogen atom and to identify those terms which are associated with the increase in apparent mass of the electron through its interaction with the radiation field. Here one assumes that the electromagnetic mass of the electron is a small effect and that its apparent divergence arises from a failure of present day quantum electrodynamics above certain frequencies. It is impossible at present to say just what these frequencies are, but one might suppose them to be of the order of 137 mc^2/h, or of nuclear dimensions, so that there is a region in which relativistic effects can manifest themselves and in which our present electrodynamics might be supposed to have a sort of validity. As long as the major contributions to the line shift come from considerably lower frequencies, it is possible to schematize this cut-off by using the phenomenological mass of the electron, which must include these effects. Under these conditions, it is unlikely that the exact nature of the failure of our electrodynamics can appreciably affect the results.

This viewpoint suggests that one re-examine some other areas in which the electrodynamics has failed, to see whether these considerations affect the conclusions that have been drawn. In particular, a problem closely connected to the line shift is that of the radiative effects on the scattering of electrons from an electrostatic field, which is just the dynamic analog to the line shift, both involving the simultaneous interaction of an electron with the electrostatic field of a scattering center, and with the electromagnetic field. Indeed, if one considers the line shift non-relativistically for a highly excited continuum level and expands the wave function in Born approximation, one obtains for the line shift just a sum of radiative scattering corrections of the form (2) below, corrected for the fact that the scatterings involved are virtual rather than real. We would like, therefore, to study the radiative effects on electron scattering in order to see whether the electromagnetic mass of the electron plays any part in the problem.

II. REACTIVE EFFECTS ON ELECTRON SCATTERING

This problem has been studied in a non-relativistic approximation by Bloch and Nordsieck,[4] Braunbeck and Weinmann,[5] and Pauli and Fierz,[6] relativistically by Dancoff,[7] and then discussed in detail by Bethe and Oppenheimer.[8]

If one calculates non-relativistically in perturbation theory, the cross section for the elastic

[1] W. E. Lamb, Jr. and R. C. Retherford, Phys. Rev. 72, 241 (1947).
[2] H. A. Bethe, Phys. Rev. 72, 339 (1947).
* We use the term reactive to apply to the radiative effects which survive after the electromagnetic inertial effects are properly taken into account.
[3] W. E. Lamb, Jr., unpublished.
[4] F. Bloch and A. Nordsieck, Phys. Rev. 52, 54 (1937).
[5] W. Braunbeck and E. Weinmann, Zeits. f. Physik 110, 360 (1938).
[6] W. Pauli and M. Fierz, Nuovo Cimento 15, 167 (1938).
[7] S. M. Dancoff, Phys. Rev. 55, 959 (1939).
[8] H. A. Bethe and J. R. Oppenheimer, Phys. Rev. 70, 451 (1946).

scattering of an electron of momentum $\mathbf{k}$ into the solid angle $d\omega$, with final momentum $\mathbf{p}$, one obtains

$$d\sigma = (mV_{kp}/2\pi\hbar^2)^2 d\omega, \tag{1}$$

where m is the mass of the electron, and V_{kp} the matrix element of the electrostatic scattering potential V between the initial and final states. If one now includes the effects of interaction with the radiation field, in the usual way, one finds that the cross section is changed by an amount

$$\delta d\sigma = -\frac{2\alpha}{3\pi}\frac{(\mathbf{p}-\mathbf{k})^2}{m^2c^2}\cdot d\sigma \cdot \int_T^\infty \frac{dq}{q}, \tag{2}$$

where α is the fine structure constant, T the kinetic energy of the electron, q the frequency of the photon whose emission and re-absorption produces this effect, and, for consistency, m in both (1) and (2) must be specified to be the mechanical mass of the electron. This result is in itself somewhat surprising since, as is well known, the electromagnetic mass of the electron diverges linearly in non-relativistic approximation, so that the expression (2) seems to have no effects of a mass change represented. The reason for this omission may be understood in the following way: In the use of continuum perturbation theory, one is accustomed to assuming that the first- and second-order energy shifts caused by the perturbation are zero, which is quite correct for a scattering potential, but not for the interaction with radiation. The factor of m^2 in (1) comes from the density of states and from the flux corresponding to a given momentum, hence from a factor $p^2(dp/d\epsilon)^2$. If one carried out the perturbation theory consistently, one would insert the energy-momentum relationship that is given by the Hamiltonian to first order in α, therefore involving the linear divergence of the electromagnetic mass. However, one has made a sort of inadvertent separation of effects of order α, and has used here the empirical mass of the electron. This procedure is quite analogous to Bethe's approach to the line shift calculation. However, one must be quite careful in this, since in discarding some terms of order α, and keeping others, one must be sure that the ones that are kept are the correct ones. In this non-relativistic treatment the form of the perturbation calculation makes the separation between inertial and reactive effects of radiation automatic and correct, but, as we shall see, an unambiguous separation in a relativistic calculation, while also possible, is not automatically performed by the method of calculation. It is just this difference that led to the failure of Dancoff's relativistic attack on the problem, as we shall see later.

Indeed, one can predict immediately the effect of the mass in a relativistic calculation, by considering the effect of a small variation in mass in the relativistic equivalent to (1),**

$$d\sigma_{\text{rel}} = (\epsilon V_{kp}/2\pi\hbar^2c^2)^2 d\omega\left[\frac{1+(\mathbf{p}+\mathbf{k}/2mc)^2}{1+(\mathbf{p}/mc)^2}\right], \tag{1'}$$

where, as before, $|k| = |p|$. The terms are grouped in this way since in the hybrid perturbation theory ordinarily used the explicit effects of the electromagnetic mass would only appear in the term in square brackets. The other two factors of ϵ arise exactly as the m^2 term above, and one would ordinarily use the empirical mass of the electron in them. If one now increases the mass in the square brackets by a small amount μ, the change in cross section, to order v^2/c^2, is given by

$$\frac{\delta d\sigma_{\text{rel}}}{d\sigma_{\text{rel}}} = \frac{\mu}{2m}\frac{(\mathbf{p}-\mathbf{k})^2}{m^2c^2}, \tag{3}$$

and if one inserts for μ the electromagnetic mass of the electron, calculated in hole theory, $\mu = (3\alpha m/2\pi)\int^\infty (dq/q)$, one obtains an expression which differs only in the multiplicative constant from the divergent terms that Dancoff found, suggesting quite strongly that these are identifiable as manifestations of the electromagnetic mass of the electron. In fact, the numerical difference arises from Dancoff's omission of certain electrostatic transitions, which are, of course, essential to the covariance of the scheme, and, if included, make the agreement exact.

We will discuss this situation in somewhat greater detail in the next section.

** This argument is due Dr. S. Epstein, to whom I am indebted for permission to quote his results.

III. RELATIVISTIC EFFECTS

As motivation to a relativistic attack on the problem, Dancoff argued that, for energetic virtual photons, the relativistic mass increase of the recoil electrons cuts down the current matrix elements, and thereby would induce convergence into the expression (2) at the upper limit, if one were to consistently treat the recoil particles relativistically in hole theory. He performed a relativistic calculation of the radiative effects, and did indeed find that this was the case, but the relativistic treatment introduced a new set of terms with no non-relativistic analogs, which brought in a new divergence. In this calculation, he used the same hybrid perturbation theory that was discussed in the preceding section, thereby leaving out some divergent effects of the electromagnetic mass. It will be pertinent to our discussion to analyze in some detail the nature and origin of the new divergent terms, and we will show that they are all attributable to the (divergent) mass increase of the electron, as was suggested in the preceding section. What remains is just the expression (2) with an upper limit at kmc^2, where k is a number of order unity that can be calculated directly from the theory. Thus, the change of cross section caused by interaction with radiation is just

$$\delta d\sigma = -\frac{2\alpha}{3\pi}\frac{(\mathbf{p}-\mathbf{k})^2}{m^2c^2}\cdot d\sigma\cdot\ln\frac{kmc^2}{T}. \tag{4}$$

All of Dancoff's divergent terms (his 4*d*, 4*d'*, 4*e*, 4*e'*) involve transitions in which a negative energy electron excites itself to a positive energy state of the same momentum and spin through its interaction with the radiation field, or vice versa. Thus, an electron with momentum $\mathbf{p}$, and energy $-|\epsilon|$, could emit a photon with momentum $\mathbf{q}$, recoiling to the positive energy state $\mathbf{p}-\mathbf{q}$, and then re-absorb the photon, going to the state $\mathbf{p}, |\epsilon|$. The net effect of the transition is just that the electron has changed the sign of its energy. There are also electrostatic terms of exactly this same nature, which Dancoff has omitted. The matrix element for the process above is

$$-\sum_{q\lambda}\frac{2\pi e^2}{q(q+\epsilon_p+\epsilon_{p-q})}\times\overline{X}_f(\alpha\cdot 1_\lambda)(\Lambda_{p-q}{}^+-\Lambda_{p-q}{}^-)(\alpha\cdot 1_\lambda)X_i, \tag{5}$$

where λ is the photon polarization, 1_λ a unit vector in the direction of polarization, the X normalized spinors, and the Λ projection operators as indicated. The corresponding electrostatic term is

$$\sum_q\frac{2\pi e^2}{q^2}\overline{X}_f(\Lambda_{p-q}{}^+-\Lambda_{p-q}{}^-)X_i, \tag{5'}$$

and the sum of (5) and (5'), since $\overline{X}_fX_i=0$, is

$$U_{p-p+}=\sum_q\frac{2\pi e^2}{q^2\epsilon_{p-q}}\overline{X}_f\left\{H_{p-q}-\frac{q}{q+\epsilon_p+\epsilon_{p-q}}\sum_\lambda(\alpha\cdot 1_\lambda)H_{p-q}(\alpha\cdot 1_\lambda)\right\}X_i, \tag{6}$$

where H is the Dirac Hamiltonian. For large q this gives a divergent term

$$U_{p-p+}=-\sum_q\frac{3\pi e^2}{q^3}\overline{X}_f\alpha\cdot\mathbf{p}X_i=+\sum_q\frac{3\pi e^2}{q^3}\overline{X}_f\beta mX_i$$

$$=\frac{3e^2m}{2\pi}\int^\infty\frac{dq}{q}\cdot\overline{X}_f\beta X_i, \tag{7}$$

so that these transitions behave as if they were caused by a perturbation equal to $\beta\cdot(3\alpha mc^2/2\pi)\times\int^\infty(dq/q)$. However, the coefficient of β here is just the divergent part of the electromagnetic mass of the electron, so that these transitions result from the electromagnetic mass effects of the radiation field and, if the empirical mass is used in the Hamiltonian $\alpha\cdot\mathbf{p}+\beta m$, one must omit transitions of this kind. Thus Dancoff's divergent terms arise entirely from the fact that the mass term is not diagonal in the Dirac Hamiltonian, so that a small (but divergent) increment in mass mixes positive and negative energy states, and makes new transition schemes possible.

In the case of the Pauli-Weisskopf theory, the situation is exactly analogous. The terms that give the highest (quadratic) divergence, are the terms in the square of the vector potential, whose matrix element for creating a pair in the sense discussed above is $(e^2/\pi\epsilon_p)\int_0^\infty qdq$, while the electromagnetic mass due to these terms gives exactly the same result when added to the zero-order Hamiltonian.

It should be noted that we have only shown that the divergent part of these matrix elements corresponds to a mass effect and, in fact, there are finite parts that do not, so that transitions of this type should properly be included to a finite extent. However, one is faced, in doing this, with the problem of separating a finite part of a formally infinite term, so that a specification of the way in which the infinite integral is performed is required for an unambiguous result.*** Schwinger[9] has given a procedure for separation of mass terms, by means of a canonical transformation on the Hamiltonian, which is equivalent to ours for this problem and which leads to finite terms of this character.

We conclude, therefore, that one can adopt a fairly clear procedure for eliminating the divergent mass effects from these transition problems. In the first place, one must use the empirical mass of the electron wherever the energy-momentum relationship is required, and second, must omit from the transition schemes transitions that are caused by mass increments.

*** An estimate of these finite terms indicates that they produce effects which are of order unity compared with the logarithm in (4), so that they are not important for low velocities.

[9] J. Schwinger, unpublished.

IV. CONCLUSIONS

We have seen that the use of the perturbation method in certain transition problems provides an automatic separation between the inertial and reactive effects of the radiation field. In a relativistic calculation, however, the non-diagonal character of βm in the Dirac Hamiltonian makes the separation of inertial effects a slightly more subtle procedure, and it must be performed explicitly. However, an unambiguous identification of divergent terms can indeed be made, and the reactive terms in the scattering of an electron by an electrostatic field are found to converge. The suggested procedure is easily extended to other types of fields, and one can see no clear obstacle to the calculation of the reactive effects on other problems involving electrons.

In conclusion, I would like to express my sincere appreciation to Professor J. R. Oppenheimer, for having suggested this problem, and for many helpful conversations concerning it.

Letters to the Editor

PUBLICATION of brief reports of important discoveries in physics may be secured by addressing them to this department. The closing date for this department is five weeks prior to the date of issue. No proof will be sent to the authors. The Board of Editors does not hold itself responsible for the opinions expressed by the correspondents. Communications should not exceed 600 words in length.

Remarks on H. W. Lewis' Paper "On the Reactive Terms in Quantum Electrodynamics"[1]

SAUL T. EPSTEIN
The Institute for Advanced Study, Princeton, New Jersey
November 25, 1947

IN connection with the results of Lewis, it should be noted that once one knows the differential cross section, $\varphi\sigma$, to the first non-vanishing order in $\alpha(=e^2/\hbar c)$ for a process in which a free particle interacts with an electromagnetic field, there is an almost trivial method for determining the correction of order α which has to be applied to this result because one has used the experimental, not the mechanical rest mass of the particle in computing it. This correction, combined with the usual radiative corrections of order α, may be expected to yield a finite result.

To find the correction we remark that the effect of a change in the particle's rest mass (that is, the difference between experimental and mechanical rest masses) on the plane waves, density of states, incident flux, and other quantities entering into the calculation of a cross section is to change the value of M, the parameter representing the mass, and through this the value of the energy defined by $E^2=C^2P^2+M^2C^4$, where P is the particle momentum. P is, of course, unchanged. Hence the first-order correction in $\varphi\sigma$, due to the mass difference δM, is

$$\delta(\varphi\sigma)=\frac{\delta(\varphi\sigma)}{\delta M}\cdot\delta M,$$

where, before differentiation, $\varphi\sigma$ has been expressed as a function only of the mass and of the momenta, and where for δM we substitute the electromagnetic rest mass of the free particle to order α, however, with a minus sign because the experimental mass is greater than the mechanical mass.

Lewis has mentioned my application of this simple method to the problem of radiative corrections to electron scattering; we will consider here the corrections to the scattering of a Pauli-Weisskopf particle by a central field. Two cases will be discussed: (*I*) the potential is an electrostatic potential and (*II*) the potential is a world scalar $V(\Lambda)\Psi\Psi^*$, Ψ, being the particle wave function.

We have, keeping just the relevant terms,

$$\varphi\sigma_I\alpha P^2+M^2C^2,$$

$$\varphi\sigma_{II}\alpha\frac{P^2+M^2C^2}{P^2+M^2C^2},$$

$$\delta M=-\frac{\alpha}{\pi M}\int K\varphi K+\cdots,$$

where the dots represent both infinite and finite terms.[2] Therefore, for small momenta

$$\frac{\delta(\varphi\sigma_I)}{\varphi\sigma_I}=-\frac{2\alpha}{\pi M^2}\left(1-\frac{P^2}{M^2C^2}\right)(\int K\varphi K+\cdots),$$

$$\frac{\delta(\varphi\sigma_{II})}{\varphi\sigma_{II}}=-\frac{2\alpha}{\pi M^2}\left(1-\frac{P^2}{M^2C^2}\right)(\int K\varphi K+\cdots)+\frac{2\alpha}{\pi M^2}\left(1-\frac{P^2}{M^2C^2}\right)(\int K\varphi K+\cdots).$$

Dancoff[3] has studied the radiative corrections to this problem. Since in *I* the part of $\varphi\sigma_I$ which contributes is just the product of the density of states and the incident flux, he found only finite corrections, and did not find the negative of the mass correction because, as Lewis has discussed, he used an inconsistent perturbation method. For the same reason he did not find the negative of the first term in *II*. However, he does find the nagative of the second term (when the electrostatic terms found by Lewis are included) plus finite terms. Thus, we see that by considering all the corrections we get a finite result in both cases, removing the anomaly found by Dancoff.

Clearly this same procedure will be helpful in determining the mass corrections in Compton scattering, bremsstrahlung, and other processes.

I would like to thank H. W. Lewis and Professor J. R. Oppenheimer for many stimulating discussions.

[1] H. W. Lewis, Phys. Rev. **73**, 173 (1948).
[2] V. Weisskopf, Phys. Rev. **56**, 72 (1939).
[3] S. M. Dancoff, Phys. Rev. **55**, 959 (1939).

On the Mean Life of Negative Mesons

G. E. VALLEY AND B. ROSSI
Laboratory for Nuclear Science and Engineering, Massachusetts Institute of Technology, Cambridge, Massachusetts
November 24, 1947

THE cloud-chamber apparatus, previously described by one of us,[1] has been reconstructed in such a way as to allow measurement of the decay times of individual positive or negative mesons which stop in the specimen block *S* (compare Fig. 1, reference 1). The time-measuring apparatus is in principle similar to that described by Rossi and Nereson.[2,3]

The decay time is registered by a ballistic meter which is photographed on the same picture as is the cloud chamber.

With this apparatus we have observed that slow mesons of both signs decay in a specimen of type 61-S Duralumin (98 percent Al, 1 percent Mg) and have succeeded in accumulating sufficient data to make rough determinations of the mean lives of the positive and negative mesons.

Our results are shown in Fig. 1 in the form of integral decay distributions. When analyzed by the method of Peierls[4] the mean lifetime is, for the positive mesons 2.19 $\pm$0.24 microseconds, and for the negative mesons 0.74 $\pm$0.17 microsecond.

During the experiment, 32 negative and 147 positive mesons were observed to decay after 1.1 microsecond from their time of arrival at the apparatus. This is in agreement with a previous finding of Bernardini and Pancini[5] to the effect that in aluminum both positive and negative mesons decay, but that the *observed* number of positive decays is considerably larger than that of negative decays.

Our value for the mean lifetime of positive mesons is in agreement with previous determinations of the mean lifetime of mesons brought to rest in absorbers of high atomic number; in this case it is known that only positive mesons give rise to delayed emission of decay electrons. According to our results, the composite decay curve of positive and negative mesons in aluminum is the sum of two exponentials. However, the fact that within the experimental accuracy the decay curves in aluminum published by Nereson and Rossi[1] and by Ticho[6] can be represented by a simple exponential for times longer than one microsecond, does not contradict our findings because at one microsecond the number of surviving negative mesons is a small fraction of the number of surviving positive mesons. For the same reason it would not be expected that this effect would have been detected by Sigurgiersson and Yamakama.[7]

From the approximate equality in the number of positive and negative mesons in the atmosphere it is known that the natural lifetime of negative mesons cannot be appreciably shorter than that of positive mesons. The large difference which we find between the *apparent* lifetimes of positive and negative mesons in aluminum can be explained easily if one assumes that mesons may be captured by nuclei. This nuclear capture process will only take place for negative mesons because the electrostatic interaction brings negative mesons close to the nuclei and keeps positive mesons away. If $\tau 0$ is the mean lifetime before decay (which is here assumed to be exactly the same for positive and negative mesons) and τc is the mean lifetime of negative mesons before capture, the apparent mean lifetime of negative mesons, τa, is given by the expression $1/\tau a = 1/\tau 0 + 1/\tau c$.[8] Under the same assumption, the fraction of negative mesons which undergo spontaneous decay is $f = \tau a/\tau 0$. With the values of $\tau 0$ and τa quoted above, one obtains $f = 0.36 \pm 0.08$. On the other hand, extrapolation of the decay curves of negative and positive mesons to $t = 0$ gives the following value for the ratio N^-/N^+ between the numbers of negative and positive mesons which give rise to delayed coincidences: $N^-/N^+ = 0.6 \pm 0.2$. This ratio does not represent the exact fraction f of negative mesons which decay in aluminum because (1) positive mesons are slightly more abundant than negative mesons, (2) some of the mesons are absorbed in the brass walls of the counters rather than in the aluminum, (3) the natural time lags of G-M counters slightly affect the absolute number of observed delayed coincidences. After correcting for the above effects, one obtains for f the value: $f = 0.7 \pm 0.25$, which is greater than that calculated on the basis of the observed mean lifetimes. Not much weight, of course, can be attached to this discrepancy until the statistical errors have been reduced by further experiments which are now in progress. Also the possibility that the apparatus may discriminate in favor of negative mesons has not yet been carefully tested. If the discrepancy were confirmed, it might be interpreted to indicate that the nuclear capture of negative mesons is often accompanied by the emission of particles which can be detected by the G-M counters. Another interesting possibility is that negative mesons are never captured by nuclei, but that their natural lifetime is shortened by the proximity of the nucleus, perhaps on account of the strong electric field existing in this region. If this is the case, the fraction f should turn out to be one, a value consistent with our determinations. The assumption that negative mesons do not undergo nuclear capture would explain the failure to detect stars at the end of meson tracks in cloud-chamber pictures, and would also be in agreement with the recent results of Lattes, Occhialini, and Powell.[9] However, some of Rasetti's early results[10] may be difficult to explain under the hypothesis that in heavy elements the disappearance of a meson is always accompanied by the emission of a decay electron.

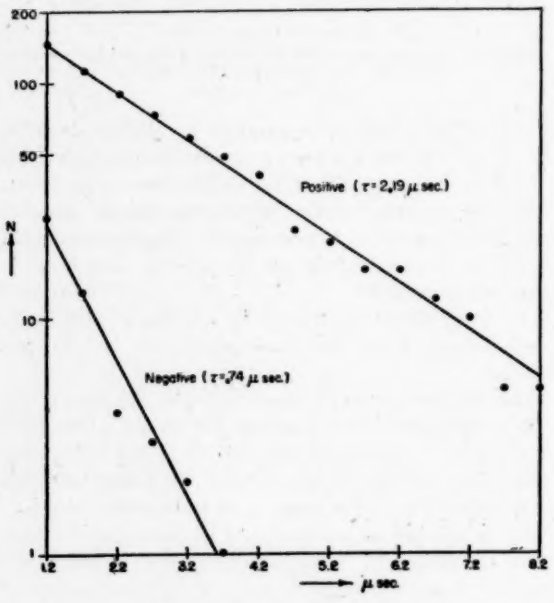

FIG. 1. Integral decay plots for positive and negative mesons which have been stopped in aluminum.

This work was supported in part by the Office of Naval Research, Contract N5 ORI-78, U. S. Navy Department.

[1] G. E. Valley, Phys. Rev. **72**, 772 (1947).
[2] B. Rossi and N. Nereson, Phys. Rev. **62**, 417 (1942).
[3] N. Nereson and B. Rossi, Phys. Rev. **64**, 199 (1943).
[4] R. Peierls, Proc. Roy. Soc. **149**, 467 (1935); Dr. Peierls has kindly extended the scope of these calculations for us in a private memorandum.
[5] The writers are much indebted to Dr. Bernardini and Dr. Pancini for a private communication of this still unpublished result, which concentrated their interest upon aluminum.
[6] H. K. Ticho, Phys. Rev. **72**, 255 (1947).
[7] T. Sigurgiersson and A. Yamakama, Phys. Rev. **71**, 319 (1947).
[8] The thought that the apparent lifetime of negative mesons must be different from their natural lifetime if a competition exists between spontaneous decay and nuclear capture, appears to have occurred independently to various physicists, including the writers. It has been described by H. K. Ticho and M. Schein in a recent letter to this journal. (Phys. Rev. **72**, 248 (1947).)
[9] C. M. G. Lattes, G. P. S. Occhialini, and C. F. Powell, Nature **160**, 453 (1947).
[10] F. Rasetti, Phys. Rev. **60**, 198 (1941).

Further Results on Burst Production by Penetrating Cosmic-Ray Particles

H. BRIDGE, W. E. HAZEN,* AND B. ROSSI
Laboratory for Nuclear Science and Engineering, Massachusetts Institute of Technology, Cambridge, Massachusetts
November 28, 1947

FROM a coincidence experiment made by means of a pulse ionization chamber and a bank of G-M tubes, Bridge, Rossi, and Williams[1] concluded: (1) that there exist in cosmic rays, ionizing particles capable of producing bursts in an ionization chamber after traversing 15 cm of lead; (2) that the number of these particles increases with height much more rapidly than the number of ordinary mesons; (3) that most of the bursts are the result of showers rather than of heavily ionizing nuclear fragments.

These conclusions have been confirmed by recent experiments. (a) The equipment used by Bridge, Rossi, and Williams was run at 10,000 and 14,000 feet in the Rocky Mountains, and it was found that the coincidence rate increased by a factor of 2.9 ± 0.4 between these two altitudes. The corresponding increase in the total number of penetrating particles (most of which are ordinary mesons) is only a factor of 1.2. (b) The G-M tubes ion chamber equipment was used in combination with a cloud chamber arranged as shown in Fig. 1. The chamber was 11 in. in diameter. It contained eight ½-in. lead plates, 9 in. long, and spaced 1 in. between centers. The cloud chamber was triggered by coincidences between the G-M tray and the ionization chamber. The pulse required from the ionization chamber was equivalent to the average pulse produced by 15 fast particles traversing the chamber perpendicularly to the axis. A number of pictures were obtained showing the production of electron showers by penetrating ionizing particles. An example is shown in Fig. 2. The particle which is seen to initiate a shower in the sixth lead plate cannot possibly be a high energy electron because no such electron can come out of a large thickness of lead unaccompanied by many low energy electrons. The shower represents an energy of at least several Bev, so that the energy of the penetrating particle which is responsible for it is probably more than 10^{10} ev.

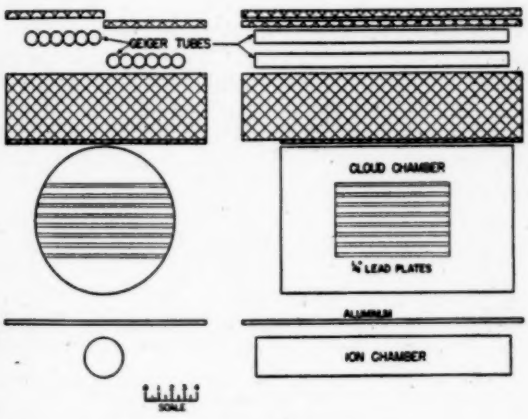

FIG. 1. Experimental arrangement.

Some of the pictures showed associated production of penetrating particles and/or "stars." Occasionally, one of the penetrating particles with low energy could be identified as a meson. The absence of detectable penetrating particle tracks in many of the showers, however, is not evidence for their absence, since we should expect most of such tracks to be completely lost in the dense electron cascades.

The simultaneous appearance of electron showers, penetrating particles, and stars in cloud-chamber pictures has been reported by other experimenters[2] and has been interpreted as showing that electrons and/or photons are are occasionally produced in nuclear interactions.

The very rapid increase with altitude of such nuclear interaction proves that this phenomenon does not represent a rare kind of secondary process by an abundant component of the local cosmic radiation but rather a frequent kind of secondary process by a component of the local cosmic radiation which is very scarce at sea level but becomes rapidly more abundant as the altitude increases. As indicated in the previous paper by Bridge, Rossi, and Williams,[1] we believe that this component consists of protons, probably, in part, of protons belonging to the primary cosmic radiation. Of course, we must expect that phenomena of the same type are produced also by secondary protons and neutrons arising from nuclear disruptions provided their energy is sufficiently high.

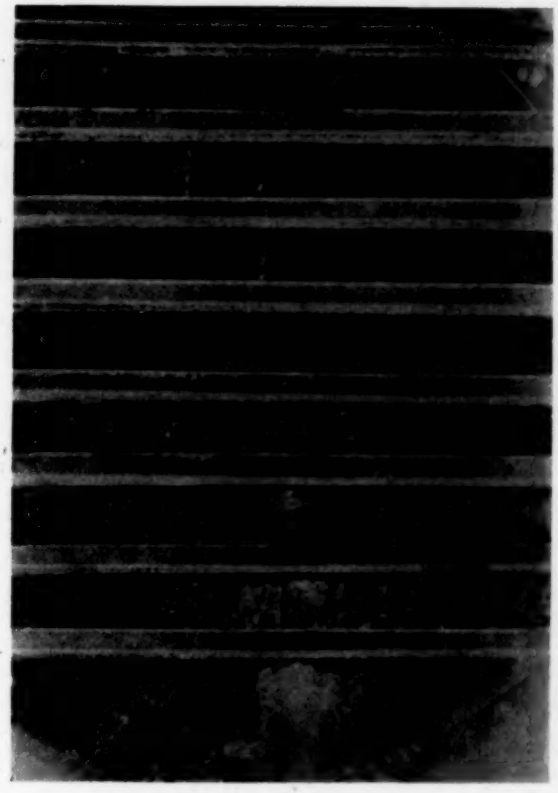

FIG. 2. Cloud-chamber photograph showing the production of electron showers by penetrating ionizing particles.

It is possible, even likely on theoretical grounds, that nucleons do not generate electrons or photons directly, but rather through the production and subsequent almost immediate decay of neutral mesons. It also appears possible, in view of the recent experiments with photographic emulsions,[3] that the primary products of nuclear collisions are heavy mesons, which then disintegrate into neutral mesons and ordinary mesons. It is hoped that a more complete analysis of existing data as well as the results of new experiments now in progress will throw some light on the exact mechanism of production of electrons and photons by nucleons. The research described in this letter was supported partially by Contract N5 ORI-78, U. S. Navy Department, Office of Naval Research.

* John Simon Guggenheim Memorial Fellow, now at the University of Michigan, Ann Arbor, Michigan.
[1] H. Bridge, B. Rossi, and R. W. Williams, Phys. Rev. **72**, 257 (1947).
[2] See, for instance, J. Daudin, Comptes Rendus (May 1944); G. D. Rochester, Proc. Roy. Soc. **A187**, 464 (1946); W. B. Fretter, Phys. Rev. **71**, 462 (1947).
[3] C. M. G. Lattes, G. P. S. Occhialini, and C. F. Powell, Nature **160** 453 (1947).

Isotopic Composition of Samarium

MARK G. INGHRAM, DAVID C. HESS, JR., AND RICHARD J. HAYDEN
Argonne National Laboratory, Chicago, Illinois
December 1, 1947

DURING the last three years several measurements of the abundance of the samarium isotopes were made at the Metallurgical Laboratory. The only previous measurements were those of Aston,[1] which were made from incompletely resolved spectra and were admittedly not very accurate. The observation of the neutron absorption by the isotope at mass 149 by Lapp, Van Horn, and Dempster[2,3] required a new measurement. For their measurements mass spectra were made on Eastman III-O ultraviolet sensitive spectroscopic plates with a double focusing instrument in which the ion source was a vacuum spark between nickel tubes packed with the oxide of samarium. The gadolinium abundances as measured by Wahl[4] were used as intensity standards. There is, however, some question as to the slope of the density curve used by Wahl in determining the gadolinium abundances, since the intensity standards were printed by x-rays.

A second measurement was a photometric comparison of samarium with the neodymium isotopes by Wilfrid Rall and A. J. Dempster,[5] using the abundances given by J. Mattauch and V. Hank[6] for the latter element as standards. In their determination of the neodymium standards these authors fixed the slope of the photographic density curve by means of exposures with different exposure times on the same plate, assuming constancy of discharge. These values are given in the third row of Table I.

Our own measurements were made using electrometric recording of the ion currents. This eliminates the difficulties in determining the density curves so that the isotopic abundances determined are independent of any other measurements. The analysis was made with a 60°, six-inch radius of curvature single focusing mass spectrometer in the same manner as our previously reported measurements of lanthanum and cerium.[7] The ions were produced by heating the oxide of samarium on a tungsten filament. Ion currents were measured with a vibrating reed electrometer connected to a Brown Electronik Strip Chart Recorder. No source magnet was used, and the ion beams were swept across the final collector by changing the analyzer magnetic field. Thus all discriminations are believed to be below 1 percent.[7] The results are tabulated in the fourth row of Table I. Except in the case of mass 144 the errors tabulated are larger than the mean deviations by amounts sufficient to include possible systematic errors in the mass spectrometer. The actual mean deviations are about three times smaller than the deviations quoted in the table.

Calculations of the chemical atomic weight from these abundances, assuming a packing fraction for samarium of -2.4×10^{-4} and the factor 1.000275 in converting from the physical to the chemical atomic weight scales, gives a value of 150.35 as compared with the chemically determined value of 150.37.

The following upper limits for possible samarium isotopes of neighboring masses were obtained: 140, 141, 142, less than 0.001 percent; 143, 145, and 146, less than 0.002 percent; 151, less than 0.02 percent; 153 and 155, less than 0.01 percent; 156, 157, and 158, less than 0.002 percent.

These limits are of special interest in connection with the alpha-activity of samarium which corresponds to a half-life for all the nuclei of 10^{12} years. Because the location of this activity is still uncertain, and because the isotope of mass 146 has been assumed to be undetected because it is alpha-active, it is of interest to consider this isotope as the source of the activity. Since if it is present, it is present to less than 0.002 percent, the upper limit on the half-life of the isotope is 2×10^{7} years. This is too short a half-life from geological considerations to explain the present activity, so this activity must still be located in one of the known isotopes. Thus, if the 146 is absent because of alpha-activity, it is a different activity from the alpha-activity now existing in samarium.

TABLE I. Abundance of samarium isotopes.

144	147	148	149	150	152	154	Obs.
3	17	14	15	5	26	20	Aston[1]
3	14.2	9.5	12.7	5.0	31.9	23.7	L,VH,D[2,3]
2.7	15.2	10.8	14.1	7.7	27.1	22.4	R,D[5]
3.16 ±.10	15.07 ±.15	11.27 ±.11	13.84 ±.14	7.47 ±.07	26.63 ±.26	22.53 ±.22	I,H,H

[1] F. W. Aston, Proc. Roy. Soc. **A146**, 50 (1934).
[2] R. E. Lapp, J. R. Van Horn, and A. J. Dempster, Manhattan Project Report CP-2975.
[3] R. E. Lapp, J. R. Van Horn, and A. J. Dempster, Phys. Rev. **71**, 745 (1947).
[4] Wahl, Soc. Sci. Fenn. **11**, 1 (1941). According to a paper by J. Mattauch and H. Ewald, Zeits. f. Physik, **122**, 321 (1944), the standards were made with x-rays.
[5] W. Rall and A. J. Dempster, Manhattan Project Report CP-3537.
[6] J. Mattauch and V. Hank, Naturwiss. **25**, 780 (1937).
[7] M. G. Inghram, R. J. Hayden, and D. C. Hess, Jr. Phys. Rev. **72**, 967 (1947).

Fast Modulation Effects in the Optical Region

ARTHUR RUARK

The Applied Physics Laboratory and the Institute for Cooperative Research, The Johns Hopkins University, Baltimore, Maryland

November 26, 1947

IN these columns Forrester, Parkins, and Gerjuoy[1] have suggested the possibility of observing beat frequencies between closely neighboring lines in the optical region. They propose to detect microwave beats between two Zeeman components of a spectral line by allowing the light to fall on a photo-cathode. Thence, pulses of electrons go to a cavity in the same vacuum. It may be useful to call attention to the viewpoints presented in a paper by Breit, Ruark, and Brickwedde.[2] Experiments with rotating Nicols and other modulators were discussed on ordinary wave theory, and on the basis of absorption and emission by a large quantized rotating oscillator, representing the modulator. The analysis showed clearly that rays of different frequencies can be coherent and that the "only reason why we are not conscious of the fact is that their frequency differences are (ordinarily) too large. Thus, the Zeeman effect corresponding to 0.01 gauss would cause a frequency difference of the order of 10^8 a second, and hence no stationary pattern could be observed."

I wish to describe an interesting light-modulation experiment which I set up at the Bureau of Standards in 1926. It was not completed because of a change of residence. Light from a narrow slit fell on a lens of diameter D, the slit being at the focus. Behind the lens there was a mirror of width D rotating with a high angular velocity ω. Thus the reflected light could be swept rapidly over the narrow slit of a spectroscope, placed also at the focal distance. This experiment was designed to "cut photons in two." (The idea seemed sensible then, since Dirac's radiation theory had not been published.) Let us see what can be done to get very brief light pulses by this method. The lens forms a diffraction maximum of width $r\lambda/D$ at the focal distance r. Thus the effective duration of the pulse passing the final slit is $\lambda/D\omega$. Now, $D\omega/2$ is limited to a value of the order of 30,000 cm/sec. by the strength of present-day mirror materials; so, for green light, *the pulse duration cannot now be less than 10^{-9} sec., in order of magnitude.* This time interval is shorter than the duration of the fastest sparks, which must be superior to the decay time of the excited atoms, so this result may be interesting. Because of the short pulse length, the light transmitted has a relative band width $\Delta\lambda/\lambda = D\omega/c$, but if the mirror has a width equal to D there is a further broadening of the same magnitude, resulting from Doppler effect at the edges of the mirror face. The two effects are physically different, and not merely two ways of looking at the same thing. I have had the opportunity to discuss speedy rotators and short sparks with Drs. L. B. Snoddy and J. W. Beams, and wish to thank them for relevant information.

[1] Forrester, Parkins, and Gerjuoy, Phys. Rev. 72, 728 (1947).
[2] Breit, Ruark, and Brickwedde, Phil. Mag. 3, 1306 (1927).

Gamma-Radiation from Light Nuclei under Proton Bombardment

W. A. FOWLER, C. C. LAURITSEN, AND T. LAURITSEN

Kellogg Radiation Laboratory, California Institute of Technology, Pasadena, California

November 24, 1947

STUDIES of the gamma-radiation emitted in the disintegration of lithium, beryllium, carbon, and fluorine by protons at several well-known resonances have recently been completed. The thick-target yield of the radiation, the half-width of the resonance, and the range in aluminum of the secondary electrons produced by the radiation have been determined.

The results are tabulated in Table I. The resonance energies given in the second column are based on the resonance in $Li^7(p\gamma)$ at 440 kev as standard.* The values for the energy of the gamma-radiation which are listed are in most cases those which have been previously determined in this laboratory by magnetic analysis of the energy of secondary electrons and pairs produced in thin laminae suspended in a cloud chamber. The values have been corrected for new calibrations of the field coils used in these measurements. In the case of the 1077-kev resonance in $Be^9(p\gamma)$ the energy of the more energetic gama-ray (6.7 Mev) has been determined from secondary absorption measurements, while the 0.8-Mev radiation has been established in measurements employing a focusing beta-ray spectrometer.

The secondary ranges given in the table have been determined with coincidence counters and are those ranges at which the number of secondaries is reduced to 0.8 percent (2^{-7}) of the number without absorber between the counters.[1,3] The high order intersections of the absorption curves with the background are about 10 percent greater than these ranges but cannot be determined as accurately.

The thick-target yield of the radiation has been determined simultaneously with electroscopes and counters housed in aluminum. In the calculations we used the curves of Fig. 1, which give the counts per incident quantum produced in a counter and the ion pairs/cc per quantum/cm² produced in the ionization chamber of an electroscope as a function of the quantum energy. The quantum efficiency curve for a counter with aluminum walls was calculated from 2.5 to 25 Mev in a manner described by Bleuler and Zünti[2] and will be discussed in detail in a future publication. The electroscope curve is taken from Streib, Fowler, and Lauritsen.[3]

The yields are in disintegrations per incident proton for the actual targets employed, namely, LiOH with the natural Li^7 abundance, beryllium metal, natural Acheson graphite, and CaF_2. In the case of $C^{13}(p\gamma)$ there are 50 percent more quanta than disintegrations, since the disintegration branches about equally to give one 8.1-Mev quantum and one 2.3-Mev quantum followed by a 5.8-Mev quantum.[4] It is well to note that the approximate linearity of the detector sensitivity curves with energy makes the disintegration yield relatively independent of the branching or the number of steps in the radiation as long as the total energy radiated in the various transitions is the same.

TABLE I. Summary of Yield and Energy Measurements.*

Source	Resonance energy kev	Energy of radiation Mev	Range of secondaries d_7 (Al) cm	Thick-target yield Electroscope Disintegrations/proton	Thick-target yield Counter Disintegrations/proton	$\omega\gamma$ ev	Γ kev	σ_R cm²
$Li(p\gamma)$	439	17.5[a]	2.91	5.6×10^{-9}	5.1×10^{-9}	8.9	12[d]	5.7×10^{-22}
$Be^9(p\gamma)$	988	7.4	1.26	1.82×10^{-8}	1.74×10^{-8}	12.5	94	4.4×10^{-23}
	1077	6.7,0.8	1.11	1.05×10^{-9}	0.97×10^{-9}	0.77	4	5.8×10^{-23}
$C^{12}(p\gamma)$	453	2.3[b]			7.3×10^{-10}	0.63	35	1.2×10^{-23}
$N^{13}(\beta^+)$		1.25[c]			7.2×10^{-10}			
$C^{13}(p\gamma)$	550	2.3,5.8,8.1			1.8×10^{-10}	15	40	2.0×10^{-23}
$F^{19}(p\alpha',\gamma)$	338	6.3		1.67×10^{-8}	1.74×10^{-8}	30	4	6.5×10^{-23}
	All ≤960	6.3	1.06	6.80×10^{-7}	6.95×10^{-7}			

* Target materials: LiOH, Be metal, Acheson graphite, CaF_2.
[a] Weak radiation near 14 Mev neglected in these calculations.
[b] Plus two annihilation quanta.
[c] Maximum energy of the positrons.
[d] Corrected for radiation observed above resonance.

The agreement between electroscope and counter yields is satisfactory. In the carbon[5] and lithium[6] reactions the results do not depart markedly from the widths and yields which have been determined previously. In the case of $C^{12}(p\gamma)$ which results in the production of radioactive N^{13} the positron yield has been measured with counters and is in agreement with the quantum yield. In the $F^{19}(p\alpha',\gamma)$ reaction the yield values are 20 percent higher than that given for the alpha-particles by Van Allen and Smith[7] ($1.43\times10^{-8}\alpha/p$), and further studies of this discrepancy are contemplated.

From the absolute thick-target yields it is possible to compute the term $\omega\gamma=\omega\Gamma_p\Gamma_x/\Gamma=2\epsilon Y/\lambda^2$, which appears in the Breit-Wigner dispersion formula. The quantity ω is the statistical factor, Γ_p is the width for re-emission of a proton, Γ_x is the width for the primary process in the gamma-radiation ($\Gamma_{\alpha'}$ in the case of fluorine, Γ_γ in all the others), and Γ is the width for all competing processes. Y is the yield, λ is the wave-length of the incident protons at resonance, and ϵ is the stopping cross section of the target for protons per disintegrable nucleus. The quantity γ is approximately equal to the smaller of Γ_p and Γ_x when $\Gamma=\Gamma_p+\Gamma_x$ and is thus equal to Γ_γ in all but the $F^{19}(p\alpha',\gamma)$ case where it is equal to Γ_p.

The width at resonance, Γ, has been determined for the case of lithium and carbon from the thick-target curves and in the case of beryllium from thin-target curves. The proton beam was passed through the electrostatic analyzer previously described[8] and had a spread in energy of the order of 300 e-volts at 1 Mev. In the case of carbon the widths are great enough so that the curves are distorted by the proton barrier penetration factor from that of a simple dispersion curve, and a correction has been made to give the width at resonance. A similar correction has been made for the position of the resonance. The total width is approximately equal to Γ_p in all but the $F^{19}(p\alpha',\gamma)$ case where it is equal to $\Gamma_{\alpha'}$.

The theoretical implication of these results will be discussed in a future publication. The experimental results should serve to aid in standardizing information concerning the disintegrations of light elements. This work was carried out under contract with the Office of Naval Research.

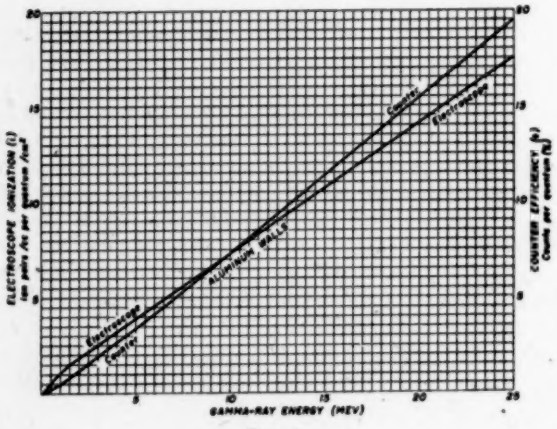

FIG. 1.

* A correction for radiation observed above the resonance indicates that the true resonance position is 439 kev on the conventional energy scale.

[1] Bradt, Gugelot, Huber, Medicus, Preiswerk, and Scherrer, Helv. Phys. Acta 19, 77 (1946).
[2] E. Bleuler and W. Zünti, Helv. Phys. Acta 19, 375 (1946).
[3] J. F. Streib, W. A. Fowler, and C. C. Lauritsen, Phys. Rev. 59, 253 (1941).
[4] T. Lauritsen, C. C. Lauritsen, and W. A. Fowler, Phys. Rev. 59, 241 (1941).
[5] R. B. Roberts and N. P. Heydenburg, Phys. Rev. 53, 374 (1938); S. C. Curran, P. I. Dee, and V. Petržílka, Proc. Roy. Soc. 169A, 269 (1939).
[6] L. R. Hafstad and M. A. Tuve, Phys. Rev. 48, 306 (1935); W. A. Fowler, E. R. Gaerttner, and C. C. Lauritsen, Phys. Rev. 53, 628 (1938).

Superconductivity and the Debye Characteristic Temperature

K. R. DIXIT
Royal Institute of Science, Bombay, India
December 1, 1947

A PAPER[1] with the above title was published recently in the Physical Review. In this paper a curve is drawn showing the relation between the superconducting threshold temperature (T_s) and the Debye characteristic temperature (Θ_D), and some conclusions are derived on the basis of this assumption. If this relation is justifiable we could also say that substances which do not become superconducting by about 0.7°K will not become superconducting at all. This conclusion is not drawn in the paper mentioned, but a similar conclusion was drawn in an

earlier paper[2] by the writer. The relevant part is quoted below:

"On this assumption substances which have no conductivity electrons and substances in which the interaction between the conductivity electrons and the lattice vibrations is not negligible will not show superconductivity. According to Debye (Ann. d. Physik **32**, 85 (1938)) the effect of the lattice oscillations is very small for all temperatures below 1°K. From this we can conclude that substances which do not become superconducting by about 1°K will not become superconducting at all. This seems to agree with the observed fact that the lowest transition temperature recorded (Smith and Wilhelm, Rev. Mod. Phys. **7**, 237 (1935)) is 0.6°K for cadmium."

[1] J. de Launay and R. L. Dolecek, Phys. Rev. **72**, 141 (1947).
[2] Dixit, Curr. Sci. **9**, 274 (1940).

Index of Refraction for Electrons in Crystalline Media

LORENZO STURKEY
The Dow Chemical Company, Midland, Michigan
December 4, 1947

THE Schrödinger equation for electrons in a crystalline medium may be written[1]

$$\nabla^2\psi+(8\pi^2me/h^2)(E+V_0+\sum_{g\neq 0}V_g e^{2\pi i g\cdot r})\psi=0,$$

where E is the accelerating potential of the electrons, V_0 the "inner potential," and the V_g are the coefficients in the Fourier expansion of the periodic potential in the crystal.

It is usually assumed that the index of refraction n for electrons is given by

$$n^2=(E+V_0)/E.$$

However, if electrons are incident on a crystal at the Bragg angle for a set of planes (hkl), a correction must be made to the inner potential. This correction may be calculated by finding the value of ΔE that diagonalizes the energy matrix

$$\begin{pmatrix}\Delta E & -V_{hkl}\\ -V_{-h-k-l} & \Delta E\end{pmatrix},$$

i.e., $\Delta E=\pm V_{hkl}$. In this case

$$n^2=(E+V_0\pm V_{hkl})/E$$

and double refraction occurs, with $P=V_0\pm V_{hkl}$ as effective inner potential.

In a previous communication,[2] refraction effects were discussed for electrons in crystals of cubic habit like MgO and CdO. The vector angular deviations from the Bragg reflection position due to refraction for such crystals may be expressed as:

$$\delta=(P/2E)(u\tan<r,n_1+V\tan<r,n_2)=(P/2E)K, \quad (1)$$

where

$u=(r\times n_1)/|r\times n_1|$,
$V=(r\times n_2)/|r\times n_2|$,
r is unit vector in direction of electron ray,
n_1 and n_2 are face normals of crystal.

Since $P=V_0\pm V_{hkl}$ when the Bragg conditions are satisfied, one should expect two values of δ for each incident direction. On account of the cubic shape of the crystal, equal positive and negative values of δ will occur for the same setting of the crystal, making a total of *four* spots in a line:

$$\delta_1=+K(V_0+V_{hkl})/E,$$
$$\delta_2=-K(V_0+V_{hkl})/E,$$
$$\delta_3=+K(V_0-V_{hkl})/E,$$
$$\delta_4=-K(V_0-V_{hkl})/E.$$

Since V_{hkl} may be calculated with a much higher degree of accuracy than V_0, this phenomenon allows V_0 to be calculated from V_{hkl} without evaluating K or even knowing E.

$$V_0=V_{hkl}(\delta_1-\delta_2+\delta_3-\delta_4)/(\delta_1-\delta_2-\delta_3+\delta_4). \quad (2)$$

In electron diffraction patterns from MgO and CdO smokes, groups of spots as described are frequently observed on diffraction rings having a V_{hkl} of the same order of magnitude as V_0—i.e., [200] and [220] rings. Since K in (1) often cannot be determined unambiguously, (2) provides a more reliable method for obtaining V_0. Some representative measurements are found in Table I.

TABLE I.

	(hkl)	meas. V_{hkl}/V_0	calc. V_{hkl}	calc. V_0
MgO	200	0.54	7.42 volts	13.7 volts
		0.59		12.6
		0.58		12.8
	220	0.415	5.37	12.9
		0.425		12.6
CdO	200	0.69	13.9	20.0
	220	0.55	9.8	18.0
		0.57		17.5
		0.52		19.0
		0.55		18.0

In cases where the angle of incidence is such that the Bragg reflection conditions are satisfied for more than one set of planes, multiple values of the inner potential occur. Such cases often occur in electron diffraction since the wave-length is usually much smaller than the interplanar spacings. For an angle of incidence such that the (200), (022), and (222) reflections are obtained simultaneously, *four* values of P should occur, with eight values of δ:

$$\Delta E=\pm(V_1+V_2)-V_3, \qquad V_1=V_{200},$$
$$\Delta E=\pm(V_1-V_2)+V_3, \qquad V_2=V_{022},$$
$$V_3=V_{222}.$$

When measurements are to be made on spots in diffraction patterns from crystals of various geometrical shapes, it should be remembered that each member of a group may be affected differently by extinction. Consequently, measurements using (1) on a single spot may give an error of $\pm V_{hkl}$, and such measurements should be made only when $V_{hkl}\ll V_0$, a condition not frequently valid for planes of low indices. Observations made on a large number of patterns indicate that spots resulting from the smallest values of the inner potential occur most frequently. Such considerations should explain anomalous inner potential values reported in the literature for planes of low indices.[3,4]

[1] H. A. Bethe, Ann. d. Physik **87**, 55 (1928).
[2] Sturkey and Frevel, Phys. Rev. **68**, 56 (1945). An extended discussion was given in a paper by L. Sturkey at the 1946 meeting of ASXRED at Silver Bay, Lake George, New York.
[3] Yamaguti, Proc. Phys. Math. Soc. Japan **16**, 95 (1934).
[4] Thomson and Cochrane, *Theory and Practice of Electron Diffraction* (The Macmillan Company, New York, 1939), Chapter 10.

Diffraction of Electromagnetic Waves

W. Owen Tranter
Physics Branch, Military College of Science, Shrivenham, N. Swindon, England
November 19, 1947

In a recent article, C. L. Andrews investigated some interesting variations of the intensity in the front of an electromagnetic wave that has passed through a circular aperture.[1] In this connection the writer would like to call attention to some work of his, now in progress, which may throw light on Andrews' results.

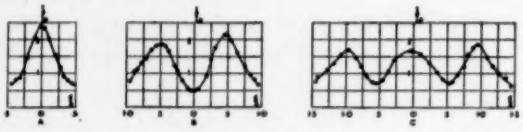

FIG. 1. Experimental determination of the intensity in the plane between two unactivated dipoles separated by distances λ, 2λ, 3λ, respectively.

Two vertical unactivated dipoles supported by thin glass rods replaced the aperture used by Andrews. Their separation in the H plane was successively λ, 2λ, and 3λ and the field between them was investigated by a receiving dipole moved in this plane. The results are shown in Figs. 1A, B, and C, respectively. The ordinates represent the ratio of the resultant to the undisturbed intensity, and the abscissae the distance of the receiving dipole from the center of the "aperture" in fractions of a wave-length. There is a striking resemblance to the results obtained by Andrews when he used a circular aperture.[2]

An approximate explanation of these results may be obtained in the following terms. Consider the resultant field in the plane of the dipoles to be a combination of the undisturbed incident wave and the waves reradiated in antiphase from the unactivated dipoles. An instantaneous picture of the waves in the "aperture," when it is of diameter λ, is shown in Fig. 2A. The undisturbed incident

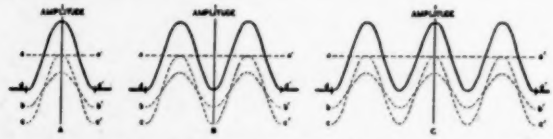

FIG. 2. Theoretical prediction of the instantaneous wave form in the plane of the aperture when its diameter is λ, 2λ, and 3λ, respectively.

wave is represented by aa', the reradiated wave from the left-hand dipole by bb', while cc' represents the combination of this with a similar reradiated wave from the right-hand dipole. The resultant dd' is obtained by combining aa' with cc'. Figures 2B and 2C show the resultant field in the plane of the "aperture" when its diameter is 2λ and 3λ, respectively. Although these results are in general agreement with experiment it must be pointed out that no allowance has been made for the fall-off of the reradiated field with distance, and clearly, this requires further investigation. In this simple theory it has been assumed quite arbitrarily that the dipoles reradiate 50 percent of the incident energy. Experiment shows the effective reradiation to be nearer 15 percent, but this does not alter the form of the curves obtained.

It would therefore seem likely that in dealing with diffraction of electromagnetic waves it is necessary to superimpose upon the formal diffraction pattern the effects due to reradiation from the sides of the aperture. Experiments are already in progress to investigate this more fully.

[1] C. L. Andrews, Phys. Rev. **71**, 777 (1947).
[2] Reference 1, Figs. 3A, B, and C.

The Deuteron Problem with Gaussian Potentials*

S. Moszkowski and R. G. Sachs**
Argonne National Laboratory, Chicago, Illinois
November 26, 1947

As a preparatory step for a calculation of the triton binding energy, the constants have been determined for a Gaussian neutron-proton potential, including a tensor interaction. The results are presented here on the chance that they may be of use to other workers in the field. The calculation was performed by means of the variation method. Both the S and D wave functions were assumed to be Gaussian functions, and the variation was carried out with respect to the ranges of each of these functions and with respect to the relative coefficient of the S and D terms. The variation was subject to the condition that the quadrupole moment have the experimental value[1] $Q=2.73\times10^{-27}$ cm². In this way the depth of the potential and the relative strength of the ordinary and tensor potentials were determined as a function of the range of the interaction.

Explicitly, the form of the interaction was assumed to be[2]

$$V=(1+\gamma S_{12})J(r),$$

where

$$J(r)=-J_0\exp(-r^2/\alpha^2),$$

and

$$S_{12}=[3(\sigma_1\cdot r)(\sigma_2\cdot r)-(\sigma_1\cdot\sigma_2)r^2]/\sqrt{8}r^2.$$

The S wave function was taken to be

$$\psi_S=c_S\exp(-\lambda r^2/2),$$

and the D function,

$$\psi_D=c_D\mu S_{12}\exp(-\mu r^2/2).$$

The total energy calculated for the normalized wave function $\psi=\psi_S+\psi_D$ was then varied with respect to λ, μ, and c_D/c_S. The minimum binding energy obtained in this way is a function of J_0, γ, and α. The constants J_0 and γ were then determined as a function of α by setting the binding energy equal to E, the binding energy of the deuteron, and the quadrupole moment equal to the value given above.

For the conventional value[2,3] $\alpha=2.80\times10^{-13}$ cm we find $J_0=10E$, $\gamma=1.50$, $\alpha^2\mu=2.92$, $\alpha^2\lambda=0.92$, and the D state probability is 4.0 percent.

It is to be expected that this method for obtaining J_0 will lead to a considerable overestimate, since the variation method would yield an underestimate of the binding energy if the correct potential were used. That this expectation is realized can be seen from the fact that the

value of J_0 is considerably greater than the square well depth ($6.40E$) obtained more accurately by Rarita and Schwinger.[2]

* This work has been carried out under the auspices of the Atomic Energy Commission. It was completed and submitted for declassification on July 1, 1947.
** Present address: Department of Physics, University of Wisconsin, Madison, Wisconsin.
[1] A. Nordsieck, Phys. Rev. **58**, 310 (1940).
[2] W. Rarita and J. Schwinger, Phys. Rev. **59**, 436 (1941).
[3] See also H. A. Bethe, *Elementary Nuclear Theory* (John Wiley and Sons, Inc., New York, 1947), p. 54.

On the Binding Energy of the Triton*

M. GOEPPERT-MAYER AND R. G. SACHS**
Argonne National Laboratory, Chicago, Illinois
November 26, 1947

IT has been shown[1] that the measured[2] magnetic moment of the triton can be accounted for without reference to meson exchange currents in the nucleus if the wave function of the ground state of the nucleus is assumed to contain a large admixture of ^2P and ^4P functions. Therefore, it seemed worth while to calculate the binding energy of the triton with a wave function of that form. For this calculation the potential energy was assumed to be the sum of an ordinary interaction term and a tensor interaction term *without* exchange. The potential function was taken to be a Gauss function with a range of $\alpha=2.80\times10^{-13}$ cm. The constants used in the interaction were those obtained from the deuteron calculation presented in the foregoing letter.[3]

The calculation was carried out by means of the variation method with a trial function consisting of a linear combination of those functions ψ_1, ψ_4, ψ_5, and ψ_8 which were used to account for the magnetic moment in reference 1. The radial part of each of these functions was taken to be Gaussian in both the distance $\boldsymbol{\rho}$ between the neutrons and the distance $\mathbf{r}$ from the center of gravity of the neutrons to the protons. To be consistent with reference 2, no dependence on $(\mathbf{r}\cdot\boldsymbol{\rho})$ was assumed. The binding energy was calculated as a function of the range in r and the range in ρ of each of the radial functions and as a function of the coefficients of the S, ^2P, ^4P, and D wave functions.

The resulting expression for the energy is much too complicated to minimize analytically. A careful inspection of this expression did, however, lead to the conclusion that the introduction of the ^2P or ^4P state reduces the binding energy. The best wave function which could be obtained by inspection contains 96 percent S state and 4 percent D state in agreement with the results of Gerjuoy and Schwinger.[4] It was found that, without loss in binding, the radial factors in the S and D functions could be taken to be of the form $\exp[-\beta(r_{12}^2+r_{13}^2+r_{23}^2)]$, where r_{ij} is the distance between the pair of particles i, j. This is the form of the function used by Gerjuoy and Schwinger.[4] For the S function $\beta\approx0.35\alpha^{-2}$ and for the D function $\beta\approx0.70\alpha^{-2}$. With this wave function the binding energy turns out to be 9.5 Mev. The excessively large binding is a consequence of the method used to obtain the strength of the potential.

From these results one may conclude that the tensor interaction will not introduce a large amount of ^2P or ^4P function into the ground-state wave function of the triton. The introduction of exchange forces would seem to strengthen this conclusion since repulsive potentials would thereby be introduced for the P functions. If a wave function containing a large P state probability is required to account for the magnetic moment, it will probably be necessary to assume that there are three-body interactions between nucleons. However, it should be kept in mind that only the four functions ψ_1, ψ_4, ψ_5, ψ_8, out of a possible nine functions, have been used for this calculation. Although these functions seem to account best for the magnetic moment, they may not give the best account of the binding energy and magnetic moment simultaneously.

* This work was carried out under the auspices of the Atomic Energy Commission. It was submitted for declassification on July 23, 1947.
** Present address: Department of Physics, University of Wisconsin, Madison, Wisconsin.
[1] R. G. Sachs, Phys. Rev. **72**, 312 (1947).
[2] H. L. Anderson and A. Novick, Phys. Rev. **71**, 372 (1947); F. Bloch, A. C. Graves, M. Packard, and R. W. Spence, Phys. Rev. **71**, 373 (1947).
[3] S. Moszkowski and R. G. Sachs, preceding letter.
[4] E. Gerjuoy and J. Schwinger, Phys. Rev. **61**, 138 (1942).

Excitation of Infra-Red Phosphors by Alpha- and Beta-Particles*

R. H. THOMPSON AND R. T. ELLICKSON
Reed College, Portland, Oregon
December 5, 1947

RECENTLY, a group of phosphors has been discovered that shows a marked response to infra-red light, if previously excited by ultraviolet light. Among the most responsive of these phosphors to infra-red is the one known as Standard VII, which is a strontium sulfide phosphor activated with cerium and samarium.[1]

It is true that some of these phosphors, especially Standard VII, are also excited by the radiations from radium in equilibrium with its products. At the Conference on Luminescent Materials held at Cornell University in October, 1946, there was a good deal of discussion of the question whether the alpha-particles or the beta-particles were responsible for this excitation. It was the contention

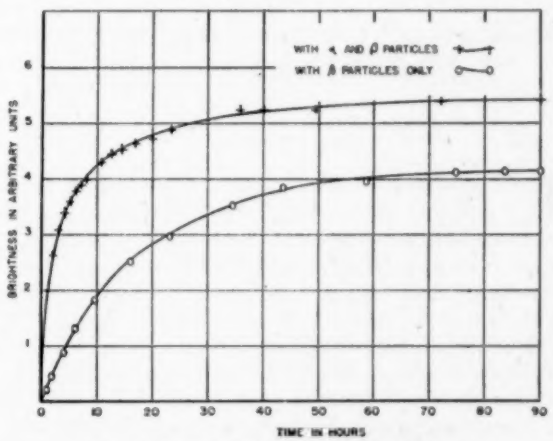

FIG. 1. Excitation of Standard VII phosphor.

of one of the authors (R.T.E.), based on the results of a single experiment, that there was no great difference between the degree of excitation produced by a combination of alpha- and beta-particles and the excitation produced by the same source with the alpha-particles removed. Others at the conference maintained that beta-particles are completely ineffective and that only the alpha-particles produce excitation.

The experiment has been repeated here with considerable care; the results are shown in Fig. 1. The crosses show the increase in brightness, measured under constant, low intensity infra-red radiation of a Standard VII sample excited for various times by a source consisting of a radium salt on a metal plate covered by a gold foil thin enough to allow alpha-particles to pass through it. The foil serves to contain the products of disintegration, and the excitation in this case is due to a combination of alpha- and beta-particles. The circles show the increase in brightness of the same sample excited by the same source, but with the alpha-particles removed by an absorber. As is evident from the curve, the beta-particles produce a final brightness about three-fourths as large as the combination source does. The thickness of the paper absorber used was fifty percent greater than that needed to remove all alpha-particles, as shown by the rate of discharge of an electroscope. This absorber removed about thirty percent of the beta-particles also. It may be significant that the fraction of the beta-particles removed by the absorber is about equal to the fractional decrease in the brightness with the absorber over the exciting source. In any case, there seems to be no doubt but that beta-particles are effective in exciting the Standard VII phosphor.

The phosphor sample used was supplied to us by Professor R. Ward of the Polytechnic Institute of Brooklyn, to whom we are greatly indebted. We wish also to acknowledge the assistance of Mr. Paul Hansen, who made the absorption measurements, and Mr. Robert Scott, who built the electron multiplier apparatus with which the brightness measurements were made.

* Supported by the Office of Naval Research.

[1] F. Urbach, D. Pearlman, and H. Hemmendinger, J. Opt. Soc. Am. 36, 372 (1946).

Extension of Crocco's Theorems to Flows Having Non-Uniform Stagnation Enthalpy*

R. C. PRIM
Naval Ordnance Laboratory, Washington, D. C.
November 28, 1947

TWO remarkable theorems relating the vorticity and pressure in plane and in axially symmetric steady flow of an ideal gas (non-viscous, thermally non-conducting, with constant specific heats) in the absence of body forces have been established by Crocco.[1] The first theorem states that the pressure and vorticity are proportional along each streamline of a plane flow in a region between two shock fronts. The second theorem states that the vorticity and the product of pressure and radial distance are proportional along each streamline of an axially symmetric flow in a region between two shock fronts.

As has been shown by Vazsonyi[2] and Emmons,[3] these theorems are valid only for flows of uniform stagnation enthalpy ("tank" flows). However, in terms of the reduced velocity field $\bar{v}$ defined by

$$\bar{v}=v/v_{\text{ultimate}}=v/[2\gamma/(\gamma-1)][p/\rho]+v^2$$

(where v denotes the actual velocity vector, γ the adiabatic exponent, p the pressure, and ρ the density) more general theorems are valid:

Theorem 1: Along each streamline of any steady, plane flow of an ideal gas in the absence of body forces, the pressure is proportional to the vorticity of the reduced velocity field in a region between two shock fronts.

Theorem 2: Along each streamline of any steady, axially symmetric flow of an ideal gas in the absence of body forces, the vorticity of the reduced velocity field is proportional to the product of the radial distance and the pressure in a region between two shock fronts.

These extended theorems are readily established by recourse to the substitution principle established by Munk and Prim.[4] First, for any *tank flow* the extended theorems are valid by virtue of Crocco's theorems and the simple proportionality between reduced velocity and actual velocity in a tank flow. Second, by the substitution principle, for any steady flow of an ideal gas in the absence of body forces there exist *tank flows* having the *same streamline pattern, reduced velocity field, and pressure distribution.* Since the extended theorems are valid for these substitute tank flows, they are valid for the original flow as well.

In the paper cited above, Crocco establishes the differential equations for stream functions for steady plane and axially symmetric gas flows having a uniform stagnation enthalpy. An argument paralleling that used above easily shows that these stream-function equations are also valid for flows of non-uniform stagnation enthalpy.

Alternative proofs to those employed here can be constructed by formal vector manipulations.[5]

* This generalization was undertaken at the suggestion of P. F. Nemenyi.

[1] L. Crocco, "Eine neue Stromfunktion für die Erforschung der Bewegung der Gase mit Rotation," Zeits. f. angew. Math. u. Mech. (Feb. 1937).

[2] A. Vazsonyi, "On two-dimensional rotational gas flows," Bull. Am. Math. Soc. 50, 188 (1944).

[3] H. W. Emmons, "The numerical solution of compressible fluid flow problems," NACA TN932, pp. 24–25, May 1944.

[4] M. M. Munk and R. C. Prim, "On the multiplicity of steady gas flows having the same streamline pattern," Proc. Nat. Acad. Sci. (May 1947).

[5] M. M. Munk and R. C. Prim, "On the canonical form of the equations of steady motion of a perfect gas," Nav. Ord. Lab. Memorandum No. 9169 (June 1947).

Ultraviolet Transmission of "Counting" Diamonds

H. FRIEDMAN, L. S. BIRKS, AND H. P. GAUVIN
Naval Research Laboratory, Washington, D. C.
December 1, 1947

DIAMONDS that exhibit crystal counting properties are relatively rare. It has been observed thus far that gamma-ray counting diamonds are "water-white," but this quality in itself is not sufficient to guarantee counting properties. Van Heerden,[1] who first demon-

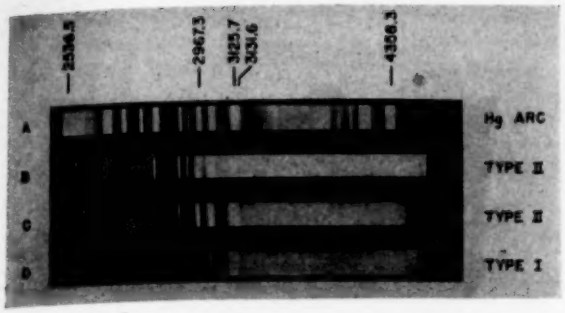

FIG. 1. Spectral transmission of Type-I and Type-II diamonds. A. Mercury spectrum from H-4 lamp. B. Transmission of Type-II diamond (borrowed from Bureau of Standards). C. Type-II diamond (NRL). D. Type-I diamond.

strated the phenomenon of crystal counting in AgCl, experimented unsuccessfully with a diamond of gem quality. Curtiss and Brown[2] recently examined 100 industrial diamonds out of which only two responded well to gamma-rays. This experience has since been duplicated at this and other laboratories. In the experiments reported thus far no comparisons of other physical properties of counting and non-counting diamonds were included.

The existence of two types of diamonds, one much rarer than the other, was described by Robertson, Fox, and Martin, in 1934.[3] The rarer type, which they designated Type II, is characterized by transparency in the ultraviolet down to λ2250, and in the infra-red at 8μ. Type I, the common variety, is opaque below λ3000 and also at 8μ. Among all the physical properties examined by Robertson and his colleagues, the most striking difference between the two diamond types was this greater optical transparency of the rare Type II. Type II also exhibited much greater photo-conductivity and was more nearly optically isotropic. As evidence of the rareness of Type-II diamonds, they remark that, following the discovery of their first Type-II diamond, between two and three hundred diamonds were examined without another being found transparent in the ultraviolet. We have examined a number of counting diamonds, sorted out of a collection of industrial diamonds at this laboratory and one borrowed from L. F. Curtiss of the National Bureau of Standards, for transparency in the ultraviolet. The diamonds were also tested here for their counting characteristics. The amplitude of the largest pulses in Curtiss' diamond was about 50 microvolts,[2] which was roughly 10 times background noise as observed without equipment; those in the best NRL diamond were only 5 times background.

Figure 1 shows the mercury line spectrum of an H-4 lamp, together with the spectral transmission of the two best counting diamonds and the corresponding transmission of a non-counting diamond, which was typical of ten examined. The ten non-counting diamonds each showed a similar abrupt absorption below λ3000, whereas, the two best counting diamonds transmitted well below λ2536. Two relatively poor counting diamonds showed correspondingly faint transmission in the ultraviolet, beyond the limit exhibited by non-counting diamonds. From this correlation between counting and ultraviolet transparency, it appears that the counting characteristic is another exclusive property of the Type-II diamond.

[1] P. J. Van Heerden, *The Crystal Counter* (Dissertation, Utrecht, 1945).
[2] L. F. Curtiss and B. W. Brown, Phys. Rev. **72**, 643 (1947).
[3] R. Robertson, T. J. Fox, and A. E. Martin, Phil. Trans. Roy. Soc. London **463**, 232(A) (1934).

The Beta- and Gamma-Spectra of Ga^{72} *

S. K. HAYNES
Clinton Laboratories, Oak Ridge, Tennessee
AND
Vanderbilt University, Nashville, Tennessee
November 26, 1947

THE beta- and gamma-spectra of Ga^{72} have been investigated with a thin lens spectrometer. The results are given in Table I where a parenthesis means that the line intensity is so close to the statistical fluctuations that its existence is not certain. The energies are accurate to better than two percent, while the relative intensities are probably accurate to twenty percent except for the two highest energy beta-ray groups and the very weak gamma-ray lines. The large uncertainty in the intensities of the two highest energy beta-particle groups arises from the assignment to these groups of the particles associated with an additional apparent end point at 1.48 Mev with an apparent abundance of 10.5 percent. The intensity of the most intense gamma-ray line (0.84 Mev) has been arbitrarily taken as 100 percent in the table. The four most intense gamma-ray lines have been previously reported.[1-3] The four beta-ray groups are in qualitative agreement with the absorption results of Siegel and Glendenin.[4]

Although a complete decay scheme cannot be given on the basis of these spectra, the four most intense gamma-ray lines can be assigned with very little uncertainty as shown in the accompanying partial decay scheme (see Fig. 1). The assignment of the 0.84-Mev gamma-ray to a position in series with all or nearly all of the transitions is necessitated both by its very high intensity and by the value of 2.6 Mev of gamma-ray energy per beta-particle given by Barker,[5] which is in good agreement with the beta-ray energies and intensities of Table I, provided the 1.48-Mev group is not considered real. The four weak gamma-rays probably all help to make up the fourteen percent discrepancy between the 0.64-Mev beta-ray group and the 2.51-Mev gamma-ray line. Considering energy alone the

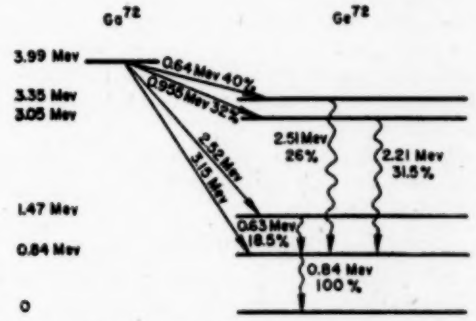

FIG. 1. A partial decay scheme of Ga^{72}.

TABLE I. Gamma-ray spectra of Ga^{72}.

Ga^{72} beta-groups		Ga^{72} gamma-rays	
Energy	Intensity	Energy	Intensity
3.15 Mev	9.5 to 20%	2.51	26%
2.52 Mev	8 to 18.5%	2.21	31.5%
0.955 Mev	32%	1.87	7.5%
0.64 Mev	40%	(1.60)	(4.5%)
		1.05	4.5%
		0.84	100%
		0.68	2%
		0.63	18.5%

1.87-Mev line fits well between the levels of Ge^{72} at 3.35 Mev and 1.47 Mev, while the sum of the other three lines, 0.68+1.05+1.60=3.33, is very close to the difference between the 3.35-Mev level of Ge^{72} and the ground state. However, the intensity of the 0.68 line appears to be much too small to be in a sequence with the 1.05-Mev line and probably the 1.60-Mev line, even allowing for rather large uncertainty in intensity measurements.

The 0.68 line was found by means of its conversion electrons which appear in about 0.5 percent of the disintegrations. The gamma-ray line intensity is so small as to be very difficult to measure. It would appear, however, that the conversion coefficient was between 10 and 50 percent which, for such a high energy and such a low atomic number, would indicate a metastable level with a considerable half-life. The decay period of the beta-ray spectrum and conversion line differs inappreciably from 14.1 hours, indicating that the delay of the line is not longer than a few hours at most.

* This document is based on work performed under Contract No. W-35-058-eng-71 for the Atomic Energy Project at the Clinton Laboratories.

[1] C. E. Mandeville, Phys. Rev. 64, 147 (1943).
[2] L. C. Miller and L. F. Curtiss, Phys. Rev. 70, 983 (1946).
[3] A. Wattenburg, Phys. Rev. 71, 497 (1947).
[4] Siegel and Glendenin, Rev. Mod. Phys. 18, 513 (1946).
[5] E. C. Barker, Phys. Rev. 72, 167 (1947).

Stark Spectrum of HDO*

M. W. P. STRANDBERG, T. WENTINK, JR., R. E. HILLGER, GREGORY H. WANNIER,** AND MURRAY L. DEUTSCH**
Research Laboratory of Electronics, Massachusetts Institute of Technology, Cambridge, Massachusetts

December 4, 1947

THE $5_{4,3;0}$–$5_{4,2;1}$ rotation line of HDO[1] has been measured in the 1.25-cm region at a frequency of 22,307.67 ±0.05 mc/sec. The Stark spectrum of this line was studied in a wave-guide cell by use of equipment and methods that have been described previously.[2–4] Five components were detected, but only three of them were measured. Line breadths were of the order of 250 kc/sec. and, qualitatively, intensities followed theoretical predictions, i.e., proportional to M^2.

In Fig. 1 is plotted the experimental data for the three Stark components that were measured. The data may be fitted with the formula:

$$\Delta\nu = 9.00 E^2 M^2 \times 10^{-8} \text{ mc/sec.},$$

where E is measured in volts per cm and M is the magnetic quantum number, $|M| \leq 5$.

In deriving this equation theoretically, the calculation

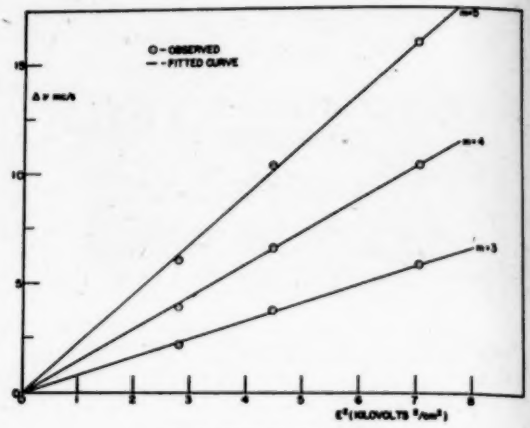

FIG. 1. HDO Stark pattern.

turned out to be considerably more straightforward than expected for an asymmetric rotor. Most of the energy denominators in the second-order terms of conventional perturbation theory are in the infra-red and can be neglected in comparison with the line $5_{4,3;0}$–$5_{4,2;1}$. The largest neglected term corrects the simplified formula in two ways: (*a*) The entire Stark pattern is shifted toward the undisturbed line by an amount about 2.5 percent of its total width. (*b*) The term in M^2 is increased by about 2 percent. The contribution of all the other terms is negligible. For HDO, $K=-0.7$ so that in calculating the direction cosine matrix elements an additional approximation was made by using the symmetric rotor wave functions without further transformation. This approximation involves an error of less than 2 percent of the total Stark pattern width. The resulting theoretical formula is:

$$\Delta\nu = \frac{\mu^2 E^2 \sin^2\delta M^2}{h^2(\nu_{4,1}-\nu_{4,0})}\frac{1}{50},$$

where: μ=dipole moment in e.s.u.-cm, δ=angle between ellipsoid of inertia and dipole moment=20°38′,[5] E=applied electric field in e.s.u./cm, ν=frequency in c.p.s.

By using the dipole moment of H_2O(1.84×10^{-18} e.s.u.-cm),[6] the above equation becomes

$$\Delta\nu = 9.56\times10^{-8} E^2 M^2 \text{ mc/sec.},$$

which is to be compared with the experimental formula.

The agreement is reasonable since, in fact, the dipole moment of HDO can only be approximated by that of H_2O. Using the experimental formula, the value of the dipole moment of HDO obtained, is:

$$\mu = 1.78\pm0.06\times10^{-18} \text{ e.s.u.-cm.}$$

Errors in field strength constitute about 1.5 percent of the indicated error.

* This work has been supported in part by the Signal Corps, the Air Materiel Command, and the O.N.R.
** Socony-Vacuum Laboratories, Paulsboro, New Jersey.
[1] C. H. Townes and F. R. Merritt, Phys. Rev. 70, 558 (1946).
[2] Golden, Strandberg, Wentink, and Hillger, Phys. Rev. 73, 92 (1948).
[3] R. H. Hughes and E. B. Wilson, Jr., Phys. Rev. 71, 562 (1947).
[4] B. P. Dailey, Phys. Rev. 72, 84 (1947).
[5] G. W. King, R. M. Hainer, and P. C. Cross, Phys. Rev. 71, 433 (1947).
[6] See, for example, "Tables of electric dipole moments," Tech. Report No. II, Laboratory for Insulation Research, Massachusetts Institute of Technology.

On the Production of Mesotrons in Cosmic-Ray Stars in the Stratosphere*

MARCEL SCHEIN AND JERE J. LORD
Department of Physics, University of Chicago, Chicago, Illinois
December 5, 1947

TWO Ilford type C2 plates sent along with a free balloon experiment in the stratosphere were exposed to cosmic radiation at an altitude greater than 60,000 feet for a period of eight hours. The one plate examined was covered with 0.15 mm of Al foil and placed about 30 centimeters above some Pb used in conjunction with a counter-telescope arrangement. A thin layer of Cellophane then surrounded the whole apparatus.

By examining the plate, it was found that there was a very large number of cosmic-ray stars present in the emulsion of the film. In the two square centimeters of the plate examined so far, the rate of star production corresponded to approximately 6000 stars of more than 4 long-range particles per cubic centimeter of emulsion per day. This is very considerably higher than the corresponding figure for mountain altitudes (3400 meters). In some of the stars, nuclei heavier than α-particles were emitted which then disintegrated at the end of their range into two particles ("hammer track").[1] In one case the heavier nucleus ejected from the center of the star had a range of 70 microns.

Figure 1 is a mosaic of microphotographs of a high energy star in which ten well separated particles were observed to be emitted from a common center. Tracks (*a*) and (*b*), ending in the emulsion, were identified as protons of long range since their total number of grains along the track *versus* range is in best agreement with the proton calibration curve given for the same type of plate by Lattes, Occhialini, and Powell.[2] Two shorter tracks, (*f*) and (*g*), are very probably nuclei heavier than α-particles since a careful examination of the tracks under the microscope (1350 magnification) shows that they are almost a solid pencil of silver atoms. The other five tracks in the star, which appear as sharp tracks under the microscope, are out of focus in the mosaic, and since those tracks fail to end in the emulsion, they could not be identified.

A particle having an unusually long range was emitted in the star reproduced in Fig. 2. This track (1) was emitted from the center of the star in a nearly horizontal plane and extended 917 microns in the emulsion before it stopped. The end of the track is very close to the glass of the plate. The number of grains were counted in each 50-micron range and found to be in excellent agreement with the

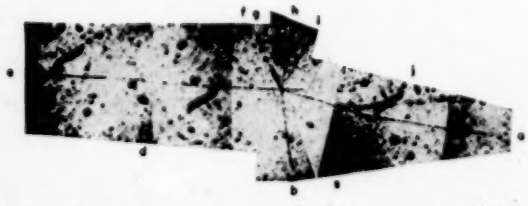

FIG. 1. Mosaic of microphotograph of a high energy star. Tracks (*a*) and (*b*) are protons of long range. Shorter tracks (*f*) and (*g*) are probably nuclei heavier than alpha-particles. The other tracks are not identified.

FIG. 2. An unusually long track (1) from a star. It is probably due to a mesotron. Tracks (*h*), (*i*), and (*j*) are particles which appear to be heavier than alpha-particles. Tracks (*k*) and (*m*) are not identified.

grain *versus* range curve of mesotrons published by Powell and his collaborators.[3] For the residual ranges of 100, 300, 500, 700, and 917 microns the corresponding number of grains were 111, 285, 419, 525, 618. All of these grain counts are considerably below that of a proton of corresponding range and are as low as Powell's grain count for a mesotron. Tracks (*h*), (*i*), and (*j*) end in the emulsion and are particles which appear to be heavier than α-particles. Of these tracks, (*j*) shows a sharp bend (1.7 microns long) at the end of its range (3.9 microns) which is either a scattering (90°) or a secondary disintegration. The other tracks (*k*) and (*m*) are out of focus, and, since they pass out of the emulsion, identification was not possible.

In another part of the plate, a second long-range particle stopping in the emulsion was found. This particle probably originated in the glass of the plate and traveled 1512 microns in a nearly horizontal plane before it stopped. The grains were counted along the track and the following results were found: for the residual ranges 96, 576, 864, 1152, and 1512 microns, the corresponding grain counts were 108, 442, 610, 776, and 959. These figures are in very satisfactory agreement with Powell's data for a mesotron. It is, therefore, concluded that both long-range tracks must have masses considerably lower than that of a proton and, hence, must be mesotrons. The relatively large scattering observed along the tracks is in agreement with this finding.

We wish to thank Dr. J. A. Simpson for supplying the Ilford plates used in the experiment.

* This research was supported in part by Navy Contract N6ori-20, Task Order XVIII.

[1] Nature **159**, 93 (1947).
[2] Lattes, Occhialini, and Powell, Nature **160**, 453 (1947).